Investigating the contribution of synaptic and vascular pathology to neurodegeneration in mitochondrial disease

Alexia Chrysostomou

BSc (Hons) MRes

This thesis is submitted for the degree of Doctor of Philosophy at Newcastle University

Wellcome Trust Centre for Mitochondrial Research

Institute of Neuroscience

Newcastle University

October 2015

Author's Declaration

This thesis is submitted for the degree of Doctor of Philosophy at Newcastle University. The research was conducted in the Wellcome Trust Centre for Mitochondrial Research, Institute of Neuroscience, and is my own work if not stated otherwise. The research was completed under the supervision of Professor D.M. Turnbull, Professor R.W. Taylor and Dr N.Z. Lax from September 2012 to October 2015.

I certify that none of the material offered in this thesis has been previously submitted by me for a degree or any other qualification at any other university.

Abstract

Mutations in mitochondrial DNA (mtDNA) lead to a genetically and phenotypically heterogeneous group of human diseases, mitochondrial disorders. Though patients with mtDNA disease present with multisystemic abnormalities, the central nervous system is usually severely affected. Of the neurological deficits, cerebellar ataxia is the most frequently presenting symptom of patients recruited to the UK MRC Mitochondrial Disease Patient cohort, with a prevalence of 70%. Furthermore, stroke-like episodes are prominent, but not restricted, to patients with the Mitochondrial Encephalomyopathy, Lactic Acidosis and Stroke-like episodes (MELAS) syndrome, due to the m.3243A>G point mutation. Both neurological symptoms are associated with pronounced neurodegeneration. The aim of this thesis was to gain further insights into the mechanisms responsible for neuronal loss in patients who manifest with cerebellar ataxia and stroke-like episodes.

A reliable, reproducible and quantitative quadruple immunofluorescent technique has been developed that allowed the quantification of respiratory chain protein expression in specific neuronal domains and cellular populations. Furthermore, three-dimensional reconstruction helped examine the structural characteristics of sub-cellular compartments. Close investigation of the intracerebellar microcircuitry provided evidence for respiratory chain protein expression defects in Purkinje cell bodies, dendrites and presynaptic terminals. Altered Purkinje cell innervation of respiratory chain deficient dentate nuclei neurons likely leads to neuronal disinhibition and is accompanied by partially disturbed glutamatergic connectivity to the region.

Additionally, respiratory chain deficiencies were detected in the vasculature of vulnerable to stroke-like episodes brain regions (cerebellum, occipital and temporal lobe) in patients harbouring the m.3243A>G point mutation. Preliminary data suggest that stroke-like episode manifestation and cortical lesion development is due to an additive effect between neuronal/interneuronal and vascular pathology.

These observations set the basis for studying the impact of mtDNA defects in synaptic, neuronal and vascular health *in-vitro* and have important implications for identifying good candidates for drug targeting in mitochondrial disease.

For my mum xx

Acknowledgments

Firstly I would like to thank Professor Doug Turnbull and Dr Nichola Lax for their continuous guidance and support throughout my PhD, without which I would not have been able to reach this stage. Their precious advice has helped me overcome obstacles and their encouraging words have given me strength when lab work became very frustrating. I would particularly like to thank Nichola, who has been so much more than just a supervisor.

I would also like to thank those with whom I have collaborated throughout my PhD. Primarily I would like to thank Dr Trevor Booth and Dr Alex Laude (Bio-Imaging Unit, Newcastle University) for trusting me with their valuable equipment and for allowing me to use it anytime needed. Special thanks to Dr Alex Laude for his important contribution in experimental design and his patience with all the technical questions I had at the time. I am also grateful to Catherine Hossain for investigating respiratory chain protein expression in the occipital lobe endothelium (described in Chapter 6) as part of her MRes project.

Huge thanks to various member of the Mitochondrial research group, who have given vast amounts of support. I would particularly like to thank Jonathan for putting up with me and Amy and Hannah for listening to me complain when lab work was not going to plan. I am very grateful to John Grady for all the help with analysing the data and for making numbers meaningful.

Thanks to my close friends for their support all these years. I am honoured to have such amazing people around me – friends in Cyprus who make me feel that I never left home, Nicolas and Athina who make life in the UK so enjoyable. I am greatful to all my family for their constant encouragement and endless love. For secretly worrying but always encouraging me to move forward. Last (but not least!), I would like to thank Giannis for standing by my side and supporting me in everyting I do. This means the world to me!

Finally I am grateful to the sponsors of my studentship for the opportunity to complete this PhD.

Table of Contents

List of Figures

List of Tables

Publications

Chrysostomou, A., Grady, J.P., Laude, A., Taylor, R.W., Turnbull, D.M. and Lax, N.Z. (2015) 'Investigating complex I deficiency in Purkinje cells and synapses in patients with mitochondrial disease', Neuropathol Appl Neurobiol.

Chrysostomou A, Turnbull D.M. "Mitochondria, the synapse and neurodegeneration". Invited contribution to "Mitochondrial Dysfunction in Neurodegenerative disorders" – 2nd Edition. Springer, November 2015

Abbreviations

3D	Three-dimensional
ADP	Adenosine diphosphate
AHS	Alpers-Huttenlocher syndrome
AIF	Apoptosis-inducing factor
AMPA	A-amino-3-hydroxy-5-methylisoxazole-4-propionic acid
ANS	Ataxia neuropathy spectrum
Apaf-1	Apoptotic protease activating factor 1
ATP	Adenosine triphosphate
BBB	Blood-brain barrier
Ca^{2+}	Calcium
CF	Climbing fibre
CFV	Cresyl Fast Violet
CM	Cristae membrane
CNS	Central nervous system
COX	Cytochrome *c* oxidase
CPEO	Chronic progressive external ophthalmoplegia
D –loop	Displacement loop
DAB	Diaminobenzidine
DCN	Deep cerebellar nuclei
DN	Dentate nucleus
DNA	Deoxyribonucleic acid
dNTPs	Deoxynucleotides
Drp1	Dynamin-related protein 1
ETC	Electron transport chain

Fe-S	Iron-sulphur
FFPE	Formalin-fixed paraffin-embedded
GABA	Γ-aminobutyric acid
GAD	Glutamic acid decarboxylase
GAD^+	GAD-positive
GADnL	Large GAD-negative
GLUT1	Glucose transporter 1
H^+	Protons
HRP	Horseradish peroxidase
HSP	Heavy strand promoters
IBM	Inner boundary membrane
IHC	Immunohistochemistry
IMM	Inner mitochondrial membrane
IO	Inferior olive
IOSCA	Infantile-onset spinocerebellar ataxia
KSS	Kearns-Sayre syndrome
LHON	Leber's hereditary optic neuropathy
LSP	Light strand promoter
MAMs	Mitochondrially associated endoplasmic reticulum membranes
MELAS	Mitochondrial encephalopathy with lactic acidosis and stroke-like episodes
MERRF	Myoclonic epilepsy with ragged-red fibres
MF	Mossy fibre
MFN	Mitofusins
MLKL	Mixed-lineage kinase domain-like
ML	Molecular layer

MNGIE	Mitochondrial Neurogastrointestinal encephalopathy
MRI	Magnetic resonance imaging
mRNA	Messenger ribonucleic acid
MtDNA	Mitochondrial DNA
MtEF	Mitochondrial elongation factors
MtERF	Mitochondrial transcription termination factors
MtSSB	Mitochondrial single-stranded DNA binding protein
NBT	Nitro blue tetrazolium
NBTR	Newcastle brain tissue resource
NGS	Normal goat serum
NMDAS	Newcastle Mitochondrial Disease Adult Scale
NPA	No-primary antibody
NSA	No-secondary antibody
O_H	Origin of heavy strand replication
O_L	Origin of light strand replication
OMM	Outer mitochondrial membrane
OPA1	Optic Atrophy 1
OXPHOS	Oxidative phosphorylation system
PCR	Polymerase chain reaction
PFA	Paraformaldehyde
PEO	Progressive external ophthalmoplegia
PGAM5	Phosphoglycerate Mutase Family Member 5
PGC-1α	Peroxisome proliferator-activated receptor γ, coactivator 1α
PMI	Post-mortem interval
POLγ/G	Mitochondrial polymerase gamma

POLMRT	Mitochondrial RNA polymerase
PPARγ	Peroxisome proliferator-activated receptor γ
PSF	Point spread function
Q	Ubiquinone
RIPK3	Receptor-interacting serine/threonine-protein kinase 3
RITOLS	Ribonucleotide incorporation throughout the lagging strand
RNA	Ribonucleic acid
ROS	Reactive oxygen species
rRNA	Ribosomal RNA
RT	Room temperature
SANDO	Sensory ataxia neuropathy dysarthria and ophthalmoplegia
SB	Sudan black b
SD	Standard Deviation
SDH	Succinate dehydrogenase
SMA	Smooth muscle actin
SY	Synaptophysin
SVs	Synaptic vesicles
TBS	Tris-buffered saline
TBST	Tris-buffered saline-Tween
TCA	Tricarboxylic acid cycle
TFAM	Transcription factor A
TFEM	Mitochondrial elongation factor
TIM23	Translocase Of Inner Mitochondrial Membrane 23
tRNA	Transfer RNA
VDAC	Voltage-dependent anion channel

VGLUT	Vesicular glutamate transporter
WT	Wild-type
W/V	Weight/volume

Chapter 1

Chapter 1 Introduction

1.1 Mitochondria

Mitochondria are highly dynamic cytoplasmic organelles present in all nucleated mammalian cells (with the exception of red blood cells). Although they are most well known for their capacity for energy production (in the form of adenosine triphosphate – ATP), their importance in calcium homeostasis (Vandecasteele *et al.*, 2001), reactive oxygen species (ROS) production (Sena and Chandel, 2012), iron-sulphur (Fe-S) cluster biogenesis (Rouault and Tong, 2005) and apoptosis (Wang and Youle, 2009) places mitochondria at the centre of cellular life and death.

According to evolutionary biology, mitochondria have derived from a mutually beneficial relationship between free-living bacteria (Gray, 2012). The "serial hypothesis" suggests that an alpha-proteobacterium was incorporated into a primitive eukaryote cell, which originated from an Archaebacterium and lacked mitochondria, to eventually become the mitochondrion (proto-mitochondrion) (Margulis, 1970). However, more recent observations have led to the "hydrogen hypothesis" which states that mitochondria have evolved after an endosymbiotic relationship between a hydrogen-dependent Archaebacterium and a hydrogen-producing Eubacterium (Martin and Muller, 1998). Regardless of the evolutionary mechanisms that gave rise to modern day mitochondria, a single endosymbiotic event occurred which was followed by either partial loss or transfer of genetic material from the proto-mitochondrion to the cell nucleus (Timmis *et al.*, 2004).

1.1.1 Mitochondrial structure

Upon electron microscopy, mitochondria appear as double-membraned organelles that have a rod or ovoid shape and measure 1-4μm in length x 0.3-0.7μm in diameter (Palade, 1953). The intermembrane space separates the outer from the inner mitochondrial membrane, whereas the interior of the mitochondrion is termed the matrix (Figure 1- 1) (Palade, 1953). The mitochondrial matrix contains multiple copies of the mitochondrial genome and the machinery necessary for its expression.

The outer mitochondrial membrane (OMM) very much resembles normal cell membranes. Its lipid layer is enriched for the voltage-dependent anion channel (VDAC) protein porin, which allows for the exchange of small molecules and ions, <5kDa, between the cytoplasm and the intermembrane space (Alberts B, 2002).

In contrast to the OMM, the high proportion of cardiolipin present within the lipid bilayer of the inner mitochondrial membrane (IMM), accounts for the membranes' impermeability to

macromolecules and ions. Instead, the membrane only allows the perfusion of O_2, CO_2 and H_2O into the matrix, whereas transport proteins located throughout the membranous layer allow small molecules to enter the interior of mitochondria. The IMM is extremely rich in protein (75% protein content) and has traditionally been though to project into the mitochondrial matrix through highly folded conformations, known as cristae (Palade, 1952; Ardail *et al.*, 1990). However, advances in high-resolution microscopy have revealed that the IMM is in fact comprised of the inner boundary membrane (IBM) and the cristae membrane (CM), which are connected through crista junctions (Perkins *et al.*, 1997; Frey and Mannella, 2000). Complexes of the oxidative phosphorylation system (OXPHOS) and proteins involved in Fe-S cluster biogenesis, local protein synthetic machinery and transport are primarily localised within the CM, whilst the IBM is enriched for proteins associated with mitochondrial fusion and related with nuclear DNA-encoded protein import (Vogel *et al.*, 2006).

However, this is not how mitochondria appear *in vivo* which are often organised into syncytia. Mitochondrial ultrastructure is highly variable and depends on the cellular physiological state at the time.

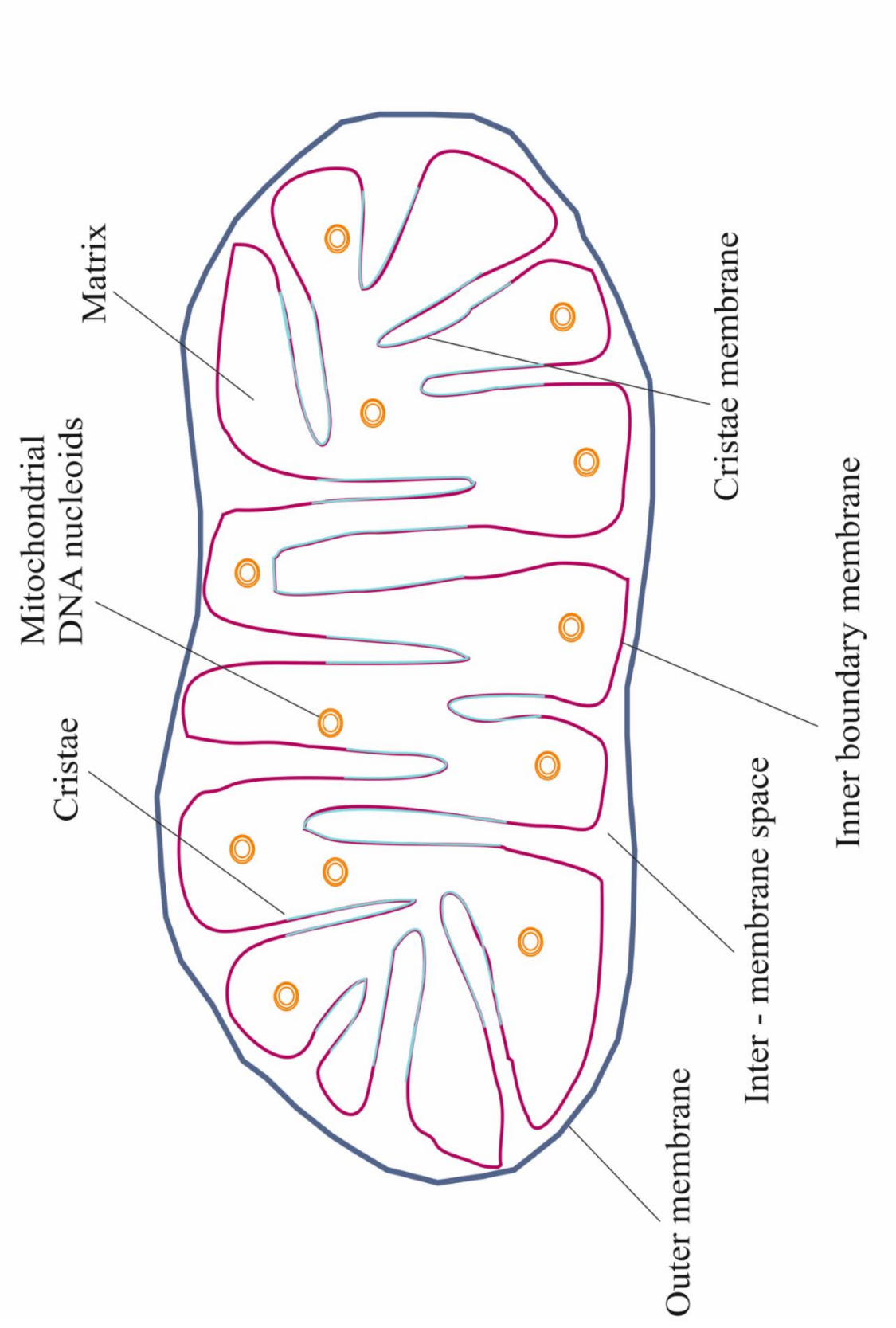

Figure 1- 1: Mitochondrial structure according to recent electron microscopic observations

1.1.2 Mitochondrial biogenesis

The number of mitochondria within tissues varies greatly, depending on the metabolic demand of its cellular populations, and as such mitochondrial biogenesis is tightly regulated so as the ATP requirements of the tissue are met. Its primarily regulated by the peroxisome proliferator-activated receptor γ, coactivator 1α (PGC1-α) and has long being considered to take place within the cell nucleus (Jornayvaz and Shulman, 2010).

1.1.3 Mitochondrial dynamics

Mitochondria are dynamic organelles and as such rarely appear as single entities. Instead, they are usually arranged in networks constantly undergoing fusion and fission allowing for nutrient exchange and support between the individual components (Bereiter-Hahn and Voth, 1994; Chen and Chan, 2004). The balance between mitochondrial fusion and fission is vital since altered fusion/fission rate and/or disturbed fusion/fission machinery have been linked to human neurodegenerative disease (Chen and Chan, 2009). Proteins that are involved in mitochondrial fusion include mitofusins 1 and 2 (MFN1 and MFN2) and optic atrophy 1 (OPA1), whereas the dynamin-1 like protein (DNM1L) is responsible for mitochondrial fission (Liesa *et al.*, 2009).

Further to fusion and fission, mitochondrial dynamics also comprise mitochondrial autophagic degradation, mitophagy (Kim *et al.*, 2007; Twig *et al.*, 2008). Unwanted or damaged organelles are selectively targeted via the Pink1-Parkin signalling pathway and removed via lysosomal degradation (Clark *et al.*, 2006; Park *et al.*, 2006).

1.1.4 Neuronal mitochondria

Neuronal mitochondria are generated in cell bodies and reach the distal parts of an axon via motor protein-assisted transport. There are two types of axonal mitochondrial transport, anterograde and retrograde. Anterograde transport is promoted via Kinesin motors and involves mitochondrial transport towards the axon terminal end of microtubules (Hirokawa and Noda, 2008). Dyneins on the other hand, facilitate retrograde mitochondrial transport back to the cell body (towards the minus-end of microtubules) (Vallee *et al.*, 2004). Mitochondria constantly undergo cycles of moving, stopping and restarting. They are capable of moving in both directions, whereas specific neuronal and physiological signals promote mitochondrial anchoring to particular neuronal sites (Hollenbeck and Saxton, 2005; MacAskill and Kittler, 2010; Schwarz, 2013; Sheng, 2014).

Interestingly, recent evidence on the existence of axonal and presynaptic protein synthetic machineries suggest that mitochondrial biogenesis does not only take place in neuronal cell bodies (Schacher and Wu, 2002; Hillefors *et al.*, 2007; Natera-Naranjo *et al.*, 2010). This is

explained by the fact that some peripheral neurons can possess axons that are several centimetres long, making it difficult for slow-moving mitochondria to meet the energetic demand of distal synapses at any given point. Likewise, Pink1 and Parkin recruitment locally by damaged axonal mitochondria suggests that mitophagy may also occur in the axons (Ashrafi *et al.*, 2014). Local response to focal damage presents a neuroprotective mechanism that does not require retrograde mitochondrial transport.

1.1.5 Oxidative phosphorylation and ATP synthesis

ATP synthesis via the oxidative phosphorylation system (OXPHOS) meets approximately 80% of the total cellular energetic demand. Intermediate products from the tricarboxylic acid (TCA) cycle (also referred to as the citric acid cycle or Kreb's cycle) donate electrons to the respiratory chain, the transfer of which results in ATP generation (Hatefi, 1985; Saraste, 1999).

The primary step of cellular respiration involves cytoplasmic glycolysis, whereby glucose is broken down into pyruvate according to Equation 1- 1 (Berg JM, 2002b):

$$Glucose + 2NAD^+ + 2ADP + 2P_i \rightarrow 2Pyruvate + 2NADH + 2H^+ + 2ATP + 2H_2O$$

Equation 1- 1: Glycolysis

Cytoplasmic pyruvate is then transported into the mitochondrial matrix, within which it undergoes decarboxylation in a reaction catalysed by pyruvate dehydrogenase (Equation 1- 2):

$$Pyruvate + CoA + NAD^+ \rightarrow Acetyl\ CoA + NADH + H^+ + CO_2$$

Equation 1- 2: Pyruvate decarboxylation

Acetyl CoA feeds into the TCA cycle along with NAD^+ and FADH. The two substrates are reduced into NADH and $FADH_2$, to later become electron carriers, and Acetyl CoA is oxidised to CO_2. The overall TCA cycle reaction is summarised in Equation 1- 3 (Berg JM, 2002a):

$$Acetyl\ CoA + 3NAD^+ + FAD + ADP + P_i + 2H_2O \rightarrow CoA + 3NADH + FADH_2 + 2H^+ + ATP + CO_2$$

Equation 1- 3: Outcome of TCA cycle

The ETC consists of four transmembrane multimeric complexes (complex I-IV) and two mobile electron carriers (coenzyme Q and cytochrome *c*), which along with ATP synthase (complex V) comprise the OXPHOS system (Figure 1- 2). Electrons from NADH and $FADH_2$ are donated to complexes I and II respectively which in turn transfer the electrons across the chain. The energy released from electron transfer at complexes I, III and IV, is used to pump protons (H^+)

from the mitochondrial matrix into the intermembrane space creating an electrochemical gradient. This gradient drives protons through complex V that facilitates the phosphorylation of adenosine diphosphate (ADP) to produce ATP (Figure 1- 2) (Berg JM, 2002c).

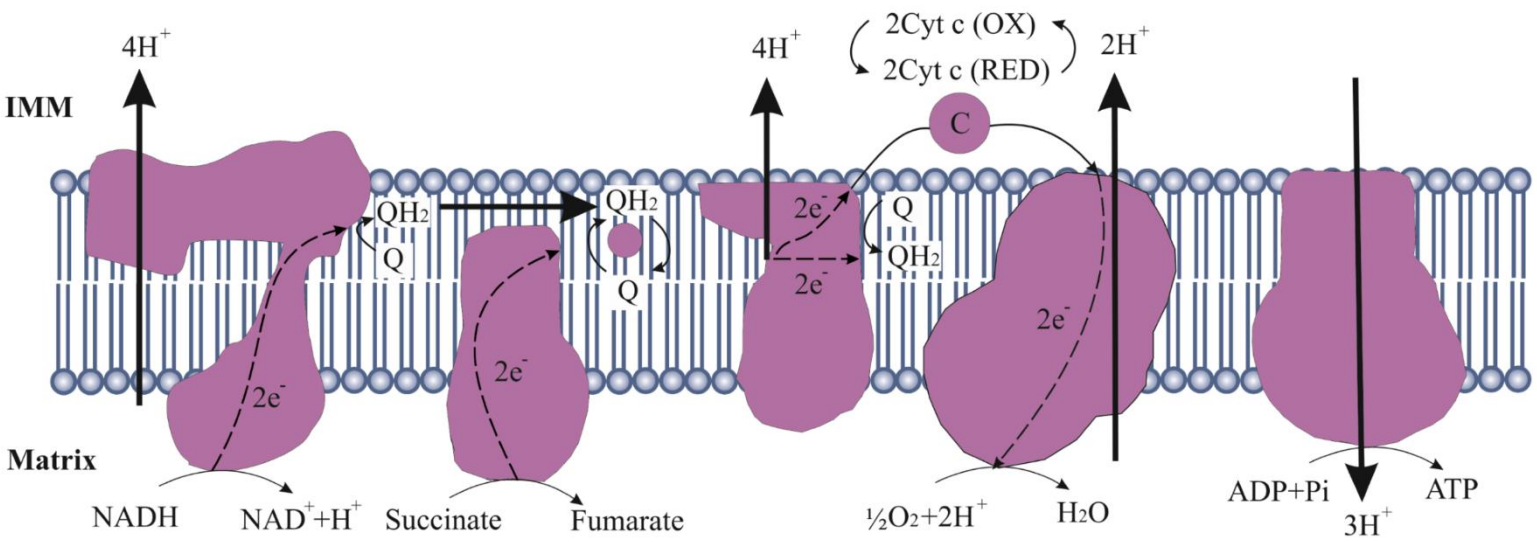

	Complex I	Complex II	Complex III	Complex IV	Complex V
mtDNA/nDNA subunit ratio	7/39	0/4	1/10	3/10	2/14

Figure 1- 2: The oxidative phosphorylation system.

The five transmembrane complexes of the mitochondrial respiratory chain are located within the cristae membrane of the inner mitochondrial membrane and undergo a series of oxidation and reduction reactions. Electrons enter the chain at complexes I and II and reach complex III via reduction of ubiquinone (Q) to ubiquinol (QH_2). Re-oxidation to ubiquinone by complex III generates electrons that are transported to complex IV via cytochrome *c* (C). Passage of electrons across complexes I, III and IV results in proton pump into the mitochondrial matrix and the generation of an electrochemical gradient, used by complex V (ATP synthase) for ATP production. The 13 polypeptides encoded by the mtDNA constitute essential subunits of the respiratory chain. Complex II is entirely encoded by nuclear DNA.

1.1.5.1 Complex I

Complex I (NADH: Ubiquinone oxidoreductase) is the largest of the respiratory chain complexes with a molecular weight of approximately 1,000kDa. The mammalian mitochondrial complex consists of 46 protein subunits, 7 of which are encoded by mitochondrial DNA (mtDNA) (Ugalde *et al.*, 2004b). Electron donation to this complex results to the oxidation of NADH to NAD^+ (by ubiquinone) and to the translocation of four protons into the intermembrane space. The reaction is shown below (Equation 1- 4):

$$NADH + Q + 5H^+_{matrix} \rightarrow NAD^+ + QH_2 + 4H^+_{ims}$$

Equation 1- 4: Complex I reaction

1.1.5.2 Complex II

Complex II (succinate dehydrogenase or succinate ubiquinone oxidoreductase) is the smallest of all respiratory chain complexes since it is comprised of four protein subunits, solely encoded by nuclear DNA. Transfer of electrons across this complex does not drive proton translocation into the intermembrane space, though it reduces FAD^+ to $FADH_2$ while converting succinate to fumarate. The electrons released by the reoxidation of $FADH_2$ to FAD^+ are used to reduce ubiquinone to ubiquinol (Equation 1- 5) (Hagerhall, 1997).

$$succinate + Q \rightarrow fumarate + QH_2$$

Equation 1- 5: Complex II reaction

1.1.5.3 Complex III

Complex III (Ubiquinol: cytochrome *c* oxidoreductase) is composed of 11 protein subunits, one of which is mtDNA-encoded (cytochrome *b*). Complex III utilises the transfer of electrons from ubiquinol to cytochrome *c*, via s process known as the Q cycle, during which two protons are pumped into the intermembrane space (Equation 1- 6) (Mitchell, 1976).

$$2QH_2 + Q + 2Cytc_{oxidised} + 2H^+_{matrix} \rightarrow 2Q + QH_2 + 2Cytc_{reduced} + 4H^+_{ims}$$

Equation 1- 6: Complex III reaction, the Q cycle

1.1.5.4 Cytochrome c

Cytochrome *c* is a small, nuclear encoded hemoprotein that facilitates the transfer of a single electron from complex III to complex IV. It's function extends beyond respiration, since its cytosolic release has been linked to apoptotic cell-death pathways (Huttemann *et al.*, 2011).

1.1.5.5 Complex IV

Complex IV (cytochrome *c* oxidase) is the terminal enzyme of the ETC which also catalyses its rate-limiting reaction. The complex consists of 13 protein subunits, 3 of which are mitochondrially encoded, and catalyses the reduction of oxygen (O_2) to water (H_2O). One reduction reaction requires 4 electrons and results in the translocation of 4 protons into the intermembrane space (Equation 1- 7) (Huttemann *et al.*, 2011).

$$4Cytc_{reduced} + 8H^+_{matrix} + Q_2 \rightarrow 4Cytc_{oxidised} + 4H_2O + 4H^+_{ims}$$

Equation 1- 7: Complex IV reaction

1.1.5.6 Complex V

Complex V ($F_o F_1$ ATP synthase) employs the electrochemical proton gradient, generated by the passage of electrons across the ETC, to drive the phosphorylation of ADP to ATP according to Equation 1- 8:

$$ADP + P_i + 2.7H^+_{ims} \rightarrow ATP + 2.7H^+_{matrix}$$

Equation 1- 8: ATP synthesis

The complex contains two domains, the F_o is located in the membrane and the F_1 extents into the mitochondrial matrix. Proton movement through the F_o domain drives F_1 rotation and generation of ATP. Eight protons are required for a full 360^o rotation of the F_1, which produces 3 molecules of ATP. Thus, the production of one ATP molecule costs 2.7 proton ions (Ferguson, 2010; Watt *et al.*, 2010).

1.1.5.7 Supercomplexes

Free-floating single respiratory chain complexes within the IMM are believed to co-exist with sophisticated supramolecular complexes, termed supercomplexes (Dudkina *et al.*, 2010). Evidence for the existence of OXPHOS supercomplexes arises from blue-native PAGE gels (Schagger and Pfeiffer, 2000) as well as electron microscopic images that illustrate the presence of defined interaction within isolated supercomplexes (Dudkina *et al.*, 2005; Schäfer *et al.*, 2006). Almost all mammalian complex I and III form stable interactions with four copies of complex IV, giving rise to "respirasomes" (Schagger and Pfeiffer, 2000). These can indeed respire independently to the rest of the chain in the presence of ubiquinone and cytochrome *c* (Acin-Perez *et al.*, 2008). Remarkably, respirasome activation requires the incorporation of the catalytic subunit of complex I (NADH dehydrogenase) to the pre-assembled supercomplex (consisted of a complex I scaffold, complex III and IV) (Moreno-Lastres *et al.*, 2012), whereas supercomplex formation is likely to be advantageous to the oxidative phosphorylation capacity

of the cell (Schagger and Pfeiffer, 2000). The time needed for ETC substrates to travel across supercomplexes is decreased, resulting in enhanced catalytic activity of the unit (Schagger and Pfeiffer, 2000). Moreover, the demonstration that electron transport chain complexes are interconnected could account for combined respiratory chain deficiencies in human mitochondrial disease.

1.1.6 Other mitochondrial functions

1.1.6.1 Ca^{2+} signalling and homeostasis

The mitochondrial membrane potential (~180mV), established by a series of oxidation and reduction reactions across the ETC, enables cytoplasmic Ca^{2+} sequestration and contributes to intracellular calcium homeostasis. Cytoplasmic Ca^{2+} crosses the OMM via the VDAC pore (Simamura *et al.*, 2008) and is imported to the mitochondrial matrix via a calcium uniporter (MCU) found at the IMM (Kirichok *et al.*, 2004). Within the matrix, Ca^{2+} functions as a signalling molecule serving to regulate cellular communication (Hofer *et al.*, 2000), apoptosis (Orrenius *et al.*, 2003), ATP production (Tarasov *et al.*, 2012) and metabolism (Duchen, 2000).

The importance of mitochondrial calcium buffering within neurons should not be underestimated. Elevated cytosolic [Ca^{2+}] drives mitochondrial anchoring to synaptic sites, whereas mitochondrial-mediated calcium buffering is key for rapid recovery and therefore synaptic transmission preservation in glutamatergic synapses (Billups and Forsythe, 2002). Moreover, calcium buffering by mitochondria is central to neuronal polarity and axonal differentiation (Mattson and Partin, 1999). Interestingly, synaptic mitochondria appear to have a lower threshold for calcium uptake before their membrane potential collapses and their function is impaired relative to their non-synaptic counterparts (Yarana *et al.*, 2012), implying that the ability of mitochondria to buffer calcium differs across the neuron.

1.1.6.2 Reactive oxygen species production

Mitochondrial reactive oxygen species (ROS) have historically being considered to be damaging to the cells, though more recent investigations have highlighted their importance in cellular physiology, particularly for cell signalling. Complexes I and III possess collectively 10 sites that are capable of producing superoxide radicals (O2-) and thus mitochondrial ROS (Chen et al., 2003; Brand, 2010). Excessive ROS production has been linked to neurodegenerative disorders, cancer and ageing, whereas it's tight regulation facilitates cell differentiation, immune cell activation, autophagy and metabolic adaptation (Sena and Chandel, 2012).

1.1.6.3 Apoptosis and other cell death mechanisms

Apoptosis or programmed cell death is the process by which unwanted or damaged cells are degraded so that the whole organism can survive. Mitochondria are directly involved in apoptotic cell death pathways since intracellular Ca^{2+} built-up drives pro-apoptotic factors (e.g. Bax, Bad) to act on mitochondria. Organelle depolarization and opening of permeability transition pore releases cytochrome *c* that facilitates apoptosome formation via interaction with the apoptotic protease activating factor 1 (Apaf-1). Caspase-9 activation and downstream signaling cascades eventually lead to cellular death. (Kroemer *et al.*, 1998; Wang and Youle, 2009).

Mitochondrial importance in non-apoptotic cell death mechanisms has also been reported and includes their involvement in necroptosis, ferroptosis, and caspace-independent cell death pathways (Tait et al., 2014; Yang and Stockwell, 2015). Serving as a regulated active type of cell death that resembles necrosis (Galluzzi et al., 2011), necroptosis initiation (following DNA damage, viral infection and death receptor-ligand binding) leads to necrosome formation (containing the receptor-interacting serine/threonine-protein kinase 3 (RIPK3) and the mixed-lineage kinase domain-like (MLKL) protein) which is then translocated to mitochondrially associated endoplasmic reticulum membranes (MAMs) (Chen et al., 2013). Phosphorylation of a mitochondrial phosphatase (PGAM5) by RIPK3 drives DNM1L activation followed by mitochondrial fission, ROS production and necroptosis (Wang et al., 2012). Mitochondrial importance in necroptosis is however controversial since organellar depletion does not affect the kinetics or the extent of necroptosis induced by factors other than ROS (Tait et al., 2013).

Ferroptosis is an iron-dependent form of oxidative cell detah that is genetically, morphologically and biochemically unique (Dixon et al., 2012). Two cellular events are suggested to be necessary for ferroptosis to occur; one being the disruption of cellular antioxidant defences (by chemical compounds like erastin, Sorafenib and p53 and/or following ischemia/reperfusion injury) and the other being an increase of intracellular iron (Bogdan et al., 2015; Yang and Stockwell, 2015). The presence of small mitochondria with increased membrane density in cells treated with erastin (Dixon et al., 2012) and the identification of VDAC2/3 as direct erastin targets (Yagoda et al., 2007), suggests for mitochondrial participation in erastin-induced cell death.

Mitochondrial outer membrane permeablisation is a shared mechanism between apoptosis and caspase-independent cell death pathways (Tait and Green, 2008), which are overall biochemically and kinetically distinct. Mitochondria may contribute to caspase-independent

cellular death directly, via a loss-of-function mechanism or a combination of the two (Tait et al., 2014). Outer membrane permeabilisation leads to intermembrane protein release (e.g cytochrome *c*, apoptosis-inducing factor (AIF), endonuclease G etc) and cellular death however, definitive proof that this is indeed the case is lacking (Jones et al., 2003; Bahi et al., 2006). Instead, mitochondrial permeabilisation is proposed to be crucial for mitochondrial function since TIM23 (an inner mitochondrial membrane translocase subunit) (Goemans et al., 2008) and cytochrome *c* degradation (following permeabilisation) (Ferraro et al., 2008) collectively contribute to respiratory chain (complex I and IV) dysfunction (Lartigue et al., 2009) and loss of mitochondrial membrane potential. These eventually lead to cellular death. Finally, reversal of ATPase function (following mitochondrial permeabilisation) is proposed to result in ATP hydrolysis and cellular ATP depletion, thus accelerating caspase-independent cell death (Tait et al., 2014).

1.1.6.4 Iron homeostasis and Fe-S cluster biogenesis

Mitochondria are central to cellular iron metabolism since the majority of intracellular iron is imported into the organelles, via the IMM protein mitoferrin (Shaw *et al.*, 2006). Organellar iron is then utilised for haem production and Fe-S cluster biogenesis (Wang and Pantopoulos, 2011). Fe-S cluster biogenesis is a complex and multi-stage process during which the mitochondrial proteins Isu1/2 and Isa1/2 serve as the scaffold for cluster biogenesis and Grx5 and Abcb7 are involved in cluster maturation (Wang and Pantopoulos, 2011). The primary role of Fe-S clusters is to facilitate electron transport, exemplified by the presence of 12 different Fe-S clusters in the ETC (Schultz and Chan, 2001), while they are also involved in the sensing and regulation of oxidative stress and intra-mitochondrial iron levels (Olsson and Norrby, 2008; Yeh *et al.*, 2009).

1.2 The mitochondrial genome

Mitochondria contain their own genetic material, mitochondrial DNA (mtDNA) (Nass and Nass, 1963), which is a small (16,569bp) and circular double-stranded molecule that resides within the mitochondrial matrix. MtDNA is composed of a guanine-rich heavy strand and a cytosine-rich light strand, which collectively house the 37 mtDNA genes. The mitochondria genome encodes for 13 proteins necessary for the assembly and function of the oxidative phosphorylation system, 2 ribosomal RNAs (rRNAs) and 22 transfer RNAs (tRNAs) (Figure 1- 3) (Anderson *et al.*, 1981). The only non-coding region within mtDNA is known as the strand-displacement loop (D-loop), a triple-stranded sequence that serves as the site for heavy strand replication and contains elements necessary for mtDNA transcription (Arnberg *et al.*, 1971; Kasamatsu *et al.*, 1971; Shadel and Clayton, 1997). Unique features of the mitochondria

genome include the absence of intronic sequences and scarcity of non-coding regions (termination codons created after transcription) within its structure, accounting for the compactness of the molecule (Anderson *et al.*, 1981).

Multiple mtDNA copies (2-10) are present within each mitochondrion (Lee and Wei, 2005) and numerous mitochondria are contained within each mammalian cell, thus some cells of the human body can have up to 10^4 mtDNA copies (Lightowlers *et al.*, 1997). Though originally believed to be naked and unprotected, mtDNA molecules are packaged into small (~100nm) protein-DNA complexes known as nucleoids (Chen and Butow, 2005; Kukat *et al.*, 2011). Nucleoids have been reported to contain between 1.4 (Kukat *et al.*, 2011) and 3 (Brown *et al.*, 2011) mtDNA copies and are highly abundant for the mitochondrial transcription factor A (TFAM) (Parisi and Clayton, 1991; Kukat *et al.*, 2011). Other proteins documented to be associated with mammalian nucleoids include the mitochondrial DNA helicase - TWINKLE, the single-stranded DNA binding protein - mtSSB and the mitochondrial DNA polymerase - POLγ (Chen and Butow, 2005).

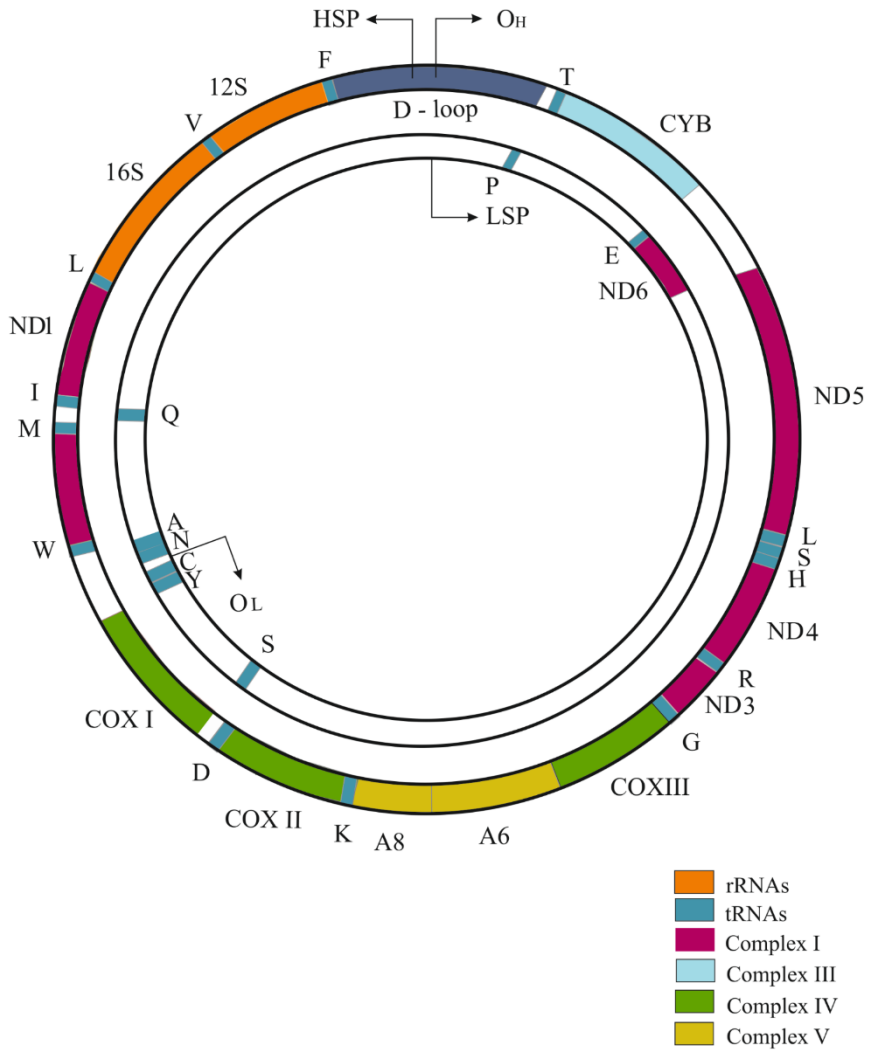

Figure 1- 3: The human mitochondrial genome.

The human mtDNA is a compact, circular double-stranded molecule comprised of a heavy and a light strand. MtDNA encodes for 37 genes: 13 polypeptides, 2 rRNAs and 22 tRNAs. The outer (heavy strand) houses 12 of the protein encoding genes: 5 complex I subunits (*MT- ND1-5*), 1 complex III subunit (*MT -CYB*), 3 complex IV subunits (*COX I-III*) and 2 subunits of complex V (*ATP 6&8*). The ND6 subunit of complex I is transcribed from in the inner light strand, whereas tRNA genes are dispersed throughout both stands and interspersed between protein coding regions. The D-loop is the only non-coding region within mtDNA and contains the sites for mtDNA transcription (HSP and LSP). The origins for heavy (H) and light (L) strand replication (O_H and O_L) are also shown.

1.3 MtDNA transcription and translation

The three sites of transcription initiation are found within the D-loop: the light strand promoter (LSP) and the heavy strand promoters 1 and 2 (HSP1 and HSP2 respectively). The LSP transcribes the full length of the light strand (containing mt-*ND6* and 8 tRNAs), so does HSP2 for the heavy strand (12 mitochondrial proteins, 2 rRNAs and 14 tRNAs). On the contrary, HSP1 only transcribes 2 tRNAs and both rRNAs of the heavy strand (Figure 1- 3) (Montoya *et al.*, 1982; Chang and Clayton, 1984). Once TFAM binds directly upstream of the promoter region, the mtDNA undergoes conformational changes that allow the mitochondrial RNA polymerase (POLMRT) and mitochondrial transcription factor B1/B2 (TFB1M/TFB2M) to access mtDNA and thus initiate the transcription process (Fisher *et al.*, 1987; Dairaghi *et al.*, 1995). MtDNA is transcribed bi-directionally, producing a polycistronic molecule that will subsequently be processed and give rise to mature mRNAs, tRNAs and rRNAs (Rebelo *et al.*, 2011). Following transcription initiation, the mitochondrial transcription elongation factor (TEFM) associates with POLMRT assuring for transcription elongation followed by the incorporation of the mitochondrial transcription termination factor (mTERF) and termination of the process (Rebelo *et al.*, 2011). There are currently four members of the mTERF family of proteins, the function of which might not be restricted to transcription termination but in fact also be associated with mtDNA transcription initiation and replication (Roberti *et al.*, 2009).

Although mammalian mitochondrial translation holds many unique features, it follows the canonical initiation, elongation and termination steps (Smits *et al.*, 2010). Mitochondrial mRNA translation is performed within mitoribosomes, structures equivalent to nucleolar ribosomes that are extremely rich in protein. Mitoribosomes are comprised of a small 28S subunit (SSU), a large 39S subunit (LSU) and the 2 mitochondrial rRNAs (12S and 16S) (O'Brien, 2003). The translation initiation factors IF2 (Ma and Spremulli, 1995) and IF3 (Koc and Spremulli, 2002), the elongation factors mtEFTu (Ling *et al.*, 1997), mtEFTs (Xin *et al.*, 1995) and mtEFG (Hammarsund *et al.*, 2001) and the release factor RF1 assist the initiation, elongation and termination of the translation procedure respectively. An AUA or AUU codon, located within the highly compact and uncapped mitochondrial mRNAs, marks the initiation of protein synthesis by the 22 mitochondrial tRNAs (contrary to what is suggested by the wobble hypothesis) (Barrell *et al.*, 1980). The site of translation termination is marked by the presence of an AGG or AGA triplet, in addition to UAA and UAG (Osawa *et al.*, 1992), which is recognised by mtRF1α.

1.4 MtDNA replication

MtDNA replication occurs independently of nuclear DNA and of the cell cycle, justifying the term "relaxed replication" (Bogenhagen and Clayton, 1977; Birky, 1994). In post-mitotic cells mtDNA is turned over in a much slower rate than in actively dividing cells (Wang *et al.*, 1997), and there are evidence to suggest that mtDNA synthesis in neurons might take up to 20 hours (Calkins and Reddy, 2011). There is an on-going debate as to the exact mechanism(s) that account for mtDNA replication, the most popular of which being: the asynchronous or strand-displacement model and the synchronous model (Holt and Reyes, 2012). According to the former, mtDNA replication starts at the origin of heavy strand replication (O_H) and processes around two-thirds of the mtDNA molecule (synthesizing the leading strand), before initiation of lagging strand synthesis starts at the origin of light strand replication (O_L) (Kasamatsu and Vinograd, 1973; Clayton, 1982). Later, Holt and colleagues (2000) have identified the presence of replication intermediates with differing sensitivities to single-stranded nucleases giving rise to the synchronous replication model (Holt *et al.*, 2000). A refined version of the model is suggestive of bidirectional mtDNA replication, initiated in more than one regions (encompassing *MT-CYB*, *ND5* and *ND6*) and terminated at the O_H (Bowmaker *et al.*, 2003). The latest model of mtDNA replication is similar to the strand-displacement model but further proposes the incorporation of ribonucleuotides (RNAs) in the lagging strand during leading strand synthesis, hence its name: RITOLS (ribonucleotide incorporation throughout the lagging strand) (Yang *et al.*, 2002; Yasukawa *et al.*, 2006).

Although numerous mtDNA replication models have been proposed, few enzymes are currently known to be necessary for mtDNA replication. These include: the mtDNA polymerase γ (POLG) (Hance *et al.*, 2005), the mitochondrial TWINKLE DNA helicase (Tyynismaa *et al.*, 2004), the mitochondrial RNA polymerase (POLMRT) (Fuste *et al.*, 2010) and the mitochondrial single-stranded binding protein (mt-SSB) (Maier *et al.*, 2001).

1.5 Mitochondrial genetics

1.5.1 Maternal inheritance and the bottleneck effect

MtDNA inheritance does not follow the Mendelian rules; instead mtDNA is strictly inherited through the maternal germline (Giles *et al.*, 1980). The mechanisms responsible for paternal mtDNA destruction are species-specific and take place both pre- and post-fertilisation (Sato and Sato, 2013). Selective proteasomal degradation and autophagy account for paternal mtDNA elimination in mammalian (Kaneda *et al.*, 1995; Sutovsky *et al.*, 1999) and nematode fertilised eggs (Sato and Sato, 2011) respectively. On the contrary, paternal mtDNA is degraded during

spermatogenesis in flies (DeLuca and O'Farrell, 2012), whereas nucleoid density is decreased in fish sperm and degraded following fertilisation (Nishimura *et al.*, 2006). However, the paternal origin of an inherited deletion in mt-*ND2* has been documented providing evidence for the only case of human mtDNA inherited from the father (Schwartz and Vissing, 2002).

Pathogenic mtDNA mutations are therefore transmitted from the mother to her children, though there is extensive variability in the number of mutated mtDNA molecules that are passed onto the next generation (Taylor and Turnbull, 2005). This genetic variability accounts for phenotypic variability amongst patients with the same genetic defect (Chinnery *et al.*, 1997) and is attributed to a phenomenon known as genetic bottleneck (Chinnery *et al.*, 2000). There is an on-going debate as to the exact mechanism by which the genetic bottleneck occurs, the most widely accepted being the rapid replication of mtDNA molecules during embryonic development (~200 mtDNA molecules in primordial germ cells, giving rise to oocytes which contain ~100,000 copies of mtDNA) (Cree *et al.*, 2008). The level of pathogenic mutations in offspring are defined by random genetic drift although specific inheritance patterns for the various mtDNA defects exist (Brown *et al.*, 2001).

1.5.2 MtDNA mutagenesis and repair mechanisms

Both the compact structure of mtDNA and its close proximity to the ETC render the mtDNA susceptible to acquiring defects. The absence of histones (Richter *et al.*, 1988) and the less robust mtDNA repair mechanisms (Clayton, 1982) (relative to ones in place for nuclear DNA) constitute mtDNA vulnerable to genetic alterations with a 10-fold increased mutation rate compared to chromosomal DNA (Brown *et al.*, 1979). Furthermore, the presence of mtDNA nucleoids in the vicinity of ROS production sites, occurring during normal OXPHOS conditions, has a negative impact on mtDNA integrity.

MtDNA point mutations, single large-scale or multiple deletions, insertions or duplications can occur as a consequence of DNA strand breaks (el-Khamisy and Caldecott, 2007; Kasparek and Humphrey, 2011), replication errors or incorporation of modified nucleotides (Kamiya, 2003; Boesch *et al.*, 2011). Somatic mtDNA mutations can also be acquired as a result of normal ageing whilst ancient genetic variants occur as an adaptive response to differential environmental conditions (Wallace, 2010). However, pathogenic nuclear and mtDNA mutations associated with adult mitochondrial disease are the focus of this study, detailed discussion of which will be provided at the appropriate section.

Contrary to what was previously believed, the mitochondrial DNA repair pathways are very similar to the nuclear ones (Larsen *et al.*, 2005). These include direct reversal (though its

function in mammalian mitochondria is yet to be verified) (Yasui *et al.*, 1992), base excision repair (Stierum *et al.*, 1999), mismatch repair (Mason *et al.*, 2003) and single-strand break repair (Hegde *et al.*, 2012). Mitochondria have also evolved a unique DNA repair mechanism according to which damaged mtDNA fractions are degraded and replaced by replicated segments of the healthy genome (Gross and Rabinowitz, 1969).

1.5.3 Heteroplasmy and the threshold effect

The presence of multiple mtDNA copies within a cell allows for a mixture of wild type and mutant mtDNA molecules to co-exist. This significant characteristic of mitochondrial genetics is termed heteroplasmy and determines the phenotypic presentation of mitochondrial disease (Larsson and Clayton, 1995). Heteroplasmy is expressed as the percentage of mutant mtDNA copies within a cell or tissue, whereas a homoplasmic state exists if all the mtDNA molecules contained within a cell are identical (either homoplasmic wild type or homoplasmic mutant) (Taylor and Turnbull, 2005).

Random genetic drift controls the levels of pathogenic mutations within a cell via a process known as clonal expansion (Elson *et al.*, 2001); that is the selective multiplication of the mutant genome during successive mitotic events and eventually the accumulation of high heteroplasmic levels in post-mitotic tissues (Weber *et al.*, 1997). However, there exists a critical threshold level before a metabolic defect occurs and a clinical phenotype is observed. The value that the threshold level occupies is variable and depends on the individual, the tissue metabolic requirements and the mutation type. Indeed, the threshold level for mtDNA point mutations involving tRNA genes is ~90% (Yoneda *et al.*, 1995), whilst for single large-scale mtDNA deletions is ~70-80% (Sciacco *et al.*, 1994). Furthermore, tissue specificity is evident since isolated brain mitochondria are thought to have a lower threshold for complex I deficiency (compared to heart, muscle, liver and kidney), whilst mitochondria isolated from muscle were more vulnerable to complex IV defects (Rossignol *et al.*, 1999).

1.6 Mitochondrial disease

There are two sides to every coin and the same is certainly true for mitochondria. The respiratory chain serves to provide the cell with the majority (~90%) of its energetic requirements and as such defects in the energy production machinery is a common cause of inherited disease. Mitochondrial disease encompasses a genetically and phenotypically heterogeneous group of disorders that commence due to either primary mtDNA mutations or defects in nuclear DNA encoded-genes involved in mtDNA maintenance, respiratory chain

assembly and function. Furthermore, mitochondrial disease can arise due to altered mitochondrial dynamics, disturbed IMM structure and aberrant mitochondrial protein transport.

Since the publication of the human mtDNA sequence in 1981 (Anderson *et al.*, 1981) and its association with disease in 1988 (Holt *et al.*, 1988; Wallace *et al.*, 1988), over 270 mtDNA point mutations have been identified and numerous syndromes are linked to mitochondrial dysfunction. The emergence of new technologies enables the identification of nuclear gene mutations responsible for respiratory chain deficiencies, expanding the list of nuclear DNA genes involved in mitochondrial disease (Taylor *et al.*, 2014). Meanwhile, phenotypic heterogeneity is pronounced since distinct syndromes have unique as well as overlapping symptoms, constituting clinical diagnosis extremely challenging (McFarland and Turnbull, 2009). Common disease features might include lactic acidosis, mitochondrial proliferation in muscle fibres (ragged-red fibres) and muscular respiratory chain deficiency, though exceptions do occur (DiMauro *et al.*, 2006).

Mitochondrial disorders are much more prevalent than originally anticipated and in fact, the frequency of pathogenic mtDNA mutations is likely to be underestimated. Data gathered from around the world (England, Finland, Sweden and Australia) suggest that approximately every 1 in 8,500 individuals (adults and children) are affected by mitochondrial disease (both due to mtDNA and nuclear DNA defects) (Chinnery, 2000). According to Schaefer and colleagues (2008) every ~1 in 10,000 adults in the North East of England are clinically affected, whereas ~1 in 6,000 are at risk of developing mitochondrial disease (Schaefer *et al.*, 2008). More recently, the estimated prevalence of adult mitochondrial disease in the same region (North East of England) was ~1 in 4,300 (Gorman *et al.*, 2015b).

Mitochondrial disease is progressive (Arpa *et al.*, 2003; Majamaa-Voltti *et al.*, 2006; Coku *et al.*, 2010) and valuable work has been performed that allows the prediction of disease progression rate (Grady *et al.*, 2014) and the presence of specific system involvement (Grady, 2013). No treatments are currently available for patients with mitochondrial disease however, recent advances in reproductive medicine enable the prevention of mitochondrial disease transmission to the next generations (Craven *et al.*, 2010; Craven *et al.*, 2011; Gorman *et al.*, 2015a).

1.6.1 Primary mitochondrial DNA disorders in adults

Primary mtDNA disorders arise due to pathogenic mtDNA defects, including point mutations, large-scale deletions, duplications and inversions. MtDNA point mutations involve protein

encoding (e.g. *ATP6*) and rRNA genes but are largely associated with tRNA genes, thus affecting respiratory chain protein synthesis. Similarly, mtDNA deletions usually span a 2-10 kb region and are accompanied by short repeats on the deletion breakpoints, high density of which is found within mitochondrial tRNA genes (Schon *et al.*, 1989; Mita *et al.*, 1990; Damas *et al.*, 2012).

Given the high copy number of mtDNA within each cell, every tissue is likely to possess defective mtDNA copies explaining the multisystemic nature of mitochondrial disorders and the presence of neurological and non-neurological symptoms. Neurological disease is the most common feature (McFarland *et al.*, 2010) and symptoms include ataxia, stroke-like episodes, myopathy, peripheral neuropathy and deafness. Clinical syndromes with characteristic features do exist yet many patients are left undiagnosed (Chinnery *et al.*, 2015).

1.6.1.1 Mitochondrial encephalomyopathy with lactic acidosis and stroke-like episodes

The presence of stroke-like episodes, encephalopathy and elevated lactate is reminiscent for the phenotypic manifestation of the mitochondrial encephalomyopathy with lactic-acidosis and stroke-like episodes (MELAS) syndrome (Hirano *et al.*, 1992). Originally described by Pavlakis (1984), this multisystemic disorder affects normally developed adults who upon disease may present with cerebellar ataxia, cardiomyopathy, diabetes mellitus, gastrointestinal dysmotility, hearing loss and retinitis pigmentosa (Pavlakis et al., 1984; Hirano et al., 2006; Chinnery *et al.*, 2015). Regardless of the numerous neurological deficits, stroke-like episodes are the prominent feature of these patients concomitant with headache, nausea and seizures (Chinnery *et al.*, 2015; Hirano et al., 2006). Stroke-like episodes predominantly affect posterior brain regions (including parietal and occipital lobes) detected as hyperintense lesions upon MRI scan, which do not follow the major vascular territories (Ohama *et al.*, 1987; Sue *et al.*, 1998).

The m.3243A>G point mutation within the *MT-TL1* gene (encoding $tRNA^{Leu(UUR)}$) accounts for 80% of the MELAS cases (Goto *et al.*, 1990), although other less frequent mutations have been described. Some of the mutations within tRNA genes include the thymine (T) to cytosine (C) transition at position 3271 (m.3271T>C) in *MT-TL1* (Goto *et al.*, 1991), m.1642G>A in *MT-TV* ($tRNA^{VAL}$) (Taylor *et al.*, 1996) and m.5814A>G in *MT-TC* ($tRNA^{Cys}$) (Manfredi *et al.*, 1996). Mutations within protein encoding genes also exist and involve *MT-ND1* (Kirby *et al.*, 2004; Malfatti *et al.*, 2007), *MT-ND5* (Santorelli *et al.*, 1997; Corona *et al.*, 2001; Liolitsa *et al.*, 2003; McKenzie *et al.*, 2007), *MT-CO2* (Tam *et al.*, 2008), *MT-CO3* (Manfredi *et al.*, 1995) and *MT-CYB* (De Coo *et al.*, 1999; Emmanuele *et al.*, 2013). Interestingly, not all point mutations are unique to MELAS patients since some are also associated with overlapping

syndromes, exemplifying the phenotypic heterogeneity of mitochondrial disease (Ruiter *et al.*, 2006).

1.6.1.2 Myoclonic epilepsy with ragged-red fibres

Characteristic features of patients diagnosed with myoclonic epilepsy with ragged-red fibres (MERRF) syndrome include progressive myoclonus, epilepsy (focal and generalised), cerebellar ataxia and myopathy (Hirano et al., 2006; Chinnery et al., 2015). Peripheral neuropathy, bilateral deafness, dementia and muscle weakness are frequently observed, whereas optic atrophy, cardiomyopathy, pyramidal signs and lipomatosis may also manifest (Hirano and DiMauro, 1996).

Patients usually present with symptoms in childhood, though adult onset has been reported, significantly lowering the life expectancy (Chinnery *et al.*, 2015). The $tRNA^{Lys}$ gene (*MT-TK*) is considered a mutation hotspot for this syndrome since it houses ~90% of pathogenic mutations associated with MERRF, the most frequent of which being the m.8344A>G (Shoffner *et al.*, 1990; Hirano et al., 2006). Point mutations in other tRNA genes, whilst rare, also exist (*MT-TF*, *MT-TL1*, *MT-TI* and *MT-TP*) and may also give rise to a differential diagnosis (Yoon *et al.*, 1993; Shtilbans *et al.*, 2000; DiMauro S, 2003; Nishigaki *et al.*, 2003; Emmanuele *et al.*, 2011).

1.6.1.3 Kearns-Sayre syndrome

Serving as the first multisystem mitochondrial disorder to be clinically defined, the Kearns-Sayre syndrome (KSS) is characterised by ophthalmoplegia and pigmentary retinopathy that presents before the age of 20 (Kearns and Sayre, 1958). Patients with KSS have a relatively low life expectancy and the majority of them display with short stature, hearing loss, limb weakness and cognitive impairment (executive function and visuospatial perception) (Bosbach *et al.*, 2003). Additional features include cerebellar ataxia, cardiac condition block, elevated cerebrospinal fluid protein and proximal myopathy (Maceluch and Niedziela, 2006). Genetically, KSS is defined by sporadic large-scale deletions or complex rearrangements of mtDNA (Zeviani *et al.*, 1988; Moraes *et al.*, 1989).

1.6.1.4 Leber's Hereditary Optic Neuropathy

Leber's hereditary optic neuropathy (LHON) predominantly affects young males that lose their bilateral central vision sequentially. The vast majority of LHON cases (over 95%) are due to mtDNA point mutations within genes encoding for complex I protein subunits: m.11778G>A (*MT-ND4*), m.3460G>A (*MT-ND1*) and m.14484T>C (*MT-ND6*) (Mackey *et al.*, 1996), but rare secondary mutations have also been documented (Carelli *et al.*, 2004; Yum *et al.*, 2014).

Symptoms develop in a small percentage of homoplasmic mutation carriers (~50% of male and ~10% of female) implying that epigenetic modification and/or environmental factors are important for the clinical manifestation of the disease (Newman, 2002). Moreover, the strong disease predilection for males suggests that nuclear X-linked loci control disease phenotypic presentation (Bu and Rotter, 1991; Nakamura *et al.*, 1993).

1.6.1.5 Chronic progressive external ophthalmoplegia

Chronic progressive external ophthalmoplegia (CPEO) is the most common mitochondrial myopathy in adults (Jean-Francois *et al.*, 1997). Dating back from 1867 CPEO is characterized by ptosis, ophthalmoparesis and mitochondrial myopathy (Jean-Francois *et al.*, 1997). Proximal limb muscle weakness, facial muscle paralysis, early fatigue, exercise intolerance, sensorineural hearing loss, axonal neuropathy, ataxia, depression, cataracts and cardiomyopathy may also manifest (Cohen and Naviaux, 2010).

CPEO can be sporadic or familial, a primary or secondary mitochondrial disorder. Single mtDNA deletions account for the majority of CPEO cases, whereas mtDNA duplications and single nucleotide substitutions in tRNA genes may occur (Holt *et al.*, 1988; Fassati *et al.*, 1994; Silvestri *et al.*, 1996; Taylor *et al.*, 1998). Mutations in nuclear genes involved in mtDNA maintenance result in secondary mitochondrial disease due to multiple mtDNA deletions (Carrozzo *et al.*, 1998; Moslemi *et al.*, 1999).

1.6.2 Mitochondrial disease in adults due to nuclear defects

In addition to primary mtDNA mutations, nuclear genetic defects can result in aberrant oxidative metabolism and mitochondrial disease. Mutations in genes encoding for respiratory chain protein subunits and/or assembly factors directly impair OXPHOS, whereas mtDNA integrity is negatively affected by defects in nuclear genes involved in mtDNA maintenance. There exists an ever-increasing list of nuclear genetic mutations involved in mitochondrial disease whilst multiple alterations in a single gene can account for a plethora of distinct clinical syndromes (Lightowlers *et al.*, 2015). Nuclear genes most frequently associated with mitochondrial disease will be discussed below.

1.6.2.1 Polymerase gamma

Polymerase gamma (POLG) is the sole mtDNA polymerase described to date, mutations in which are an important cause of mitochondrial disease (Cohen BH, 2010). Over 160 mutations are spread throughout the gene, giving rise to secondary mtDNA alterations (mtDNA depletion and deletion) (Fonzo *et al.*, 2003; Tzoulis *et al.*, 2009) and consequent Mendelian inherited diseases. A wide spectrum of syndromic diseases are related to *POLG* mutations, which may

have an infantile or adult onset. These include the Alpers-Huttenlocher syndrome (AHS), autosomal dominant and recessive PEO and the ataxia neuropathy spectrum (ANS) (Horvath *et al.*, 2006).

AHS usually has a childhood onset and is characterised by severely impaired development (psychomotor regression), liver failure, intractable seizures and cortical blindness (Naviaux and Nguyen, 2004; Davidzon *et al.*, 2005; Isohanni *et al.*, 2011). Upon magnetic resonance imaging (MRI), multiple lesions and severe atrophy are apparent in cortical regions (Saneto *et al.*, 2008; Gropman, 2013). Patients with PEO typically present with ptosis and strabismus, consequent to progressive weakness of the extraocular eye muscles, and generalised myopathy (Van Goethem *et al.*, 2001). Deafness, ataxia, neuropathy, parkinsonism, depression and hypogonadism further affect those who acquire the disease due to *POLG* mutations, giving rise to the so called PEO+ phenotypes (Filosto *et al.*, 2003; Mancuso *et al.*, 2004). ANS encompasses the previously distinct mitochondrial recessive ataxia syndrome (MIRAS) and sensory ataxia neuropathy dysarthria and ophthalmoplegia (SANDO) (Cohen BH, 2010). Further to ataxia and neuropathy (maybe sensory, motor or both), patients with ANS may manifest with encephalopathy, myoclonic seizures, blindness and liver dysfunction (Wong *et al.*, 2008).

1.6.2.2 Twinkle

Twinkle helicase is an important protein of the mtDNA replicative machinery and a constituent of mitochondrial nucleoids, present within the matrix. The protein is encoded by the *C10orf2* gene, also known as PEO1, mutations in which result in qualitative (deletions) and quantitative (depletions) mtDNA alterations (Spelbrink *et al.*, 2001).

Large mtDNA deletions are thought to arise due to impaired helicase activity, resulting in adult-onset PEO or PEO+ phenotypes (Spinazzola and Zeviani, 2005). On the contrary, hepatocerebral depletion syndrome and infantile-onset spinocerebellar ataxia (IOSCA) are examples of mitochondrial disease due to quantitative mtDNA changes due to *C10orf2* mutations (Hakonen *et al.*, 2007; Sarzi *et al.*, 2007). Infants with hepatocerebral depletion syndrome present with elevated lactate, liver enlargement, hypotonia and psychomotor delay. Neurological abnormalities are progressive and include ataxia, ophthalmoplegia, nystagmus and epilepsy (El-Hattab and Scaglia, 2013). Infants with IOSCA suffer from ataxia, ophthalmoplegia, sensory neuropathy, encephalopathy with seizures and muscle hypotonia due to mitochondrial depletion in liver and brain (Nikali *et al.*, 2005; Hakonen *et al.*, 2007; Hakonen *et al.*, 2008).

1.7 Mitochondrial disease and the brain

Despite the fact that the brain only occupies 2% of our bodies' mass, it consumes 20% of the organisms' oxygen at rest (Mink *et al.*, 1981), exemplifying the extensive metabolic requirements of the tissue. The highly specialised neuronal networks formed in the brain facilitate information processing that occurs via synaptic transmission. This process is highly dependent on mitochondrial function, constituting mitochondrial biogenesis, transport and quality control in neurons vital to neuronal health and brain function. It therefore comes as no surprise that the central nervous system (CNS) is vulnerable to mitochondrial respiratory chain deficiencies and as such, neurological deficits are one of the most common features of patients with mitochondrial disease.

1.7.1 Brain atrophy

Primary evidence of CNS abnormalities arise from neuroradiological data as well as macroscopic observations upon post-mortem examination. Despite the great variability in the phenotypic manifestation of mitochondrial disease, neurodegeneration is a unifying feature amongst patients with different disorders and is due to brain atrophy and structural abnormalities. Indeed, decreased fresh brain weight (by about ~19%) in 12 patients with mitochondrial disease (m.3243A>G, m.8344A>G, m.14709T>C, single large mtDNA deletion and *POLG*) compared to aged-matched controls is due to profound neuronal loss throughout the brain (Lax and Jaros, 2012).

1.7.2 Neuroradiological observations

Neuroradiological examination of patients with the m.3243A>G and m.8344A>G point mutation and of those with mtDNA rearrangements and deletions signifies the presence of hyperintense lesions in the brain stem and basal ganglia, whereas white matter and cortical changes also exist (Haas and Dietrich, 2004; Saneto *et al.*, 2008; Gropman, 2013). Cerebral atrophy is commonly observed in many disease subgroups, though not a specific finding. Cerebellar atrophy might serve as the main finding for some patients (Valanne *et al.*, 1998; Scaglia *et al.*, 2004; Scaglia *et al.*, 2005), whereas it can be linked to more severe disease in others (Sue *et al.*, 1998). Such an example includes the documentation of enlarged fourth ventricles in six pedigrees with MELAS (due to the m.3243A>G) predicted to result in cerebellar atrophy during disease progression (Sue *et al.*, 1998).

Neuroimaging findings are variable and often depend on the experimental setting (Magnetic resonance imaging, Computerised Tomography scan, diffusion tensor imaging, magnetic resonance spectroscopy); they may hint towards signature features for a specific disorder, non-

specific abnormalities or even demonstrate the occurrence of structurally normal brains (Saneto *et al.*, 2008). Such a characteristic feature is the presence of stroke-like cortical lesions in posterior brain regions (parieto-occipital region) of patients harbouring the m.3243A>G. Lesions affect predominantly grey matter and adjacent white matter areas, while they do not conform to the major vascular territories. They may be unilateral or bilateral, they may resolve with time or reappear in neighbouring regions upon sequential examination (Haas and Dietrich, 2004; Gropman, 2013). Neuroradiological imaging of patients with MELAS (due to m.3243A>G) performed in 1998 reports mineral deposition (calcification) in the basal ganglia as the most common finding, documented in the majority of patients (54%) (Sue *et al.*, 1998).

Contrary to the specific neuroradiological abnormalities of patients with MELAS, MERRF patients present with a variety of neuroimaging changes ranging from white matter lesions, to basal ganglia haemorrhage and atrophy of the cerebral cortex and cerebellum (Haas and Dietrich, 2004). Moreover, scattered cerebral infarcts are documented in a 39-year-old woman (harbouring the m.8344A>G point mutation) who did not present with the classical clinical features for MERRF (Tanji *et al.*, 2003).

A clinicopathological investigation of 26 patients with a combined mitochondrial spinocerebellar ataxia and Alpers phenotype due to mutations in *POLG* (homozygous or compound heterozygotes for A467T and W748S) revealed the presence of focal lesions involving (with order of frequency) the occipital lobe, deep cerebellar nuclei, the thalamus and basal ganglia (Tzoulis *et al.*, 2006). Early onset Alpers syndrome (in childhood) is linked to progressive occipital lobe hyperintensities, whilst lesions may resolve and the brain may be structurally normal even by the time of death (Saneto *et al.*, 2008).

White matter changes are the distinctive feature of patients with Mitochondrial Neurogastrointestinal Encephalopathy (MNGIE) and KSS syndrome. Termed leukodystrophy, these lesions are diffuse sparing the corpus callosum in patients with MNGIE (Nishino *et al.*, 1999; Labauge *et al.*, 2002) who also present with demyelinated sensory neurons (Hirano *et al.*, 1994). In patients with KSS, subcortical, basal ganglia, thalamic and brain stem white matter lesions are observed, whilst cerebral and cerebellar atrophy are commonly reported (Chu *et al.*, 1999; Lerman-Sagie *et al.*, 2005).

1.8 Neuropathological features of mitochondrial disease

Further to focal lesions detected macroscopically in the brains of patients with mitochondrial disease, microscopic neuropathological investigations are indicative of profound neuronal cell loss, spongiform degeneration (mainly in the white matter), glial cell proliferation and axonal

demyelination (Sparaco *et al.*, 1993). Respiratory chain deficiencies and decreased ETC protein expression in vulnerable neuronal, inter-neuronal and vascular cell populations have also been documented (Tanji *et al.*, 2001; Betts *et al.*, 2006; Lax *et al.*, 2012b; Lax *et al.*, 2012c; Lax *et al.*, 2015). These are usually associated with high heteroplasmic percentages, cellular loss and structural abnormalities.

1.8.1 m.3243A>G

The presence of pan-necrotic foci is a characteristic feature of patients with MELAS, due to the m.3243A>G, associated with neuronal loss, inflammatory response activation and astrocytic and capillary proliferation (Sparaco *et al.*, 1993; Sue *et al.*, 1998; Tanahashi *et al.*, 2000; Betts *et al.*, 2006). These infarct-like foci are commonly observed in cerebral cortices (bilateral) and cerebellum, whilst the basal ganglia, the thalamus, the brain stem and subcortical white matter may also be affected (Sparaco *et al.*, 1993; Sue *et al.*, 1998; Betts *et al.*, 2006; Lax *et al.*, 2012c). Calcium deposition constitutes the second most frequent lesion in patients with MELAS, whereas cortical vacuolation (spongiform degeneration) is observed in the cerebrum and spinal cord (lateral and posterior columns (Sparaco *et al.*, 1993).

Vascular abnormalities include vessel wall calcification reported in globus pallidus, basal ganglia and thalamus (Sue *et al.*, 1998; Tanahashi *et al.*, 2000), decreased immunoreactivity against mtDNA-encoded respiratory chain subunits (Sparaco *et al.*, 2003) and COX-deficient blood vessels with high heteroplasmic percentages in various brain regions (Betts *et al.*, 2006; Lax *et al.*, 2012c). COX-deficiency is not only observed in association with lesions since it's particularly prominent in meningeal, cortical and white matter vessel walls (Betts *et al.*, 2006; Lax *et al.*, 2012c). Thinning of the smooth muscle and endothelial cell layers in the cerebellum is indicative of vascular cell loss, whilst plasma protein (fibrinogen and IgG) extravasation (Tanji *et al.*, 2001; Lax *et al.*, 2012c) and decreased tight junction protein expression (Lax *et al.*, 2012c) are reminiscent of blood-brain barrier (BBB) permeability problem. According to electron microscopic observations, enlarged mitochondria are aggregated within the smooth muscle and endothelial cell layer of cerebral and cerebellar arterioles and small arteries (Ohama *et al.*, 1987; Mizukami *et al.*, 1992; Tanahashi *et al.*, 2000). Likewise, mitochondrial proliferation in choroid plexus epithelial cells is documented and accompanied by COXII immunodeficiency (Ohama and Ikuta, 1987; Tanji *et al.*, 2001).

Generalised cerebellar atrophy is observed, whilst the extent of neurodegeneration in the olivo-cerebellar pathway varies and involves inferior olivary, Purkinje cell and dentate nucleus neurons (Sparaco *et al.*, 1993; Tanahashi *et al.*, 2000; Lax *et al.*, 2012b). Preserved neurons

contain high percentage of mutant mtDNA species and have severely decreased respiratory chain protein expression (complex I and IV) (Lax *et al.*, 2012b; Chrysostomou *et al.*, 2015). Selective deficiency in mtDNA-encoded respiratory chain protein subunits (COXII and ATPase8) are documented in 2 patients harbouring the m.3243A>G point mutation (Sparaco *et al.*, 2003). Swollen Purkinje cell axons ("torpedoes") and thickened dendritic trees (cacti) are documented (Mori *et al.*, 2000; Tanahashi *et al.*, 2000; Betts *et al.*, 2006; Lax *et al.*, 2012b) and the latter is usually associated with increased mitochondrial density upon light (Lax *et al.*, 2012b) and electron (Tanahashi *et al.*, 2000) microscopic observations. Moreover, grumose degeneration around dentate nucleus neurons (Tanahashi *et al.*, 2000) and decreased synaptophysin immunoreactivity at the region (Lax *et al.*, 2012b) suggests altered synaptic input (probably inhibitory) to the dentate nucleus. Indeed, complex I protein expression defects detected in GABAergic presynaptic terminals contacting dentate nucleus neurons combined with inhibitory synapse loss denote aberrant inhibitory neurotransmission to the region (Chrysostomou *et al.*, 2015). Intracerebellar synaptic remodelling is proposed since enlarged residual inhibitory synapses may represent means to compensate for synaptic loss (Chrysostomou *et al.*, 2015).

Profound inhibitory interneuronal loss is documented in occipital, temporal and frontal cortices of four patients with MELAS, accompanied by severe complex I protein expression deficiencies and high heteroplasmic percentages (≥79%) in residual interneurons. This is in accordance with near homoplasmic (≥92%) mutation load percentages detected in various brain regions of an autopsy case (Betts *et al.*, 2006).

1.8.2 m.8344A>G

Selective neurodegeneration within the cerebellum, brain stem and spinal cord is characteristic of patients harbouring the m.8344A>G point mutation (Sparaco *et al.*, 1993). The cerebellar dentate nucleus neurons and Purkinje cells, the inferior olivary neurons within the brain stem and cells in Clarke's nucleus of the spinal cord are preferentially lost, whereas cytoplasmic eosinophilia, neuronal atrophy and astrocytic proliferation is apparent in affected areas (Sparaco *et al.*, 1993; Zhou *et al.*, 1997; Lax *et al.*, 2012b). Heteroplasmic levels for the m.8344A>G point mutation in individual neurons do not necessarily correlate with percentage cell loss (Zhou *et al.*, 1997; Lax *et al.*, 2012b) and axonal demyelination in cerebellar peduncles and posterior spinocerebellar tracts is likely consequent to neuronal/axonal degeneration (Sparaco *et al.*, 1993; Lax *et al.*, 2012b).

Preserved neurons have combined complex I and IV protein expression deficiencies (Lax *et al.*, 2012b), contrary to selective decrease in COXII protein expression in the frontal cortex, cerebellum and medulla documented during autopsy (Sparaco *et al.*, 1995). Abnormal intracerebellar microcircuitry is suggested following the documentation of structurally abnormal Purkinje cell axons (spheroids), degenerative Purkinje cell presynaptic terminals (grumose degeneration) and decreased synaptophysin immunoreactivity (mainly involving the dentate nucleus) (Sparaco *et al.*, 1993; Lax *et al.*, 2012b). This notion is strengthened by observations made by Chrysostomou and colleagues who report complex I deficiency in Purkinje cell presynaptic terminals, associated with inhibitory synapse loss from the dentate nucleus (Chrysostomou *et al.*, 2015).

Additional to neuronal populations, GABAergic interneuronal density is severely decreased in the occipital, temporal and frontal lobe (Lax *et al.*, 2015). Near homoplasmic percentages for the mutated mtDNA species is detected on homogenised tissue, whilst surviving interneurons have combined respiratory chain protein expression deficiencies involving complex I and IV (Lax *et al.*, 2015).

Necrotic foci detected in MERRF are accompanied by vascular proliferation, whilst respiratory chain deficiency, high heteroplasmy (≥86%) and cellular loss have been detected in cerebellar blood vessels (Lax *et al.*, 2012c). Moreover, Purkinje cell and dentate nucleus neurons immunoreactive against plasma proteins and decreased tight junction protein expression suggests BBB leakage (Lax *et al.*, 2012c).

1.8.3 MtDNA rearrangements and deletions

The most frequent neuropathological manifestation in patients with KSS is spongy degeneration in the cerebrum, cerebellum and spinal cord, although grey matter changes have been observed in the brain stem (Oldfors *et al.*, 1990; Sparaco *et al.*, 1993; Lax *et al.*, 2012b). Axonal demyelination is related to spongiform degeneration since its most frequently detected in cerebral and cerebellar white matter (Sparaco *et al.*, 1993). Lax and colleagues (2012) attribute demyelination to oligodendrocyte dysfunction since loss of myelin associated glycoprotein from the dentate nucleus is accompanied by high mtDNA deletion levels, glial depletion and respiratory chain protein expression deficiencies (Lax *et al.*, 2012a).

Extensive neurodegeneration and gliosis is detected in brain stem and the cerebellum, most commonly affecting the substantia nigra, the red, vestibular and oculomotor nuclei as well as cerebellar Purkinje cells and dentate nuclei neurons (Oldfors *et al.*, 1990; Sparaco *et al.*, 1993; Tanji *et al.*, 1999; Lax *et al.*, 2012b). Cactus-like Purkinje cell dendrites (Tanji *et al.*, 1999; Lax

et al., 2012b), axonal swellings (torpedoes) proximal and distal to Purkinje cell bodies (Lax *et al.*, 2012b) and decreased axonal density in the white matter (Tanji *et al.*, 1999) are reminiscent of neuronal structural disorganisation and likely altered intracerebellar signalling. Indeed, synaptophysin immunoreactivity to the dentate nucleus is scarce and Purkinje cell terminal arborisations are swollen (Tanji *et al.*, 1999). Structurally abnormal mitochondria (enlarged with disturbed cristae organisation) have been detected in the Purkinje cells of a single case (Adachi *et al.*, 1973), whereas residual Purkinje cell and dentate nuclei neurons have marked complex I and IV protein expression deficiencies (Lax *et al.*, 2012b).

GABAergic interneuron loss has recently been documented in the occipital and (to a lesser extent) temporal cortex of a KSS patient accompanied by severe complex I and IV protein expression deficiencies detected upon quadruple immunofluorescence (Lax *et al.*, 2015). COX-deficient interneurons and blood vessels in these regions have also been reported (Lax *et al.*, 2015).

Vascular proliferation is evident in various brain regions, whereas iron and calcium deposition is found within and around capillary and arterial walls (Sparaco *et al.*, 1993; Tanji *et al.*, 1999). Moreover, fibronectin extravasation in the cerebral cortex provides evidence towards BBB breakdown (Oldfors *et al.*, 1990), though no fibrinogen or IgG extravasation was detected by Lax and colleagues (Lax *et al.*, 2012c). Remarkably, decreased COX II immunoreactivity in the epithelial cells of the choroid plexus and high levels of deleted (Δ) mtDNA species implies that the threshold for impaired mtDNA translation has been exceeded (Tanji *et al.*, 2001).

1.8.4 Leber's hereditary optic neuropathy

Degeneration of the ganglion cell layer and optic nerve along with relative preservation of the rest of the retina constitutes the typical pathological finding in patients with LHON (Kwittken and Barest, 1958; de Gottrau *et al.*, 1992; Kerrison *et al.*, 1995; Sadun *et al.*, 2000). Marked axonal depletion in the optic nerve has been observed in association with demyelination of the spinal cord and peripheral nerves (Kwittken and Barest, 1958) and gliosis within the optic nerve (Kermode *et al.*, 1989; Smith *et al.*, 1990; Kerrison *et al.*, 1995) and spinal cord (Kwittken and Barest, 1958). Lateral geniculate body loss suggests for transneuronal degeneration (Kwittken and Barest, 1958), whereas calcium deposition is detected on preserved swollen retinal ganglion cells which contain swollen mitochondria (Kerrison *et al.*, 1995).

1.8.5 Mitochondrial disease associated with Polymerase γ mutations

Originally described by Cottrell and colleagues, neuropathological changes in a patient with multiple mtDNA deletions involved selective neuronal degeneration, axonal demyelination,

diffuse astrocytosis and a mosaic pattern of neuronal COX deficiency (Cottrell *et al.*, 2000). Astrogliosis was pronounced in superficial occipital cortex and hippocampal layers depleted of neurons (CA1-4), in the dorsal columns of the spinal cord and in the white matter of the cerebellum, basal ganglia, thalamus and hypothalamus. Extensive neurodegeneration is reported in pyramidal cell layers of the hippocampus (CA1-4), the substantia nigra of the midbrain, the inferior olivary nucleus of the medulla and the Purkinje cells and dentate nucleus of the cerebellum. Degenerative changes are also detected in the dorsal root and paraspinal sympathetic ganglia, whereas myelin pallor in the inferior olivary nucleus, the cerebellar white matter and the cervical spinal cord suggest axonal demyelination. Neuronal respiratory chain deficiency is detected throughout the brain, though variable, and does not necessarily correlate with the extent of neuropathological changes (Cottrell *et al.*, 2000).

Considerable substantia nigra neuronal loss has also been documented in association with Lewy body pathology, high mtDNA deletion levels, COX deficiency (Betts-Henderson *et al.*, 2009) and severely decreased complex I and IV protein expression in remaining neurons (Reeve *et al.*, 2013). Betts and colleagues further document gracile nucleus, Purkinje cell and dentate nucleus neurodegeneration and cervical spinal cord axonal demyelination in accordance with neuropathological features of mitochondrial disease (Betts-Henderson *et al.*, 2009).

Tzoulis and colleagues have described the neuropathological changes observed in patients with POLG-related encephalopathy (Alpers syndrome and spinocerebellar ataxia) (Tzoulis *et al.*, 2006; Tzoulis *et al.*, 2010; Tzoulis *et al.*, 2014). Cerebral cortical lesions detected upon neuroradiological examination were associated with extensive neurodegeneration, cortical vacuolation, astrocytic proliferation and microglia activation (Tzoulis *et al.*, 2010). Vacuolation and eosinophilic necrosis was also detected in the thalamus, where neuronal loss appeared more selective compared to the cortex. The cerebellar cortex (Purkinje cell layer) suffered neuronal loss, gliosis and eosinophilic necrosis, which was also detected in the dentate nucleus.

A sequential study performed by the same group reports the presence of acute focal lesions in the neocortex, hippocampus, thalamus and cerebellar cortex, all associated with selective neuronal loss, eosinophilic necrosis, neuropil vacuolation, astrocytosis and microglia activation (Tzoulis *et al.*, 2014). Stroke-like cortical lesions detected on MRI correlated with the lesions documented on post-mortem tissue. The thalamus, substantia nigra and dentate-olivary and dentatorubral systems suffered severe neuronal loss and gliosis, whereas more selective changes were observed in the spinal cord. Interestingly, complex I protein expression defects were more severe in regions with chronic changes and higher neuronal density (compared to

regions with acute focal lesions), where complex IV deficiency also occurred to a lesser extent. The most severe electron transport chain protein expression deficiencies were detected in the substantia nigra, red, olivary and pontine nuclei (Tzoulis *et al.*, 2014).

Similarly, Lax and co-workers report the presence of cerebellar microinfarcts and associated astrogliosis in patients with heterozygous *POLG* mutations (Lax *et al.*, 2012b). Marked neuronal loss in the dentate nucleus correlates with massive outflow tract demyelination, though neurodegeneration across the olivo-cerebellar pathway does not relate to the low heteroplasmic levels for mtDNA deletion detected (Lax *et al.*, 2012b). More recently, profound inhibitory interneuron loss has been detected in the occipital, temporal and frontal cortices with associated complex I and IV (to a lesser extent) protein expression deficiencies in preserved GABAergic interneurons (Lax *et al.*, 2015).

Neurophysiological examination of 11 patients with compound heterozygous changes in *POLG* confirmed sensory neuropathy (usually in association with motor neuropathy) due to dorsal root ganglion abnormalities. Neuropathological examination revealed extensive neurodegeneration in the dorsal root ganglia, axonal and myelin loss in posterior spinal funiculus. Mitochondrial density and complex IV protein expression was intact in posterior horn neurons of the spinal cord, whereas complex I protein expression was severely decreased. On the contrary, altered mitochondrial mass, defective oxidative metabolism (COX-deficiency), decreased respiratory chain protein expression and mtDNA deletion and depletion is documented in dorsal root ganglia (Lax *et al.*, 2012d).

1.9 Animal and cell culture models of mitochondrial disease

Examining human post-mortem brain tissue and characterising the biochemical defects and neuropathological features of patients with mitochondrial disease is important since it strengthens our understanding of the consequences of mitochondrial dysfunction in a biological system. However, this only provides the chance to document chronic, end-stage disease changes without providing any information as to the molecular pathways and mechanisms responsible for initiation and progression of the neurodegenerative process. Animal models and cell culture systems that successfully recapitulate the human disease are therefore an invaluable tool for exploring mechanisms of neurodegeneration and choosing appropriate drug targets.

Skin fibroblasts extracted from patients with mitochondrial disease are routinely employed in order to investigate the pathophysiological changes in different tissues as a consequence of disease. Fibroblast reprogramming, into induced pluripotent stem cells (iPSCs), may alter the heteroplasmic levels for any given mtDNA mutation (Hamalainen *et al.*, 2013; Kodaira *et al.*,

2015) however it provides the opportunity to model specific mitochondrial disorders (Kodaira *et al.*, 2015) and screen potential therapeutic compounds (Breuer *et al.*, 2013). High mutation load for the m.3243A>G point mutation in iPSCs (Kodaira *et al.*, 2015), differentiated neurons and teratomas (Hamalainen *et al.*, 2013) was demonstrated to selectively impair complex I activity, in accordance with observations in tissue from MELAS patients. Interestingly, complex I-positive mitochondria were clustered around neuronal cell bodies and were eliminated by mitophagy with time (Hamalainen *et al.*, 2013). Likewise, aberrant complex I activity was detected in fibroblasts extracted from patients with Leigh syndrome, due to *Ndufs4* mutations, accompanied by complex III deficiencies and subassembled complex I and IV units (Scacco *et al.*, 2003; Ugalde *et al.*, 2004a). Moreover, altered mitochondrial morphology, membrane potential, calcium signalling and ROS production levels demonstrate organellar vulnerability to damaging factors (Valsecchi *et al.*, 2013).

Further to neurons differentiated from patient iPSCs, mouse embryonic stem cells engineered to express pathogenic mtDNA mutations were exploited in order to establish the impact of mitochondrial dysfunction on neuronal morphology and health (Kirby *et al.*, 2009; Abramov *et al.*, 2010; Trevelyan *et al.*, 2010). *Trans*-mitochondrial cybrids with severe complex I (~10% residual activity) and mild complex IV (40% residual activity) defects were able to successfully differentiate into neurons and form functional synaptic connections (Kirby *et al.*, 2009). However, cybrids harbouring severe respiratory chain defects had decreased neuronal differentiation capacity (Kirby *et al.*, 2009) and increased membrane potential upon neuronal maturation (Abramov *et al.*, 2010). Increased ROS production rate (Abramov *et al.*, 2010) and altered Ca^{2+} handling following repetitive stimulation (Trevelyan *et al.*, 2010) in both neuronal cell lines suggests that more than one mechanisms are likely to collectively contribute to neurodegeneration observed in patients with mitochondrial disease.

An ever-increasing number of mouse models have been developed in an attempt to mimic mitochondrial disease, both in terms of pathophysiology and neuropathology. Pioneering work from Sligh (2000) and Inoue (2000) involved the introduction of pathogenic mtDNA molecules into embryonic stem cells (Sligh *et al.*, 2000) or fertilised embryos (Inoue *et al.*, 2000), achieving the transmission of pathogenic mutations (Sligh *et al.*, 2000) and deletions (Inoue *et al.*, 2000) into successive generations. A similar approach to directly manipulate mtDNA involved the introduction of severe complex I (*MT-ND6*) and mild complex IV (*MT-COXI*) mutations into the female germline, though severe defects were selected against during oogenesis (Fan *et al.*, 2008).

Alternatively, manipulation of nuclear DNA-encoded genes involved in mtDNA maintenance has proved to be an effective method for altering mtDNA integrity. Examples include the "deletor" and the "mutator" mouse due to mutations in *Twinkle* (Tyynismaa *et al.*, 2005) and *POLG* (Trifunovic *et al.*, 2004) respectively. Accumulation of multiple mtDNA deletions in the deletor mouse induces the muscle features of patients with PEO. Respiratory chain deficiency has mainly been detected in muscle and hippocampus, though low percentage of COX-deficient neurons exists in the cerebellum, olfactory bulbs, substantia nigra and hypothalamus (Tyynismaa *et al.*, 2005). In contrast, the mutator mouse demonstrates an accelerated ageing phenotype with weight and hair loss, kyphosis, osteoporosis, anaemia, reduced fertility and cardiomegaly (Trifunovic *et al.*, 2004). Accumulation of mtDNA mutations with time results in extensive respiratory chain deficiencies without elevated ROS production (Trifunovic *et al.*, 2005).

Recent technologies allow inactivation of genes in selective tissues or cell types providing the opportunity to replicate the features of specific mitochondrial disorders. Such an example is the inactivation of *Ndufs4* from Purkinje cells and glia in an effort to simulate Leigh syndrome (Quintana *et al.*, 2010). Spongiform degeneration, astrogliosis and vascular proliferation in the cerebellum constitute the main neuropathological findings, accompanied by abnormal mitochondrial structure within presynaptic terminals contacting Purkinje cell bodies (Quintana *et al.*, 2010). Phenotypic manifestations of these mice recapitulate those of Leigh syndrome including ataxia, failure to thrive, motor dysfunction and premature death (Quintana *et al.*, 2010). However, no basal ganglion pathology is detected, contrary to observations in patients with the disease, highlighting the need for interpreting the results with caution.

1.10 Aims and Objectives

How do synapses and microvessels contribute to neurodegeneration due to mitochondrial disease?

Cerebellar ataxia is the most common neurological deficit of patients with mitochondrial disease. Neuropathological observations include pronounced neuronal degeneration, documented in association with synaptic disturbances and likely consequent altered intracerebellar circuitry. The relatively simple and well-studied cerebellar microcircuitry will be used in this thesis to answer the following questions:

- Is synaptic pathology a primary event in neurodegeneration or consequent to the degenerative process?
- Is there any evidence for structural synaptic abnormalities and/or respiratory chain deficiency in Purkinje cell presynaptic terminals contacting dentate nucleus neurons?
- How do presynaptic abnormalities relate to postsynaptic neuronal deficiency and loss?

Extensive neurodegeneration and pan-necrotic foci are also detected in association with stroke-like cortical lesions. These are prominent but not restricted to patients with MELAS syndrome. The brain microvasculature will be examined in this thesis to answer the following questions:

- Is there any evidence of respiratory chain protein expression deficiency in arterioles and capillaries of posterior cortical regions?
- How do neuropathological observations relate to clinical and neuroradiological data for these patients?

Chapter 2

Chapter 2 Materials and methods

2.1 Equipment and consumables

2.1.1 Equipment

2100 Antigen Retriever	Aptum Biologics
3510 benchtop pH meter	Jenway
AxioCam ICc1	Carl Zeiss microscopy
AxioCam MRc	Carl Zeiss microscopy
AxioCam MRm	Carl Zeiss microscopy
ChemiDoc™ Imaging System	Bio-Rad
Eppendorf Centrifuge 5418	Eppendorf
Veriti® 96-Well Thermal Cycler	Life Technologies
Horizontal gel electrophoresis tank	Peqlab
IKA Magnetic stirrer hotplate RCT basic	Fisher Scientific
MP-250V power supply	Cleaver Scientific
OHAUS adventurer® balance	OHAUS
Nikon A1R scanning confocal system	Nikon
Olympus microscope BHX54	Olympus
PALM MicroBeam Observer 21	Carl Zeiss microscopy
Pyromark Q24 workstation	Qiagen
Zeiss Axio Imager M1	Carl Zeiss microscopy

2.1.2 Software

ZEN imaging software	Carl Zeiss microscopy
Volocity® 3D image analysis and deconvolution software (v.6.1)	PerkinElmer
IMARIS scientific 3D/4D Image processing & analysis software	Bitplane
ImageLab software (v.4.1)	Bio-Rad

PALM RoboSoftware	Carl Zeiss microscopy
StereoInvestigator software	MBF Bioscience

2.1.3 Consumables

0.2ml Thin-Walled PCR Tubes	Thermo Scientific
0.5ml PCR Tubes	Thermo Scientific
1.5ml Eppendorf Tubes	Thermo Scientific
2ml Eppendorf tubes	Biogene
96-well plate Semi-Skirted with Raised Rim	Starlabs
AdhesiveCap 200 clear (D) PCR Tubes (0.2ml)	Zeiss
Aerosol resistant Pipette tips	Starlabs
Coverslips (22x20, 22x32mm, 22x40mm, 22x50mm)	VWR International
Charged adhesion slides (26x76x1.0-1.2mm)	CellPath
ErgoOne® Single-channel Pipettes (P1000, P200, P20, P10)	Starlabs
Gel extraction Kit	Qiagen
HiQA Mega converslips (37x58mm)	CellPath
HiQA Supa Mega coverslips (50x64mm)	CellPath
HISTOBOND® + supa mega slides (75.2 x 50.4 x 1mm)	CellPath
ProLong® Gold Antifade Mountant	Life Technologies
PyroMark Gold Q24 Reagents	Qiagen
SuperFrost™ Plus Adhesion slides (38x75x1mm)	ThermoScientific

2.2 Solutions and chemicals

2.2.1 Solutions

Solutions and buffers were prepared in Nanopure (18 Mega Ohms activity) water and subsequently autoclaved.

1% Acid-alcohol solution	500ml Ethanol 5ml HCL
3% Hydrogen Peroxide	485ml dH2O 15ml Hydrogen peroxide
3% Sudan Black B	0.3g of Sudan black B 100ml of 70% ethanol
Acetate Buffer pH 4.5	13.5ml Acetic acid 23.5g Sodium acetate 2L dH2O
Cresyl fast violet (CFV) staining solution	500ml Acetate Buffer pH 4.5 500ml dH2O 50ml CFV
DNA Loading Buffer	0.25% (w/v) Bromophenol Blue 0.25% (w/v) Xylene Cyanol 30% (v/v) Glycerol
Electrophoresis Buffer (1l)	100ml 10x TAE 900ml Nanopure water
50µl 0.5M TrisHCL pH 8.5	30.275g Trisma base 500ml dH2O
Scott's tab water	2g Sodium bicarbonate 20g Magnesium sulphate 1L tap water
Single cell Lysis Buffer (500µl)	250µl 1% Tween 20 50µl 0.5M TrisHCL pH 8.5 195µl dH2O 5µl proteinase K

Phosphate Buffered Saline pH 7.4	0.276g $NaH_2PO_4*H_2O$
	1.136g Na_2HPO_4
	8.5g NaCl
	1L dH2O
Tris-Buffered Saline pH7.4	1.2g Trisma base
	17g NaCl
	2L dH20
Tris-Buffered Saline – Tween pH7.4	1.2g Trisma base
	17g NaCl
	2L dH20
	1ml Tween 20
10mM Tri-sodium citrate pH6.0	2.941g tri-sodium citrate
	1L dH20
1mM EDTA pH8	0.416g EDTA
	1L dH20

2.2.2 Chemicals

2.2.2.1 Antibodies

Anti-Synaptophysin	DAKO
Anti-GAD65/67	Sigma-Aldrich
Anti-Gephyrin	BD Biosciences
Anti-Calbindin	Swant
Anti-pan-AMPA	Millipore
Anti-VGLUT1	NeuroMab
Anti-GLUT1	Thermo Scientific
Anti-α-SMA	Abcam

Anti-VDAC1	Abcam
Anti-NDUFB8	Abcam
Anti-NDUFA13	Abcam
Anti-COX I	Abcam
Anti-COX IV	Abcam
Alexa Fluor®405	Life technologies
Alexa Fluor®488	Life technologies
Alexa Fluor®546	Life technologies
Alexa Fluor®647	Life technologies
Biotin-XX	Life technologies
Streptavidin, Alexa Fluor® 647 conjugate	Life technologies
Biotin-SP	Jackson ImmunoResearch
Rhodamine Red™-X	Jackson ImmunoResearch

2.2.2.2 Histological reagents

Acetic acid	VWR
Anti-Mouse/Rabbit PolyVue HRP Labe	Diagnostic BioSystems
Cresyl violet acetate	Sigma
3, 3’ Diaminobenzidine Tetrahydrochloride	Sigma
Di-Sodium hydrogen orthophosphate anhydrous	VWR
DPX™	Merck
Ethanol	Fischer Scientific
Ethylenediaminetetraacetic Acid, Disodium Salt, Dihydrate	Affymetrix
Histoclear™	National Diagnostics
30% w/v Hydrogen Peroxide	Sigma
Mayers Haematoxylin	TCS Biosciences Ltd

Normal goat serum	Sigma
Paraformaldehyde solution 4% in PBS	Santa Cruz Biotechnology
Polymer Penetration Enhancer	Diagnostic BioSystems
Sodium acetate	VWR
Sodium chloride	Sigma
Sodium dihydrogen orthophosphate 1-hydrate	VWR
Sudan Black B (Noir Soudan)	RAL diagnostics
Tri-sodium citrate	VWR
Trizma base	Sigma
Tween 20	Sigma

2.2.2.3 Molecular Biology reagents

Agarose MP	Roche
AmpliTaq GOLD® DNA polymerase	Life Technologies
10X AmpliTaq Gold® PCR Buffer	Life Technologies
Buffer QX1	Qiagen
Buffer PE	Qiagen
Deoxynucleotide Triphosphates	Rovalab
Diethylpyrocarbonate (DEPC) -treated water	Life Technologies
GelRed nucleic acid stain	Biotium
GO Taq Hot Start DNA Polymerase	Promega
Hyperladder IV	Bioline
La Taq DNA polymerase	Takara
Proteinase K	Invitrogen
PyroMark Annealing buffer	Qiagen
PyroMark Binding buffer	Qiagen

PyroMark Gold Q24 Reagents (5 x 24)	Qiagen
PyroMark Wash buffer (x10)	Qiagen
Quick-load 1kb DNA ladder	BioLabs
Streptavidin sepharoseTM high performance beads	GE Healthcare
Tris-HCl	Sigma

2.3 Central nervous system samples

2.3.1 Patient cohort

Central nervous system (CNS) tissue from thirteen adult patients was obtained from the Newcastle Brain Tissue Resource (NBTR). All patients included in this study were clinically and genetically diagnosed with mitochondrial disease and received regular clinical assessments using the validated Newcastle Mitochondrial Disease Adult rating Scale (NMDAS) (Schaefer *et al.*, 2006). Patients and their families provided informed consent to donate their tissue for research purposes and ethical approval for this study was gained from Newcastle and North Tyneside Local Research Ethics Committee (LREC 2002/205). A summary of the clinical, genetic and neuropathological details of patients is provided in Table 2- 1 (patient numbering is the same throughtout the thesis for consistency).

Upon patient death, NBTR pathologists remove the whole brain for dissection. Half of the cerebral hemisphere (left hemisphere) is snap frozen and stored at -80^{o}C for molecular genetic investigation, whilst the other half (right hemisphere) is fixed in 10% formalin and embedded in paraffin wax.

Frozen tissue was cut at 15µm-thick sections using a cryostat (-12^{o}C) and mounted on SuperFrost glass slides. Frozen sections were left to air dry before stored at -80^{o}C until required. Formalin–fixed Paraffin-Embedded (FFPE) tissue was cut using a microtome at either 20µm or 5µm-thick sections and mounted on SuperFrost glass slides. Fixed tissue was then incubated at 37^{o}C for 3-5 days in order to ensure tissue adhesion onto the slide and was then stored at 4^{o}C until required.

2.3.2 Control tissue

To determine the extent of neuropathological changes in patients with mitochondrial disease, neurologically normal age-matched controls are used. Frozen control tissue was obtained from the NBTR, whereas FFPE brain sections were obtained from the NBTR and the MRC Sudden Death Brain and Tissue Bank, Edinburgh. The neuropathological details of controls are summarised in Table 2- 2.

	Pt1	Pt2	Pt3	Pt4	Pt5	Pt6	Pt7	Pt8	Pt9	Pt10	Pt11	Pt12	Pt13
Age	36	60	30	45	20	57	42	58	59	79	55	24	55
Gender	Female	Female	Male	Male	Female	Female	Female	Male	Male	Male	Male	Female	Male
Genotype	m.3243A>G	m.3243A>G	m.3243A>G	m.3243A>G	m.3243A>G	m.3243A>G	m.8344A>G	m.8344A>G	POLG (p.Gly848Ser and p.Ser1104Cys)	POLG (p.Thr251Ile/p.Pro587Leu; p.Ala467Thr)	POLG (p.Trp748Ser and p.Arg1096Cys)	POLG (p.Ala467Thr and p.Trp748Ser)	m.14709T>C
Disease duration (years)	15	33	11	ND	10	32	37	23	37	23	50	4	21
Fixation length (weeks)	1	6	10	8	6	50	8	6	4	8	7	18	17
Post-mortem Interval (hours)	42	10	69	43	187	36	59	66	67	85	112	83	10
Neurological manifestations													
Cerebellar ataxia	+	+	+	+	+	+	+	+	+	+	+	+	+
Stroke-like episodes	+	+	-	+	+	+	-	+	-	-	-	+	-
Epilepsy	+	+	-	+	+	-	+	+	-	-	+	+	-

Table 2- 1: Summary of the clinical, genetic and neuropathological details of patients included in this study.

Type	Age (years)	Sex	Length of fixation (weeks)	Post-mortem delay (hours)	Cause of death	Source
Control 1	69	Female	6	16	Gastric cancer	NBTR
Control 2	68	Male	8	54	Bowel cancer	NBTR
Control 3	78	Female	5	23	metastatic oesophageal carcinoma	NBTR
Control 4	74	Female	13	67	Lung cancer	NBTR
Control 5	55	Male	14	41	Liver cancer	NBTR
Control 6	74	Female	9	53	Heart failure and lung cancer	NBTR
Control 7	70	Male	11	72	Metastatic prostate cancer	NBTR
Control 8	73	Male	7	25	ND[1]	NBTR
Control 9	78	Female	8	34	Metastatic cancer - primary origin unknown (probably ovarian)	NBTR
Control 10	45	Male	13	13	ND	NBTR
Control 11	48	Male	1	72	Coronary artery atherosclerosis	Edinburgh
Control 12	48	Male	1	46	Coronary artery atherosclerosis	Edinburgh
Control 13	61	Male	1	61	ND	Edinburgh
Control 14	48	Male	1	43	Coronary artery thrombosis and atherosclerosis	Edinburgh
Control 15	25	Male	1	53	ND	Edinburgh
Control 16	44	Male	1	83	Complications of bronchopneumonia and coronary artery atherosclerosis	Edinburgh
Control 17	43	Male	1	96	Coronary artery thrombosis and atherosclerosis	Edinburgh
Control 18	74	Female	1	41	Pulmonary thromboembolism	Edinburgh
Control 19	70	Male	1	ND	Hypertensive and ischaemic heart disease, Type 2 diabetes and Fatty degeneration of the liver	Edinburgh
Control 20	52	Male	1	52	Ischaemic heart disease, Coronary artery atherosclerosis and Type 2 Diabetes Mellitus	Edinburgh
Control 21	71	Female	1	41	Ischaemic and hypertensive heart disease	Edinburgh
Control 22	75	Male	1	78	Ischaemic heart disease and Coronary artery atherosclerosis	Edinburgh
Control 23	51	Male	1	71	Ischaemic heart disease and Coronary artery atherosclerosis	Edinburgh
Control 24	41	Female	1	50	Unascertained	Edinburgh
Control 25	33	Male	1	47	Ischaemic heart disease and Coronary artery atherosclerosis	Edinburgh
Control 26	68	Male	1	96	Complications of familial amyloid polyneuropathy	Edinburgh

Table 2- 2: Neuropathological details of controls included in this study

[1] ND – not determined

2.4 Two-dimensional neuronal density

In order to assess the degree of neuronal loss in the cerebellum of patients with mitochondrial disease, 20µm-thick FFPE sections from patients and controls were subjected to a two-dimensional neuronal density protocol previously described (Lax *et al.*, 2012). In summary:

2.4.1 Cresyl Fast Violet (CFV) stain

Dewaxed and rehydrated sections (see section 2.6) were fixed in 1% acid alcohol solution for 5 minutes and rinsed 3-4 times in distilled water. Following this, sections were incubated in pre-warmed CFV staining solution for 10-15 minutes at 60ºC and were then left to cool for 5 minutes at room temperature in staining solution. A final wash in distilled water for 1 minute was followed by dehydration in a graded ethanol series (70%, 95% and 100%) and mounting on DPX™ (Merck).

2.4.2 Quantification of Purkinje cell and dentate nucleus neuronal populations

For Purkinje cell neuronal count, the cerebellar cortex was identified at x10 magnification and the boundaries of the Purkinje cell layer were outlined to give distinct lobular areas (Figure 2-1) using the closed contour function of the StereoInvestigator software. Cells with a visible nucleolus and a clear cytoplasm were counted in each lobular area at x40 magnification using the Meander scan. Purkinje cell density for each lobule was deviated after dividing the number of identified neurons by the lobule's area (number of neurons per mm^2 lobular area) and overall Pukrinje cell density was evaluated after pooling together the data for each lobule.

Similarly, the dentate nucleus (DN) grey matter ribbon was identified at x2.5 magnification and was divided into quadrants according to Su and colleagues (Su *et al*., 2000) (Figure 2- 1). Cells that fulfilled the criteria of a visible nucleolus and a clear cytoplasm were counted for each quadrant at x100 magnification using the Meander scan. Dentate nucleus neuronal cell densities for each quadrant were calculated after dividing the number of identified neurons by the quandrant's area (number of neurons per mm^2 quadrant area), whereas the overall dentate nucleus neuronal cell density deviated after combing the data for each quadrant.

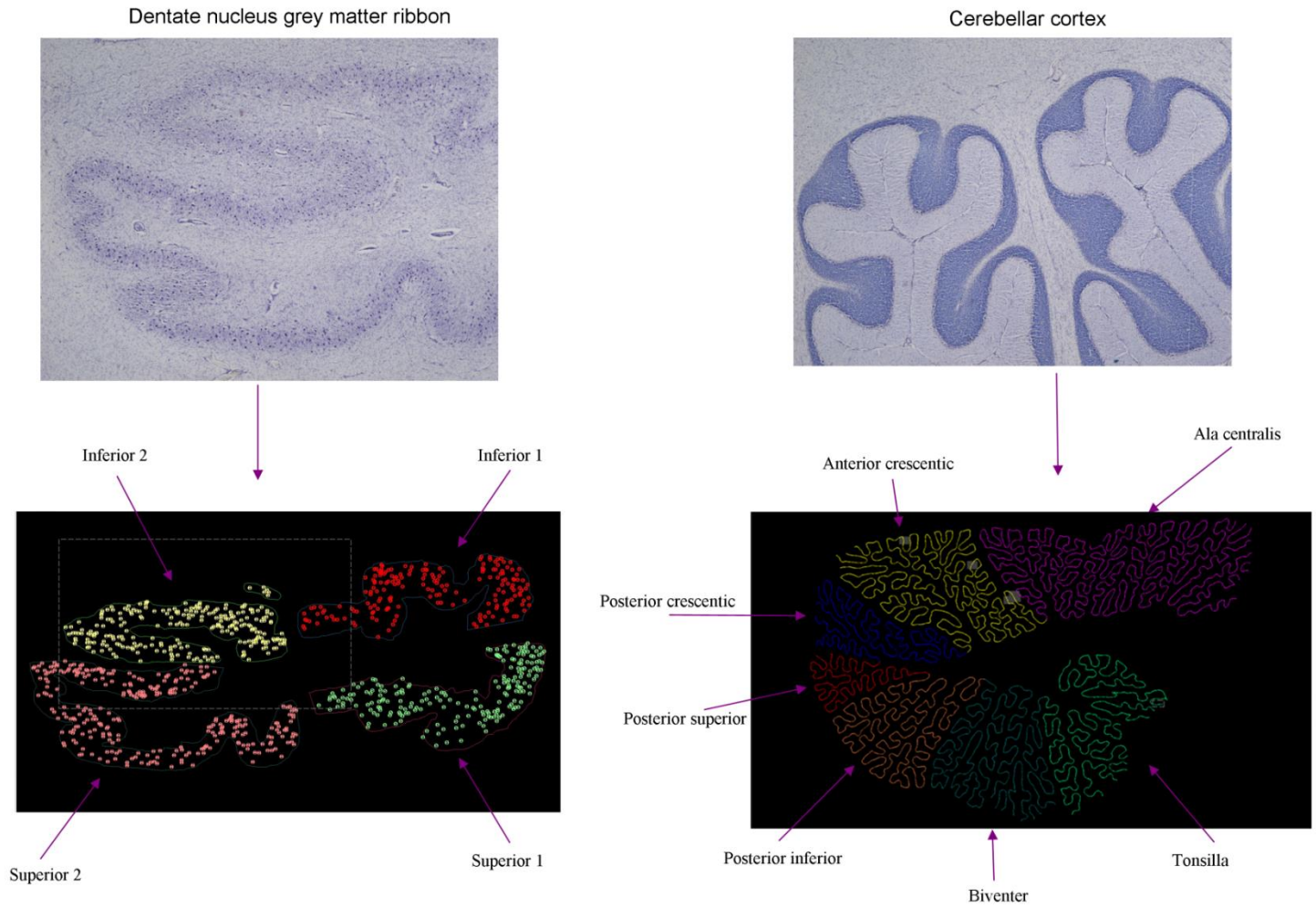

Figure 2- 1: Dentate nucleus and cerebellar cortex division.

The dentate nucleus was divided into distinct quadrants and the cerebellar cortex into the different lobular areas, within which neuronal density counts were performed.

2.5 Dual cytochrome *c* oxidase (COX)/ Succinate dehydrogenase (SDH) stain

Frozen brain tissue sections mounted on SuperFrost glass slides (15µm thick) were left to air-dry for one hour before being subjected to a dual COX/SDH histochemical protocol. COX medium was prepared by adding 200µl of cytochrome *c* stock solution (500µM cytochrome *c* in 0.2M phosphate buffer, pH 7.0) to 800µl of 3,3'diaminobenzidine tetrahydrochloride (DAB) stock solution (5mM DAB in 0.2M phosphate buffer, pH 7.0) with 20µg.ml-1 catalase. Each section was incubated with 200µl of the COX solution for 50 minutes at 37ºC. Following incubation, sections were washed in phosphate-buffered saline (PBS) (3x5 minutes). SDH medium was prepared by adding 800µl NitroBlue tetrazolium (NBT) stock solution (1.5mM NBT in 0.2M phosphate buffer pH 7.0) to 100µl sodium succinate stock solution (1.3M sodium succinate in 0.2M phosphate buffer pH 7.0), 100µl phenazine methosulphate (PMS) stock solution (2mM PMS in 0.2M phosphate buffer pH 7.0) and 10µl sodium azide stock solution (100mM sodium azide in 0.2M phosphate buffer pH 7.0). Sections were incubated with the SDH solution (200µl on each section) for 45 minutes at 37ºC. Tissue sections were washed in PBS (3x5 minutes), dehydrated through graded ethanol series (70%, 95% and 2x 100%), cleared in two changes of Histoclear™ (National Diagnostics, Charlotte, NC) and mounted in DPX™ (Merck).

2.6 Immunohistochemical staining

FFPE (5µm) cerebellar tissue sections mounted on SuperFrost glass slides were dewaxed by placing in a 60ºC oven for 20 minutes and rehydrated by immersion in Histoclear™ (x2) (National Diagnostics, Charlotte, NC) and graded ethanol series (2x100%, 95% and 70%) for 5 minutes. Following a thorough wash under distilled water, heat mediated antigen retrieval was performed. This involved immersing the sections in 1mmol Ethylenediaminetetraacetic Acid (EDTA) (pH 8.0) and pressure cooking for 40 minutes or microwaving in boiling Tri-sodium citrate (10mM; pH 6.0) for 10 minutes and cooling, depending on the antibody used. Endogenous peroxidase activity was blocked by incubating in 3% Hydrogen peroxide (Sigma) solution for 30 minutes at room temperature (RT). Sections were washed (3x5 minutes) with tris-Buffered saline-Tween (TBST) followed by incubation in the appropriate primary antibody dilution (Table 2- 3) for 1 hour at RT. The sections were washed with TBST (3x5 minutes) and a Polymer Penetration Enhancer (Diagnostic BioSystems) was applied for 30 minutes, followed by further washes (TBST; 3x5 minutes) and incubation with an Anti-Mouse/Rabbit PolyVue horseradish peroxidase (HRP) (Diagnostic BioSystems) for 30 minutes, all at RT. Antibody binding to the epitope of interest was detected after incubation with 3, 3'-diaminobenzidine (DAB) (Sigma-Aldrich) for 5 minutes at RT. Sections were then washed in running water and

counterstained with Mayer's haematoxylin for 10 minutes. "Blueing" of the nuclei was achieved after incubating in Scott's tab water for 1 minute and dehydration was achieved by immersing the sections in 70%, 95%, 2x100% ethanol and 2x Histoclear™ (National Diagnostics, Charlotte, NC) for 5 minutes. Finally, coverslips are mounted on to tissue sections using DPX™ (Merck).

2.7 Immunofluorescent staining

2.7.1 FFPE tissue

Using a microtome 5µm-thick FFPE CNS tissue sections were mounted on SuperFrost glass slides and subjected to immunofluorescent staining to allow for co-localisation studies. Sections were dewaxed by placing in a 60ºC oven for 20 minutes and rehydrated by immersion in Histoclear (National Diagnostics, Charlotte, NC) and graded ethanol series (100% to 70%). Antigen retrieval was performed using the 2100 retriever unit (Electron Microscopy Sciences©, Hatfield) by immersing sections in 1mmol EDTA (pH 8) and pressure cooking for 40 minutes. Sections were blocked in 1 or 10% normal goat serum (NGS) (Sigma) (depending on the antibody used) for 1 hour at RT and incubated in primary antibodies (Table 2- 3) at the optimal dilution overnight at 4ºC. Mouse monoclonal and rabbit polyclonal primary antibodies were applied to the sections at the appropriate dilution and for the appropriate time depending on the experimental protocol (details of these are given in Chapter 3 of this thesis). Following incubation with primary antibodies, sections were washed with 10mM PBS (3x5 minutes) and subjected to incubation with a biotinylated secondary antibody (when necessary). Quadruple immunofluorescent labelling involved tissue incubation with secondary anti-mouse, anti-rabbit or streptavidin-conjugated antibodies coupled with Alexa Fluor 405, 488, 546 and 647 (Life Technologies). The signal-to-noise ratio was increased by quenching autofluorescence with 3% Sudan Black b solution for 10 minutes. Sections were then washed in distilled water and mounted in Prolong Gold (Life Technologies). All the primary and secondary antibodies used for this study are listed in Table 2- 3.

Immunofluorescence was performed on positive controls (all antibodies), no-primary-antibody (NPA) and no-secondary-antibody (NSA) controls for each of the four fluorophores to allow background correction and cross-reactivity checks respectively. All patient and control samples were stained under the same conditions and slides were kept at -20C until required.

2.7.2 Frozen tissue

Frozen cerebellar tissue sections (15μm) were air-dried for 1.5 hours at RT before being fixed in 4% Paraformaldehyde (PFA) (Santa Cruz Biotechnology) for 10 minutes. Washes with 10mM Tris-buffered saline (TBS) (2x2 minutes and 1x10 minutes) were followed by section blocking with 10% NGS for 30 minutes at RT and primary antibody incubation overnight at 4^{o}C (Table 2- 3). Following TBS washes (3x5 minutes) a biotinylated secondary antibody (Table 2- 3) was applied for 30 minutes at RT. Double immunofluorescence was achieved after incubating the sections with secondary streptavidin-conjugated and anti-goat antibodies coupled with Rhodamine Red-X and Alexa Fluor 488 respectively (Table 2- 3) for 2 hours at 4^{o}C. Tissue auto-fluorescence was blocked by incubating with 3% Sudan Black b solution for 3 minutes.

Immunohistochemistry					
Primary antibody	**Epitope**	**Host and isotype**	**Source**	**Catalog No.**	**Antigen retrieval**
Synaptophysin	presynaptic vesicles	Mouse monoclonal - IgG1	DAKO	M0776	Microwaving in Tri-sodium citrate (10mM) pH6 for 10 minutes
Glutamic acid decarboxylase 65/67	GABAergic neurons - GAD67 and Inhibitory axonal terminals - GAD 65	Rabbit polyclonal - IgG	Sigma-Aldrich	G5163	Microwaving in Tri-sodium citrate (100mM) pH6 for 10 minutes
Immunofluorescence					
Primary antibody	**Epitope**	**Host and isotype**	**Source**	**Catalog No.**	**Antigen retrieval**
Synaptophysin (SY-38)*	presynaptic vesicles	Mouse monoclonal - IgG1	DAKO	M0776	EDTA (1mM); 2100 antigen retriever
Glutamic acid decarboxylase 65/67 (GAD 65/67)*	GABAergic neurons (GAD67) and inhibitory axonal terminals (GAD 65)	Rabbit polyclonal - IgG	Sigma-Aldrich	G5163	EDTA (1mM); 2100 antigen retriever
Gephyrin	Inhibitory postsynaptic compartments	Mouse monoclonal - IgG1	BD Biosciences	610585	EDTA (1mM); 2100 antigen retriever
Calbindin D-28k	Calcium binding protein; Calbindin-expressing neurons	Mouse monoclonal - IgG1	Swant	CB300	EDTA (1mM); 2100 antigen retriever
Glucose transporter 1 (GLUT-1)	Endothelial cell layer	Rabbit polyclonal - IgG	Thermo Scientific	PA1-21041	EDTA (1mM); 2100 antigen retriever
Alpha- Smooth muscle actin (SMA)	Smooth muscle layer	Rabbit polyclonal - IgG	Abcam	ab5694	EDTA (1mM); 2100 antigen retriever
Complex I subunit NDUFA13	NDUFA13	Mouse monoclonal - IgG2b	Abcam	ab110240	EDTA (1mM); 2100 antigen retriever
Complex I subunit NDUFB8	NDUFB8	Mouse monoclonal - IgG1	Abcam	ab110242	EDTA (1mM); 2100 antigen retriever
Complex IV subunit IV	COX4+COX4L2	Mouse monoclonal - IgG2a	Abcam	ab110261	EDTA (1mM); 2100 antigen retriever
Complex IV subunit I	COX1	Mouse monoclonal - IgG2a	Abcam	ab14705	EDTA (1mM); 2100 antigen retriever
Voltage-dependent anion channel 1 (VDAC1)	Outer mitochondrial membrane protein (VDAC1/porin)	Mouse monoclonal - IgG2b	Abcam	ab14734	EDTA (1mM); 2100 antigen retriever
Vesicular glutamate transporter 1 (VGLUT1)	Neurotransmitter transporter	Mouse monoclonal – IgG1	NeuroMab	73-066	EDTA (1mM); 2100 antigen retriever
Pan-AMPA receptor (GluR1-4)	Glutamate receptors	Mouse monoclonal – $IgG2b_k$	Millipore	MABN832	EDTA (1mM); 2100 antigen retriever

Secondary antibody	Target	Host	Source	Catalog No.	Antigen retrieval
Biotin-XX*	Mouse IgG1 (γ1)	Goat	Life technologies	A10519	N/A
Biotin-SP	Mouse IgG1 (γ1)	Goat	Jackson ImmunoResearch	115-065-205	N/A
HRP-conjugated	Mouse IgG1 (γ1)	Goat	Life technologies	A10551	N/A
Alexa Fluor® 647 Tyramide	HRP	N/A	Life technologies	T2095	N/A
Streptavidin, Alexa Fluor® 647 Conjugate	Biotin	N/A	Life technologies	S32357	N/A
Alexa Fluor® 405	Rabbit IgG (H+L)	Goat	Life technologies	A31556	N/A
Alexa Fluor® 488	Mouse IgG2b (γ2b)	Goat	Life technologies	A2114	N/A
Alexa Fluor® 488*	Rabbit IgG (H+L)	Goat	Life technologies	A11008	N/A
Alexa Fluor® 488	Mouse IgG2a (γ2a)	Goat	Life technologies	A21131	N/A
Alexa Fluor® 546	Mouse IgG2a (γ2a)	Goat	Life technologies	A21133	N/A
Alexa Fluor® 546	Mouse IgG2b (γ2b)	Goat	Life technologies	A21143	N/A
Rhodamine Red™-XD26:I34 (RRX) Streptavidin*	Biotin	N/A	Jackson ImmunoResearch	016-290-084	N/A

Table 2- 3: Primary and secondary antibodies used in this study.

* Indicates antibodies used for frozen tissue immunofluorescence.

2.8 Microscopic and image analysis techniques

2.8.1 Point-scanning confocal microscopy

Immunofluorescently stained FFPE brain sections from patients and controls were imaged using an A1R confocal system (Nikon). The system is equipped with a fully motorised inverted point scanning confocal microscope (Nikon), four spectrally unmixed lasers (405nm, 488nm, 561nm and 647nm), six different objectives (air or oil) and the NIS-Elements software (v4.2) (Nikon). Specific neuronal and sub-neuronal compartments and vascular cell populations were easily detected using an immersion oil x60 objective with numerical aperture 1.4 and working distance 0.13cm. Regions of interest were identified, a Step-by-step Nikon A1 Piezo Z scanner and Nikon TI-S-EJOY (Nikon) defined the z dimensions (top and bottom limits) of each region on the software surface. The depth of the tissue was then automatically calculated and the appropriate number of z stacks was captured at x180 magnification (x60 objective and x3 electronic zoom) according to the recommended microscope settings: Pixel size: 0.14μm, z-step size: 0.175μm, optical resolution: 0.13μm and optical sectioning 0.54μm. The resonant scanning mode was chosen that facilitated fast scanning at high resolution (512x512 frames).

Laser settings for each experiment were chosen by adjusting the photomultiplier tube gain (HV), laser power and offset functions on the software work surface. Tissue from neurologically normal controls was chosen for setting up the lasers, making sure that the intensity profiles for each channel would fall within the normal range (avoiding under- or over-exposure of samples). All the patient and control samples were imaged under the same laser settings; while laser stability and day-to-day variation was tested using FocalCheck™ Fluorescence Microscope Test slides (Molecular Probes™, Invitrogen).

2.8.2 Three-dimensional analysis software

Z stacking and confocal microscopy produced three-dimensional (3D) images (sampled on x-y- and z-planes) and enabled the investigation of respiratory chain protein expression within fine structures, for example, synapses. Two three-dimensional software packages were used throughout the study, each with certain advantages over the other. Volocity® 3D image analysis and deconvolution software (v.6.1.1, PerkinElmer) was used for image deconvolution and generation of protocols that allowed for respiratory chain protein expression quantification in neuronal cell bodies, dendrites, presynaptic terminals and vascular cell populations. For quantification of dendritic length extension and isolation of presynaptic terminals directly opposed to postsynaptic sites the IMARIS scientific 3D/4D Image processing & analysis

software (Bitplane) was used. All the patient and control images were processed using the same software and experimental protocols depending on the research question at the time.

2.9 Molecular techniques

2.9.1 Isolation of different neuronal sub-compartments

In order to dissect out individual neurons and synapses, 15µm-thick frozen cerebellar sections were mounted on SuperFrost glass slides and subjected to double immunofluorescence (as described above) followed by laser capture microdissection (Zeiss PALM microdissection system). Immunofluorescently stained sections were left to air dry for 1 hour in the dark before tissue was cut and collected into sterile 0.2ml AdhesiveCap PCR tubes (Zeiss).

Purkinje cells were identified at x40 magnification by diffuse GAD-65/67 staining. Twenty randomly selected neuronal cell bodies were then isolated using the "close cut and AUTO-LPC" function of the PALM RoboSoftware into separate PCR tubes.

Areas of co-localisation between GAD-65/67 and SY-38 at the periphery of dentate nucleus neurons indicated the presence of GABAergic presynaptic terminals at x63 magnification. Given the small size of presynaptic terminals, ≥3 inhibitory axonal terminals per dentate nucleus neuron were isolated into separate PCR tubes. The "centreRoboLPC" function was employed to isolate three terminals from twenty randomly selected dentate nucleus neurons.

2.9.2 DNA extraction

Isolated tissue captured onto the adhesive caps was later subjected to centrifugation (14 000rpm for 10 minutes) into 10 µl of cell lysis buffer (50mM Tris-HCL pH 8.5, 1% Tween-20, 20mg/ml proteinase K and nanopure water) (Taylor *et al.*, 2003). Samples were lysed after incubation at 55^{o}C overnight followed by 10 minute incubation at 95^{o}C for proteinase K inactivation.

2.9.3 Polymerase chain reaction (PCR) for pyrosequencing

Cell lysates were used as template DNA to establish the m.3243A>G or m.8344A>G mutation load in Purkinje cells and presynaptic terminals from patients harbouring the m.3243A>G or m.8344A>G mutations respectively. 1µl of the Purkinje cell and 2µl of the synaptic lysate were subjected to two rounds of PCR amplification in order to have enough DNA for pyrosequencing. All the samples were run in triplicate. PCR reactions were set up in a sterile UV hood and were implemented in 25µl volumes.

2.9.3.1 M.3243A>G point mutation

To define the levels of m.3243A>G mutation load, a forward biotinylated and a reverse primer (Primer sequences and positions are summarised in Table 2- 8) amplified a 210bp PCR

fragment that spanned the m.3243 mutation site. The PCR mastermix consisted of 11.8µl DEPC-treated water (Life Technologies), 5µl, 5x GoTaq Flexi Buffer (Promega, UK), 2µl $MgCl_2$ (Promega, UK), 2.5µl 10x dNTPs (Rovalab), 2.5µl primers (10µM) (forward and reverse) and 0.2µl Go Taq Hot Start DNA polymerase (Promega, UK). The PCR conditions on the Thermal cycler (Life Technologies) were as follows (Table 2- 4):

Process	Temperature	Time	Cycles
Initial Denaturation	95°C	10 minutes	1
Denaturation	95°C	30 seconds	30
Primer annealing	62°C	30 seconds	
Extension	72°C	30 seconds	
Final Extension	72°C	10 minutes	1
Hold	4°C	∞	

Table 2- 4: PCR conditions for the m.3243A>G point mutation assay.

2.9.3.2 M.8344A>G point mutation

The m.8344A>G assay involved the use of a biotinylated forward and a reverse primer (Table 2- 8) that generated a 147bp fragment spanning the mutation site. The mastermix for the specific PCR amplification reaction was made up of 10.8µl DEPC-treated water (Life Technologies), 5µl, 5x reaction buffer (Promega, UK), 3µl $MgCl_2$ (Promega, UK), 2.5µl 10x dNTPs (Rovalab), 2.5µl primers (10µM) (forward and reverse) and 0.2µl Go Taq Hot Start DNA polymerase (Promega, UK). The Thermal cycler conditions for this assay are summarised below (Table 2- 5):

Process	Temperature	Time	Cycles
Initial Denaturation	95°C	10 minutes	1
Denaturation	94°C	30 seconds	30
Primer annealing	62°C	30 seconds	
Extension	72°C	30 seconds	
Final Extension	72°C	10 minutes	1
Hold	4°C	∞	

Table 2- 5: PCR conditions for the m.8344A>G point mutation assay.

1µl of known heteroplasmy (74% and 33% for m.3243A>G; 81% and 20% for m.8344A>G) and wild-type (WT) human homogenate DNA and mastermix were run alongside the lysates and were employed as positive and negative controls respectively.

2.9.4 PCR amplification for known heteroplasmy DNA stock generation

For the generation of mtDNA stocks with known heteroplasmy levels, 1µl of homogenate DNA was subjected to a two-stage PCR amplification protocol with an intermediate gel extraction step. The primary PCR reaction involved the use of a forward and a reverse primer (Primer Pair B; Table 2- 8) in order to amplify mitochondrial DNA and generate a~2.5kb fragment that span the mutation site. The reaction was implemented in 50µl volumes using a mastermix that consisted of 33.5µl of DEPC-treated water (Life Technologies), 5µl 1x LA PCR buffer (Mg^{2+}) (Takara Bio Inc), 8µl 10x dNTPs (Rovalab), 2µl primers (10µM) (forward and reverse) and 0.5µl LA Taq DNA polymerase (Takara Bio Inc). The PCR conditions were as follow (Table 2- 6):

Process	Temperature	Time	Cycles
Initial Denaturation	94ºC	30 seconds	1
Denaturation	94ºC	30 seconds	35
Primer annealing	58ºC	30 seconds	
Extension	68ºC	11 minutes	
Final Extension	72ºC	10 minutes	1
Hold	4ºC	∞	

Table 2- 6: Thermal cycler conditions for the first round of DNA amplification.

Following gel extraction (see section 2.9.5), the purified DNA fragments were used as template DNA to generate a 568bp product spanning the mutation site. PCR reactions were performed at 25µl volumes using a mastermix that consisted of 14.87µl DEPC-treated water (Life Technologies), 2.5µl 10x AmpliTaq Gold PCR buffer (150mM Tris-HCL, pH 8.0, 500mM KCl), 2.5µl 10x dNTPs (Rovalab), 2µl 25µM $MgCl_2$, 2µl primers (10µM) (Primer Pair 6; Table 2- 8) and 0.13µl AmpliTaq Gold Hot Start DNA polymerase (Applied Biosystems). Thermal cycler conditions are listed in Table 2- 7.

Process	Temperature	Time	Cycles
Initial Denaturation	95ºC	10 minutes	1
Denaturation	94ºC	45 seconds	35
Primer annealing	58ºC	45 seconds	
Extension	68ºC	45 seconds	
Final Extension	72ºC	8 minutes	1
Hold	4ºC	∞	

Table 2- 7: Thermal cycler conditions for the second round of DNA amplification.

Primer Sequence	Mitochondrial DNA sequence (NC_012920.1)	Tm
m.3243A>G		
5'-biotin forward primer (nt3143-3163)	5'-TAAGGCCTACTTCACAAAGCG	62°C
Reverse primer (nt3331-3353)	5'- GCGATTAGAATGGGTACAATGAG	
Sequencing primer (nt3244-3258)	5'- ATGCGATTACCGGGC	
m.8344A>G		
5'-biotin forward primer (nt8240-8264)	5'-TTT GAA ATA GGG CCC GTA TTT ACC	62°C
Reverse primer (nt8363-8387)	5'-CGG TAG TAT TTA GTT GGG GCA TTT	
Sequencing primer (nt8347-8367)	5'-ATT TCA CTG TAA AGA GGT GT	
First round PCR amplification		
B Forward (nt2395-2415)	5'- ACCAACAAGTCATTATTACCC	58°C
B Reverse (nt4653-4633)	5'- TGAGGAAATACTTGATGGCAG	
Second round PCR amplification		
6 Forward (nt3017-3036)	5' - TGTAAAACGACGGCCAGTCAGCCGCTATTAAAGGTTCG	58°C
6 Reverse (nt3574-3556)	5'- CAGGAAACAGCTATGACCGGAGGGGGGTTCATAGTAG	

Table 2- 8: The sequence and position (within the mtDNA) of primers used for pyrosequencing and generation of known heteroplasmy DNA stocks.

2.9.5 Gel electrophoresis

Two different concentrations of agarose gel were prepared depending on the size of the PCR products to be resolved; 1.5% (W/V) for PCR pyrosequencing products and 1% (W/V) for PCR products used to generate stocks of known heteroplasmy DNA. Gels contained GelRed (4µl per 100ml) that intercalated with DNA to allow for visualisation under UV light and were loaded with either Quick-load 1kb DNA ladder (BioLabs) or 100bp Hyperladder IV (Bioline). 5µl of each PCR product was mixed with 1µl loading dye (0.25% (w/v) bromophenol blue, 0.25% (w/v) xylene cyanol, 30% (v/v) glycerol) and were loaded on to the gels. Gels were submerged in 1xTAE buffer (0.8mM Tris acetate, 0.02mM EDTA, 0.4µg/ml Ethidium Bromide) and electrophoresis was performed at 75V for 45 minutes to allow separation and sizing of the PCR products. A ChemiDoc Imaging System (Bio-Rad) was used to visualise and take digital images of the gel. An example of a 1.5% gel loaded with Purkinje cell and synaptic products is shown in Figure 2- 2.

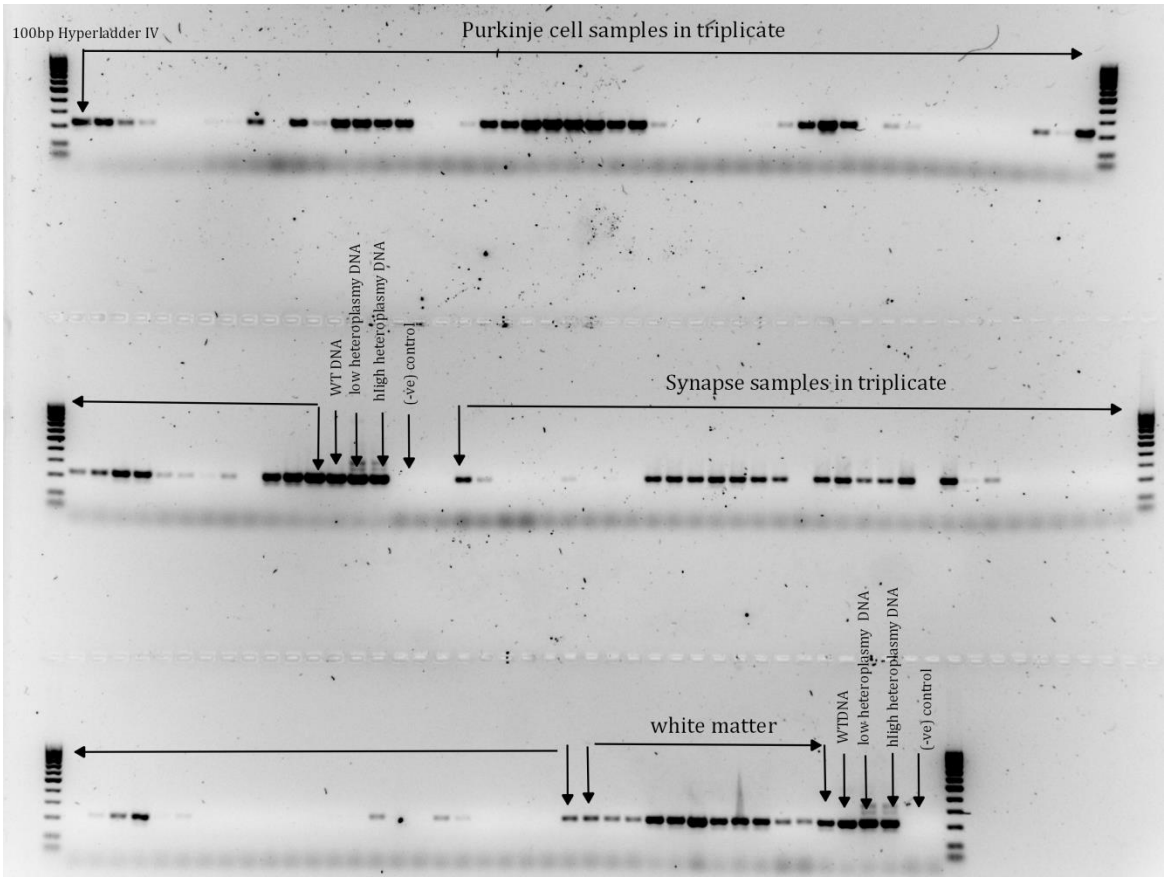

Figure 2- 2: A 1.5% gel loaded with DNA extracted from Purkinje cell bodies and synapses (in triplicate) alongside with homogenate WT and known heteroplasmy DNA.

2.9.6 Gel extraction and DNA fragment purification

Following the first PCR amplification step of known heteroplasmy mtDNA, the products were loaded on to a 1% agarose gel and were electrophoresed to allow adequate separation and sizing of the PCR products. Bands of the appropriate size were excised into 1.5ml Eppendorf tubes and were subjected to DNA extraction using a QIAEX II gel extraction kit (Qiagen) per manufacturer's instructions.

2.9.7 Pyrosequencing to define levels of mutated mtDNA

The final PCR amplification products were used to define the levels of mutated mtDNA in Purkinje cells and presynaptic terminals of patients harbouring the m.3243A>G and m.8344A>G point mutations. Depending on the intensity of the bands on the agarose gel, 10µl or 20µl of PCR product were combined with 28µl or 18µl of DEPC-treated water (Life Technologies), 40µl PyroMark binding buffer (Qiagen), and 2µl Streptavidin sepharose™ high performance beads (GE Healthcare) to give 80µl volumes of the binding solution. The samples were agitated for 10 minutes to promote DNA binding to the beads and were then transferred to the PyroMark Q24 workstation (Qiagen). A hedgehog (Qiagen), attached to a dry vacuum pump (Welch), was used to drive the samples through 70% Ethanol (5 seconds), denaturation solution (0.2M NaOH) (5 seconds) and 1x PyroMark wash buffer (Qiagen) (10 seconds). The vacuum pump was then turned off and the hedgehog was held at an angle before immersing it into a 25µl sequencing solution in a 24 well pyrosequencing plate to release the beads. The sequencing solution consisted of 24.25µl PyroMark annealing buffer (Qiagen) and 0.75µl pyrosequencing primer specific to either the m.3243A>G or the m.8344A>G assay (Table 2.4). DNA denaturation of the samples and annealing of the pyrosequencing primer required heating at 80^{o}C for 2 minutes and cooling at room temperature for 5 minutes minimum. The PyroMark Q25 cartridge (Qiagen) was then loaded with the appropriate volumes of PyroMark Gold Q24 reagents (Qiagen), enzyme mix (DNA polymerase, ATP sulfurylase, luciferase and apyrase), substrate mix (adenosine 5' phosphosulfate and luciferin) and dNTPS, suggested by the PyroMark Q24 software (Qiagen). The m.3243A>G or m.8344A>G assay was selected on the PyroMark Q24 platform (Qiagen) with each plate containing Purkinje cell samples, presynaptic terminal samples, WT and known heteroplasmy DNA. Once the pyrosequencing run was finished, results were uploaded on to and analysed using the allele quantification application of the PyroMark Q24 software (Qiagen). If the mutation load for WT and known heteroplasmy samples was within 4% of the expected value, the heteroplasmy levels for the samples to be tested were averaged amongst the triplicates.

Chapter 3

Chapter 3 Optimisation of a quadruple immunofluorescence assay to quantify respiratory chain subunit expression in human brain tissues

3.1 Introduction

3.1.1 Detection and quantification of respiratory chain deficiency

The electron transport chain (ETC), composed of four complexes and two mobile electron carriers, is located in the inner mitochondrial membrane and along with complex V (ATP synthase), constitutes a vital part of the oxidative phosphorylation system responsible for ATP production in mitochondria (Hatefi, 1985). Of the respiratory chain complexes, complexes I and IV are most frequently deficient in patients with primary mitochondrial disease (DiMauro and Schon, 2003; Swalwell *et al.*, 2011), hence many studies focus on studying the enzymatic activity and/or protein expression levels of the different complex subunits.

In order to assay the enzymatic activities of the mitochondrial respiratory chain, two approaches can be used, one which relies on fresh tissues to measure enzyme activities using spectrophotometry (Kirby *et al.*, 2007) and the other on sequential cytochrome *c* oxidase (COX)/succinate dehydrogenase (SDH) histochemistry performed on frozen tissue sections (Old and Johnson, 1989). COX/SDH histochemistry was originally developed to measure the enzymatic activity of complex IV (COX) relative to complex II (SDH) at the single cell level in human skeletal muscle (Old and Johnson, 1989) and was employed to determine the level of COX-deficiency in muscle fibres of patients with mitochondrial myopathy (Sciacco *et al.*, 1994). Complex II (SDH) consists entirely of nuclear DNA-encoded subunits, and its activity gives some indication of mitochondrial mass. COX on the other hand has both nuclear and mitochondrial DNA-encoded subunits (Chinnery *et al.*, 2008), making this respiratory chain complex vulnerable to mitochondrial DNA defects and therefore deficiency. Hence, COX/SDH histochemistry in skeletal muscle has traditionally been used as means for the clinical diagnosis of patients with mitochondrial disease.

Since similar histochemical assays are not available for complex I, measuring the enzymatic activity for this respiratory chain complex is not feasible on a single cell level (Grünewald *et al.*, 2014). Instead, enzymatic activity is quantified spectrophotometrically using homogenised tissue, and protein expression is evaluated through immunohistochemistry (IHC) using monoclonal antibodies and chromogens to visualise the protein of interest.

Employing the techniques mentioned above, enzymatic activity can only be reliably detected in homogenate tissues using spectrophotometry or by COX/SDH histochemistry; while protein

expression can be measured by presence or absence of DAB staining (IHC). The current methods do not account for mitochondrial mass and are dependent on the subjective interpretation of the pattern of staining. Hence, any mild or intermediate changes in respiratory chain protein expression may be overlooked.

Patients with mitochondrial disease have been extensively documented to be affected with a wide spectrum of neurological deficits (McFarland *et al.*, 2010), whilst research demonstrates the far-reaching signs for structural and functional neuronal abnormalities in the brains of patients with mitochondrial disease. Taking into careful consideration the urgent need for understanding the mechanisms that account for neuronal loss in mitochondrial disease combined with the short comings of current protein expression quantification techniques, one realises the necessity for developing a quantitative multiple immunofluorescent protocol that would enable the simultaneous exploration of neuronal network organisation and respiratory chain protein expression.

3.2 Aims

The major aim of this study was to develop a quantitative immunofluorescent method to allow precise detection of multiple proteins of interest, including mitochondrial respiratory chain subunits within specific neuronal subtypes, synapses and blood vessels. More specifically I aimed to:

1. Optimise a quadruple immunofluorescent technique that would allow the simultaneous detection of neuronal cell bodies, inhibitory synapses and mitochondrial populations within these.
2. Distinguish the mitochondria found in neuronal cell bodies from those located within presynaptic terminals, which would enable the precise and reliable quantification of key respiratory chain protein subunits within each neuronal sub-compartment.

3.3 Samples

3.3.1 Cerebellar tissue samples

FFPE cerebellar tissue sections (5μm thick) from ten cognitively-normal controls were employed to develop an immunofluorescent protocol for respiratory chain protein expression investigation in neuronal and sub-neuronal compartments. Tissue sections were obtained from the NBTR and the MRC Sudden Death Brain and Tissue Bank, Edinburgh. Neuropathological details of controls included in this study are summarised in Table 3- 1.

Type	Age (years)	Sex	Length of fixation (weeks)	Post-mortem delay (hours)	Cause of death	Source
Control 2	68	Male	8	54	Bowel cancer	NBTR
Control 3	78	Female	5	23	metastatic oesophageal carcinoma	NBTR
Control 4	74	Female	13	67	Lung cancer	NBTR
Control 9	78	Female	8	34	Metastatic cancer - primary origin unknown (probably ovarian)	NBTR
Control 11	48	Male	1	72	Coronary artery atherosclerosis	Edinburgh
Control 12	48	Male	1	46	Coronary artery atherosclerosis	Edinburgh
Control 13	61	Male	1	61	Suicide	Edinburgh
Control 14	48	Male	1	43	Coronary artery thrombosis and atherosclerosis	Edinburgh
Control 15	25	Male	1	53	Suicide	Edinburgh
Control 16	44	Male	1	83	Complications of bronchopneumonia and coronary artery atherosclerosis	Edinburgh

Table 3- 1: The neuropathological details of controls included in this study. NBTR – Newcastle Brain Tissue Resource.

3.4 Methodological approach

3.4.1 Immunohistochemistry for synaptic and mitochondrial protein expression

Neuropathological studies conducted on patients with mitochondrial disease suggest an intrinsic vulnerability of cerebellar Purkinje cells to mitochondrial defects and highlight their central importance to the development of cerebellar ataxia. Extensive neuronal loss is accompanied with respiratory chain protein deficiencies in remaining cells, whilst the synaptic connections between Purkinje cells and dentate nucleus neurons can appear abnormal (Tanji *et al*., 1999; Lax *et al*., 2012). These features highlight the need to study the intra-cerebellar circuitry in greater detail, including the investigation of structural synaptic characteristics and respiratory chain protein expression within these.

For the purpose of this study 5μm-thick FFPE control cerebellar tissue sections were subjected to immunohistochemical staining according to the protocol described in section 2.6. The general presynaptic marker synaptophysin and the GABA-specific neuronal and axonal terminal marker GAD-65/67 were employed in order to study the amount, the distribution and the structural characteristics of synapses to the dentate nucleus. As revealed in Figure 3- 1, synaptophysin immunoreactivity indicates synaptic connections on Purkinje cell bodies and dendrites in the Purkinje cell layer and highlights the presence of glomeruli in the granule cell layer of the cerebellar cortex. At the dentate nucleus, synaptophysin is abundantly expressed with punctate staining surrounding large glutamatergic (GADnL) and smaller GABAergic/glycinergic (GAD $^{+}$) neurons. GAD-65/67 is diffusely expressed in Purkinje cells due to their inhibitory (GABAergic) nature, outlining neuronal bodies and dendrites at the molecular layer (Figure 3- 2). The protein is also widely expressed at the boundaries and in some circumstances at the cell body of dentate nucleus neurons. When at the periphery of neurons, GAD immunoreactivity indicates the presence of inhibitory presynaptic terminals contacting dentate nucleus neurons, while cytoplasmic GAD stain is reminiscent of the presence of local GABAergic neurons (Uusisaari and Knöpfel, 2013) (Figure 3- 2).

Mitochondrial presence and distribution within neurons was examined following immunohistochemical staining against the outer mitochondrial membrane protein porin. As demonstrated in Figure 3- 3 (top panel) neurons contain a high density of mitochondria that are localised both within neuronal cell bodies and their neuritic processes. Similarly, a monoclonal antibody against NADH dehydrogenase [ubiquinone] 1 beta subcomplex subunit 8 (NDUFB8) was used to examine complex I protein expression in neurons and was indicative of cells with intact (black arrow), decreased (white asterisk) or absence (black asterisk) (compatible with

complex I deficiency) of complex I expression (Figure 3- 3) (middle panel). Furthermore, COX subunit protein expression was studied using chromogen stain against cytochrome c oxidase subunit 1 (COX1) (Figure 3- 3) (bottom panel). Some neurons were exhibitive of normal COX1 protein levels (black arrow) while others had decreased protein expression (white asterisk).

Despite the fact that synaptic proteins follow the expected pattern of expression and mitochondrial proteins indicate changes in protein expression levels, there are a number of factors that render chromogen immunohistochemistry and brightfield microscopy unsuitable for the type of analysis I am interested in performing. The pronounced levels of synaptic protein expression in the dentate nucleus neuropil makes single synapse identification challenging and often impossible (Figure 3- 1 and Figure 3- 2), while immunohistochemical staining for mitochondrial protein expression only enables the subjective identification of neurons which are intact, intermediate or negative for the protein of interest. Moreover, protein expression quantification using indirect immunohistochemistry is not reliable since the protein signal is amplified in a non-linear fashion, establishing the relationship between protein presence and signal inaccurate (Gustashaw *et al*., 2010). Chromogen immunohistochemistry is also restrictive since it only enables a single marker to be studied at a time. Hence, a direct comparison between synaptophysin and GAD expression, the potential use of synaptic and mitochondrial protein expression markers on the same tissue section or investigation of respiratory chain protein subunit loss relative to mitochondrial mass would not be feasible. Finally, two-dimensional brightfield microscopy does not provide the possibility to examine synaptic structural characteristics since synaptic size measurements cannot be derived from 2D datasets.

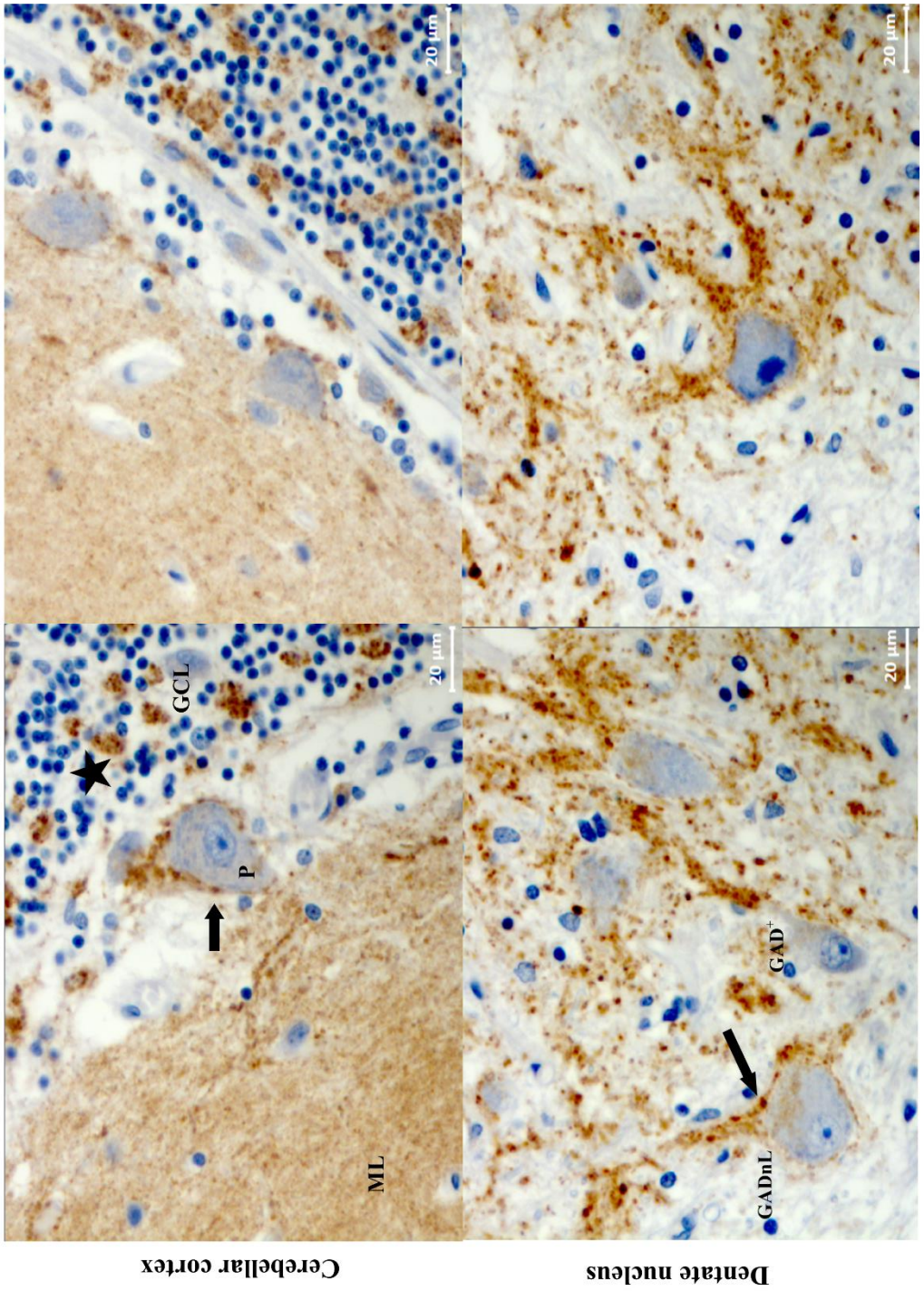

Figure 3- 1: Synaptophysin immunoreactivity in control cerebellar tissue.

At the cerebellar cortex, synaptophysin is expressed at the molecular layer (ML), around the Purkinje cell (P) body (arrow) and at the glomeruli of the granule cell layer (GCL) (asterisk). At the dentate nucleus, synaptophysin is abundantly expressed around neurons, both large glutamatergic (GADnL) and smaller GABAergic/glycinergic (GAD^+) ones, indicating the convergence of synaptic efferents. Scale bar: 20µm.

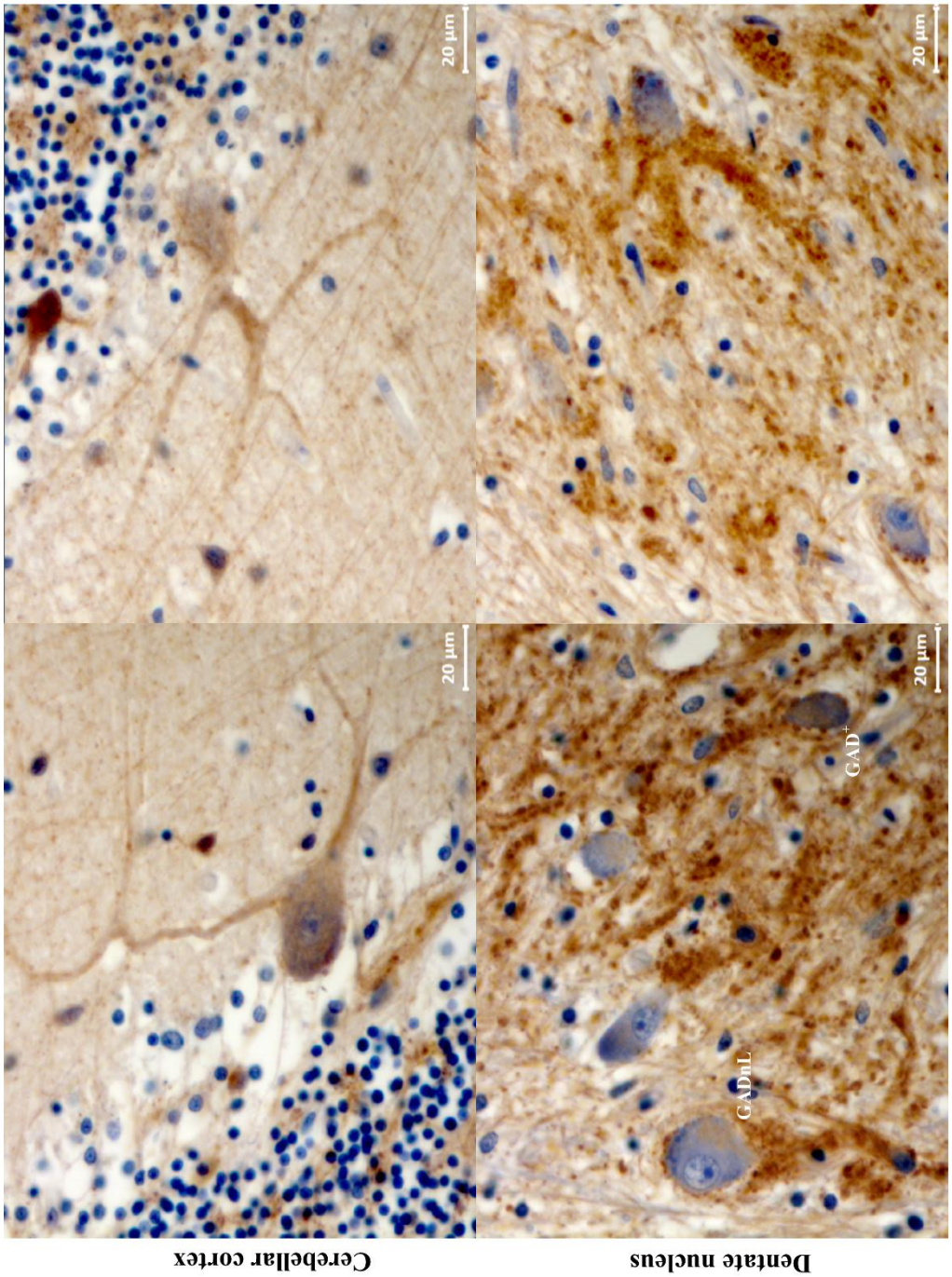

Figure 3- 2: Glutamic acid decarboxylase (GAD) immunohistochemistry in control cerebellum.

GAD-65/67 is diffusely expressed in Purkinje cells, highlighting neuronal morphology. In the dentate nucleus, GAD-65/67 is reminiscent of GABAergic synaptic input around large glutamatergic neurons (GADnL) and smaller GABAergic/glycinergic (GAD^+) neurons, while it is also expressed in the cytoplasm of GAD^+ neurons. Scale bar: 20µm.

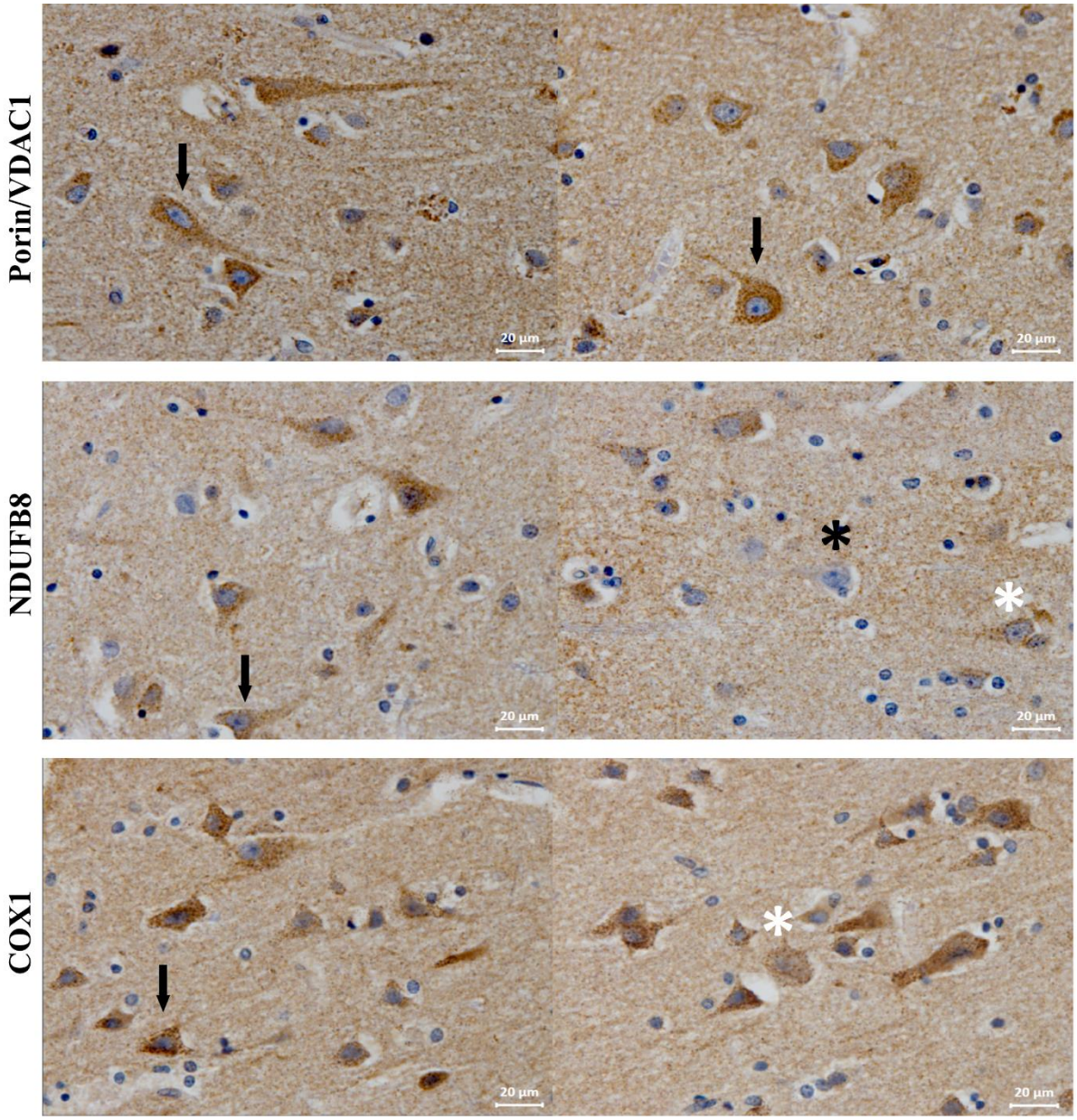

Figure 3- 3: Mitochondrial protein expression using immunohistochemical staining in control cortex.

Top panel: Neuronal mitochondria are detected using the outer mitochondrial membrane protein porin/VDAC1 as a mass marker. Cell bodies and processes (black arrows) contain high density of organelles, demonstrated by high DAB immunoreactivity. **Middle panel:** NDUFB8 is employed as a marker for complex I expression, highlighting intact (black arrow), decreased (white asterisk) and absence of immunoreactivity (black asterisk), compatible with complex I deficiency in neurons. **Bottom panel:** Complex IV subunit protein expression employing COX1 immunohistochemistry is denotive of neurons with normal (black arrow) and decreased (white asterisk) protein levels. Scale bar: 20µm

3.4.2 Optimal immunofluorescent staining conditions

Bearing the drawbacks of chromogen immunohistochemistry into consideration, I have decided to optimise an immunofluorescence technique in order to investigate respiratory chain protein expression in different cellular populations and sub-cellular compartments (neuronal cell bodies and inhibitory presynaptic terminals here). 5μm-thick FFPE cerebellar tissue sections from neurologically normal controls were subjected to a standard immunofluorescent staining protocol as previously described (see section 2.7.1).

I have decided to use mouse monoclonal antibodies against cytochrome c oxidase subunit 4 (anti-COX4 (+4L2)) and NADH dehydrogenase [ubiquinone] 1 alpha subcomplex subunit 13 (anti-NDUFA13) for mitochondrial identification and complex I protein expression investigation respectively. A mouse monoclonal antibody against the presynaptic protein synaptophysin (anti-SY-38) was employed for the identification of presynaptic terminals and a rabbit polyclonal antibody directed against Glutamic acid decarboxylase (anti-GAD-65/67) was used to mark GABAergic neurons and axonal terminals. The original choice of mitochondrial markers was based on pragmatic reasons. Since the majority of antibodies employed were raised in mice (Table 3- 2), different antibody isotypes should have been combined to avoid cross-reactivity and unspecificity. COX4 is a nuclear DNA-encoded subunit of COX that was previously shown to be preserved in patients with mitochondrial disease (Lax *et al*., 2012), hence justifying its use as a mitochondrial mass marker. Moreover, NDUFA13 served as a marker for complex I deficiency since protein expression deficiencies were previously detected in our patients (Lax *et al*., 2012).

Different antigen retrieval solutions were employed including Tri-sodium citrate (10mM) and EDTA (1mM), whereas different retrieval methods involved microwaving for 10 minutes and pressure cooking for 40 minutes. Likewise, serial dilutions of each of the antibodies were tested before the optimal working dilution for each was selected.

The optimal staining conditions (summarised in Table 3- 2) were decided for each of the four markers based on the strength, the sub-cellular distribution and the specificity of protein expression. As shown in Figure 3- 4, both COX4 and NDUFA13 demonstrate punctate staining throughout cortical grey matter and high protein expression in control neurons (white arrows) indicative of densely packed neuronal mitochondria with preserved complex I protein subunit. Furthermore, synaptophysin is widely expressed in grey matter areas with each punctum representing a single axonal terminal, whereas GAD-65/67 stains the neuronal cytoplasm of GABAergic neurons (white arrow) and inhibitory presynaptic terminals in the cortex (punctate

staining throughout grey matter) (Figure 3- 4). Once single antibody immunofluorescence was optimised, double, triple and quadruple immunofluorescent staining followed so as to verify that antibody immunoreactivity was similarly strong and specific. Indeed, COX4 co-localised with NDUFA13 in neuronal cell bodies and processes, demonstrative of mitochondria with intact complex I protein expression (double IF) (Figure 3- 5). Synaptophysin (SY-38) expression was prominent around neurons, reminiscent of synaptic terminal presence, while GAD-65/67 was punctate and co-existed with SY-38 on the periphery of neurons suggestive of GABAergic presynaptic terminal convergence.

Furthermore, antibody specificity and fluorescent channel crosstalk was tested after including no-primary-antibody (NPA) controls to the study. As verified in Figure 3- 6, each antibody is specific to the targeted protein since omitting primary antibody incubation (one antibody omitted at a time) but still incubating the sections with all the secondary antibodies demonstrates an absence of immunoreactivity in the channel to be tested.

Primary antibody	Isotype	Source	Catalogue No.	Antigen retrieval	Optimal dilution	Optimal incubation conditions
Synaptophysin (SY-38)	Mouse monoclonal - IgG1	DAKO	M0776	EDTA (1mM); 2100 antigen retriever	1 in 50	O/N at 4^{o}C
Glutamic acid decarboxylase 65/67 (GAD 65/67)	Rabbit polyclonal - IgG	Sigma-Aldrich	G5163	EDTA (1mM); 2100 antigen retriever	1 in 800	O/N at 4^{o}C
Complex I subunit NDUFA13	Mouse monoclonal - IgG2b	Abcam	ab110240	EDTA (1mM); 2100 antigen retriever	1 in 100	O/N at 4^{o}C
Complex IV subunit IV	Mouse monoclonal - IgG2a	Abcam	ab110261	EDTA (1mM); 2100 antigen retriever	1 in 200	O/N at 4^{o}C
Secondary antibody	**Isotype**	**Source**	**Catalogue No.**	**Antigen retrieval**	**Optimal dilution**	**Optimal incubation conditions**
Biotin-XX	Goat Anti-Mouse IgG1 (γ1)	Life technologies	A10519	N/A	1 in 100	30 minutes, RT
Streptavidin, Alexa Fluor® 647 Conjugate	N/A	Life technologies	S32357	N/A	1 in 100	30 minutes, RT
Alexa Fluor® 405	Goat Anti-Rabbit IgG (H+L)	Life technologies	A31556	N/A	1 in 100	30 minutes, RT
Alexa Fluor® 488	Goat Anti-Mouse IgG2b (γ2b)	Life technologies	A2114	N/A	1 in 100	1 hour, RT
Alexa Fluor® 546	Goat Anti-Mouse IgG2a (γ2a)	Life technologies	A21133	N/A	1 in 100	30 minutes, RT

Table 3- 2: The optimal working conditions for each of the primary and secondary antibodies used for immunofluorescence

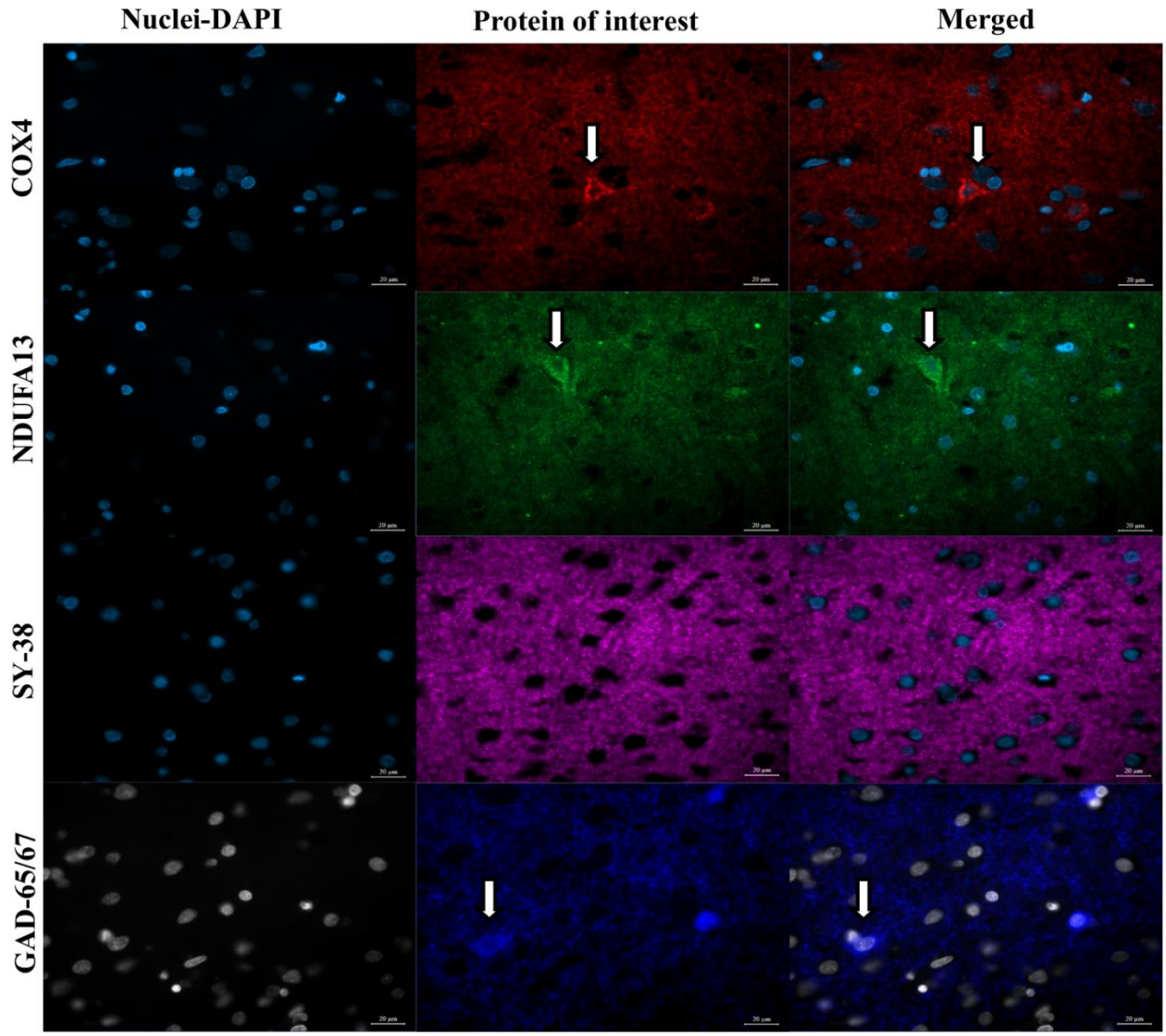

Figure 3- 4: Optimised single immunofluorescence against mitochondrial and synaptic protein markers of interest.

COX4 is employed as a mitochondrial mass marker and demonstrates punctate staining in grey matter neuropil and neurons (white arrow). Similarly, the complex I protein expression marker NDUFA13 is punctate in cortical grey matter and is enriched neurons, indicative of complex I intact cells. Synaptophysin (SY-38) is reminiscent of axonal terminal convergence and GAD-65/67 stains for inhibitory neurons (white arrows) and GABAergic synaptic terminals. Scale bar: 20µm.

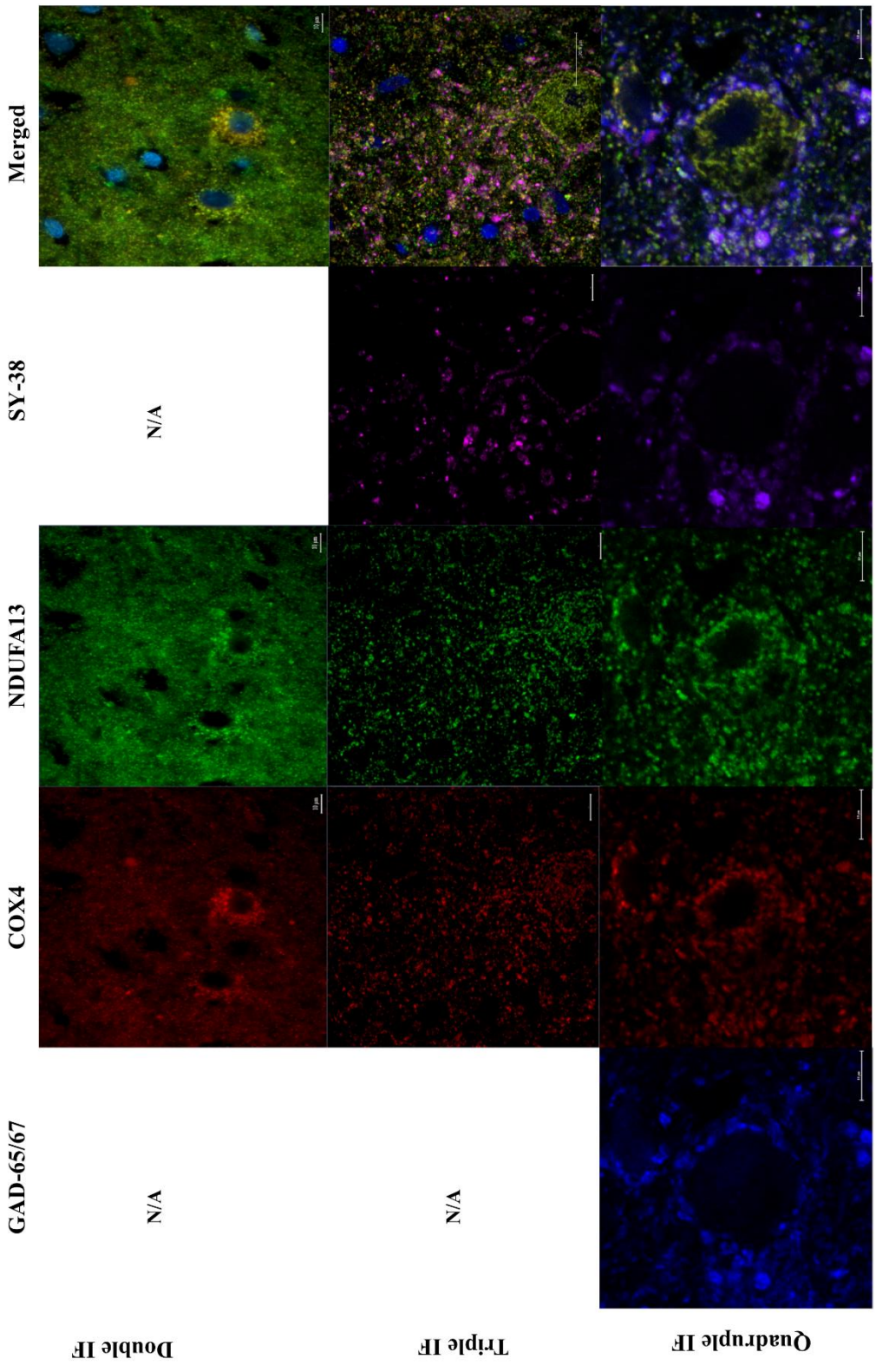

Figure 3- 5: Double, triple and quadruple staining for proteins of interest.

Double IF: COX4 and NDUFA13 are co-localised in neurons, denotive of neuronal mitochondria that have normal complex I protein expression. **Triple IF:** Synaptophysin (SY-38) – positive puncta at the periphery of neurons is reminiscent of synaptic terminal presence, whereas areas of GAD-65/67 and SY-38 co-localisation are suggestive of GABAergic terminal existence (**Quadruple IF**). Scale bar: 10µm.

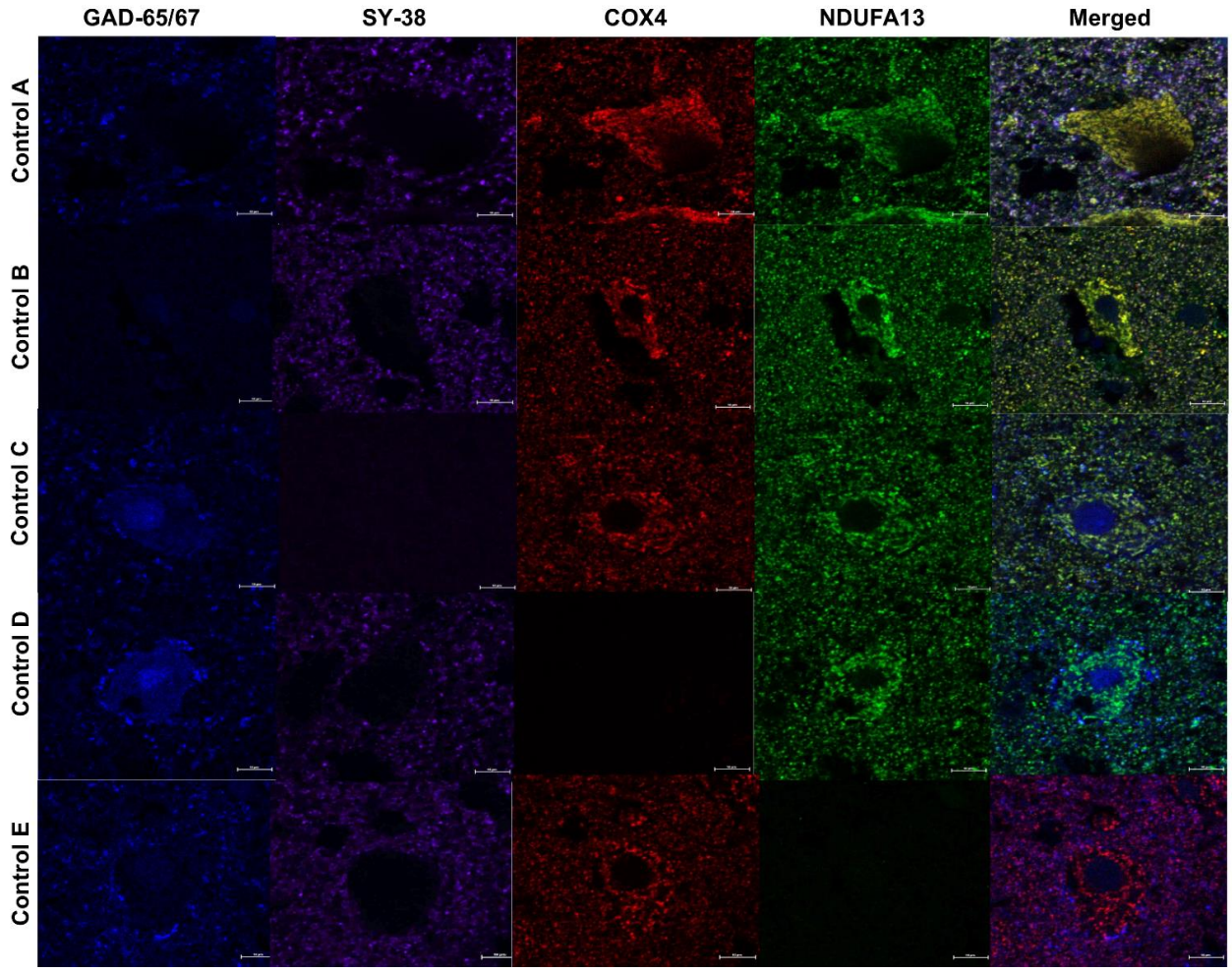

Figure 3- 6: NPA controls for cross-reactivity and assay specificity checks.

Control A: Section stained with all four markers is demonstrative of positive staining in all channels. Omission of GAD-65/67 (Control B), SY-38 (Control C), COX4 (Control D) or NDUFA13 (Control E) is accompanied by absence of signal in the corresponding channel. Scale bar: 10μm

3.4.3 Autofluorescence and Sudan Black b treatment

Tissue autofluorescence is a natural phenomenon which occurs either due to the intrinsic properties of the tissue under investigation or is induced during tissue processing (Baschong *et al.*, 2001). Nevertheless, autofluorescence is an important restricting factor when it comes to immunofluorescence analysis since it may mask true fluorescence or may be mistaken for the fluorescent label (Del Castillo *et al.*, 1989; Noonberg *et al.*, 1992; Viegas *et al.*, 2007).

Amongst the reagents frequently used to eliminate tissue autofluorescence is Sudan Black b (SB) (Baschong *et al.*, 2001) thus I have performed immunofluorescence with (+) or without (-) SB treatment to test for the this reagent's effectiveness in removing background signal and tissue autofluorescence. Control FFPE sections (5µm thick) were subjected to a standard immunofluorescent protocol (section 2.7.1), according to the previously optimised staining conditions, and included positive and NPA controls. Unspecific "staining" observed mainly in the NDUFA13 channel is removed after SB application for 10 minutes, whereas fluorescence emitted in NPA control sections is eliminated following reagent application (Figure 3- 7).

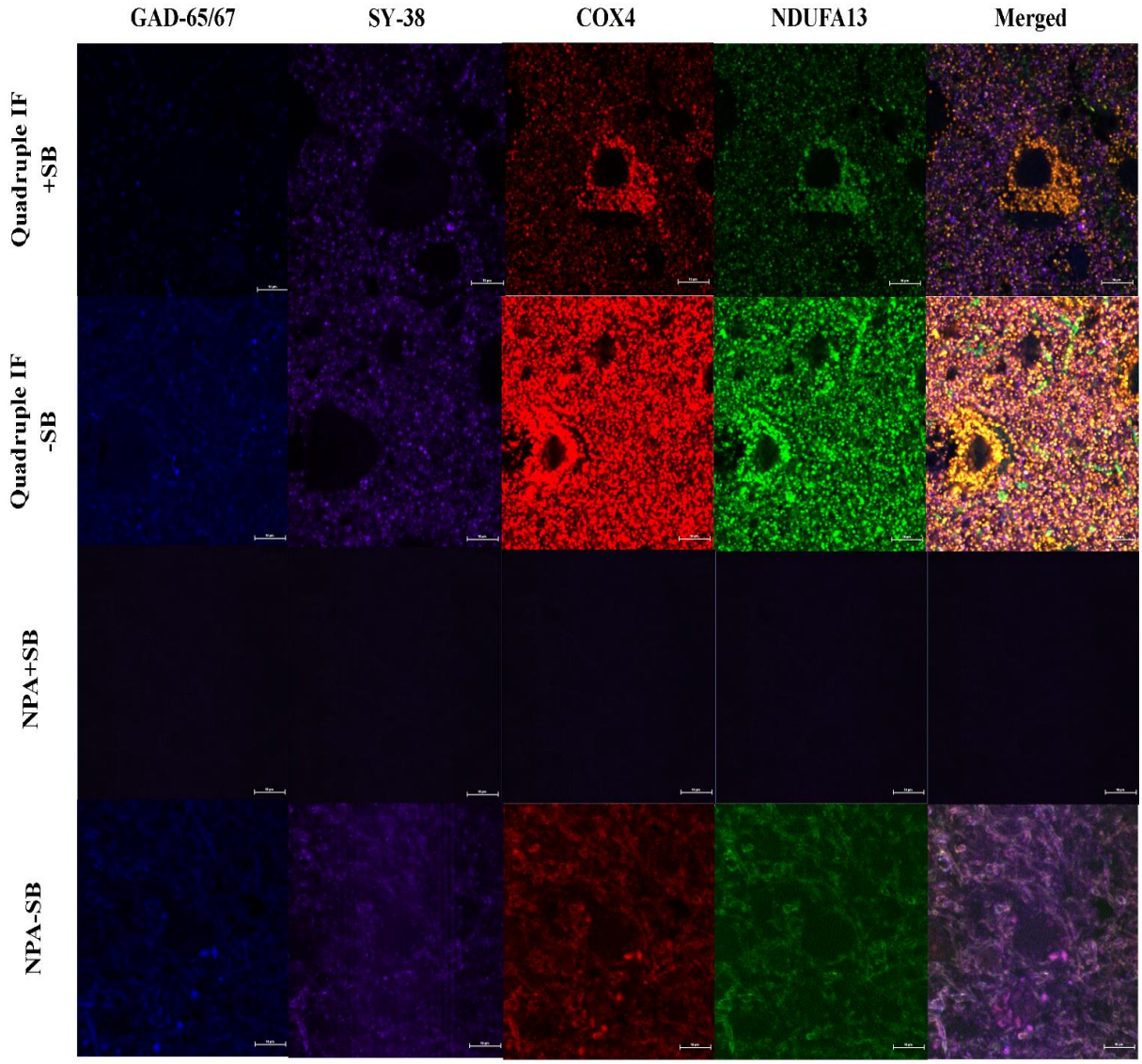

Figure 3- 7: The importance of Sudan Black b treatment in removing background and increasing signal-to-noise ratio.

Scale bar: 10µm. SB-Sudan Black, NPA – no primary antibody

3.4.4 Respiratory chain protein expression in neuronal cell bodies and presynaptic terminals

Purkinje cells utilise the inhibitory neurotransmitter GABA to suppress neurons of the deep cerebellar nuclei (Uusisaari and De Schutter, 2011), projecting inhibitory synapses mainly around neuronal cell bodies (axosomatic synapses). GAD-65/67 was uniformly and highly expressed in GABAergic neuronal cell bodies (GAD67) and inhibitory presynaptic terminals (GAD65) (Figure 3- 8) , in accordance to the anticipated subcellular distribution of the two enzymatic isoforms (Kaufman *et al*., 1991). Synaptophysin demonstrated strong and punctate staining surrounding neuronal cell bodies, representing presynaptic terminals. These terminals were suggestive of a mixture of excitatory and inhibitory synapses since only a portion of those co-localised with GAD65 (Figure 3- 8).

COX4 was expressed strongly and abundantly, with each individual puncta indicating the presence of a potentially small network of mitochondria (Figure 3- 8). Though a nuclear DNA-encoded subunit of complex I, NDUFA13 has been demonstrated to be necessary for complex assembly and stability (Angebault *et al*., 2015). Hence, by using NDUFA13 in combination with COX4 we can determine the relative loss of this complex I subunit.

Similar to Purkinje cell bodies, GAD-65/67 is expressed in different neuronal compartments of dentate nucleus neurons. When expressed in the neuronal cytoplasm, GAD67 is suggestive of Glutamic acid decarboxylase synthesis and hence of inhibitory local neuron presence (Uusisaari and Knöpfel, 2013). When expressed around the neuronal cell body, GAD65 potentially represents the occurrence of GABAergic Purkinje cell axonal terminals. To verify the existence of presynaptic terminals, synaptophysin immunoreactivity was taken into consideration. Areas of co-localisation between SY-38 and GAD-65/67 around the dentate nucleus neuronal soma are indicative of GABAergic axonal terminal divergence (Figure 3- 9). COX4 protein expression is strong throughout the dentate nucleus grey matter ribbon and within inhibitory presynaptic terminals, the same was true for the NDUFA13 subunit of complex I (Figure 3- 9). The majority of synapses demonstrated a single COX4-positive punctum, likely to be reminiscent of a small mitochondrial network (microscopic resolution does not allow for identification of single mitochondria), co-existing with NDUFA13.

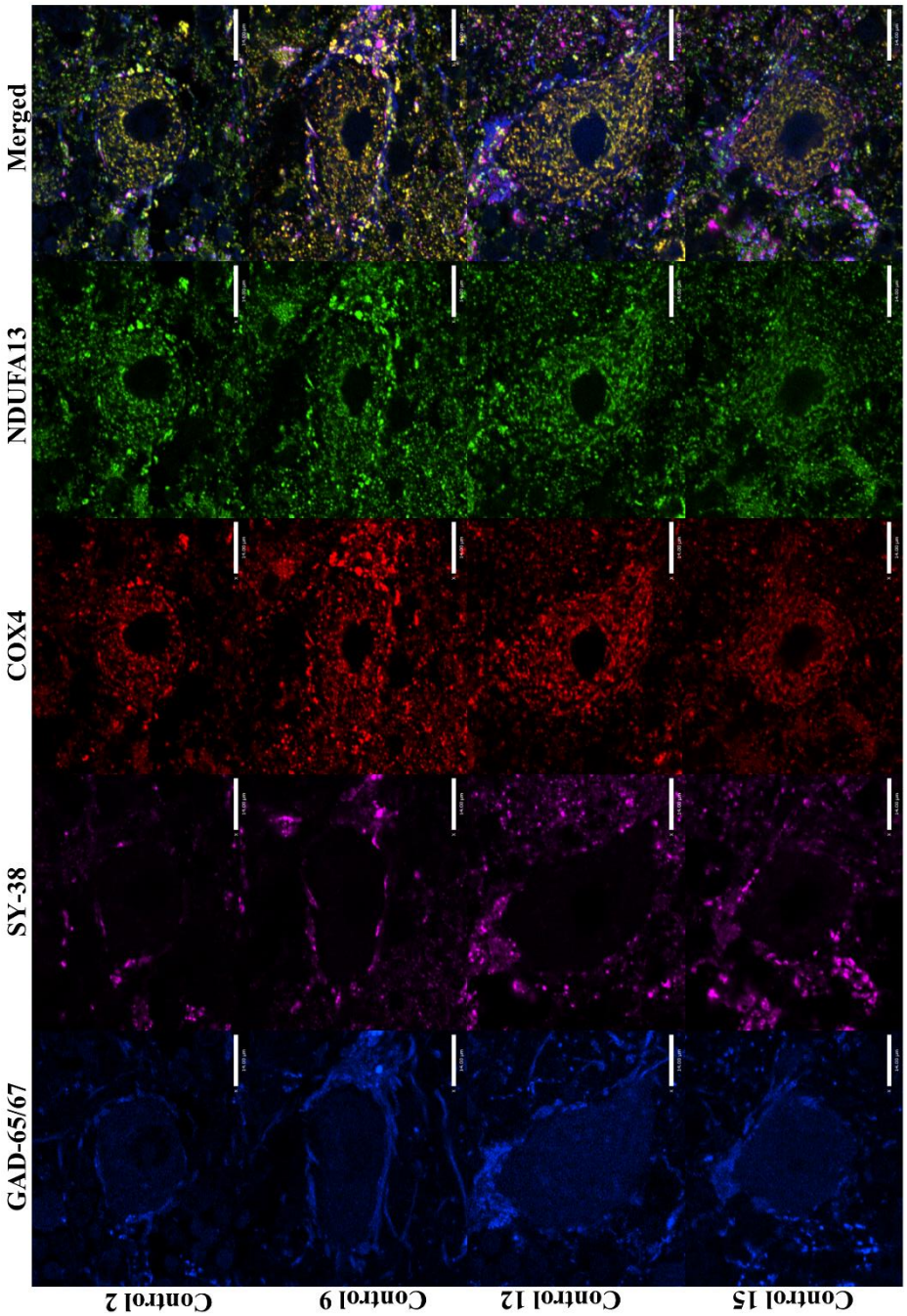

Figure 3- 8: Quadruple immunofluorescence of cerebellar Purkinje cells against Glutamic acid decarboxylase (GAD-65/67), synaptophysin (SY-38), complex IV subunit 4 (COX4) and complex I alpha subcomplex subunit 13 (NDUFA13).

GAD-65/67 is used to detect GABAergic cell bodies and inhibitory synapses. Combined with SY-38 indicates the convergence of inhibitory presynaptic terminals. COX4 is a mitochondrial mass marker and NDUFA13 protein is used to detect complex I deficiency. Control Purkinje cells demonstrate co-localisation of COX4 and NDUFA13 protein, indicating intact complex I expression. Scale bar: 14µm.

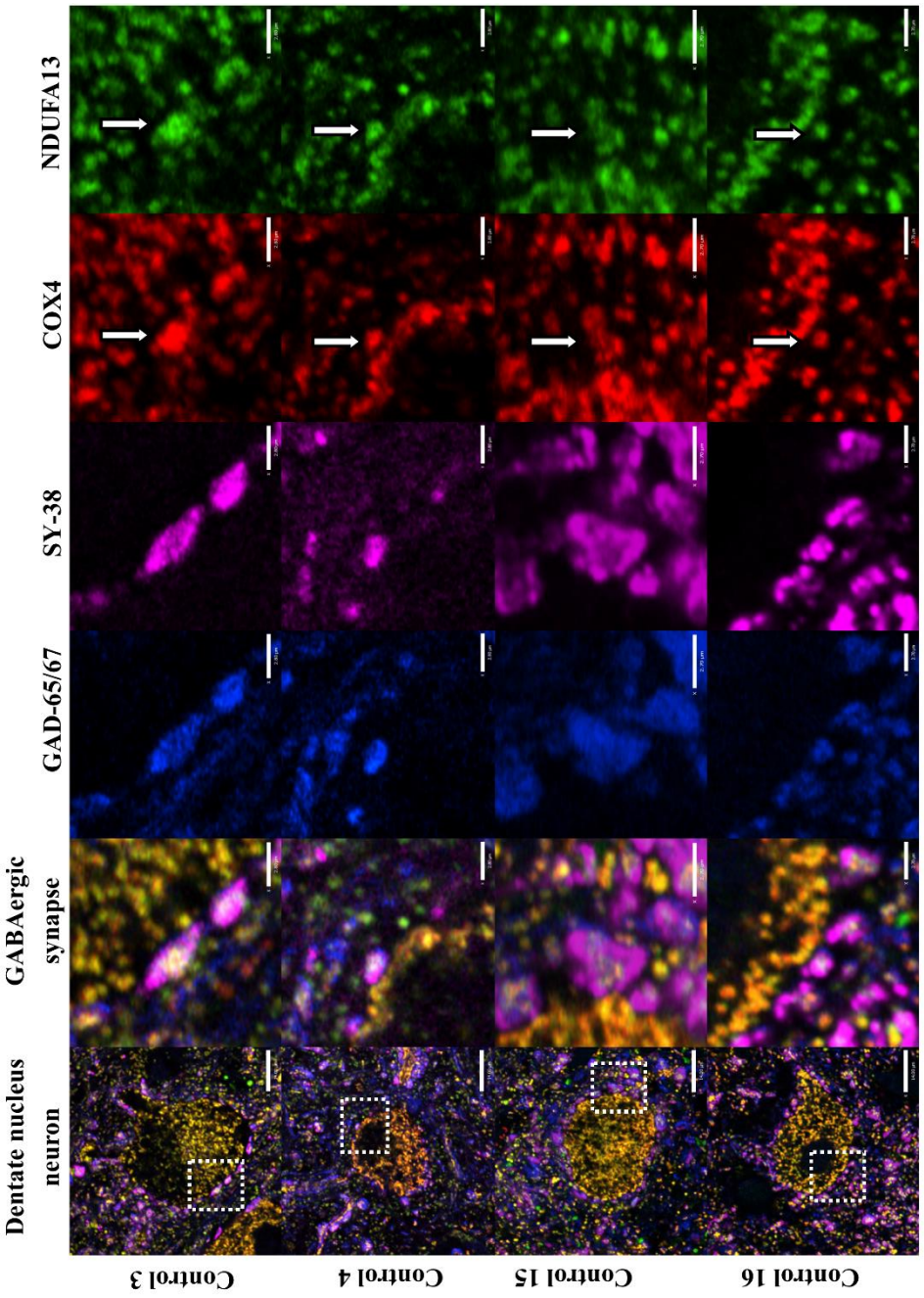

Figure 3- 9: Identification of inhibitory presynaptic terminals and respiratory chain protein expression within these.

Control dentate neurons are exhibitive of high density of synaptic efferents (Scale bar: 14µm), whilst a magnified view suggests the presence of inhibitory synapses (Scale bar: 2.8µm). Co-localisation of GAD-65/67 and SY-38 is indicative for the convergence of Purkinje cell axonal terminals that contain intact (NDUFA13-positive) mitochondria (COX4-mitochondrial mass marker) (arrows).

3.4.5 Confocal microscopy

An A1R confocal system (Nikon) was employed since it presented with significant advantages over other, conventional microscopic systems. The inverted point scanning confocal microscope enabled three-dimensional image sampling, while the four spectrally unmixed lasers (405nm, 488nm, 561nm and 647nm) allowed high resolution, multi-channel images to be acquired. Moreover, confocal laser scanning microscopy eliminates out-of-focus light interference, thus generates images specific to the plane of view.

Areas of interest (neurons or blood vessels) were identified using the microscope eyepiece at x60 magnification whilst the depth of the tissue was specified using a Step-by-step Nikon A1 Piezo Z scanner on the software surface (NIS-Elements, v4.2). Z-stacks were captured at x180 magnification (x60 objective plus x3 digital zoom) and according to the recommended microscope settings: Pixel size: 0.14μm, z-step size: 0.175μm, optical resolution: 0.13μm and optical sectioning 0.54μm. Further to image acquisition, quadruple fluorescent beads (TetraSpeck™ Fluorescent Microsphere Standards; Invitrogen) were imaged in order to measure the system's Point Spread Function (PSF).

3.4.6 Image processing

Since the data set acquired is three-dimensional, the appropriate 3D analysis software and analysis protocol is required in order to benefit from the advantages provided by laser scanning confocal microscopy. The Nikon files (.nd2) generated by the NIS-Elements software were imported into various different software, amongst which were the Volocity® 3D image analysis and deconvolution software (v.6.1.1, PerkinElmer) and IMARIS scientific 3D/4D Image processing & analysis software (Bitplane). Different analysis approaches were undertaken before the one that generated the desired output was selected.

For studying respiratory chain protein expression in Purkinje cell bodies and inhibitory presynaptic terminals to dentate nucleus neurons, z stacks were initially cropped and deconvolved using the freehand tool and the "iterative restoration" function of the Volocity software respectively. Image cropping helped analyse single neurons, whereas deconvolution facilitated light re-assignment back to its original point source giving rise to crisper images (Sarder and Nehorai, 2006) (Figure 3- 10). Thus, identifying distinct synaptic terminals would be feasible and distinguishing somatic from synaptic mitochondria would be possible.

Purkinje cell bodies were manually selected as "regions of interest", whereas GABAergic synapses were identified as areas of SY-38 and GAD-65/67 co-localisation. Mitochondrial objects within each neuronal sub-compartment were then detected, using the deconvolved

COX4 channel as a reference and the "automatic threshold" function, and were employed to acquire intensity measurements for COX4 and NDUFA13 protein expression (Figure 3- 11).

Furthermore, three-dimensional reconstruction of structures was made plausible since all images were sampled in x-, y- and z-planes. As demonstrated in Figure 3- 11 and Video 3-1, fluorescent staining can be substituted by artificial surfaces and fine sub-neuronal compartments like synapses can be modelled.

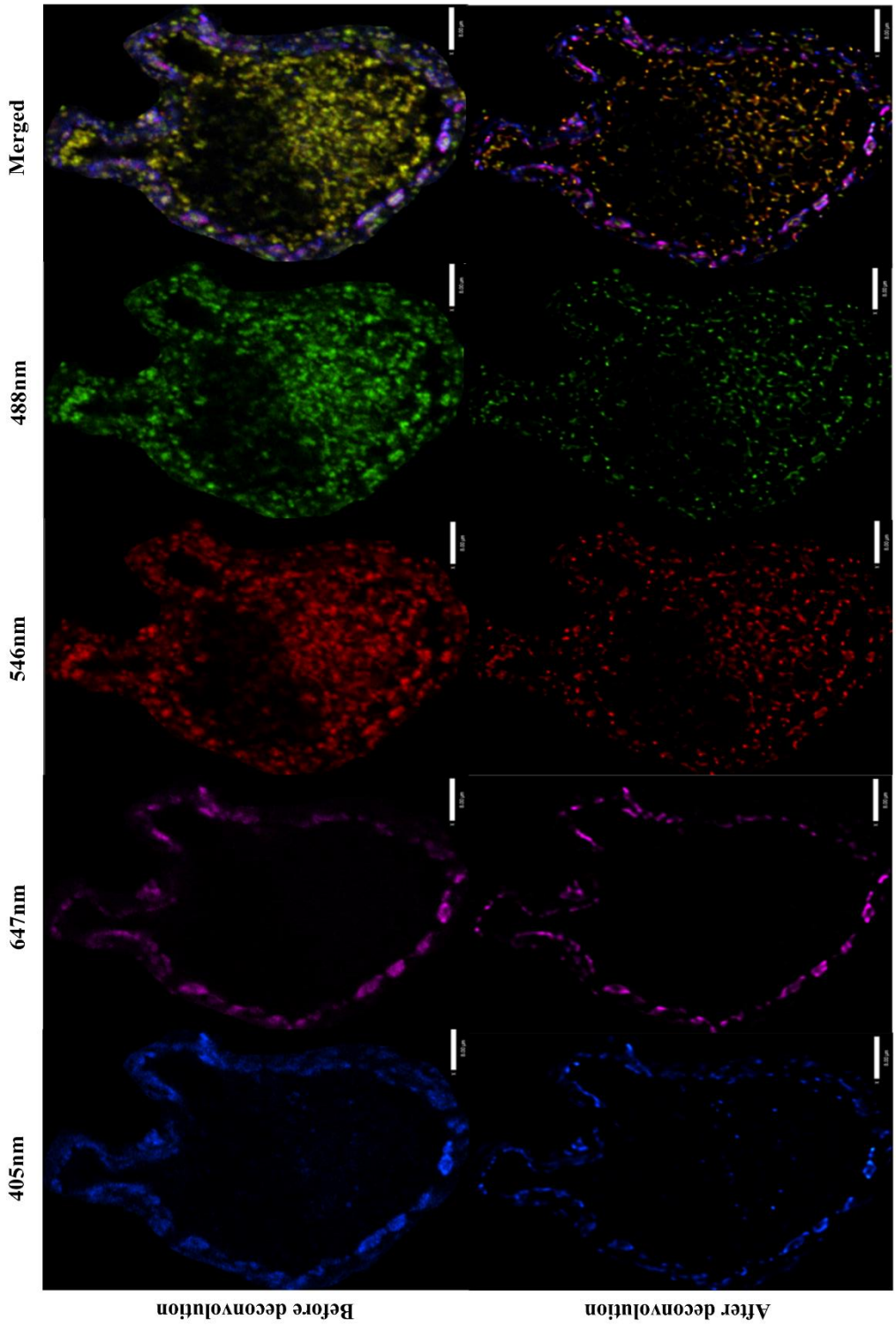

Figure 3- 10: The importance of channel deconvolutionn in producing cisper images that help identifying distinct synaptic terminals on the periphery of neurons and distinguishing synaptic from somatic mitochondria.

Scale bar: 8µm.

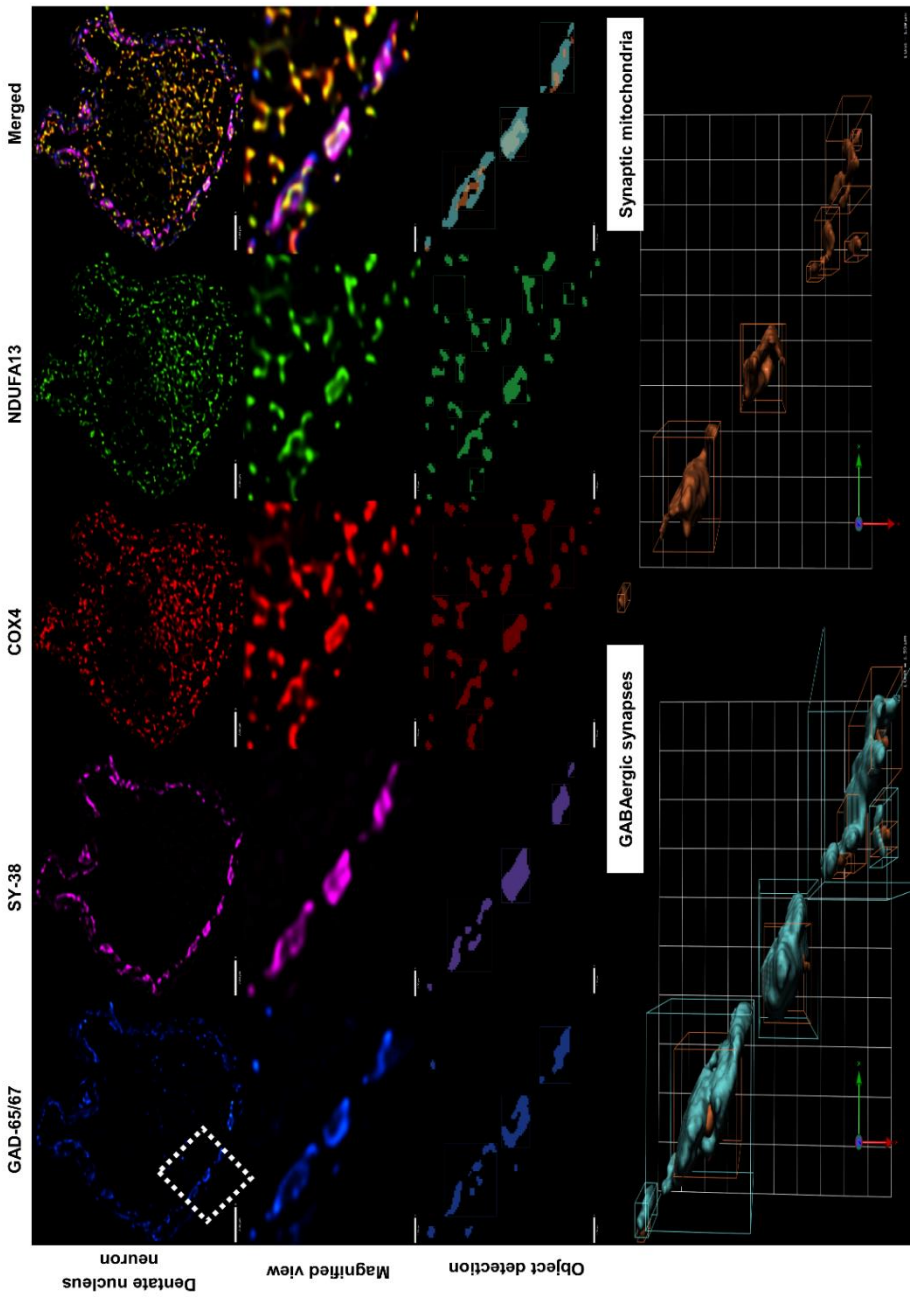

Figure 3- 11: Synaptic mitochondria detection and GABAergic synapse reconstruction.

Top panel: Confocal images of immunofluorescently stained dentate nucleus neurons were subjected to deconvolution and were later used to identify inhibitory synapses. Scale bar: 7µm. **Magnified view:** Areas on the periphery of neurons where GAD-65/67 and SY-38 puncta coexist are denotative for the presence of inhibitory synapses. COX4 – positive staining indicates mitochondrial presence and NDUFA13 immunoreactivity is used to detect respiratory chain protein deficiency. Scale bar: 1.5µm. **Object detection:** Actual staining substituted by objects that represent each of the four markers used. Mitochondrial objects can then be compartmentalized amongst GABAergic synapse objects so that only synaptic mitochondria are studied (far right). **Bottom panel:** Three-dimensional reconstruction of inhibitory synapses on the same control neuron, and localisation of synaptic mitochondria. Scale: 1 unit =1.56µm. Protocol development is achieved using the Volocity® software (v.6.3.1, PerkinElmer).

3.4.7 Quantification of respiratory chain protein expression and Z scoring

Once the mean optical density (OD) measurements for COX4 and NDUFA13 immunofluorescence were acquired using the Volocity® software (PerkinElmer), data were initially analysed manually. The $(NDUFA13)^{OD}/(COX4)^{OD}$ ratio was used to calculate the amount of NDUFA13 protein expression relative to mitochondrial presence (COX4 employed as a mitochondrial mass marker).

Later, the SAS (v.9.3) (Cary, NC) statistical software package was employed to generate z score values for each protein of interest, indicative of the degree of protein expression deviation from control values. Data normalisation and transformation was performed automatically, so was the estimation of regression parameters and standard error values.

For each area of interest (Purkinje cell body or GABAergic presynaptic terminal) the measured OD values of COX4 and NDUFA13 immunofluorescence were background corrected. Since the data were not normally distributed, the background-corrected values were then log transformed to allow for data normalisation (yielding COX4T and NDUFA13T). The distribution for COX4T and the regression of NDUFA13T against COX4T were plotted and were used to estimate the mean and standard error (from the COX4T distribution) as well as the regression parameters and the standard error of the estimate (from the regression of NDUFA13T against COX4T). For each Purkinje cell or presynaptic terminal the z score for COX4 levels was calculated, while the z score for NDUFA13 levels deviated from the linear regression based on the level of COX4. Furthermore, areas of interest were classified based on standard deviation (SD) limits (for COX4 and NDUFA13: normal if -2< z <2SD, low if z <-2SD, deficient if z <-3SD and very deficient if z <-4SD).

For example, quantification of control inhibitory presynaptic terminals (however many synapses were detected around twenty randomly selected dentate nucleus neurons) demonstrates high protein expression levels for COX4 and NDUFA13 (Figure 3- 12). Indeed, statistical analysis and z scoring for the levels of COX4 and NDUFA13 indicated normal protein expression (-2< z <2SD) (Table 3- 3), consistent with a very low percentage of GABAergic axonal terminals that were low or deficient for either of the two proteins (Table 3-3).

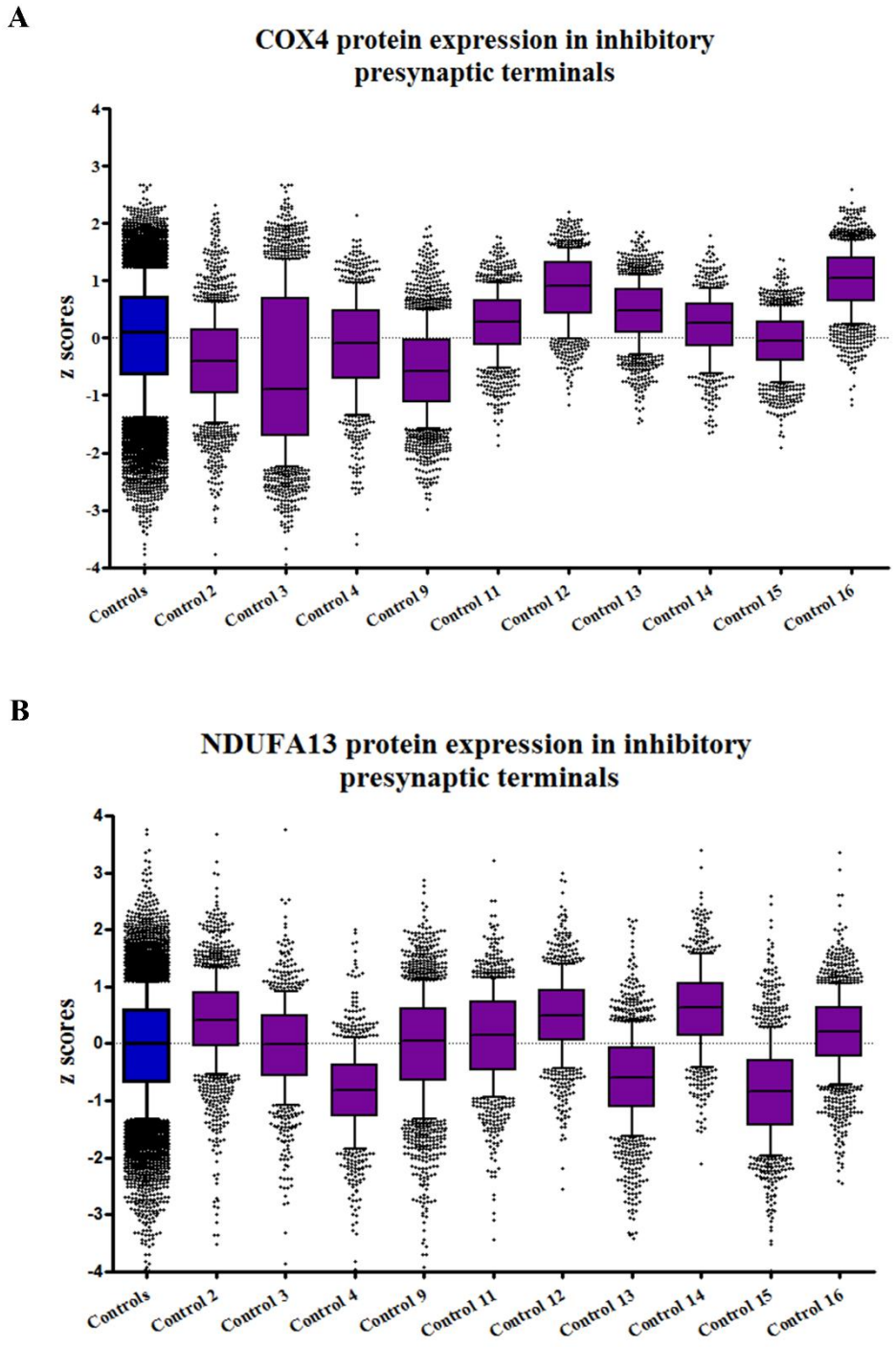

Figure 3- 12: Boxplots for the standard deviation limits of COX4 and NDUFA13 protein expression in control GABAergic presynaptic terminals.

The majority of inhibitory synapses have normal levels of COX4 **(A)** and NDUFA13 **(B)** protein expression, with few data points above or below the normal ±2 SD limits. Blue boxplots: controls grouped; Purple boxplots: individual control samples. Each data point represents protein expression in a single GABAergic presynaptic terminal.

	Control 2	Control 3	Control 4	Control 9	Control 11	Control 12	Control 13	Control 14	Control 15	Control 16
COX4 in inhibitory presynaptic terminals										
Normal (-2< z <2SD)	96.94%	83.76%	96.88%	96.96%	100%	100%	100%	100%	100%	100%
Low (z <-2SD)	2.81%	15.14%	2.88%	3.04%	0%	0%	0%	0%	0%	0%
Deficient (z <-3SD)	0.19%	1.10%	0.24%	0.00%	0%	0%	0%	0%	0%	0%
Very deficient (z <-4SD)	0.06%	0.00%	0.00%	0.00%	0%	0%	0%	0%	0%	0%
NDUFA13 in inhibitory presynaptic terminals										
Normal (-2< z <2SD)	98.75%	98.23%	92.57%	96.86%	98.75%	99.77%	94.53%	99.84%	90.75%	99.32%
Low (z <-2SD)	0.69%	1.27%	6.35%	2.43%	1.05%	0.23%	4.83%	0.16%	8.32%	0.53%
Deficient (z <-3SD)	0.25%	0.44%	0.84%	0.51%	0.19%	0.00%	0.55%	0.00%	0.75%	0.00%
Very deficient (z <-4SD)	0.31%	0.06%	0.24%	0.20%	0.00%	0.00%	0.08%	0.00%	0.19%	0.15%

Table 3- 3: The percentage of inhibitory presynaptic terminals that are Normal (-2< z <2SD), Low (z <-2SD), Deficient (z <-3SD) or Very deficient (z <-4SD) for COX4 and NDUFA13 protein expression in neurologically-normal controls.

3.5 Discussion

The severe neurological impairments affecting patients with mitochondrial disease highlight the need for developing a reliable, precise and reproducible quantitative immunofluorescent protocol that would facilitate the investigation of mitochondrial protein expression in the central nervous system. The increasing body of evidence for cerebellar vulnerability to mitochondrial dysfunction (Tanji *et al.*, 1999; Hakonen *et al.*, 2008; Lax *et al.*, 2012) and the well-known structural and functional organisation of the cerebellum, enable its use as a tool for protocol development.

Changes in mitochondrial proteins have previously been studied using conventional histochemical (COX/SDH) and immunohistochemical techniques. Despite the fact that COX/SDH histochemistry is an invaluable tool for identifying cells that are clearly deficient for COX (Ross, 2011), it relies on the subjective decision for the presence, absence or low immunoreactivity of DAB and does not allow subtle changes in protein activity to be detected. Similarly, indirect immunohistochemistry is semi quantitative, lacks correction for mitochondrial mass and requires a number of post-capture processing steps for it to serve as a reliable quantitative method (Taylor and Levenson, 2006; Nguyen, 2013). Furthermore, immunohistochemistry is restrictive in the number of proteins that can be examined per section, constituting the simultaneous investigation of several proteins impossible.

Here I report the development of an accurate, quadruple immunofluorescent technique that relies on the densitometric quantification of fluorescence to determine protein expression levels. The intra-cerebellar circuitry and more specifically the Purkinje cell-dentate nucleus inhibitory synapse is employed as an example for establishing a method that allows respiratory chain protein expression investigation in neuronal and sub-neuronal compartments. Strong and punctate staining of the inhibitory neuronal and presynaptic terminal marker GAD-65/67 and the general synaptic marker SY-38 enables the detection of GABAergic neurons and inhibitory axonal terminals, whereas the abundant immunoreactivity of antibodies against NDUFA13 and COX4 facilitates the examination of complex I protein expression relative to mitochondrial mass. Moreover, laser scanning confocal microscopy and three-dimensional analysis software enable the detection of synaptic mitochondria and inhibitory presynaptic terminal reconstruction. Hence, a single cerebellar tissue section can be employed to simultaneously examine complex I protein expression in the Purkinje cell soma and its inhibitory presynaptic terminals and to further quantify the number and the size of synaptic connections established between Purkinje cells and dentate nucleus neurons.

The technique is specific in that there is absence of antibody cross-reactivity thus channel densitometry only reflects the extent of protein expression investigated at the time. The use of a similar quadruple immunofluorescent technique for the investigation of respiratory chain protein expression in dopaminergic midbrain neurons further verifies the reliability and reproducibility of the assay (Grünewald *et al.*, 2014).

3.5.1 Future work

Given the evidence for cerebellar dysfunction and the extensive neuronal and synaptic abnormalities in patients with mitochondrial disease (Tanji *et al.*, 1999; Lax *et al.*, 2012), there needs to be an in depth study of the respiratory chain deficiencies in neuronal and sub-neuronal compartments and further a quantitative assessment of the type and nature of synaptic changes. Investigating the extent of respiratory chain protein deficiencies and of structural synaptic abnormalities and associating the observed neuropathological changes with the patients' clinical phenotype is likely to provide further insights into disease mechanisms and explain for the progression of ataxia.

Indeed, future work involves the employment of this quantitative quadruple immunofluorescent technique for the establishment of neuronal cell body and synaptic respiratory chain protein deficiencies and for the characterisation of synaptic morphological changes.

3.6 Conclusion

For the purposes of this study I have developed a quadruple immunofluorescent technique that serves as an objective, quantitative, reliable and reproducible alternative to the previously used histochemical and immunohistochemical methods. Simultaneous assessment of expression levels of four different proteins is made possible, while precise spatial distribution and morphological characterisation of synaptic terminals is possible. The method is versatile and can be adjusted to incorporate different markers depending on the research question at the time, hence serving as a valuable tool for quantifying the degree of protein expression changes in post-mortem brain tissue.

Chapter 4

Chapter 4 Cerebellar ataxia in patients with mitochondrial disease

Part 1: Synaptic terminal pathology in the cerebellum of ataxic patients

4.1 Introduction

4.1.1 Cerebellar structure

The cerebellum is crucial for muscle tone and motor movement coordination, critically defined by the fine harmonisation between ascending sensory and descending motor signals (Holmes, 1939; Chambers and Sprague, 1955; Cooper, 1958). The structure is also important for cognition (Parsons and Fox, 1997; Thach and Thach, 1997), whilst recent studies on cerebellar dysfunction were exhibitive of its importance in language, working memory and decision-making skills (Martin, 2002).

The cerebellum is located on the posterior part of the brain, dorsal to the medulla and pons when viewed on a sagittal plane. The structure's complex organisation drives its anatomic, phylogenetic and functional compartmentalisation. The cerebellum is divided into three sagittal zones (Martin, 2002; Apps and Garwicz, 2005) and further into ten lobules (I-X) (Voogd and Glickstein, 1998). Functionally, the cerebellum is organised into the spinocerebellum, the vestibulocerebellum and the pontocerebellum (cerebrocerebellum), which, as the names suggest receive, input from the spinal cord, the vestibular system and the cerebral cortex respectively (Rajakumar, 2013).

The cortex, the medullary core of white matter and the deep cerebellar nuclei make up the basic cerebellar structure. The cortex is subdivided into three stratums – the molecular, Purkinje cell and granule cell layer- and contains two neuronal and three interneuronal populations. Cortical interneurons include the inhibitory stellate and basket cells, which reside within the molecular cell layer, and the inhibitory Golgi cells found at the granule cell layer. The excitatory granule cells constitute the most abundant neuronal subtype of the granule cell layer (and of the brain as a whole), whilst the inhibitory Purkinje cells form a distinct "neuronal ribbon" interjected between the granule and molecular cell layers (Martin, 2002). Furthermore, there are three types of deep cerebellar nuclei (DCN), the dentate, the fastigial and the interposed nucleus, which contain different neuronal/interneuronal populations with distinct electrophysiological capacities (Uusisaari and Knöpfel, 2013; Cohen, 2014).

4.1.2 Cerebellar connectivity

Afferent signals to the cerebellum arrive from the inferior olive (IO), the brain stem and spinal cord. Excitatory climbing fibres (CF) project their axons from the IO and synapse onto Purkinje cells, evoking "complex spike" formation (Voogd and Glickstein, 1998; Apps and Garwicz, 2005), and onto DCN neurons. Mossy fibres (MF), originating from the brain stem and spinal cord, indirectly excite Purkinje cells (via granule cell parallel fibres) (Voogd and Glickstein, 1998; Apps and Garwicz, 2005; Rajakumar, 2013) and neurons of the DCN. Cerebellar efferents include DCN projections onto brainstem nuclei, the red nucleus of the midbrain and – via the thalamus – to premotor and primary motor cortices (Rajakumar, 2013). A summary of the intra- and extracerebellar circuitry is presented in Figure 4- 1.

The Purkinje cell-dentate nucleus neuronal synapse is the main component of intracerebellar circuitry, since Purkinje cells are the sole output neurons from the cerebellar cortex, projecting their synapses onto deep cerebellar nuclei (Uusisaari and De Schutter, 2011). Synaptic communication between the two neuronal populations is established via the inhibitory neurotransmitter γ-aminobutyric acid (GABA). The majority of Purkinje cell axonal terminals form connections on the dentate nucleus neuronal soma (cell body), giving rise to axosomatic synapses, with some synapses also being formed on neuronal dendrites or axons (axodendritic and axoaxonic synapses respectively).

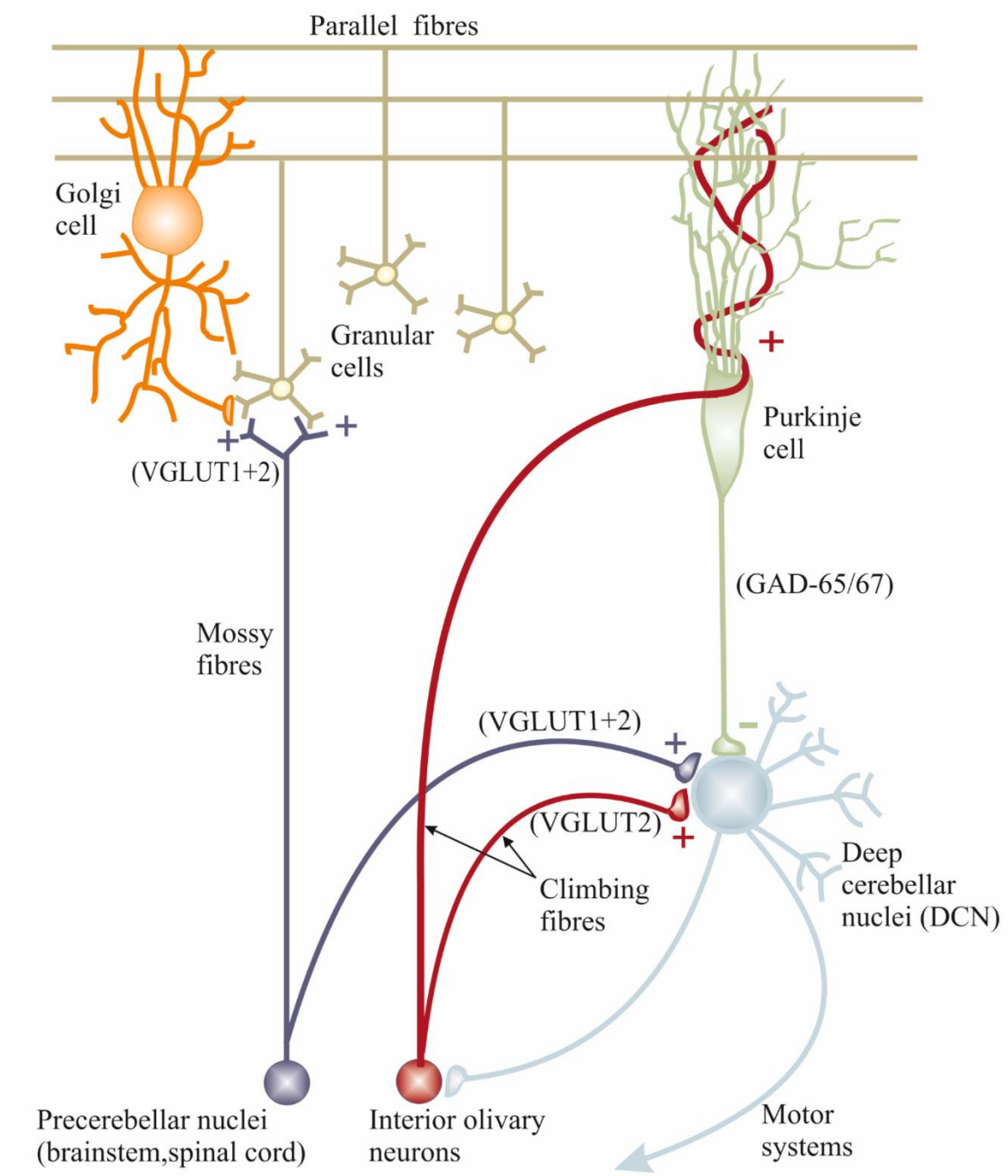

Figure 4- 1: A summary of the intra- and extracerebellar circuitry.

The cerebellum receives efferents from the inferior olive, the brain stem and the spinal cord. Climbing fibres arise from the inferior olive, project onto and excite Purkinje cells (located in the cerebellar cortex) and deep cerebellar nuclei (DCN). Mossy fibres, originating from precerebellar nuclei (brainstem and spinal cord), project their excitatory presynaptic terminals onto DCN and indirectly excite Purkinje cells (via granule cells). Intracerebellar connectivity is established via the inhibitory Purkinje cell-dentate nucleus neuronal synapse. GABAergic Purkinje cells contact DCN (principally dentate nucleus neurons), which form local feedback and global signal transduction networks by projecting their axons to the brainstem, red nucleus, premotor and primary motor cortices.

4.1.3 Cerebellar ataxia

"Lack of order" and inability to coordinate voluntary movement broadly defines ataxia. Amongst the pioneers in recognising and characterising the condition were Babinski (1899) and Holmes (1939) who introduced the terms "asynergy" (Babinski, 1899) and "delayed initiation" of voluntary movements (Holmes, 1939) to describe this pathological state. Damage to or dysfunction of the cerebellum or of its input/output pathways result in cerebellar ataxia (Marsden and Harris, 2011), with associated symptoms including dyssynergia, dysmetria, tremor, dysdiadochokinesia, asthenia and hypotonia, balance and gait dysfunction as well as dysarthria and oculomotor deficits (Klockgether, 2000).

Cerebellar dysfunction and altered intra- and extra-cerebellar connectivity is the pathological hallmark of many inherited ataxias including Spinocerebellar and Friedreich's ataxia (Scherzed *et al.*, 2012; Koeppen *et al.*, 2013). Proteins involved in hereditary forms of ataxia are associated with mitochondria and in fact, mitochondrial dysfunction is involved in the neuropathological/neurodegenerative profiles of Spinocerebellar (Das *et al.*, 2010; Sykora *et al.*, 2011), spastic (Girard *et al.*, 2012) and Friedreich's ataxia (Gonzalez-Cabo and Palau, 2013).

The intrinsic vulnerability of the cerebellum to mitochondrial dysfunction can be explained by its remarkably high neuronal density. Although it only occupies 10% of the brain's volume, the cerebellum contains 50% of the brain's total neuronal population (Knierim, 1997). Neural computation models for the estimation of energy required for signalling on principle cerebellar cells – Purkinje cells – estimates that ~10^{11} molecules of ATP are required per second (Howarth *et al.*, 2010). Surprisingly, the increased density and the excitatory nature of another cerebellar neuronal cell type –granule cells – implies that these cells outrank Purkinje neurons in terms of their energetic requirements (Howarth *et al.*, 2010). Thus, a considerable amount of energy is necessary to maintain cerebellar neuron function, assuring for the structural and functional preservation of the region (Knierim, 1997).

4.1.4 Mitochondrial disease and cerebellar ataxia

Bearing in mind the frequent involvement of mitochondria in the pathogenesis of several hereditary ataxias (Das *et al.*, 2010; Sykora *et al.*, 2011; Girard *et al.*, 2012; Gonzalez-Cabo and Palau, 2013), it comes as no surprise that patients with mitochondrial disease are frequently and severely affected by cerebellar ataxia. The increased metabolic demand of the CNS combined with the importance of mitochondria in providing the cells with the energy they require, explains the severe neurological impairments of patients with mitochondrial disease.

Despite the plethora of neurological deficits, including sensorineural deafness, cognitive decline and stroke-like episodes (McFarland *et al.*, 2010), cerebellar ataxia is the most frequently presenting symptom. In fact, approximately 70% of the patients recruited to the UK MRC Mitochondrial Disease Patient cohort are affected by ataxia which is progressive and very disabling (Lax *et al.*, 2012; Nesbitt *et al.*, 2013).

The recently developed and validated Newcastle Mitochondrial Disease Adult rating Scale (NMDAS) is routinely employed by neurologists in order to assess patient progression and decide on personalised patient care (Schaefer *et al.*, 2006). According to the NMDAS scale for cerebellar ataxia, patients are scored with 0-5. A score of zero indicates an absence of phenotype, whereas 5 is given to patients that are severely impaired and as such become wheelchair-dependent. The highly heterogenic and multisystemic nature of mitochondrial disorders implies that cerebellar ataxia affects patients with different genetic diagnoses to a currently unpredicted extent. Valuable work has been performed into understanding the progression of ataxia in patients with the m.3243A>G point mutation, suggesting that patient age and urine heteroplasmy levels can collectively help predict the severity of the ataxic phenotype. However, there is more left to do before we can confidently predict patients' progression (Grady, 2013).

Cerebellar abnormalities are routinely detected though neuroradiological imaging (Lax and Jaros, 2012). Patients with the Kearns-Sayre syndrome (KSS) demonstrate an atypical cerebellar structure (upon neuropathological examination) (Barkovich *et al.*, 1993), with Purkinje cell loss from the cerebellar cortex (Tanji *et al.*, 1999), spongiform deterioration of the white matter (Oldfors *et al.*, 1990; Tanji *et al.*, 1999) and decreased synaptic input to the dentate nuclei microscopically detected (Tanji *et al.*, 1999). Cerebellar ataxia is a prominent feature of patients with the myoclonus epilepsy with ragged-red fibres (MERRF) syndrome (Austin *et al.*, 1998; McFarland *et al.*, 2002). Patient brains have atrophic pons, cerebellar hemispheres and middle and superior cerebellar peduncles (Ito *et al.*, 2008). Neuropathologically, cerebellar lesions are pronounced (Fukuhara, 1991) whilst neuronal loss affects the inferior cerebellar cortex (Lax *et al.*, 2012). Similarly, enlarged fourth ventricles in patients with mitochondrial encephalomyopathy, lactic acidosis and stroke-like episodes (MELAS), due to the m.3243A>G point mutation, are reminiscent of the presence of cerebellar atrophy (Sue *et al.*, 1998). MELAS patients present with severe cerebellar neuropathological abnormalities, some of which include neuronal loss, axon demyelination and microinfarct presence (Lax *et al.*, 2012). Generalized pontocerebellar atrophy is evident in patients with the neurogenic weakness, ataxia and retinitis

pigmentosa (NARP) syndrome (Renard and Labauge, 2012). Ataxia also affects patients with secondary mitochondrial disease, due to mutations in mtDNA maintenance genes. Autosomal recessive polymerase γ (*POLG*) gene mutations have been associated with cerebellar ataxia (Van Goethem *et al.*, 2004; Tzoulis *et al.*, 2006), whereas neuronal loss in both the midbrain and the cerebellum of a patient suffering from multiple mtDNA deletions, due to recessive *POLG* mutations, were also detected (Betts-Henderson *et al.*, 2009).

4.1.5 Synaptic plasticity and mitochondria

The highly sophisticated neuronal structure ensures the formation of dynamic and functional networks with extensive energetic demands which can render neurons vulnerable to fluctuations in mitochondrial function. Specific neuronal sub-compartments, including synapses, are more metabolically active than others accounting for the increased mitochondrial density in these regions (Hollenbeck and Saxton, 2005). As a matter of fact, synaptic mitochondrial function goes beyond energy production, ensuring structural integrity and functional maintenance of the synaptic compartment. A summary of synaptic mitochondrial function is provided in Figure 4-2.

More specifically, signal transduction and synaptic transmission requires most of the ATP produced in the brain as demonstrated from studies on rat cerebral (Attwell and Laughlin, 2001) and human cortices (Lennie, 2003). Cortical regions enriched with neurons, and high synaptic density, consume considerable amounts of energy (Harris *et al.*, 2012), whereas ATP supplied by mitochondria is required by both axonal terminals and neuronal dendrites (pre- and post-synaptic compartments respectively) for synaptic transmission to take place.

Action potential initiation at the presynapse requires ionic flux balance, regulated by mitochondrial-generated ATP which ensures for fine tuning of ionic pumps (Attwell and Laughlin, 2001). Additionally, synaptic activity was demonstrated to "drive" synaptic mitochondrial density (Brodin *et al.*, 1999), whereas ATP supply from mitochondria is needed for synaptic vesicle transport (Verstreken *et al.*, 2005), exocytosis and recycling (Rowland *et al.*, 2000; Perkins *et al.*, 2010). Post-synaptically, the energy required for reversal of ionic gradients created following excitation (Harris *et al.*, 2012), and to a much lesser extent following inhibition (Howarth *et al.*, 2010), is provide by mitochondria.

Further to ATP production, calcium buffering by mitochondria is essential for the establishment of neuronal polarity and thus for axonal differentiation (Mattson and Partin, 1999). Also, maintenance of synaptic transmission capacity following tetanic stimulation in glutamatergic synapses is achieved thanks to mitochondrial calcium buffering that ensures for rapid recovery

(Billups and Forsythe, 2002). Moreover, studies performed on hippocampal neuronal cultures (Kang *et al.*, 2008), hippocampal slices (Levy *et al.*, 2003) and crayfish neuromuscular junctions (Tang and Zucker, 1997) are demonstrative of the importance of mitochondrial calcium buffering in synaptic plasticity.

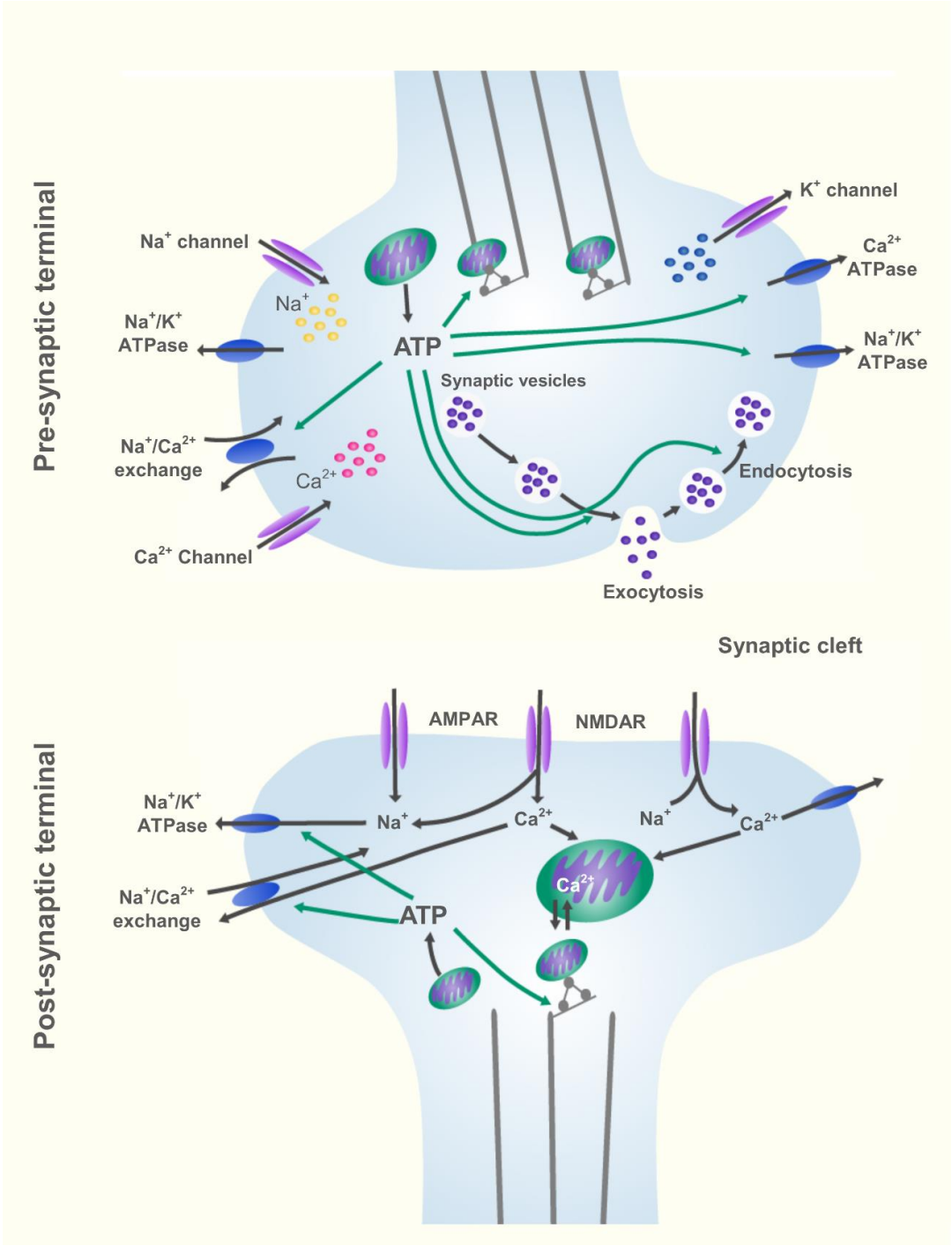

Figure 4- 2: Synaptic mitochondrial functions.

Mitochondria are enriched at synaptic sites (axonal terminals and neuronal dendrites), where their function is crucial for synaptic transmission. At the presynaptic terminal, mitochondrial generated ATP is used to drive synaptic vesicle transport, release and endocytosis (synaptic vesicle recycling), regulate ionic fluxes necessary for action potential propagation (via fuelling ATPases) and motor-protein assisted organelle transport to/from the synapse. Postsynaptic mitochondria are essential for synaptic transmission preservation since mitochondrial ATP production and calcium buffering capacities are key for reversing ionic gradients generated following transmitter release and uptake.

4.1.6 Evidence of synaptic pathology in mitochondrial disease

Generalised neurodegeneration observed in post-mortem brain samples from patients with mitochondrial disease is accompanied by structural abnormalities, specific to neuronal sub-compartments. The synaptic terminal connections linking the Purkinje cells to dentate nucleus neurons within the cerebellum have been the centre of attention, since these efferents constitute the main component of the intracerebellar circuitry (Uusisaari and De Schutter, 2011).

Detailed neuropathological studies performed by Lax and colleagues (2012) demonstrated decreased Purkinje cell efferent density to the dentate nucleus of patients carrying the m.3243A>G and m.8344A>G point mutations, despite Purkinje cell number preservation in the cerebellar cortex (Lax *et al.*, 2012). Moreover, "ghost synapses" were present in the dentate nucleus of a patient harbouring the m.14709T>C point mutation, which consisted of large presynaptic structures (detected following synaptophysin immunoreactivity) in the absence of postsynaptic dentate nucleus neurons (Lax *et al.*, 2012). Likewise, Tanji and co-workers (1999) employed synaptophysin and Calbindin immunohistochemistry in KSS patients to demonstrate the decrease in axonal terminal density and the existence of sparse and swollen Purkinje cell terminals to the dentate nucleus respectively (Tanji *et al.*, 1999).

Changes in the number and structural characteristics of Purkinje cell presynaptic terminals were followed by abnormalities in neuronal dendrites and regions proximal to Purkinje cell bodies. Main observations include swollen axons, known as "Torpedoes", and thick dendritic trees which are extensively arborized (Lax *et al.*, 2012).

The importance of mitochondrial presence and function in synaptic structural integrity and functional preservation is also demonstrated through the use of genetic modification techniques and cell culture/animal models. Mitochondrial localisation in dendritic protrusions following repetitive excitation favour the formation of new spines, whereas altered mitochondrial dynamics, via disturbed fusion/fission balance, results in decreased mitochondrial density in dendrites and decline in dendritic spine number (Li *et al.*, 2004). Moreover, disturbed Optic Atrophy 1 (OPA1) gene expression in mice is indicative of a link between mitochondrial dynamics, mitochondrial localisation and synaptic density. 10-15 month old mice heterozygous for OPA1 (a mitochondrial fusion protein) were demonstrative of mitochondrial fragmentation with retraction back to the soma and a consequent decrease in retinal ganglion cell synaptic density (Williams *et al.*, 2012). Finally, mutations of the mitochondrial fission protein Dynamin-related protein1 (Drp1) results in mitochondrial absence from the synapse in fly models (*Drosophila melanogaster*). In spite of maintained basal synaptic function under resting

conditions, flies are unable to transduce neuronal signals after high (10Hz) electrical current application (Verstreken *et al.*, 2005).

4.1.7 Synaptic protein expression

Bearing in mind Purkinje cell vulnerability to mitochondrial dysfunction, the importance of deep cerebellar nuclei in controlling cognition, emotion and language and mitochondrial significance in maintaining synaptic structure and function, I have decided to investigate dentate nucleus neuronal innervation with a focus on the Purkinje cell-dentate nucleus neural synapse.

GABA synthesis requires the enzymatic activity of Glutamic acid decarboxylase (GAD) that acts to convert L-glutamate into the inhibitory neurotransmitter (Erlander and Tobin, 1991). GAD exists in two isoforms, GAD65 and GAD67, which are encoded by two distinct genes and have differential neuronal distributions (Erlander *et al.*, 1991). The 67kDa isoform (GAD67) is expressed throughout the neuronal cell, while the 65kDa isoform (GAD65) is specific to presynaptic terminals (Kaufman *et al.*, 1991).

One of the key presynaptic proteins is synaptophysin, the most abundant (by mass) glycoprotein (Takamori *et al.*, 2006) that surrounds SVs (Jahn *et al.*, 1985). Synaptophysin is equally present in glutamate- and GABA-containing SVs (Takamori *et al.*, 2000a; Takamori *et al.*, 2000b) and has been demonstrated to control SV endocytosis following neurotransmitter release (Kwon and Chapman, 2011). Hence, synaptophysin is useful for determining the presence of a presynaptic terminal, regardless of the nature of the synaptic connection (excitatory or inhibitory).

Taking into consideration the expected neuronal distribution for GAD-65/67 and synaptophysin, these two markers can be used in conjunction in order to closely investigate the cerebellar microcircuitry. GAD67 will enable the detection of inhibitory Purkinje cell bodies within the cerebellar cortex, while areas of co-localisation between GAD65 and synaptophysin could be indicative for the presence of Purkinje cell efferents onto dentate nucleus neurons.

4.2 Aims of the study

Notwithstanding the clinical relevance of the cerebellum to mitochondrial disease and the previous detailed neuropathological studies in patients with mitochondrial disease, the presence and extent of respiratory chain defects in and the morphological characteristics of synapses have never been the point of focus. Hence, this study aims to answer the following questions:

1. Is there evidence of mitochondrial dysfunction in Purkinje cell synapses?
2. If so, does synaptic mitochondrial dysfunction have any effects on synaptic morphology and/or density?
3. Could these changes represent a primary event in neuronal degeneration? I.e. is mitochondrial disease a synaptopathy?

I will achieve these by combining a validated quantitative immunofluorescent technique with sophisticated molecular biology methods to evaluate the distribution of respiratory chain deficiencies and assess the degree of synaptic and dendritic morphological abnormalities. The frequent involvement of the cerebellum in mitochondrial disease and the simplistic architecture of the intracerebellar circuitry provide the possibility to employ the Purkinje cell-dentate nucleus synapse as a tool to gain more mechanistic insights into cerebellar ataxia and to further understand the importance of synapses in neurodegeneration due to mitochondrial disease.

4.3 Methodology

4.3.1 Cerebellar tissue samples

This study involves the neuropathological investigation of twelve adult patients who have been clinically and genetically diagnosed with mitochondrial disease. The patients were routinely assessed by neurologists using the validated Newcastle Mitochondrial Disease Adult Scale (NMDAS) (Schaefer *et al.*, 2006), while the scores for cerebellar ataxia confirm that all patients included in this study were ataxic. Patient clinical and neuropathological details are summarised in Table 4- 1.

Ten cognitively normal controls that were matched for age and post-mortem interval (PMI) with patients were included in the study (Age: Mann Whitney U test, p value =0.3390; PMI: Mann Whitney U test, p value =0.7667). Patient and control tissue characteristics are summarised in Table 4- 2.

	Pt1	***Pt2***	***Pt3***	***Pt4***	***Pt5***	***Pt6***	***Pt7***	***Pt8***	***Pt9***	***Pt10***	***Pt11***	***Pt13***
Age	36	60	30	45	20	57	42	58	59	79	55	55
Gender	Female	Female	Male	Male	Female	Female	Female	Male	Male	Male	Male	Male
Genotype	m.3243A>G	m.3243A>G	m.3243A>G	m.3243A>G	m.3243A>G	m.3243A>G	m.8344A>G	m.8344A>G	*POLG* (p.Gly848Ser and p.Ser1104Cys)	*POLG* (p.Thr251Ile/p.Pro587Leu; p.Ala467Thr)	*POLG* (p.Trp748Ser and p.Arg1096Cys)	m.14709T>C
Disease duration (y)	15	33	11	ND	10	32	37	23	37	23	50	21
Percentage cell loss												
Purkinje cells	59%	70%	0%	ND	ND	59%	67%	8%	65%	8%	ND	30%
Dentate nucleus neurons	56%	0%	20%	ND	ND	56%	75%	48%	45%	31%	ND	74%
Inferior olivary neurons	42%	50%	ND	ND	ND	42%	85%	ND	69%	ND	ND	44%

Neuropathology	Microinfarcts affecting the cerebellar cortex. Complex I and IV deficiency in ION, PCs and DNNs. Decreased synaptophysin immunoreactivity in DN. Vascular COX- deficiency in brain parenchyma	Microinfarcts in cerebellar cortex. Complex I deficiency in remaining PCs and vascular COX-deficiency	-	-	Microinfarcts in cerebellar cortex. Complex I deficiency in remaining PCs and complex I and IV deficiency in SNNs. COX-deficiency and mineralisation of blood vessels	Cerebellar lesions and mild (when existent) complex I and IV deficiency in remaining PCs and DNNs. Thinning of the endothelial cell layer	High levels of complex I and moderate levels of complex IV deficiency in surviving neurons of the olivo-cerebellar pathway. Shrunken, eosinophilic neurons and decreased synaptophysin immunoreactivity. COX-deficient vessels	Intact SN neuronal population and low levels of complex I deficiency	Cerebellar lesions and moderate complex I and IV deficiency in surviving neurons.	-	-	Severe complex I and IV deficiencies in IO. Moderate complex I and mild complex IV deficiency in PCs and DNNs. Presence of "ghost" synapses.
Ataxia (NMDAS rating)	3/5	1/5	1/5	5/5	5/5	1/5	5/5	4/5	3/5	3/5	5/5	3/5

Table 4- 1: clinical and neuropathological details of patients included in this study.

NMDAS cerebellar ataxia: 0 – none, 1 – normal gait but hesitant heel-toe, 2 – gait reasonably steady. Unable to maintain heel-toe walking or mild upper limb dysmetria. 3 – Ataxic gait (but walks unaided) or upper limb intention tremor and pointing. Unable to walk heel-toe (falls immediately). 4 – Severe ataxia – gait grossly unsteady without support, or upper limb ataxia sufficient to affect feeding. 5 – Wheel chair dependent primarily due to ataxia or upper limb ataxia prevents feeding.

Type	Age (years)	Sex	Length of fixation (weeks)	Post-mortem delay (hours)	Cause of death	Source
Control 2	68	Male	8	54	Bowel cancer	NBTR
Control 3	78	Female	5	23	metastatic oesophageal carcinoma	NBTR
Control 4	74	Female	13	67	Lung cancer	NBTR
Control 9	78	Female	8	34	Metastatic cancer - primary origin unknown (probably ovarian)	NBTR
Control 11	48	Male	1	72	Coronary artery atherosclerosis	Edinburgh
Control 12	48	Male	1	46	Coronary artery atherosclerosis	Edinburgh
Control 13	61	Male	1	61	ND	Edinburgh
Control 14	48	Male	1	43	Coronary artery thrombosis and atherosclerosis	Edinburgh
Control 15	25	Male	1	53	ND	Edinburgh
Control 16	44	Male	1	83	Complications of bronchopneumonia and coronary artery atherosclerosis	Edinburgh
Patient 1	36	Female	1	42	Cardiac arrest	NBTR
Patient 2	60	Female	6	10	Multi-organ failure	NBTR
Patient 3	30	Male	10	69	Mitochondrial disease	NBTR
Patient 4	45	Female	8	43	Mitochondrial disease	NBTR
Patient 5	20	Male	6	187	Aspiration, pneumonia and MELAS	NBTR
Patient 6	57	Male	50	36	Cardiac failure	NBTR
Patient 7	42	Male	8	59	Respiratory failure	NBTR
Patient 8	58	Male	6	66	Mitochondrial disease	NBTR
Patient 9	59	Female	4	67	Mitochondrial disease	NBTR
Patient 10	79	Female	8	85	Mitochondrial disease	NBTR
Patient 11	55	Male	7	112	Mitochondrial disease	NBTR
Patient 13	55	Male	17	10	Mitochondrial disease	NBTR

Table 4- 2: Characteristics of control and patient post-mortem tissue included in this study.

4.3.2 Immunofluorescence

Various different immunofluorescent experiments were performed depending on the research question at the time, though all protocols employed were slightly modified versions of the previously developed immunofluorescent technique (Chapter 3 of this thesis and section 2.7.1).

For evaluating complex I protein expression in Purkinje cells bodies and axonal terminals, 5µm-thick FFPE cerebellar tissue sections were immunofluorescently stained according to the protocol described in Chapter 3 of this thesis (section 3.4) (see Table 2- 3 for primary and secondary antibody combination). Triple immunofluorescence was used to study complex I protein expression in Purkinje cell dendrites and involved the use of primary and secondary antibodies included in Table 4- 3.

Triple immunofluorescence						
Primary antibodies	**Host and isotype**	**Source**	**Catalogue No.**	**Antigen retrieval**	**Optimal dilution**	**Optimal incubation conditions**
Calbindin (D-28k)	Mouse monoclonal - IgG1	Swant	CB300	EDTA (1mM); 2100 antigen retriever	1 in 1000	O/N at 4°C
Complex I subunit NDUFA13	Mouse monoclonal - IgG2b	Abcam	ab110240	EDTA (1mM); 2100 antigen retriever	1 in 100	O/N at 4°C
Complex IV subunit IV	Mouse monoclonal – IgG2a	Abcam	ab110261	EDTA (1mM; 2100 antigen retriever)	1 in 200	O/N at 4°C
Secondary antibodies	**Host and epitope**	**Source**	**Catalogue No.**	**Antigen retrieval**	**Optimal dilution**	**Optimal incubation conditions**
Alexa Fluor® 647	Goat Anti-Mouse IgG1 (γ1)	Life technologies	A21240	N/A	1 in 100	1 hour, RT
Alexa Fluor® 488	Goat Anti-Mouse IgG2b (γ2b)	Life technologies	A21141	N/A	1 in 100	1 hour, RT
Alexa Fluor® 546	Goat Anti-Mouse IgG2a (γ2a)	Life technologies	A21133	N/A	1 in 100	1 hour, RT

Table 4- 3: Primary and secondary antibodies used in this study along with their optimal working conditions.

4.3.3 Confocal microscopy and image processing

Immunofluorescently stained sections were imaged using an inverted point scanning confocal microscope (Nikon A1R) as described earlier (section 2.8.1 and 3.4.5). Z stacks were acquired for twenty randomly selected neurons - according to the recommended microscope settings - and were employed for image analysis.

Respiratory chain protein expression quantification in neuronal cell bodies involved outlining and defining the soma as a "ROI". Purkinje cell neuronal dendrites were identified due to their calbindin immunoreactivity and were manually cropped, whereas GABAergic synapses were identified as the regions of co-localisation between GAD-65/67 and SY-38 around dentate nucleus neuronal cell bodies. Once the neuronal sub-compartment of interest was manually or automatically selected, mitochondria were identified within each using COX4 as a reference channel (and the "automatic threshold" function). Mitochondrial "objects" within each sub-neuronal compartment were employed to acquire the fluorescence intensity measurements for different respiratory chain proteins (COX4 and NDUFA13). All intensity measurements were performed using Volocity® (PerkinElmer).

Synaptic terminal density quantification was performed using both Volocity® and IMARIS software. Volocity® facilitated image cropping and deconvolution (section 3.4.6), whereas IMARIS was employed for surface reconstruction. GAD- and SY-positive puncta were substituted by surfaces mimicking the pattern of staining and GABAergic synapses were detected when both surfaces were present. The number of inhibitory presynaptic terminals detected was normalised to cell circumference (per μm circumference).

Due to limited tissue availability, dendritic length extension was investigated in thin tissue sections (5 μm-thick) that were subjected to triple immunofluorescence (Table 4 – 3). Confocal images were manually cropped using Volocity® and z stacks of individual Purkinje cells were later imported into IMARIS software (Bitplane). The Filament tracer module enabled the creation of a continuous surface that resembled neuronal dendrites through the use of an "Autopath" algorithm. The Calbindin channel (Alexa Fluor 647) was employed as the source, while the filament start- and end-points were manually added. However, this technique holds significant drawbacks which are discussed below (see section 4.5).

4.3.4 Defining the levels of mutated mtDNA in neuronal cell bodies and presynaptic terminals

15μm-thick frozen cerebellar tissue sections mounted on SuperFrost glass slides were employed to determine mtDNA heteroplasmic levels in Purkinje cell bodies and axonal terminals. Sections were initially subjected to a double immunofluorescent protocol (for details see section 2.7.1 and Table 2- 3) and were then employed for single neuronal and synaptic isolation as described in section 2.9.1. DNA was extracted from the isolated tissue as previously described (section 2.9.2) and was amplified using the appropriate primers depending on the type of point mutation (section 2.9.3 and Table 2- 8). The levels of mutated over wild-type mtDNA were determined through pyrosequencing as described in section 2.9.7.

4.3.5 Statistical analyses

The mean optical density (OD) values for NDUFA13 and COX4 immunofluorescence were employed to calculate the z score values for respiratory chain protein expression in different neuronal sub-compartments using SAS 9.3 (Cary, NC). Each area was categorised according to the standard deviation limits for NDUFA13 protein expression as being normal, low, deficient or very deficient. A detailed description on data analysis is provided in Chapter 3 of this thesis (section 3.4.7).

Z score differences between sub-neuronal compartments or patients with different genetic diagnoses were assessed using two-sample (for parametric data) or Mann-Whitney U (for nonparametric data) tests. Paired nonparametric data were tested using the Wilcoxon Signed-Rank test, whilst associations between continuous variables were evaluated using Spearman's rank correlation. All statistical testing was performed in Minitab®.

4.4 Results

4.4.1 Complex I deficiency in Purkinje cells and inhibitory presynaptic terminals

Control Purkinje cells had high expression of COX4 and NDUFA13 (Figure 4- 3), indicating that control neuronal cell bodies had an abundance of mitochondria that were intact for complex I protein expression. Although patient Purkinje cells were enriched for mitochondria, in agreement to the comparable levels between control and patient COX4 protein expression (two sample t-test, p value =0.323), NDUFA13 expression was variably decreased in the majority of cells (Figure 4- 3). Protein expression quantification verified variable NDUFA13 expression and helped define the exact protein expression levels (Figure 4- 4). Some of the patients carrying the m.3243A>G point mutation (Patient 1, 3 and 5) and a patient with recessive POLG mutations (Patient 11) contained Purkinje cells deficient for complex I (NDUFA13z < -3SDs), whilst patients 4 (m.3243A>G), 6 (m.3243A>G) and 7 (m.8344A>G) had milder changes in NDUFA13 expression consistent with low protein expression levels (NDUFA13z < -2SDs) (Figure 4- 4) (Table 4- 4). Patients harbouring the m.3243A>G point mutation had more severe complex I defects relative to patients with other genetic defects (m.8344A>G, m.14709T>C and recessive *POLG*) (Mann Whitney U test, p value= 0.0306). The derived z score values for NDUFA13 expression were not affected by either PMI (Spearman's rho= -0.242, p value= 0.449) or fixation time (rho= -0.035, p=0.913) (Spearman's rank correlation). The correlations for PMI are displayed in Appendix A.

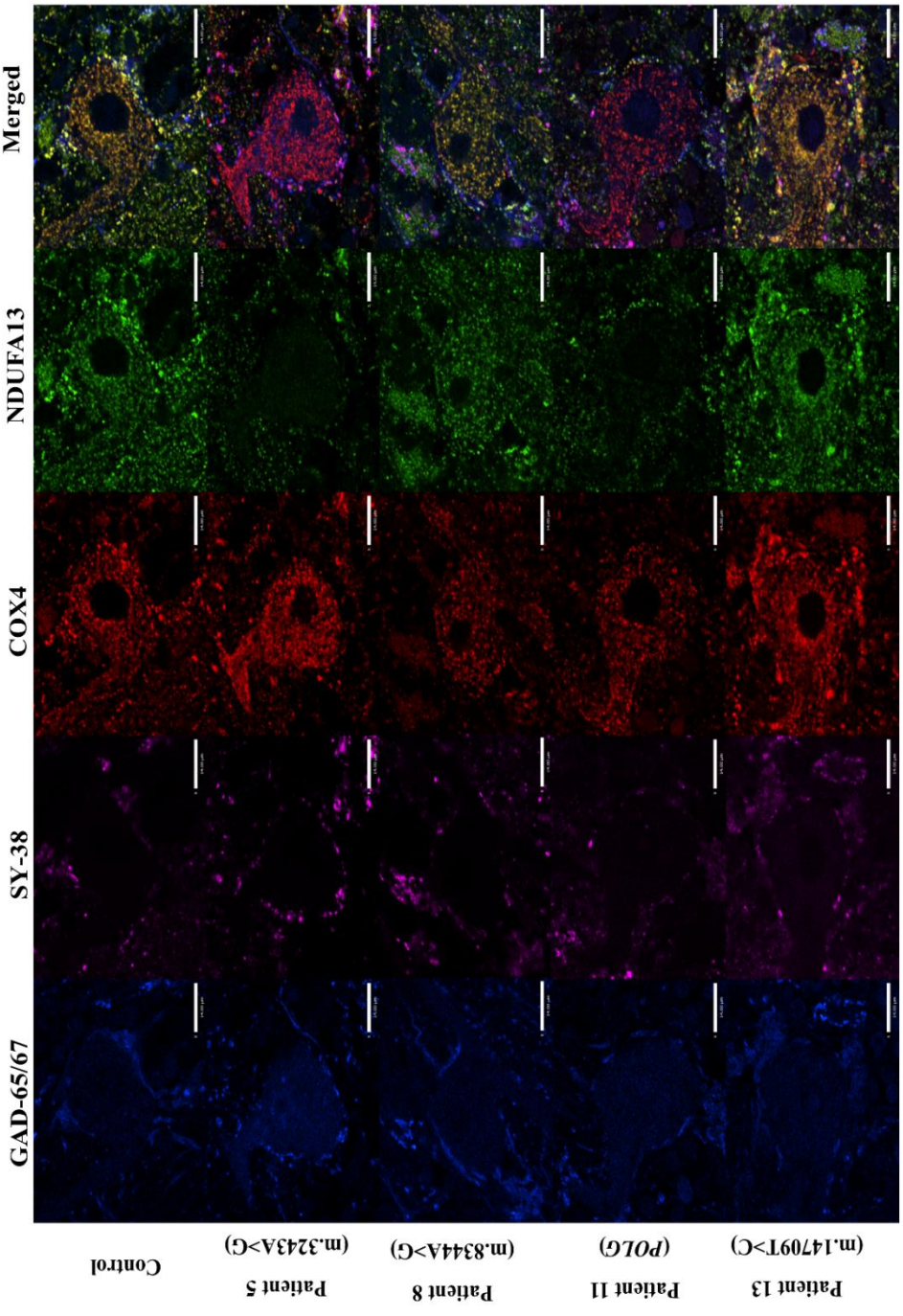

Figure 4- 3: Purkinje cell bodies immunofluorescently stained against glutamic acid decarboxylase (GAD-65/67), synaptophysin (SY-38), mitochondria (COX4) and NADH dehydrogenase [ubiquinone] 1 alpha subcomplex subunit 13 (NDUFA13).

Control Purkinje cell bodies demonstrate abundance of mitochondria with intact complex I, since COX4 is co-localised with NDUFA13. In contrast and despite maintained density of mitochondria, some patient cells are deficient for complex I demonstrated by lack of NDUFA13 immunoreactivity (Patient 5, m.3243A>G; Patient 11, POLG). For some patients though, the majority of cells were detected with normal NDUFA13 expression, constituting the levels of complex I expression comparable to that of controls (Patient 8, m.8344A>G; Patient 13, m.14709T>C). Scale bar: 14μm.

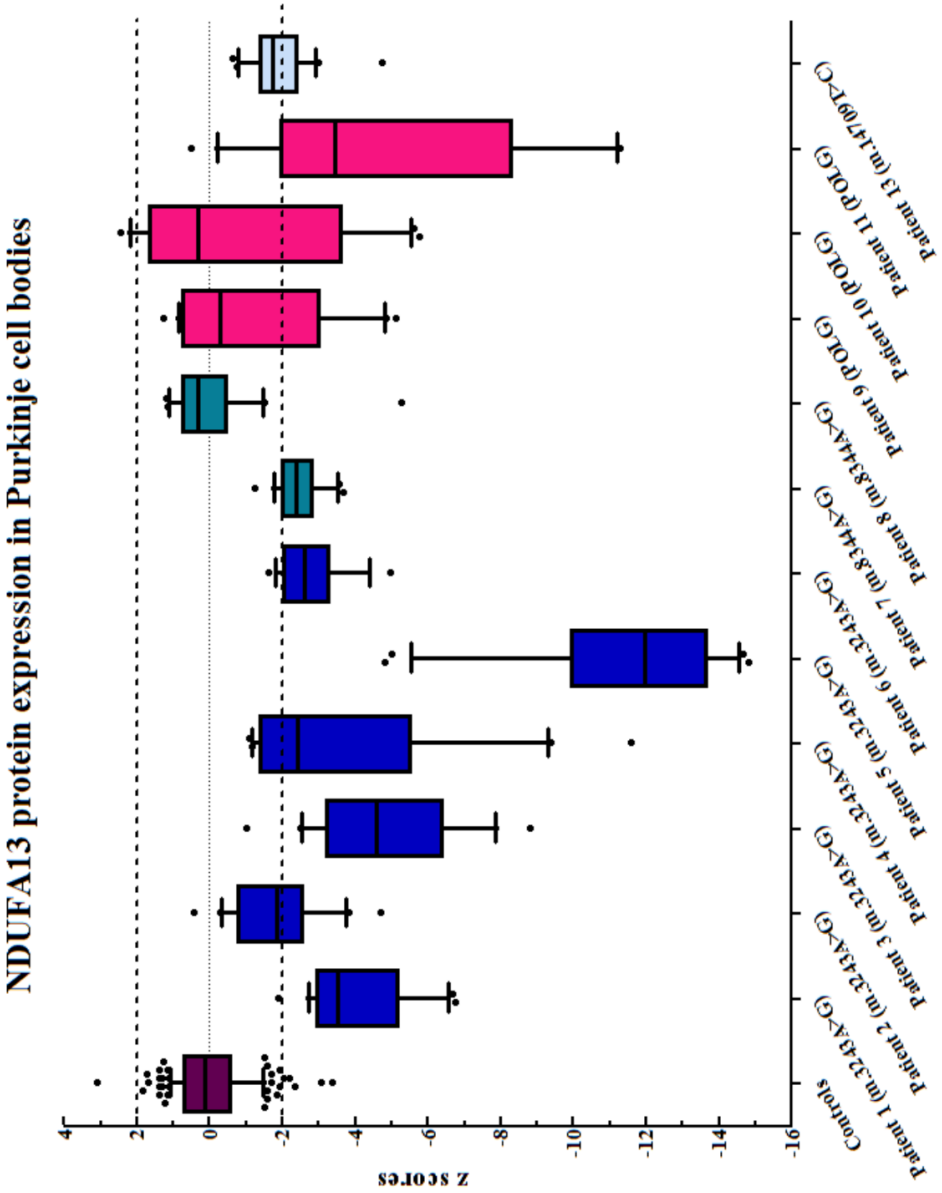

Figure 4- 4: Complex I protein expression in Purkinje cell bodies.

The z score values for NDUFA13 expression in control cells lie within the ±2 SD limits for normality, while patient values are variably different. Patients with the m.3243A>G point mutation (Patients 1-6) generally demonstrate the most severe deficiencies, with patient 5 having a median z score = -12SDs. Two patients with recessive *POLG* mutations (Patient 9 and 10) and a patient with the m.8344A>G point mutation have z score values comparable to that of controls, while patient 7 (m.8344A>G) and patient 13 (m.14709T>C) possess cells with low complex I expression (NDUFA13z< -2SDs). Each data point represents a single Purkinje cell (n=20 for each control or case).

	Controls	Pt1	Pt2	Pt3	Pt4	Pt5	Pt6	Pt7	Pt8	Pt9	Pt10	Pt11	Pt13
Purkinje cell bodies													
Normal (-2< CI_z <2SDs)	99%	5%	55%	5%	45%	0%	21%	25%	95%	70%	75%	26%	62%
Low (CI_z <-2SDs)	1%	20%	30%	15%	15%	0%	42%	60%	0%	5%	0%	16%	33%
Deficient (CI_z <-3SDs)	0%	35%	10%	20%	0%	0%	21%	15%	0%	5%	0%	21%	0%
Very deficient (CI_z <-4SDs)	0%	40%	5%	60%	40%	100%	16%	0%	5%	20%	25%	37%	5%
GABAergic presynaptic terminals													
Normal (-2< CI_z <2SDs)	98%	43%	92%	68%	67%	14%	41%	10%	66%	64%	90%	2%	12%
Low (CI_z <-2SDs)	2%	24%	5%	11%	22%	23%	30%	41%	27%	13%	6%	6%	38%
Deficient (CI_z <-3SDs)	0%	11%	1%	6%	7%	27%	18%	33%	5%	6%	1%	30%	30%
Very deficient (CI_z <-4SDs)	0%	22%	1%	15%	4%	36%	11%	15%	2%	17%	3%	62%	20%

Table 4- 4: The percentage of Purkinje cell bodies and presynaptic terminals that are normal, low, deficient or very deficient for NDUFA13 protein expression.

Although the majority of control cells and synapses are normal for NDUFA13, patients possess a mixture of normal, low, deficient and very deficient neuronal compartments.

Similarly, inhibitory presynaptic terminals present around control dentate nucleus neurons contained mitochondria with normal levels of NDUFA13 protein expression (NDUFA13z = 0.0562SDs) (Figure 4- 5). Patient GABAergic synapses had similar COX4 expression to that of control terminals (two sample t-test, p= 0.620) nevertheless, NDUFA13 expression was variably different. Inhibitory presynaptic terminals that belonged to patients had mild (Patient 1, m.3243A>G), intermediate (Patient 7, m.8344A>G) or severe (Patient 11, *POLG*) decreases in NDUFA13 expression (Figure 4- 5). Z score analysis for NDUFA13 expression demonstrated that all patients possessed a mixture of normal, low, deficient or very deficient synapses (Figure 4- 6) (Table 4- 4). In contrast to Purkinje cell bodies, synaptic NDUFA13 protein expression was similar between patients with the m.3243A>G point mutation and others when genetic defects were grouped (m.8344A>G, m.14709T>G and recessive *POLG*) (Mann Whitney U test, p value= 0.6889). Neither PMI (rho= -0.126, p value= 0.696) (Appendix A) nor fixation length (rho= -0.007, p value= 0.983) affected the z score values for NDUFA13 expression in inhibitory presynaptic terminals (Spearman's rank correlation).

Interestingly, NDUFA13 expression in synapses was negatively related to the NMDAS scores for cerebellar ataxia such that patients with higher NMDAS scores, indicative of more severe ataxia, possessed synapses with lower NDUFA13 z scores, consistent with more complex I deficiency (rho= -0.60, p value= 0.0493). Likewise, synaptic complex I protein expression is inversely related to the percentage of dentate nucleus neuronal loss. That is patients with lower synaptic complex I protein expression, indicative of more complex I deficiency, had more dentate nucleus neuronal loss (rho= -0.92, p= 0.0013) (Spearman's rank correlation).

NDUFA13 expression is variable in Purkinje cells and GABAergic synapses among patients with different genetic diagnoses. Patients harbouring the m.3243A>G point mutation have more pronounced complex I deficiency in Purkinje cell bodies compared to presynaptic terminals. On the contrary, patients with other genetic defects (m.8344A>G, m.14709T>C and recessive *POLG*) possess Purkinje cells that are less deficient relative to synapses (Table 4- 4). Following statistical analysis, there is a significant difference between the two patient groups (Mann Whitney U test for the difference between Purkinje cell and synaptic deficiency, p value= 0.0051). When taking into account the patient group as a whole, there is no difference in complex I expression levels between neuronal cell bodies and axonal terminals (Wilcoxon Signed-Rank test of differences, p= 0.666).

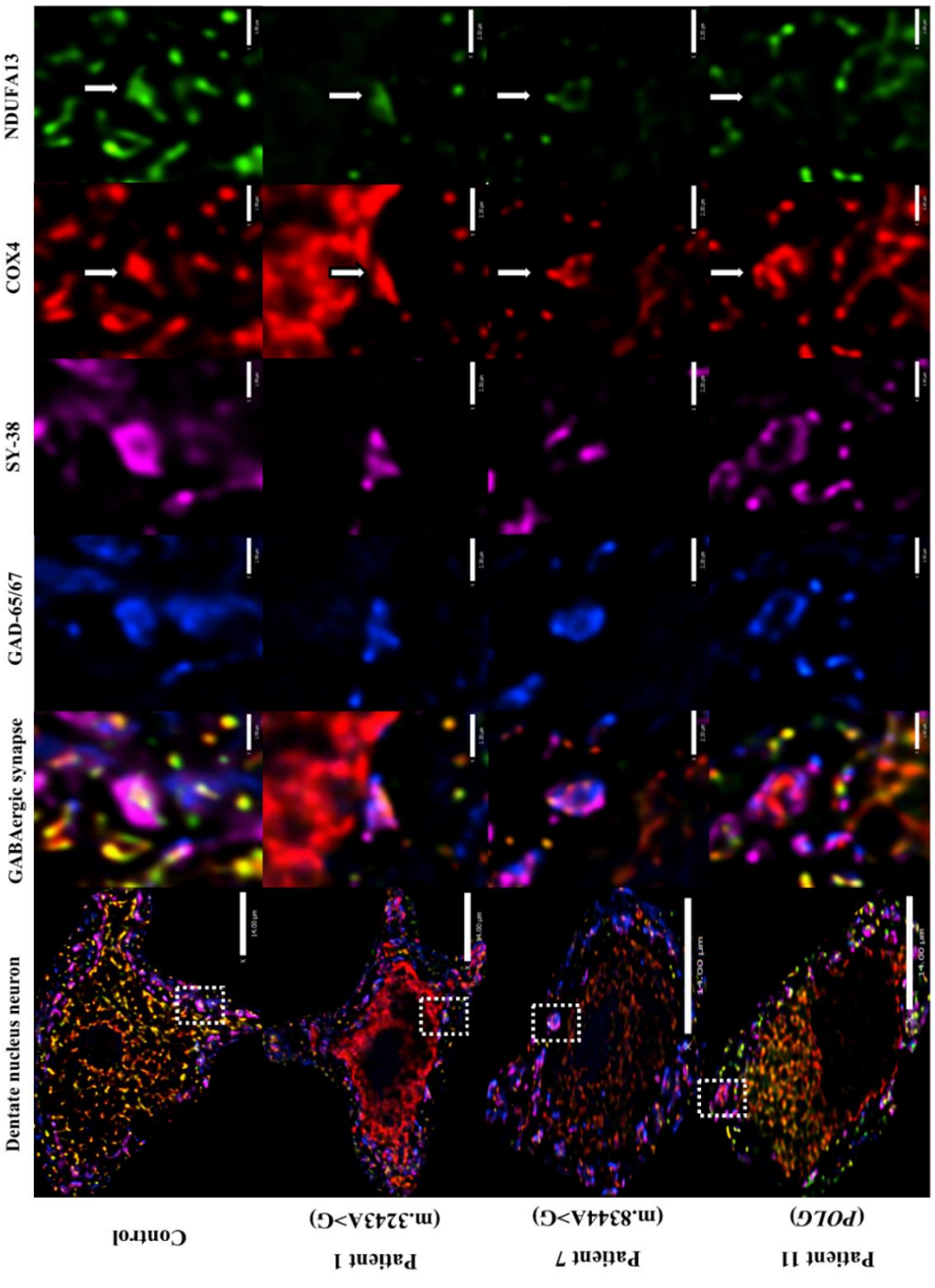

Figure 4- 5: NDUFA13 protein expression in GABAergic presynaptic terminals around dentate nucleus neurons.

Mitochondria (COX4) are co-localised with NDUFA13 (green) in control inhibitory synapses (puncta where GAD-65/67 co-exists with SY-38), indicative of complex I intact axonal terminals (Scale bar: 1.9µm). Despite maintained mitochondrial presence in patient synapses, NDUFA13 protein expression is mildly (Patient 1, m.3243A>G) (Scale bar: 2.3µm), intermediately (Patient 7, m.8344A>G) (Scale bar: 2.3µm) or severely (Patient 11, POLG) (Scale bar: 1.9µm) decreased.

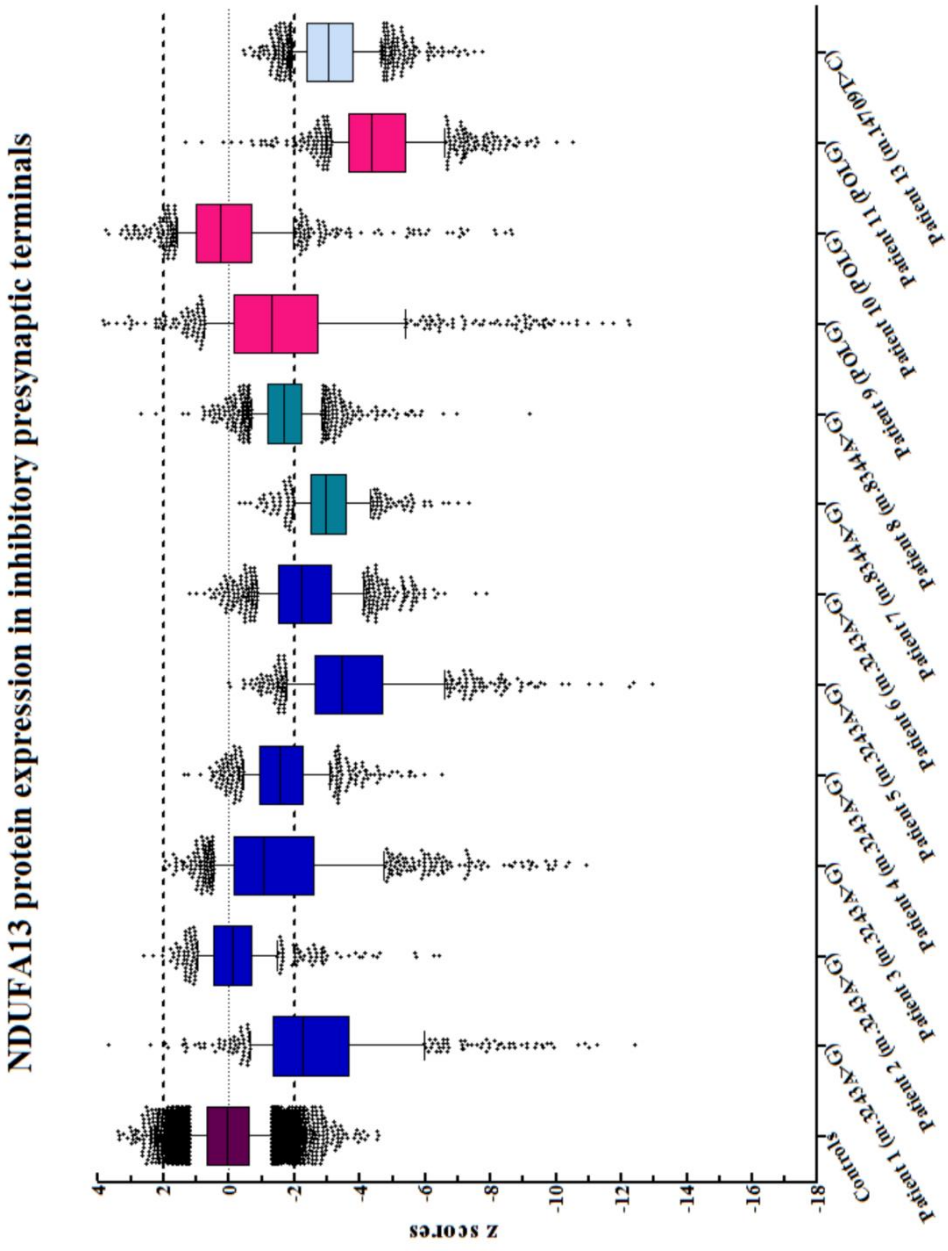

Figure 4- 6: Standard deviation limits for NDUFA13 protein expression quantification in Purkinje cell synaptic terminals.

All patients contain synapses which are normal (2< NDUFA13z <-2SDs), low (NDUFA13z<-2SDs), deficient (NDUFA13z<-3SDs) and very deficient 9NDUFA13z<-4SDs) for the protein. There is pronounced variability between patients with the same genetic defect (e.g. Patient 7 vs. Patient 8, m.8344A>G), whilst NDUFA13 protein expression is comparable amongst the whole patient cohort. Each data point represents a single synaptic readout (synaptic terminals detected around 20 neurons).

4.4.2 Heteroplasmic levels of mtDNA in neuronal cell bodies and synapses

Defining the levels of mutated over wild type mtDNA in Purkinje cell bodies and presynaptic terminals of patients with the m.3243A>G and m.8344A>G point mutation indicated high heteroplasmic levels in both neuronal compartments (Figure 4- 7). Some synaptic values were near homoplasmic (Patient 1, 2 and 3; m.3243A>G), whilst the levels of mutated mtDNA are comparable between the two neuronal sub-compartments (Wilcoxon Signed-Rank test of differences, p=1) (Figure 4- 7).

The levels of heteroplasmic mtDNA levels in Purkinje cell bodies and inhibitory presynaptic terminals are not related to NDUFA13 z score values for complex I deficiency in the corresponding sub-neuronal compartments (Purkinje cell bodies: rho= -0.6, p value= 0.285; Presynaptic terminals: rho= -0.3, p value= 0.624) (Spearman's rank correlation).

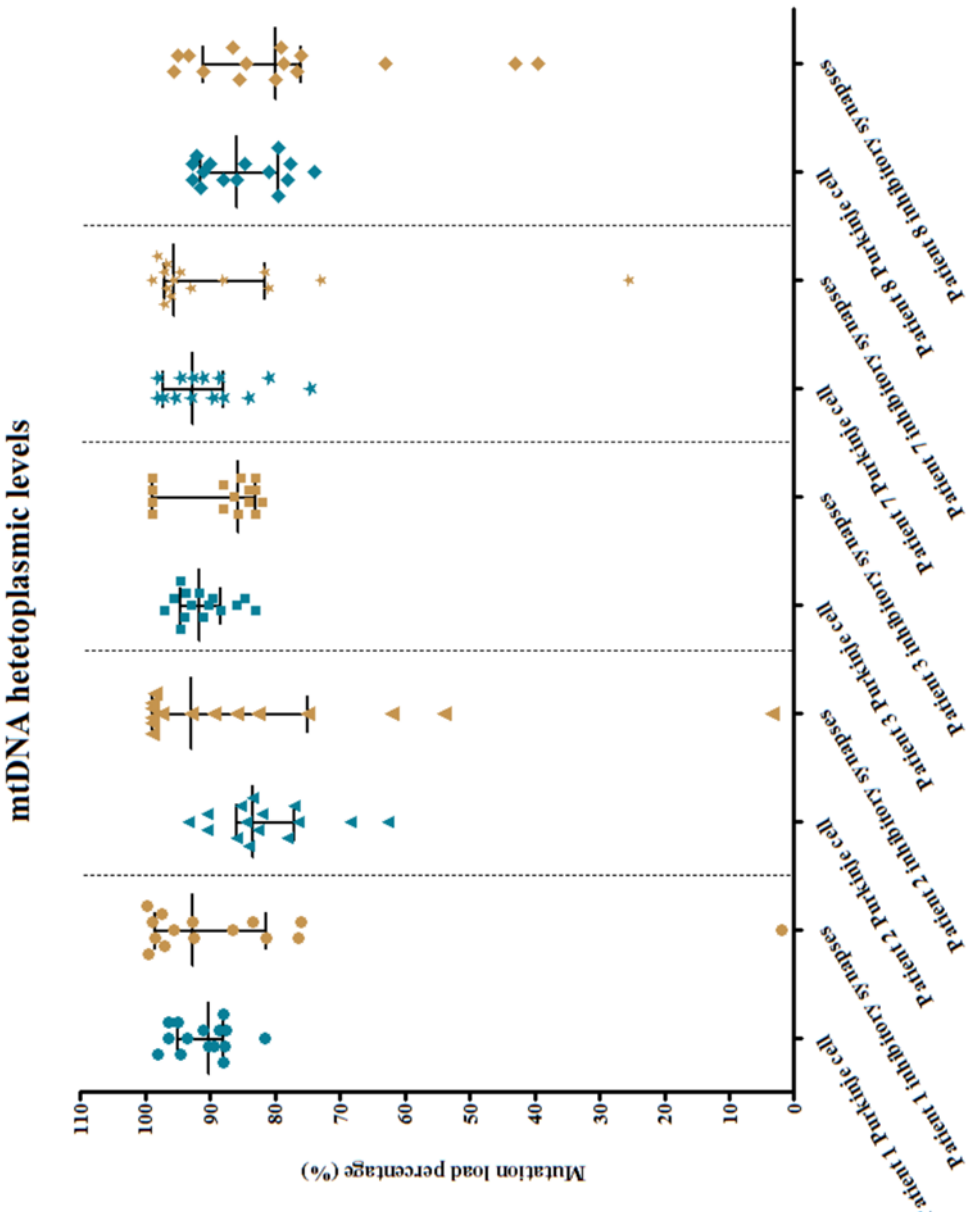

Figure 4- 7: Heteroplasmic mtDNA levels in Purkinje cells and presynaptic terminals.

The level of mutated mtDNA molecules in isolated Purkinje cell bodies and inhibitory presynaptic terminals from patients with mtDNA point mutations (m.3243A>G and m.8344A>G). Data points represent independent read-outs and bars represent medians with interquartile ranges (n=15 for both populations).

4.4.3 Remodelling of GABAergic input to the dentate nucleus

Quadruple immunofluorescence and confocal microscopy facilitated the numerical and structural investigation of GABAergic pre- and postsynaptic compartments found on the periphery and proximal dendrites of dentate nucleus neurons. Evaluating the number of inhibitory presynaptic terminals revealed decreased Purkinje cell efferent density around dentate nucleus neurons in the majority of patients (Patients 1, 2, 4, 5, 7, 9-11), though the derived z score values were within the normal ±2 SD limits (Figure 4- 8). Decreased inhibitory synapse density is in agreement with Purkinje cell loss previously documented for these patients (Table 4- 1) (Lax *et al*., 2012) and indeed, there is a significant negative relationship between the percentage of Purkinje cell loss and the number of synapses detected (rho= -0.74, p value= 0.02) (Spearman's rank correlation). Moreover, patients 3 (m.3243A>G), 8 (m.8344A>G) and 13 (m.14709T>C) demonstrated maintained synaptic and preserved Purkinje cell numbers (Figure 4- 8) (Table 4- 1).

Remarkably, residual synapses were enlarged since synaptic number and size (volume – μm^3) were negative correlated (rho= -0.615, p value= 0.037). The volume of inhibitory presynaptic terminals is displayed in Appendix B. Synaptic number counts were not affected by PMI (rho=0.522, p value=0.082) (Appendix A) or fixation time (rho=0.011, p value= 0.980) nor was synaptic volume (PMI: rho= -0.595, p value= 0.120 (Appendix A); Fixation length: rho=-0.688, p value=0.059) (Spearman's rank correlation).

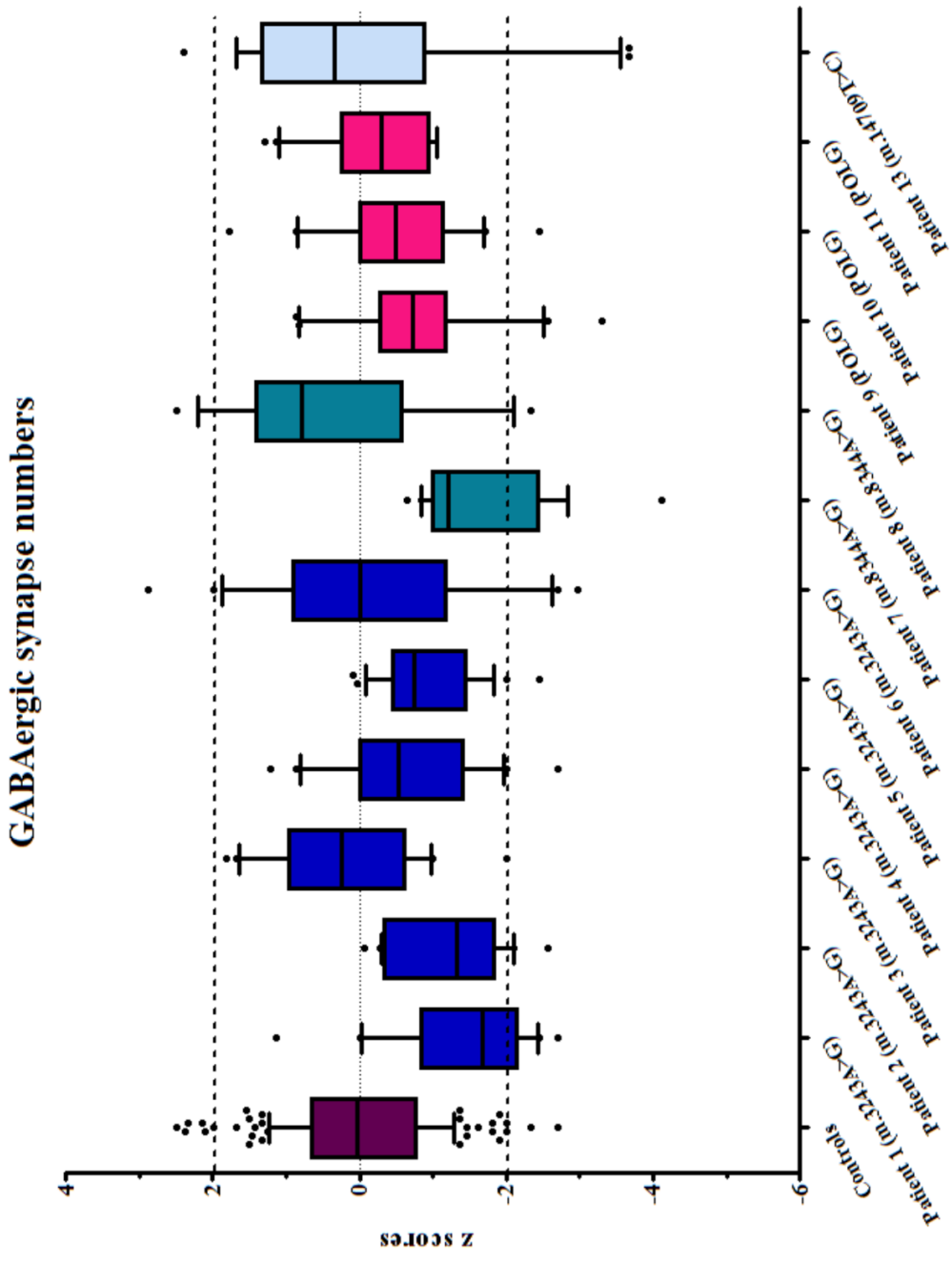

Figure 4- 8: Z scores for the number of GABAergic presynaptic terminals surrounding dentate nucleus neurons.

Most patients (8 out of 12) had decreased Purkinje cell efferent density compared to controls, the standard deviation limits for the numbers of inhibitory synapses fall within the normal limits though. Each data point reflects the number of synapses detected around a single dentate nucleus neuron (n=20).

4.4.4 Complex I deficiency in Purkinje cell dendrites

The expression of NDUDFA13 and COX4 proteins was assessed in calbindin immunoreactive Purkinje cell dendritic trees extending in the molecular cell layer of the cerebellar cortex using triple immunofluorescence. As with other neuronal sub-compartments, control neuronal dendrites contained a high density of mitochondria with intact complex I protein expression (Figure 4- 9). COX4 was a reliable marker for mitochondrial abundance since protein expression in neuronal dendrites did not show any difference between controls and patients (two sample t-test, p value= 0.232), however NDUFA13 protein expression was variably decreased in line with complex I deficiency.

As shown in Figure 4- 9, there were patients whose dendrites completely lack NDUFA13 immunoreactivity (Patient 4, m.3243A>G), in others NDUFA13 expression was considerably lower relative to COX4 expression (Patient 7, m.8344A>G), while there were also patients which possessed dendrites with preserved complex I expression (Patient 10, POLG). In agreement with observations made on neuronal cell bodies and GABAergic axonal terminals, there is a great extent of intra- and inter-patient variability in dendritic NDUFA13 protein expression (Figure 4- 10). A patient may contain cells whose dendrites have normal levels of the protein (2 <NDUFA13z< -2SDs) and cells whose dendrites are deficient for complex I (NDUFA13z< -4SDs) (e.g. Patient 6, m.3243A>G), whilst patients with the same genetic defect might have very different dendritic complex I expression levels (Patient 7 vs. Patient 8, m.8344A>G) (Figure 4- 10). Patients with the m.3243A>G point mutation (Patients 1-6) generally demonstrate lower z score values for NDUFA13 in neuronal dendrites (Figure 4- 10), compatible with the increased percentage for dendrites that are low, deficient or very deficient for NDUFA13 when these are quantified (Table 4- 5).

Indeed, dendritic complex I deficiency is more pronounced in patients with the m.3243A>G mutation compared to other patients when genetic defects are grouped (m.8344A>G, m.14709T>C and *POLG*) (two sample t-test, p value= 0.018). Furthermore, the level of complex I deficiency in Purkinje cell dendrites is comparable to that of Purkinje cell bodies (Wilcoxon Signed-Rank test of differences, p= 0.290). Z score values for NDUFA13 protein expression in neuronal dendrites were not affected by the length of formalin fixation (rho= -0.298, p value= 0.347) or by post-mortem interval (rho= -0.018, p value= 0.957) (Spearman's rank correlation) (Appendix A).

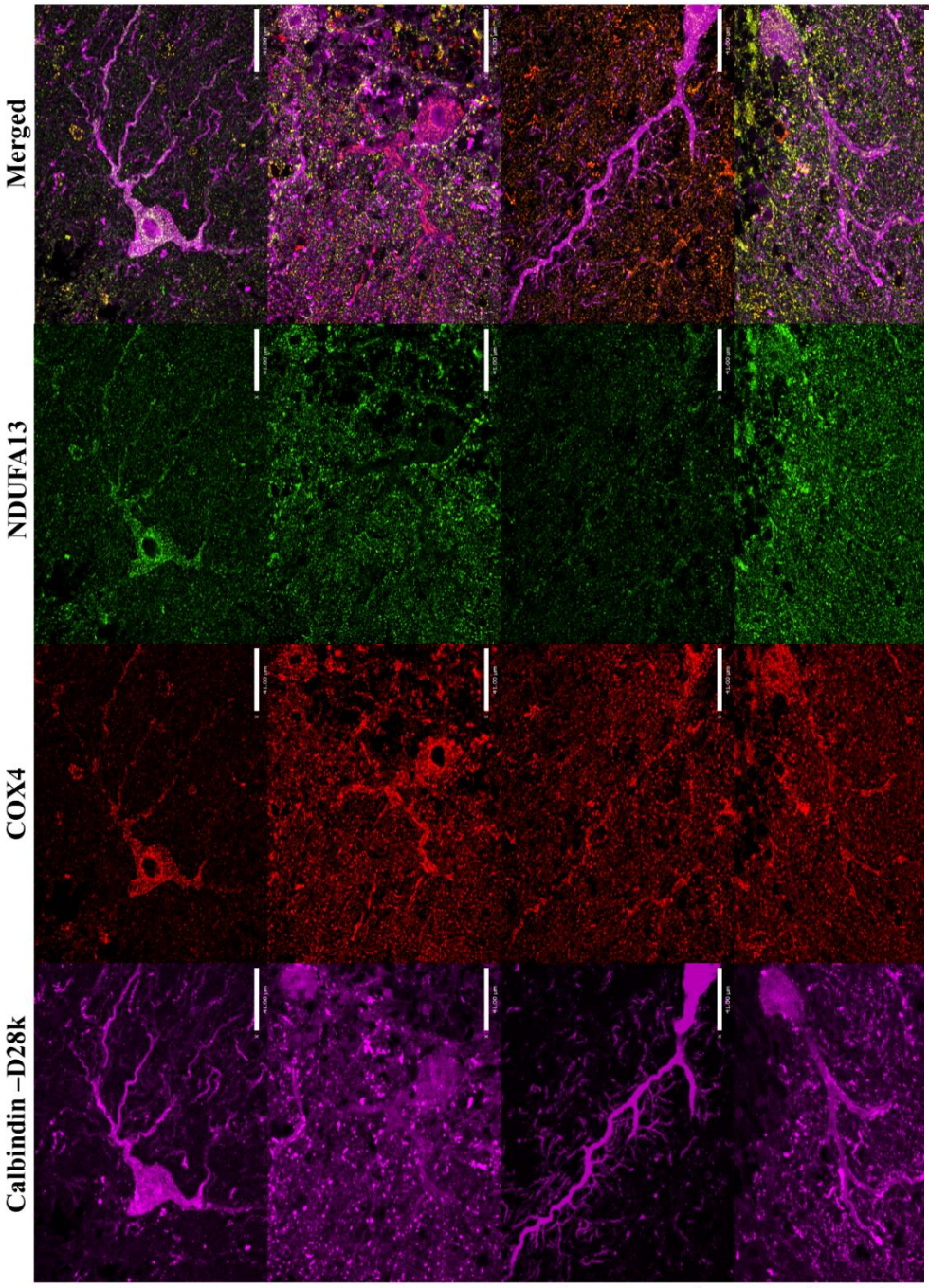

Figure 4- 9: Triple immunofluorescence for the investigation of NDUFA13 protein expression in Purkinje cell dendrites.

Whilst control neuronal dendrites have high mitochondrial density with equally high expression of NDUFA13, NDUFA13 protein expression in patient dendrites differs. Patient 4 (m.3243A>G) is exhibitive of dendritic complex I deficiency (lack of NDUFA13 immunoreactivity), while Patients 7 (m.8344A>G) and 10 (*POLG*) have decreased or normal protein expression respectiveley. Scale bar: 41µm.

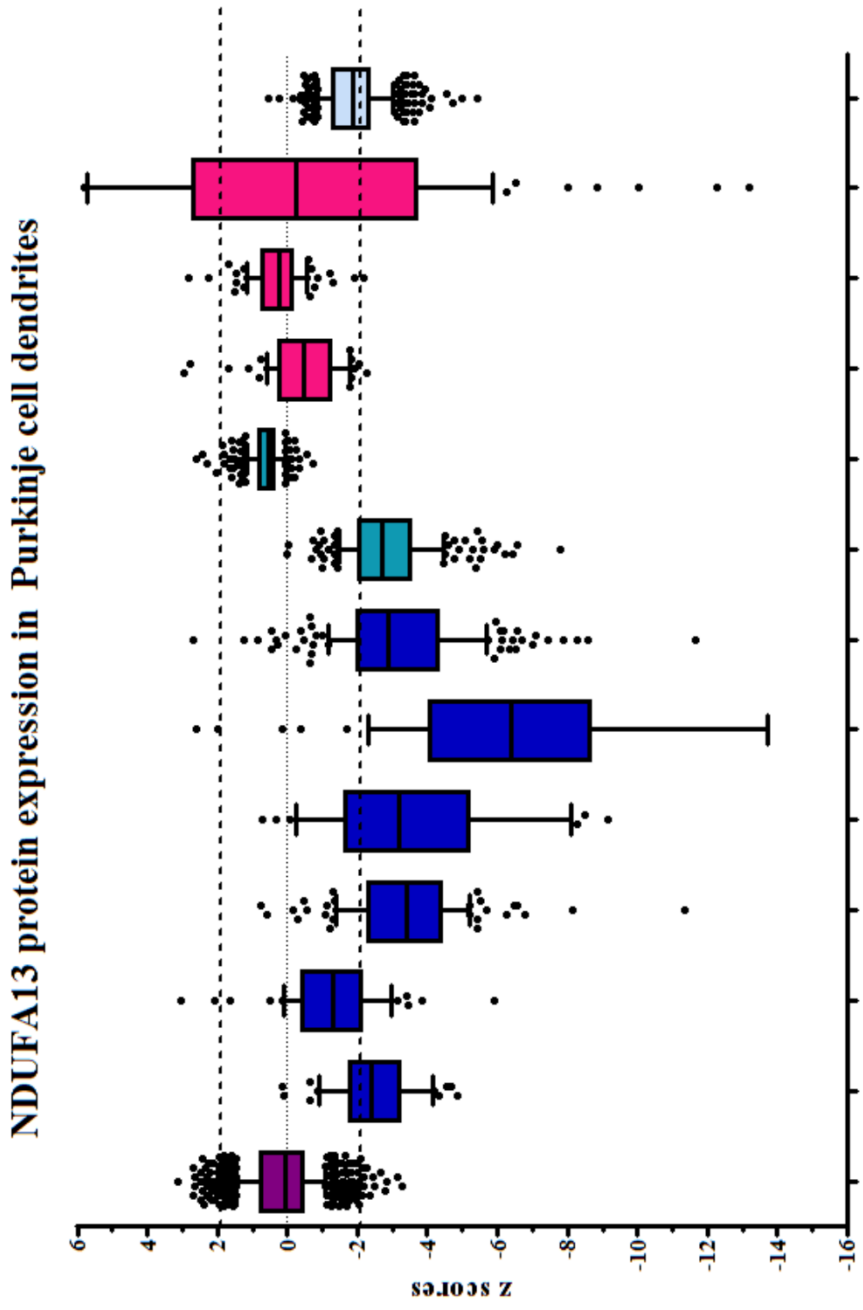

Figure 4- 10: NDUFA13 protein expression quantification in Purkinje cell dendrites.

Generally, patients with the m.3243A>G point mutation (Patient 1-6) have more severe complex I defects in neuronal dendrites compared to the remaining patients (Patient 7-13; m.8344A>G, *POLG*, m.14709T>C). Each data point reflects a single dendritic arbor (dendrites sampled from twenty Purkinje cells in each control and case).

	Controls	Pt1	Pt2	Pt3	Pt4	Pt5	Pt6	Pt7	Pt8	Pt9	Pt10	Pt11	Pt13
Purkinje cell dendrites													
Normal (-2< CI_z <2SDs)	99%	29%	69%	22%	29%	9%	25%	23%	100%	97%	99%	63%	58%
Low (CI_z <-2SDs)	1%	34%	21%	16%	19%	9%	28%	40%	0%	3%	1%	6%	32%
Deficient (CI_z <-3SDs)	0%	27%	8%	27%	13%	7%	16%	23%	0%	0%	0%	10%	8%
Very deficient (CI_z <-4SDs)	0%	10%	2%	35%	39%	75%	31%	14%	0%	0%	0%	21%	2%

Table 4- 5: The percentage of Purkinje cell dendrites that are normal, low, deficient or very deficient for each of the twelve patients included in this study

4.4.5 Calbindin immunoreactivity and dendritic extension

As demonstrated in Figure 4- 11, the patient neuronal dendrites are equally as expanded as control dendrites, since all the patient z score values for dendritic length lie within the normal ±2SD limits. Likewise, Calbindin expression is normal in all patients (2 <Calbindinz< -2SDs) though some patient median z score values are decreased relative to controls (Figure 4- 12). Dendritic extension was not affected by fixation length (rho= 0.340, p value= 0.279) or by PMI (rho= -0.567, p value= 0.054) (Appendix A), neither were Calbindin z score values (Fixation length: rho= 0.362, p value= 0.248; PMI: rho= 0.060, p value= 0.854 (Appendix A)).

Interestingly, there is a significant positive relationship between the z score values for Calbindin expression and dendritic extension (rho= 0.604, p value= 0.024), suggesting that the patients possessing the longest dendrites are the ones with increased Calbindin expression (Spearman's rank correlation). Surprisingly, Calbindin expression is significantly positively related to NMDAS scores for cerebellar ataxia implying that patients with higher scores, thus more severe ataxia, have high Calbindin immunoreactivity (rho= 0.627, p value= 0.039) (Spearman's rank correlation).

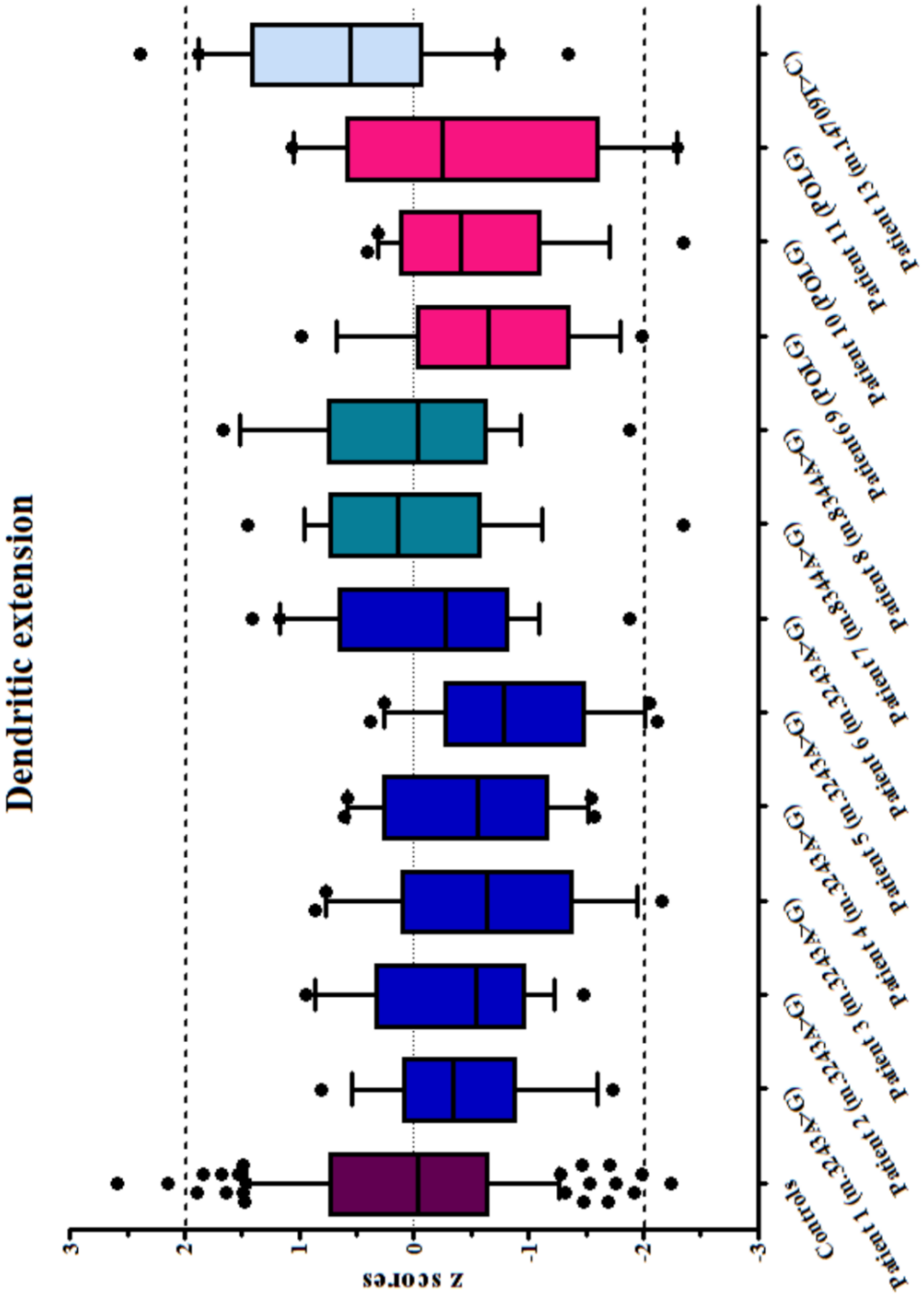

Figure 4- 11: Standard deviation limits and z score values for Purkinje cell dendritic extension.

Despite the fact that the majority of patients (9 out of 12) have decreased z score values relative to controls, all median z scores fall within normal ±2SD limits. Each data point represents a single Purkinje cell (n=20).

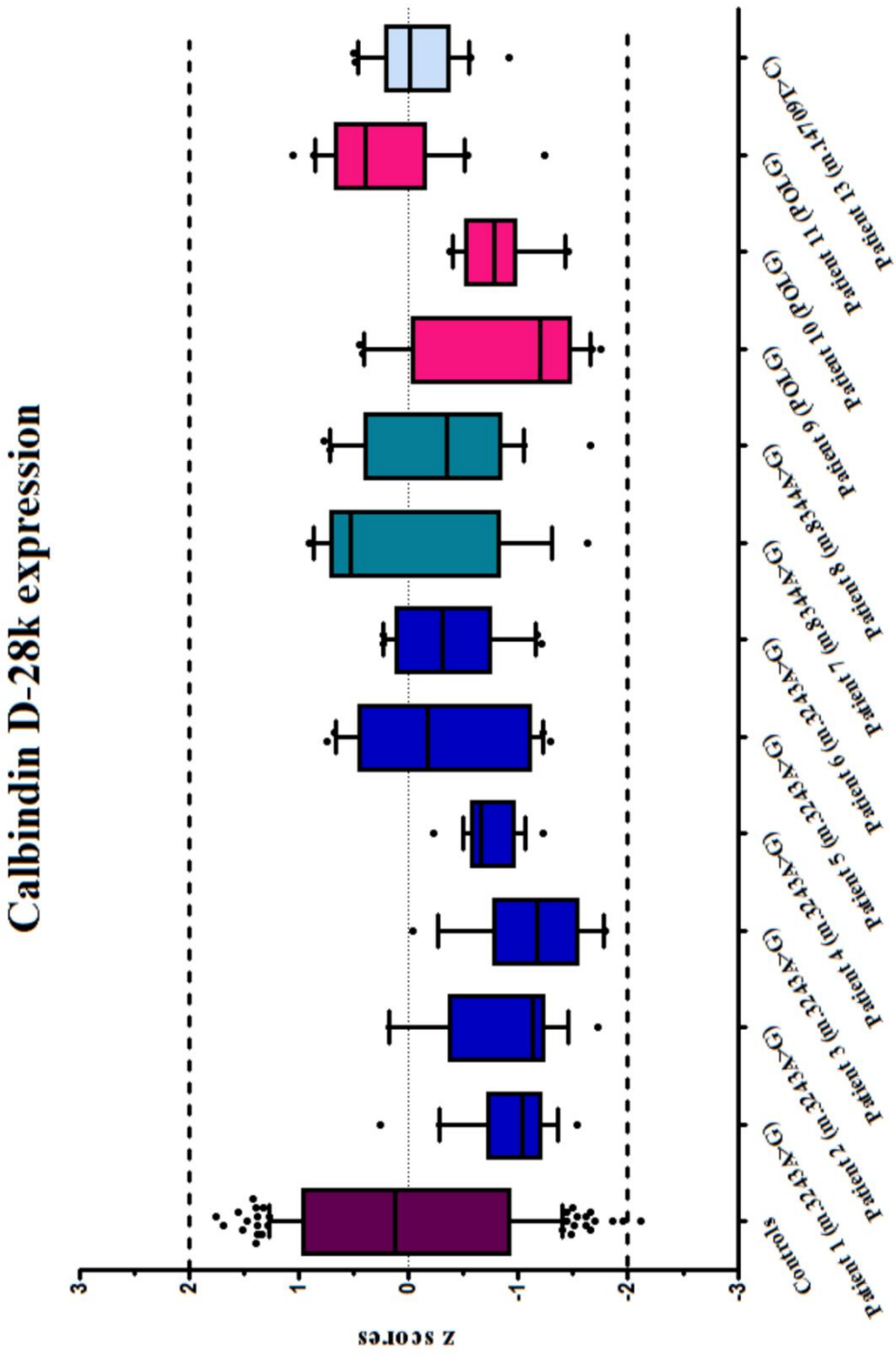

Figure 4- 12: Quantification of Calbindin protein expression in Purkinje cells using z score values and standard deviation limits.

9 out of 12 patients exhibit decreased protein immunoreactivity, as shown by lower median z score values. The difference with controls is non-significant since all patient data points fall within the normal ±2SD limits. Each data point represents a single Purkinje cell (n=20).

4.5 Discussion

Cerebellar ataxia is a common neurological deficit and an important cause of disability in patients with mitochondrial disease (Tzoulis *et al.*, 2006; Hudson *et al.*, 2008; McFarland *et al.*, 2010). The exact underlying mechanisms that account for the genesis and progression of this condition remain largely unknown, though valuable neuropathological studies performed in the past reveal Purkinje cell vulnerability to mitochondrial dysfunction (Tanji *et al.*, 1999; Sparaco *et al.*, 2003; Hakonen *et al.*, 2008; Lax *et al.*, 2012). The importance of mitochondrial function on synaptic transmission combined with the significance of the Purkinje cell-dentate nucleus synapse in establishing intracerebellar communication and extracerebellar information processing, place the inhibitory Purkinje cell synapses onto dentate nucleus neurons at the centre of attention. In this study, I have used a previously developed quantitative quadruple immunofluorescent technique (see Chapter 3) to assess the degree of complex I deficiency in Purkinje cell bodies, dendrites and inhibitory presynaptic terminals of twelve patients with mitochondrial disease. Moreover, I have quantified the density and the size of GABAergic synapses to the dentate nucleus in an attempt to gain further insights into the impact of mitochondrial dysfunction onto the synapse. Finally, I have examined the level of Purkinje cell dendritic tree arborisation and the expression of a Ca^{2+}-binding protein in order to assess the presence of neurodegenerative signs.

I demonstrate that Purkinje cell bodies, dendrites and GABAergic presynaptic terminals to the dentate nucleus have decreased NDUFA13 protein expression levels in patients relative to controls. Complex I deficiency in Purkinje cell bodies and neuronal dendrites is more prominent in patients harbouring the m.3243A>G point mutation, consistent with studies performed in skeletal muscle of patients with m.3243A>G point mutations and demonstrate low complex I activity and low complex I subunit protein expression (Moraes *et al.*, 1992; Petruzzella *et al.*, 1994; Koga *et al.*, 2000). On the contrary, complex I protein expression in Purkinje cell presynaptic terminals is similar amongst patients with different genetic diagnoses. The length of formalin fixation and post-mortem interval do not affect the levels of complex I protein expression in any of the neuronal subtypes or sub-neuronal compartments studied, implying that the observed changes are due to disease mechanisms.

There is considerable intra- and inter-patient variability across all neuronal sub-compartments investigated, exemplifying the phenotypic heterogeneity of mitochondrial disease (Moggio *et al.*, 2014). Generally, the degree of complex I expression is similar between Purkinje cell pre-/post-synaptic compartments (presynaptic terminals and dendrites respectively) and Purkinje

cell bodies. Likewise, molecular genetic investigation of patients with mtDNA point mutations (m.3243A<G and m.8344A>G) shows that mutated mtDNA heteroplasmic levels are similar between Purkinje cell bodies and inhibitory presynaptic terminals, though mutated mtDNA levels do not correlate with complex I protein expression in either of the two neuronal compartments.

Mitochondrial turnover takes place in neuronal cell bodies, via a process known as mitophagy, and assures the recycling of damaged organelles (Cai *et al.*, 2012). The high metabolic profile of a synapse implies that there needs to be a constant removal (via retrograde transport) of dysfunctional mitochondria and supply of newly-synthesised organelles to the region in order to maintain the balance between energy demand and supply (MacAskill and Kittler, 2010; Sheng, 2014). Similar complex I expression levels and mtDNA heteroplasmic percentages between synaptic and somatic neuronal compartments implies that deficient mitochondria are not efficiently removed from the synapse for degradation and/or that mitochondrial degradation mechanisms are impaired. Mitochondrial transport mechanisms to/from the synapse could therefore be malfunctional in mitochondrial disease, consistent with evidence for impaired neuronal transport in other neurodegenerative disorders (Chevalier-Larsen and Holzbaur, 2006; Morfini *et al.*, 2009; Kanaan *et al.*, 2013). Moreover, evidence for dysfunctional mitochondrial autophagic mechanisms (mitophagy) has been documented for common neurodegenerative disorders (Ghavami *et al.*, 2014), hinting towards their use as therapeutic targets (Santos *et al.*, 2011).

Remarkably, NDUFA13 protein expression in GABAergic presynaptic terminals is related to cerebellar ataxia suggesting that synaptic complex I deficiency might be important in mitochondrial disease pathogenesis. This would be compatible with other neurodegenerative disorders according to which, synaptic disturbances have a central role in disease initiation and progression (Marcello *et al.*, 2012; Picconi *et al.*, 2012). Induction and/or overexpression of a cold-shock protein (RBM3) prevents synapse loss and reverses cognitive deficits in neurodegenerative mouse models, suggesting that synaptic pathology is likely to be reversible and highlighting the potential use of synapses as a therapeutic drug target (Peretti *et al.*, 2015).

Synaptic activity drives local ATP requirements which are met by mitochondrial-generated energy (Rangaraju *et al.*, 2014). ATP generated by mitochondria fuels synaptic vesicle transport, docking, exocytosis and recycling, thus directly affects synaptic transmission (Rowland *et al.*, 2000; Perkins *et al.*, 2010). Mitochondrial function is also key in maintaining ionic gradient balance in pre- and post-synaptic terminals, allowing for the initiation of action

potentials and recovery following depolarisation respectively (Billups and Forsythe, 2002). Furthermore, the importance of mitochondrial respiratory chain function in synaptic oxygen consumption and energetic availability have been demonstrated in rat synaptosomal (Telford *et al.*, 2009) and extracted mitochondrial preparations (Davey *et al.*, 1998). Complex I deficiency in the inhibitory presynaptic terminals of patients with mitochondrial disease is therefore likely to have adverse effects for synaptic function.

Three-dimensional reconstruction of inhibitory synapses to the dentate nucleus enabled the investigation of synaptic number and size (in volume). Interestingly, the majority of patient Purkinje cells appear to have lost some of their inhibitory contacts to the dentate nucleus, while the volume of remaining ones is increased. This change can be suggestive of a compensatory mechanism that takes place to maintain the total synaptic contact area of dentate nucleus neurons, thus increasing the size of residual synapses in case of loss. Likewise, a model proposed by Scheff and Price (2003) suggests that at the early stages of Alzheimer's disease denervated neurons release signals that drive the formation of new synapses or enlargement of remaining ones in order to keep the total synaptic contact area stable (Scheff and Price, 2003).

Additional to inhibitory presynaptic terminals to the dentate nucleus, Purkinje cell dendrites and axons have previously been demonstrated to be structurally different in patients with mitochondrial disease. Purkinje cell axons proximal to neuronal cell bodies are swollen, giving rise to "Torpedoes", whereas Purkinje cell trees are thicker (forming "cactus-like" structures) and more extended (Tanji *et al.*, 1999; Lax *et al.*, 2012). Quantification of dendritic tree extension in this study demonstrates that patient Purkinje cell dendrites are equally as extended as control ones, contrary to what is commonly accepted for mitochondrial disease. It here has to be noted that quantification of dendritic length using thin tissue sections is not optimum since it only allows tissue sub-sampling and relies on the orientation that the tissue has been cut. Thus, it is likely that the results obtained from this study are not entirely reflective of Purkinje cell dendritic expansion in the cerebellum as a whole and instead only provide information for the region sampled. Alternatively, the use of thicker tissue sections (250μm -500μm) combined with recently developed methods that allow tissue clearing and neuronal structure preservation (e.g. CLARITY) would be more informative with regards to Purkinje cell dendritic arborisation (Chung and Deisseroth, 2013).

Cognition and motor coordination have been demonstrated to be regulated by a calcium-binding and buffering protein, Caldindin-$D_{28k.}$ Deletions (Barski *et al.*, 2003) or null mutations (Airaksinen *et al.*, 1997) of the protein result in altered fast calcium transients accompanied by

permanent motor coordination disturbances and ataxia. The protein is suggested to have a neuroprotective role from Ca^{2+} overload (Heizmann and Braun, 1992) and excitotoxicity (Iacopino *et al.*, 1992) and decreased protein expression levels have been linked to the pathogenesis of many neurodegenerative conditions (Heizmann and Braun, 1992) and aging (Iacopino and Christakos, 1990). Elevated calbindin protein expression levels in patients with higher NMDAS scores for cerebellar ataxia detected in this study might be reflective of a protective mechanism taking place in patients with more severe ataxia. Mitochondrial dysfunction in patient Purkinje cells is highly likely to negatively affect the calcium buffering capacity of the organelles, further to their capability for ATP production, thus elevation in Calbindin expression acts to protect the remaining neurons from calcium overload and excitotoxicity. Interestingly, a positive relationship between calbindin expression and dendritic extension is detected implying that extra burden (cytosolic Ca^{2+}) to already deficient mitochondria may negatively affect dendritic arborisation and thus, synaptic contact.

4.5.1 Future work

The importance of the cerebellum in motor coordination and cognition, the frequent presentation of cerebellar ataxia in patients with mitochondrial disease and the extensive neurodegeneration in the olivo-cerebellar pathway of patients, highlight the need for understanding the mechanisms responsible for the initiation and progression of the neuronal loss process. Despite the documentation of respiratory chain protein deficiencies in neuronal cell bodies, dendrites and presynaptic terminals and the demonstration of structural synaptic changes, it is still unclear whether synaptic pathology contributes to neuronal loss.

The use of a reliable, transgenic mouse model that replicates human mitochondrial disease would help determine the sequence and timescale of events that lead to neuronal degeneration. Behavioural mouse testing in parallel with quantitative immunofluorescence against respiratory chain and synaptic proteins will help understand whether mitochondrial dysfunction at the synapse is the one to drive synaptic loss and further determine whether synaptic abnormalities are primarily affecting neuronal health or whether are secondary to neuronal disturbances. The effect exerted by synaptic plasticity and function to neuronal preservation needs to be elucidated if we are to prevent and/or delay neuronal loss progression.

A novel hybrid protein, the slow Wallerian degeneration (Wld^s) protein, has been demonstrated to protect against axonal and synaptic degeneration (Wang *et al.*, 2001; Ferri *et al.*, 2003; Sajadi *et al.*, 2004). In fact, proteomic analysis of striatal synaptic fractions from Wld^s mice revealed altered mitochondrial protein expression, suggesting that differential expression of

mitochondrial proteins and mitochondrial function is likely to play a key role in the neuroprotective phenotype (Wishart *et al.*, 2007). Crossing transgenic mouse models of mitochondrial disease with mice expressing the Wld^s protein hold significant promises for understanding the impact of synaptic mitochondrial dysfunction in neurodegeneration due to mitochondrial disease. Can Wld^s expression improve the behaviour of mice with mitochondrial disease? And if yes, could this imply that mitochondrial disease is a synaptopathy?

4.6 Conclusion

This study further emphasises the vulnerability of the cerebellum to mitochondrial respiratory chain impairment. Quantitative quadruple immunofluorescent approaches have enabled a comprehensive and accurate analysis of complex I deficiency in neuronal cell bodies, dendritic and presynaptic terminal compartments. The distribution of respiratory chain deficiencies was assessed, presynaptic terminal characteristics were evaluated and dendritic length was quantified. Generally, respiratory chain deficiency is more pronounced in Purkinje cells bodies, compared to neuronal dendrites and presynaptic terminals, whereas patients harbouring the m.3243A>G point mutation are more severely affected. Inhibitory synapse deficiency is strongly related with poor clinical rating of ataxia, whereas structural inhibitory synapse changes are reminiscent of altered intracerebellar wiring in patients with mitochondrial disease. Regardless, the question still remains: is synaptic pathology the cause or the consequence of neuronal loss?

Chapter 5

Chapter 5 Cerebellar ataxia in patients with mitochondrial disease

Part 2: Altered intra-cerebellar connectivity in mitochondrial disease

5.1 Introduction

5.1.1 Deep cerebellar nuclei and downstream neuronal networks

The three types of deep cerebellar nuclei (DCN) house a wide variety of projection neurons and interneuronal populations each of which contribute to cerebellar synaptic plasticity and learning (Uusisaari *et al.*, 2007; Uusisaari and Knopfel, 2011; D'Angelo, 2014; Mapelli *et al.*, 2015). Regardless of their neuronal subtype, all neurons located in the DCN receive inhibitory input from Purkinje cells, which comprises the main component of intracerebellar circuitry (Teune *et al.*, 1998). Neuronal excitation is achieved via glutamatergic innervation from climbing (CF) and mossy fibres (MF), which establishes cerebellar connectivity with extracerebellar regions. Inferior olivary neurons project their CFs and excite neurons of the DCN (and Purkinje cells), as do MFs which arise from the brainstem and spinal cord (Voogd and Glickstein, 1998; Apps and Garwicz, 2005; Rajakumar, 2013).

The cerebellum is involved in feedback and feedforward loops with the cortex, the integration of which is important for cognition, emotion and language (D'Angelo and Casali, 2012). Feedback information from the cortex and basal ganglia received at the cerebellar cortex, is relayed to and integrated by DCN. DCN in turn send their output (via the red nucleus) to motor, prefrontal, parietal and temporal cortices (D'Angelo and Casali, 2012).

5.1.2 Gephyrin and its importance in neuronal function

Gephyrin is a cytoplasmic scaffold protein ubiquitously present throughout the neuronal soma and the inhibitory post synapse (Waldvogel *et al.*, 2003). When located at the postsynaptic density, gephyrin interacts with the cytoskeleton and enables clustering of synaptic proteins important for inhibitory (GABAergic and glycinergic) neurotransmission including the receptor subunits for $GABA_A$ and glycine receptors (Giesemann *et al.*, 2003; Bausen *et al.*, 2006; Tyagarajan and Fritschy, 2014). Furthermore, via it's interaction with various adhesion molecules, including Neuroligins, Gephyrin has an important role in GABAergic synapse structural integrity and thus for synaptic functional preservation (Varoqueaux *et al.*, 2004; Poulopoulos *et al.*, 2009).

It has been suggested that protein localisation and aggregation at the postsynaptic compartment is actively regulated in response to changes in the excitatory-inhibitory balance with gephyrin therefore acting as a key player in neuronal network function and information processing in the

brain (Tyagarajan and Fritschy, 2014). Likewise, gephyrin functional defects in cultured hippocampal cells had adverse effects for both inhibitory and excitatory synaptic transmission (Varley *et al.*, 2011).

5.1.3 Synaptic protein expression in the dentate nucleus

The largest of the DCN is the dentate nucleus (Diedrichsen *et al.*, 2011), which is involved in local feedback and global signal transduction networks with extracerebellar regions (Dum and Strick, 2003; D'Angelo and Casali, 2012). The occurrence and timing of output signals from the dentate nucleus is defined by the balance between neuronal excitation (+) (from CF and MF) and inhibition (-) (from Purkinje cells) (Knierim, 1997). A summary of dentate nucleus neuronal connectivity and synaptic protein expression is outlined in Figure 5- 1.

As presented in Chapter 4 of this thesis, Purkinje cell loss is profound in patients with mitochondrial disease and often exceeds the percentage of dentate nucleus neuronal degeneration (Table 4- 1). However, this is not always the case since the degree of dentate nucleus neurodegeneration in some patients surpasses that of Purkinje cell loss. Purkinje cell innervation to the dentate nucleus has previously been assessed (Chapter 4) but how glutamatergic connectivity of the dentate nucleus is affected in patients with mitochondrial disease remains to be established.

The GABAergic synapse that establishes Purkinje cell to dentate nucleus neuron contact is highly sophisticated and depends on the synergistic expression and fine interaction of many proteins at the pre- and a post-synaptic level. Inhibitory presynaptic terminals (studied in Chapter 4 of this thesis) contain glutamic acid decarboxylase 65/67 (GAD-65/67) (Erlander and Tobin, 1991), and are found opposed to inhibitory postsynaptic densities which are enriched for GABA receptors and scaffold proteins (Tyagarajan and Fritschy, 2014). Amongst these is Gephyrin, a protein that mediates GABAergic ($GABA_A$) (and glycinergic) receptor clustering at inhibitory postsynaptic terminals (Kneussel and Betz, 2000b). Hence, employing the developed quantitative immunofluorescent technique (Chapter 3) and using antibodies directed against GAD-65/67 and gephyrin, the structural properties of inhibitory synapses can be studied.

Vesicular glutamate transporters (VGLUT1-3) are a group of proteins that employ electrochemical gradients in order to load synaptic vesicles with the major excitatory neurotransmitter, glutamate (Liguz-Lecznar and Skangiel-Kramska, 2007). Despite their complementary CNS distribution (Fremeau Jr *et al.*, 2001; Kaneko *et al.*, 2002), all three protein isoforms are expressed at excitatory presynaptic terminals (Bellocchio *et al.*, 1998). Studies in

mice (Gebre *et al.*, 2012) and rat (Hioki *et al.*, 2003) exhibited that CF collaterals to the cerebellum are only positive for VGLUT2, whereas both VGLUT1 and VGLUT2 are expressed by MF presynaptic terminals. Upon glutamate release into the synaptic cleft, a series of ionotropic glutamate receptors (located at the postsynaptic neuronal membrane) are activated, leading to neuronal excitation (Day *et al.*, 1995). Named after the agonist that activates them, α-amino-3-hydroxy-5-methylisoxazole-4-propionic acid (AMPA) receptors constitute one of the three ionotropic receptor subtypes that mediate fast excitatory post synaptic potentials (Collingridge and Lester, 1989; Monaghan *et al.*, 1989; Purves. D *et al.*, 2001). Thus, antibodies against VGLUTs and AMPA receptors will facilitate the investigation of glutamatergic innervation of the dentate nucleus (Figure 5- 1).

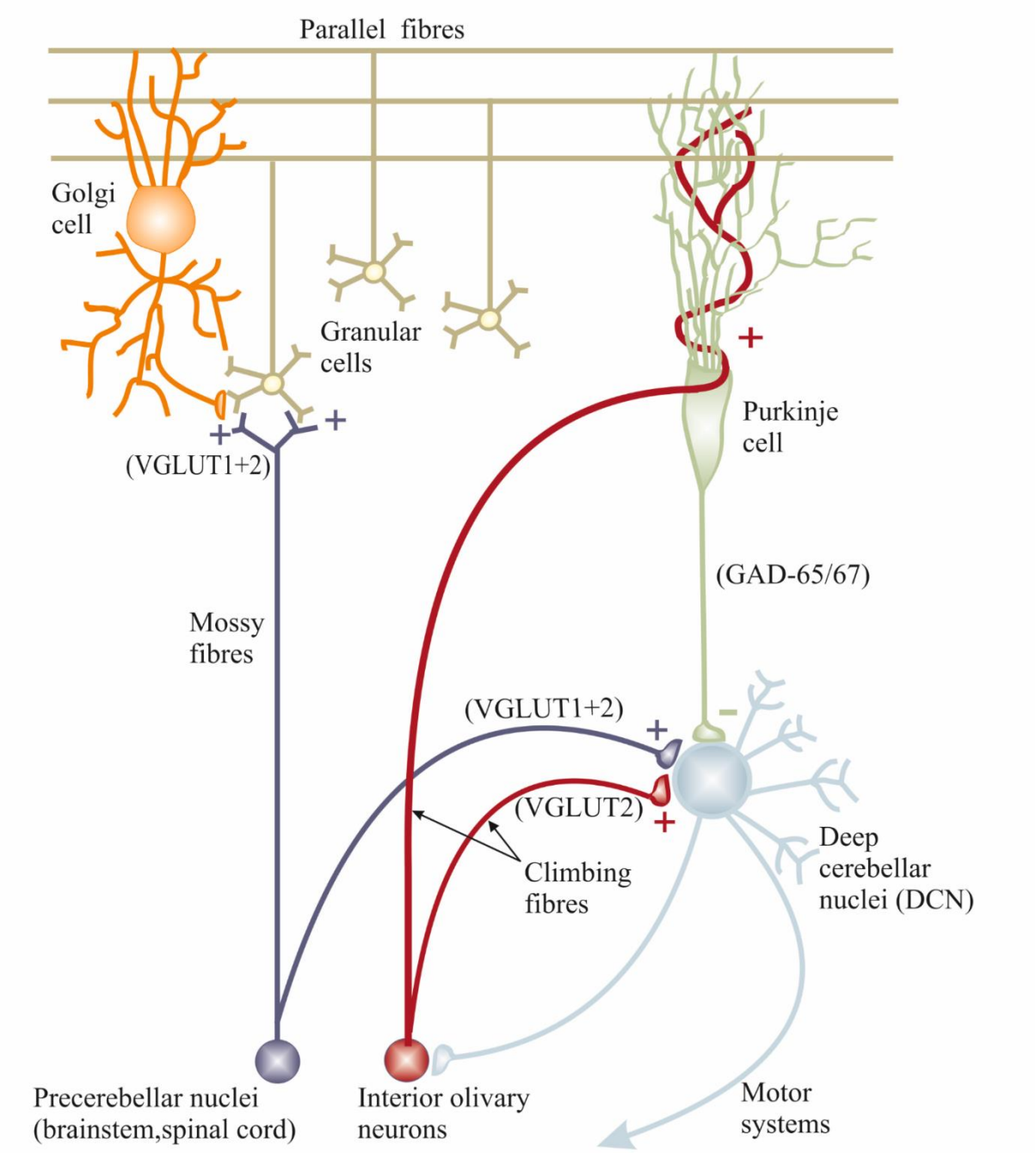

Figure 5- 1: Innervation of and synaptic protein expression in the dentate nucleus.

The dentate nucleus (the largest of the deep cerebellar nuclei – DCN) receives inhibitory input (-) from Purkinje cells and is innervated by glutamatergic (+) climbing and mossy fibres. Inhibitory presynaptic terminals to the region are positive for GAD-65/67, whereas excitatory synapses express vesicular glutamate transporters (VGLUT1+2). Gephyrin is used to detect the inhibitory and AMPA receptors are employed to identify the excitatory postsynaptic density respectively.

5.2 Aims of the investigation

The main aim of this study is to understand the impact of mitochondrial defects on intracerebellar circuitry, by now focussing on the dentate nucleus, in an attempt to gain further insights into the mechanisms responsible for the progression of ataxia. I will achieve this by:

1. Quantifying neuronal respiratory chain protein expression in the dentate nucleus
2. Investigating the density of inhibitory postsynaptic terminals and the degree of glutamatergic innervation of the dentate nucleus

5.3 Methodology

5.3.1 Cerebellar tissue samples

This study involves the neuropathological investigation of twelve adult patients that have been clinically and genetically diagnosed to suffer from mitochondrial disease and 10 age-matched controls. Patient clinical and neuropathological details are summarised in Table 4- 1, whereas patient and control tissue characteristics are summarised in Table 4- 2.

5.3.2 Immunofluorescence

5.3.2.1 Assessing respiratory chain deficiency in dentate nucleus neuronal cell bodies

5μm-thick FFPE cerebellar tissue sections mounted on SuperFrost slides were subjected to a quadruple immunofluorescent protocol as previously described (see section 2.7.1) with the following modifications:

Following antigen retrieval with EDTA, sections were incubated in 3% Hydrogen peroxide solution for 1 hour at RT and washed thoroughly with water. After tissue block with 1% NGS for 1 hour at RT, the primary antibody (Table 5- 1) solution was applied overnight at 4^{o}C. PBS washes (3x5 minutes) the next day were followed by anti-mouse and anti-rabbit secondary antibody (coupled with fluorophores) incubation for 1 hour at RT (Table 5- 1). PBS washes preceded an HRP-conjugated anti-mouse secondary antibody (Table 5- 1) incubation for 1 hour at RT, the signal of which was detected after following the Tyramide signal amplification (TSA) method per manufacturer's instructions (Life Technologies).

5.3.2.2 Evaluating glutamatergic input to the dentate nucleus

A double immunofluorescent protocol (section 2.7.1) was followed in order to stain 5μm-thick FFPE cerebellar tissue sections against excitatory pre- and postsynaptic markers (Table 2- 3). All primary and secondary antibodies (Table 5- 1) applied to the sections were diluted in 10% NGS, which was also used to block the sections prior to antibody incubation.

Quadruple immunofluorescence						
Primary antibodies	**Host and isotype**	**Source**	**Catalogue No.**	**Antigen retrieval**	**Optimal dilution**	**Optimal incubation conditions**
Gephyrin	Mouse monoclonal - IgG1	BD Biosciences	610585	EDTA (1mM); 2100 antigen retriever	1:50	O/N[1] at 4°C
Glutamic acid decarboxylase 65/67 (GAD 65/67)	Rabbit polyclonal - IgG	Sigma-Aldrich	G5163	EDTA (1mM); 2100 antigen retriever	1:800	O/N at 4°C
Complex I subunit NDUFA13	Mouse monoclonal - IgG2b	Abcam	ab110240	EDTA (1mM); 2100 antigen retriever	1:100	O/N at 4°C
Complex IV subunit IV	Mouse monoclonal - IgG2a	Abcam	ab110261	EDTA (1mM); 2100 antigen retriever	1:200	O/N at 4°C
Secondary antibodies	**Host and epitope**	**Source**	**Catalogue No.**	**Antigen retrieval**	**Optimal dilution**	**Optimal incubation conditions**
HRP-conjugated	Goat Anti-Mouse IgG1 (γ1)	Life technologies	A10551	N/A	1:100	1 hour, RT[2]
Alexa Fluor® 647 Tyramide	N/A	Life technologies	T2095	N/A	1:100	10 minutes, RT
Alexa Fluor® 405	Goat Anti-Rabbit IgG (H+L)	Life technologies	A31556	N/A	1:100	1 hour, RT
Alexa Fluor® 488	Goat Anti-Mouse IgG2b (γ2b)	Life technologies	A21141	N/A	1:100	1 hour, RT
Alexa Fluor® 546	Goat Anti-Mouse IgG2a (γ2a)	Life technologies	A21133	N/A	1:100	1 hour, RT

Double immunofluorescence						
Primary antibodies	**Host and isotype**	**Source**	**Catalogue No.**	**Antigen retrieval**	**Optimal dilution**	**Optimal incubation conditions**
Vesicular glutamate transporter 1 (VGLUT1)	Mouse monoclonal - IgG1	NeuroMab	73-066	EDTA (1mM); 2100 antigen retriever	1 in 75	O/N at 4°C
Pan-AMPA receptor (GluR1-4)	Mouse monoclonal – $IgG2b_k$	Millipore	MABN832	EDTA (1mM); 2100 antigen retriever	1 in 50	O/N at 4°C
Secondary antibodies	**Host and epitope**	**Source**	**Catalogue No.**	**Antigen retrieval**	**Optimal dilution**	**Optimal incubation conditions**
Alexa Fluor® 488	Goat Anti-Mouse IgG1 (γ1)	Life technologies	A21121	N/A	1 in 100	2 hours, 4°C
Alexa Fluor® 546	Goat Anti-Mouse IgG2b (γ2b)	Life technologies	A21143	N/A	1 in 100	2 hours, 4°C

Table 5- 1: A list of the primary and secondary antibodies used in this study, along with their optimal working conditions

5.3.3 Confocal microscopy and image processing

Immunofluorescently stained sections were imaged using an inverted laser point scanning confocal microscope (Nikon A1R) as described earlier (section 2.8.1 and 3.4.5). Twenty large glutamatergic dentate nucleus neurons were randomly selected and were employed to assess complex I protein expression in the dentate nucleus (see section 3.4.7 and 4.3.3).

Evaluating the number of Gephyrin-positive puncta around dentate nucleus neurons involved image cropping and deconvolution using Volocity® (section 3.4.6), followed by surface recreation in IMARIS. Once GAD- and Gephyrin-positive puncta were substituted by surfaces that mimic the pattern of staining, a Matlab Xtension was employed in order to filter the surfaces created. Thus, only Gephyrin puncta directly opposed to GAD were taken into account, allowing for the number of Gephyrin molecules that are associated with GABAergic presynaptic terminals to be counted. Gephyrin punctum numbers were normalised per μm^2 cell surface area.

Similarly, z stacks from sections stained against excitatory pre- and postsynaptic markers were employed to study the degree of glutamatergic innervation of dentate nucleus neurons. Volocity® helped identify, crop and measure the length of individual neuronal dendrites, whereas processed images were later imported into IMARIS. Surfaces were recreated for each pre- or postsynaptic punctum and these were used to obtain average surface number and volume measurements. Surface numbers were normalised per μm length of a dendrite.

5.3.4 Statistical analysis

The mean optical density (OD) values for NDUFA13 and COX4 immunofluorescence were employed to calculate the z score values for respiratory chain protein expression in dentate nucleus neuronal cell bodies using SAS 9.3 (Cary, NC) (section 3.4.7).

Any other statistical testing was performed as previously described (section 4.3.5).

5.4 Results

5.4.1 Complex I deficiency in dentate nucleus neuronal cell bodies

Control dentate nucleus neuronal cell bodies contain high mitochondrial mass (as judged by COX4 immunoreactivity) with matched complex I protein expression (NDUFA13 co-localisation with COX4) (Figure 5- 2). Although patient cell bodies demonstrated similarly high mitochondria mass (two sample t-test for the levels of COX4 protein expression, p value= 0.376), NDUFA13 protein expression was variably decreased relative to control neurons (Figure 5- 2). Z scoring helped define the exact levels of NDUFA13 expression and verified decreased complex I protein expression in patient neuronal cell bodies (Figure 5- 3). Heterogeneous NDUFA13 protein expression levels were evident within individual patients and across patients with the same genetic defect (e.g. patient 2 vs. patient 5; m.3243A>G) (Figure 5- 3) as previously documented (Lax *et al*., 2012). This is exemplified by the percentages of dentate nucleus neurons that are normal, low, deficient or very deficient for NDUFA13 in each patient (Table 5- 2). Although patient 2 and patient 5 harbour the m.3243A>G point mutation, the majority (81%) of dentate nucleus neurons possessed by patient 2 have normal complex I protein expression, whereas all of patient 5's neurons are low, deficient or very deficient for complex I (Table 5- 2) (Table 4- 1). Similarly, patient 10 (recessive POLG mutations) has no dentate nucleus neurons that are very deficient for complex I, whilst the majority (65%) of neurons possessed by another patient with the same genetic defect (patient 11) have very severe complex I protein expression defects (Table 5- 2) (Table 4- 1).

There is no difference in the amount of NDUFA13 between patients with the m.3243A>G point mutation and others when genetic defects are grouped (m.8344A>G, m.14709T>C and recessive POLG mutations) (Mann Whitney U test, p value = 0.4712). Z score values for NDUFA13 protein expression were not affected by either PMI (rho= -0.329, p value= 0.297) (Appendix A) or by the length of formalin fixation (rho= 0.326, p value= 0.960) (Spearman's rank correlation).

Remarkably, there is a strong positive relationship between presynaptic terminal (GABAergic synapse) (see section 4.4.1) and postsynaptic neuronal (dentate nucleus neuron) NDUFA13 protein expression. Those patients with the most severe presynaptic complex I deficiency (lower NDUFA13 z score values) possess dentate nucleus neurons with severe somatic complex I defects (rho= 0.902, p value= 0.0005) (Figure 5- 4). Furthermore, percentage dentate nucleus neuronal loss (Table 4- 1) was negatively related to somatic NDUFA13 protein expression,

since patients with the greatest degree of neuronal loss revealed lower NDUFA13 z scores, compatible with complex I deficiency, in remaining cells (rho= -0.717, p value= 0.030).

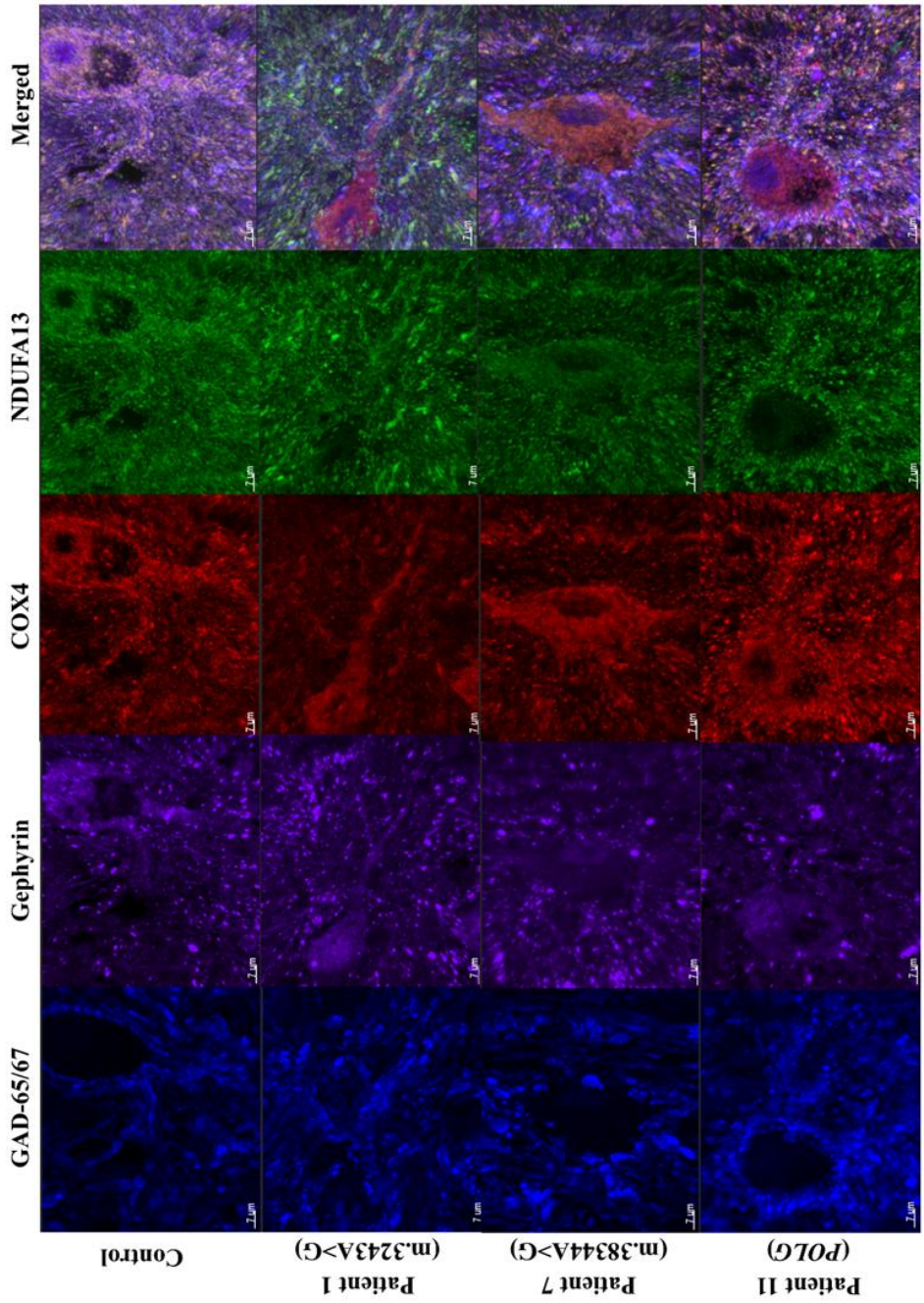

Figure 5- 2: Dentate nucleus neuronal cell bodies immunofluorescently stained against GAD-65/67, Gephyrin, COX4 and NDUFA13.

Despite mitochondrial abundance in control and patient neuronal cell bodies (COX4 immunoreactivity), NDUFA13 protein expression variably differs in patient cells. COX4 and NDUFA13 colocalisation in control cells is denotive of complex I intact organelles. On the contrary, complex I deficiency manifests in patient cells that lack NDUFA13 immunoreactivity, patient 1 (m.3243A>G) and patient 11 (POLG), or have severely decreased NDUFA13 protein expression relative to mitochondrial mass (Patient 7, m.8344A>G). Scale bar: 7µm

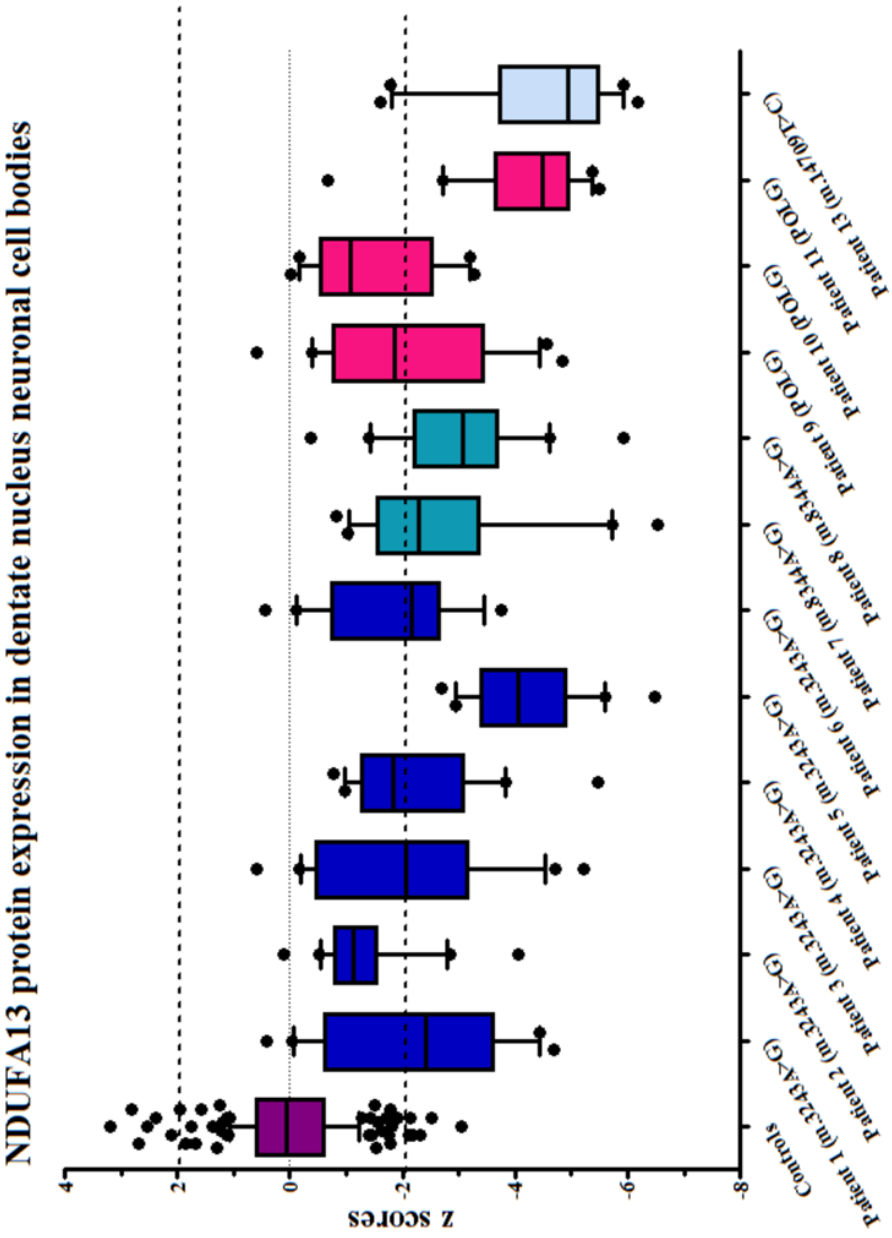

Figure 5- 3: Standard deviation limits for the levels of NDUFA13 protein expression.

Control cells have intact complex I protein expression since NDUFA13 z score values lie within the ±2SD limits for normality. Patients on the other hand possess cells that are normal (-2<NDUFA13z<2SDs), low (NDUFA13z<-2SDs), deficient (NDUFA13z<-3SDs) or very deficient (NDUFA13z<-4SDs) for complex I protein expression. Patients with the m.3243A>G point mutation have comparable z score values to patients with other genetic defects when these are grouped, whereas patients 5 (m.3243A>G), 11 (POLG) and 13 (m.14709T>C) exhibit the most severe deficiencies. Each data point represents a single dentate nucleus neuron (n=20).

	Controls	Pt1	Pt2	Pt3	Pt4	Pt5	Pt6	Pt7	Pt8	Pt9	Pt10	Pt11	Pt13
Dentate nucleus neuronal cell bodies													
Normal (-2< CI_z <2SDs)	97.00%	40.00%	81.00%	45.00%	55.00%	0.00%	47.00%	35.00%	24.00%	52.00%	68.00%	5.00%	15.00%
Low (CI_z <-2SDs)	2.50%	25.00%	14.00%	32.00%	20.00%	10.00%	37.00%	30.00%	24.00%	14.00%	18.00%	10.00%	5.00%
Deficient (CI_z <-3SDs)	0.50%	20.00%	0.00%	9.00%	20.00%	40.00%	16.00%	20.00%	33.00%	24.00%	14.00%	20.00%	10.00%
Very deficient (CI_z <-4SDs)	0.00%	15.00%	5.00%	14.00%	5.00%	50.00%	0.00%	15.00%	19.00%	10.00%	0.00%	65.00%	70.00%

Table 5- 2: The percentage of dentate nucleus neurons that are normal, low, deficient or very deficient for NDUFA13.

The majority of control neurons have intact complex I protein expression, whereas patients contain a mixture of normal, low, deficient or very deficient cells for NDUFA13.

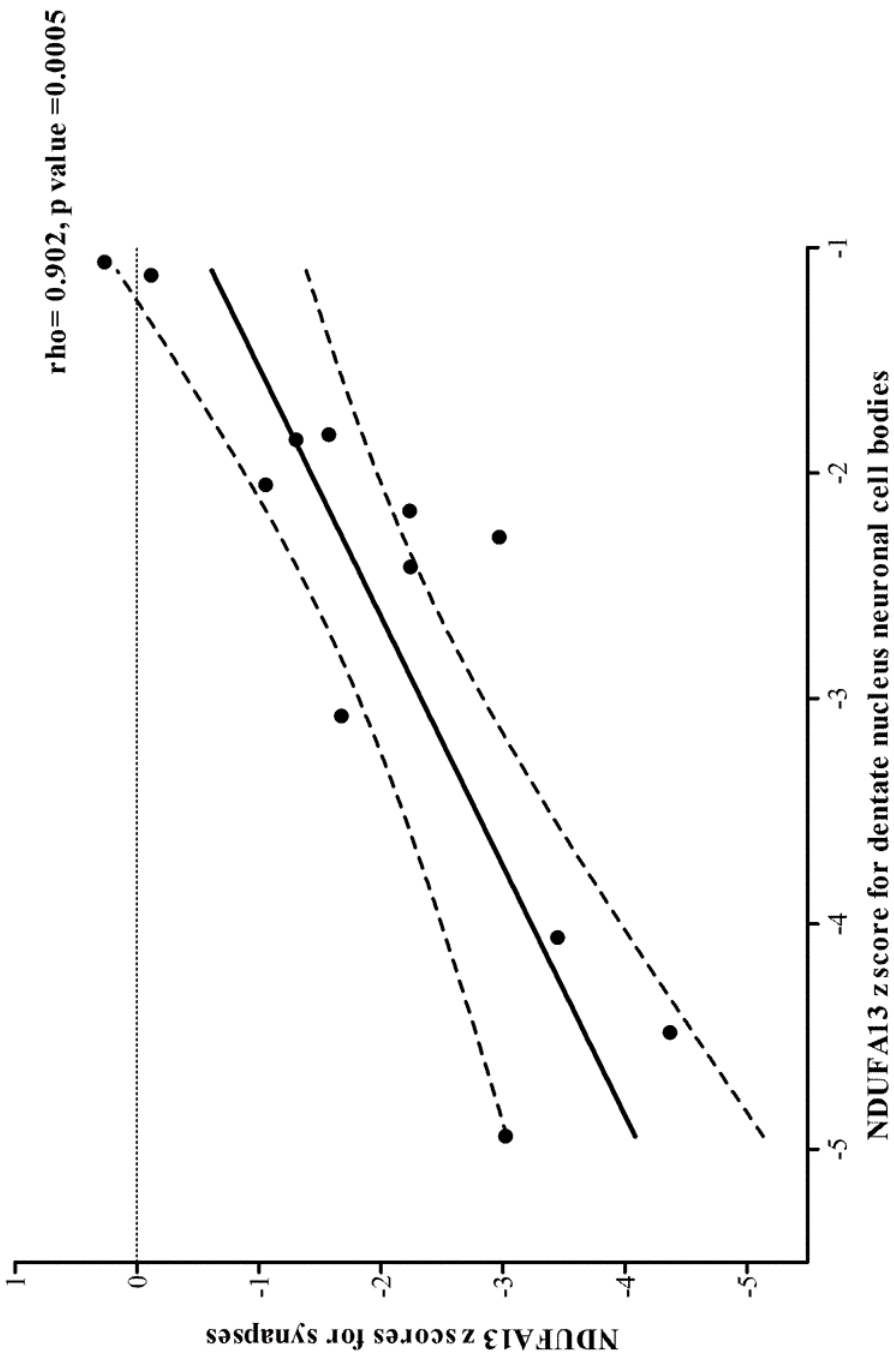

Figure 5- 4: Correlation between NDUFA13 protein expression in presynaptic terminals and postsynaptic neuronal cell bodies.

The most severe synaptic deficiencies (lower NDUFA13 z score values) are associated with the most severe neuronal cell body defects (Spearman's rho= 0.902, p value= 0.0005).

5.4.2 Loss of Gephyrin and GABAergic synapse destabilisation

Further to the amount of inhibitory input to the dentate nucleus, the number of structurally intact GABAergic pre- and postsynaptic compartments found on the periphery and proximal dendrites of dentate nucleus neurons was assessed (Video 5-1). Quantification of Gephyrin-positive puncta found opposed to GAD immunoreactive presynaptic terminals, demonstrated decreased punctum density in all patients (Figure 5- 5), though z score values fall within ±2SD limits for normality (Figure 5- 5). Decreased Gephyrin punctum density is in line with decreased Purkinje cell efferent density documented in Chapter 4 of this thesis. Indeed, there is a significant positive relationship between the number of GABAergic presynaptic terminals and Gephyrin punctum density detected on dentate nucleus neurons (rho= 0.625, p value= 0.030) (Spearman's rank correlation) (Figure 5- 6). The volume of inhibitory postsynaptic terminals is displayed in Appendix C.

Neither PMI (rho= -0.422, p value= 0.172) (Appendix A) nor fixation length (rho= -0.339, p value= 0.281) exerted an effect on inhibitory postsynaptic terminal counts.

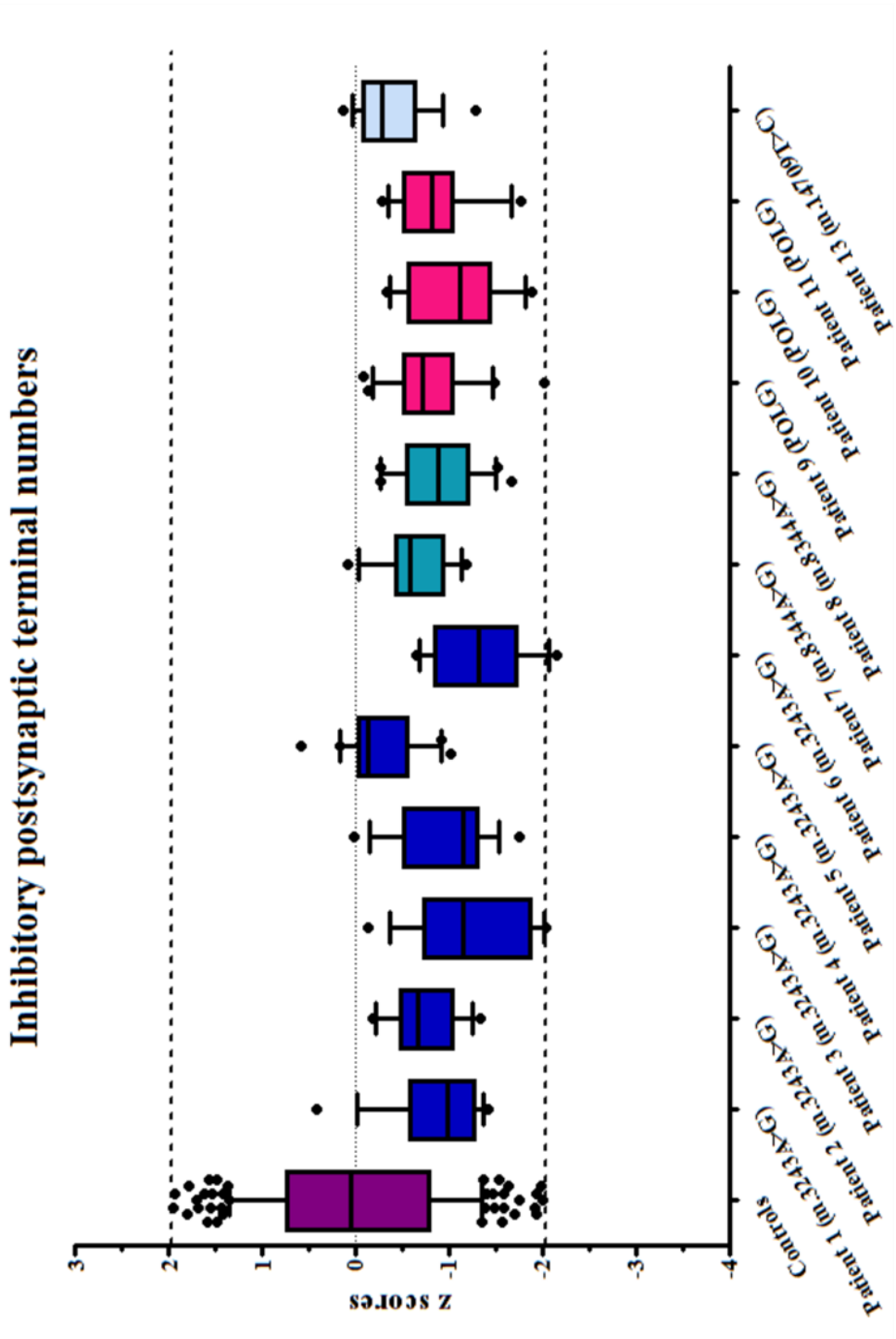

Figure 5- 5: The number of Gephyrin-positive puncta opposed to GAD-positive terminals around dentate nucleus neurons expressed as z score values.

All patients included in this study demonstrate decreased inhibitory postsynaptic terminal numbers compared to controls, though the derived z score values fall within the normal ±2 SD limits. Each data point represents the number of puncta detected around one neuron (n=20 dentate nucleus neurons).

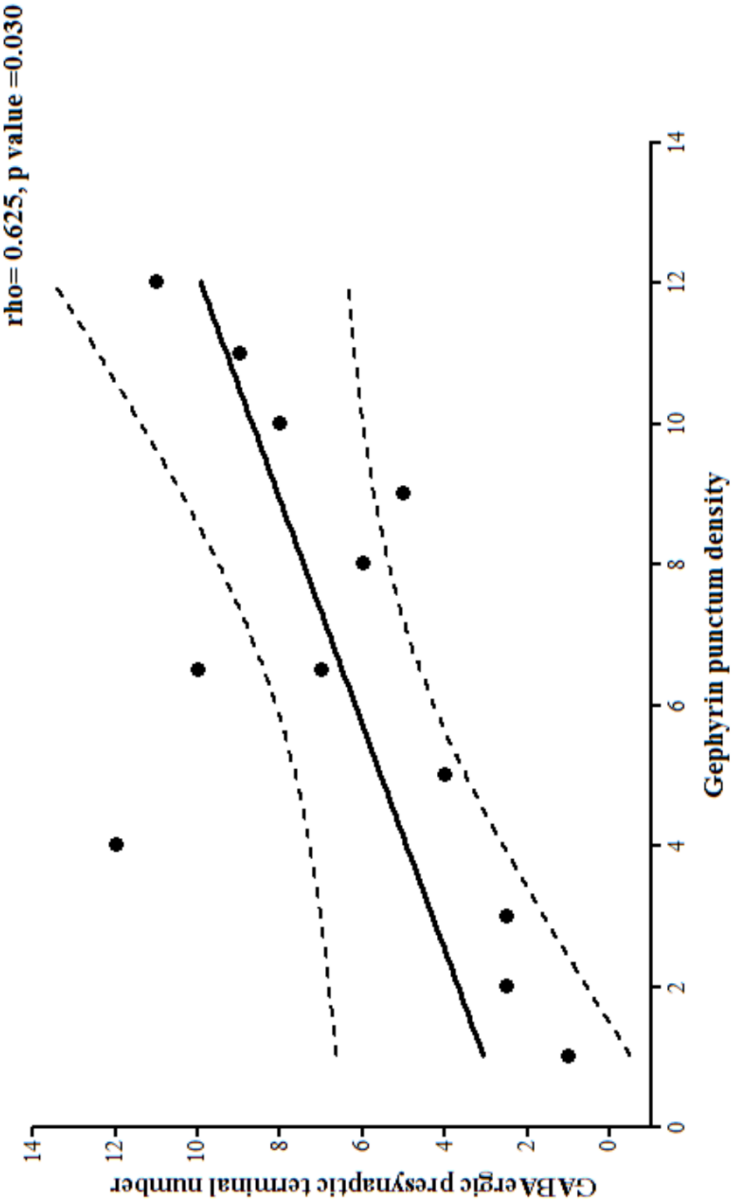

Figure 5- 6: Correlation between the number of GABAergic presynaptic terminals and Gephyrin puncta density detected around dentate nucleus neurons.

As the number of Gephyrin puncta detected on the periphery of dentate nucleus neurons increases, so does the number of GABAergic presynaptic terminals (Spearman's rho= 0.625, p value= 0.030).

5.4.3 Glutamatergic innervation of dentate nucleus neurons

Further to investigating the numerical and structural characteristics of GABAergic synapses on dentate nucleus neurons, the excitatory input to the area was partially evaluated. Control dentate nucleus neuronal dendrites (outlined in white boxes) received high density of glutamatergic input (VGLUT1-positive puncta; presynaptic terminals) and contained similarly high density of glutamate receptors (pan-AMPA-positive puncta; postsynaptic terminals) (Figure 5- 7). On the contrary, the majority of patients studied possessed dendrites with variably decreased excitatory presynaptic terminals and neurotransmitter receptors verified by decreased punctum density (Figure 5- 7). Presynaptic terminal and postsynaptic receptor number quantification verified altered glutamatergic signalling to the dentate nucleus of patients with mitochondrial disease (Figure 5- 8 and Figure 5- 9). MF input to dentate nucleus neurons was decreased in the majority of patients studied (10 out of 12) (Figure 5- 8), so was excitatory receptor number (Figure 5- 9) though the majority of z score values were within ±2SD limits for normality. Decreased glutamatergic synapse density might be consequent to extracerebellar neuronal loss (spinal cord and brainstem), however no data are available for the degree of neuronal loss in those areas.

Interestingly, remaining presynaptic terminals and glutamate receptors were smaller since punctum number was positively related to punctum size (volume - μm^3) (VGUT1: rho = 0.587, p value= 0.045 (Figure 5- 10); AMPA receptors: rho= 0.734, p value= 0.007 (Figure 5- 11) (Spearman's rank correlation). The volume of excitatory presynaptic terminals and AMPA receptors detected on dentate nucleus neuronal dendrites is displayed in Appendix D and Appendix E respectively. Presynaptic terminal number and volume was not affected by either PMI (Number: rho= -0.081, p value= 0.803; Volume: rho= 0.053, p value= 0.871) (Appendix A) or fixation length (Number: rho= 0.001, p value= 0.999; Volume: rho= -0.106, p value= 0.742). Similarly, neither PMI (Number: rho= 0.002, p value= 0.962; Volume: rho= 0.375, p value= 0.230) (Appendix A) nor fixation length (Number: rho= -0.460, p value= 0.132; Volume: rho= 0.163, p value= 0.612) affected the number and volume of AMPA receptors detected (Spearman's rank correlation).

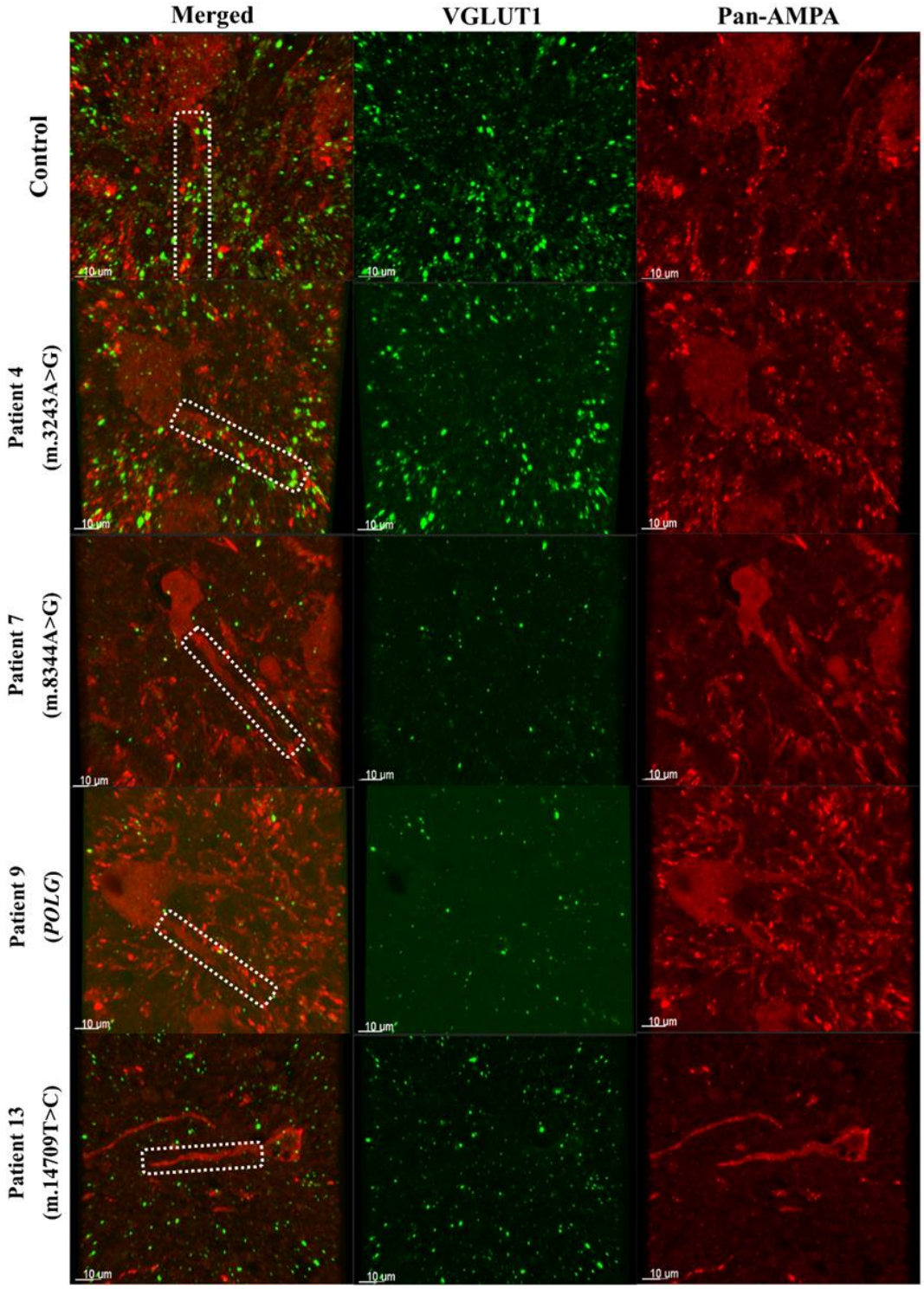

Figure 5- 7: Dentate nucleus neurons fluorescently stained against Vesicular Glutamate transporter 1 (VGLUT1) and Glutamate receptors 1-4 (pan-AMPA).

High density of excitatory presynaptic terminals (VGLUT1) synapse onto control neuronal dendrites, which are enriched for glutamate receptors (AMPA). Although the excitatory input to and the number of neurotransmitter receptors on patient 4 (m.3243A>G) neuronal dendrites are similar to that of controls, this is not the case for the majority of patients included in this study. Patients 7 (m.8344A>G), 9 (*POLG*) and 13 (m.14709T>C) are demonstrative of severely decreased presynaptic terminal and postsynaptic receptor densities. Scale bar: 10µm

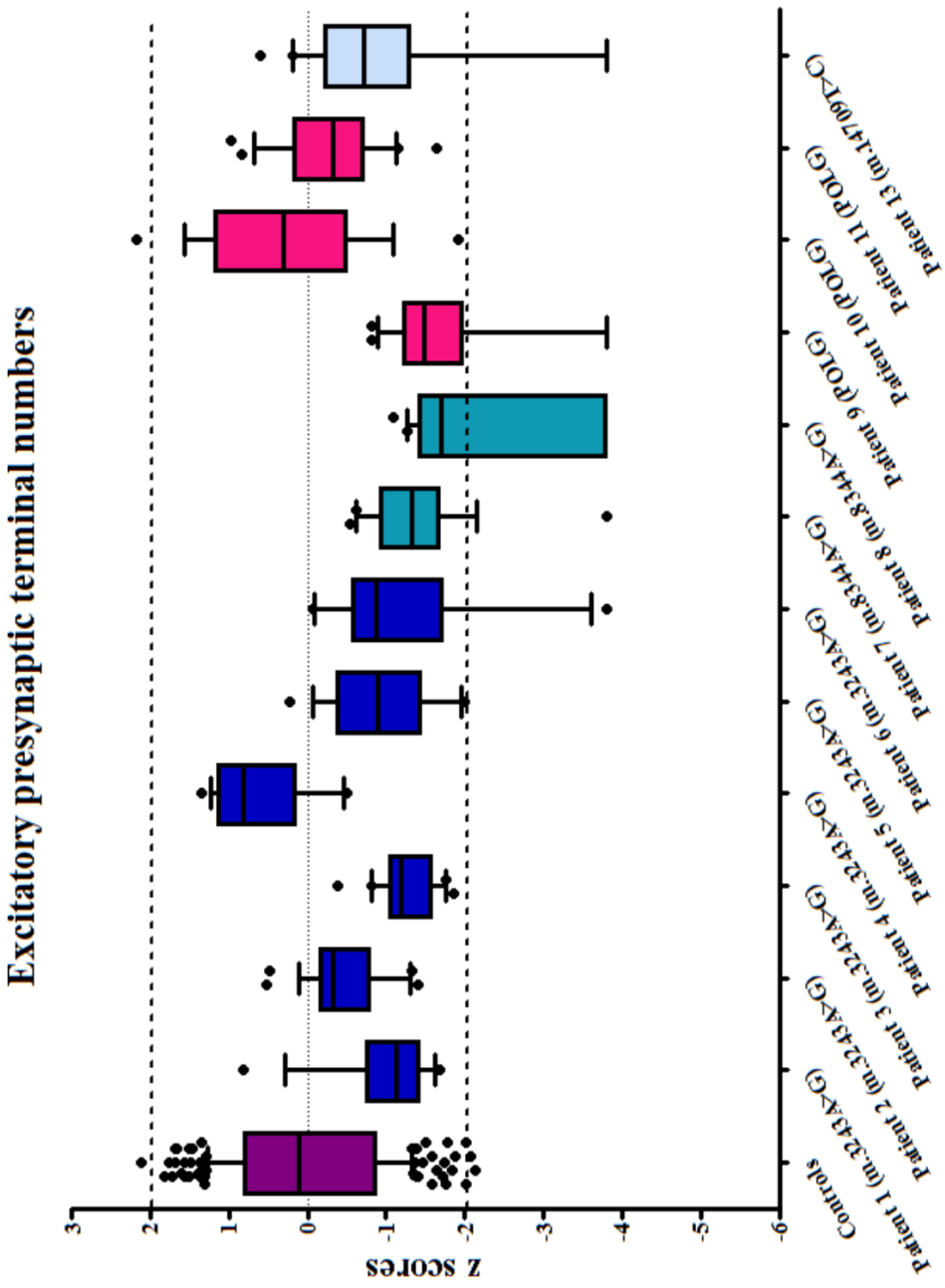

Figure 5- 8: Standard deviation limits for the number of glutamatergic presynaptic terminals detected on dentate nucleus neuronal dendrites.

Most patients (10 out of 12) had decreased glutamatergic synapse density compared to controls, although all median z score values fall within the normal limits (±2SDs). Each data point represents the number of puncta detected per µm length of dendrite (n=20 dentate nucleus neurons).

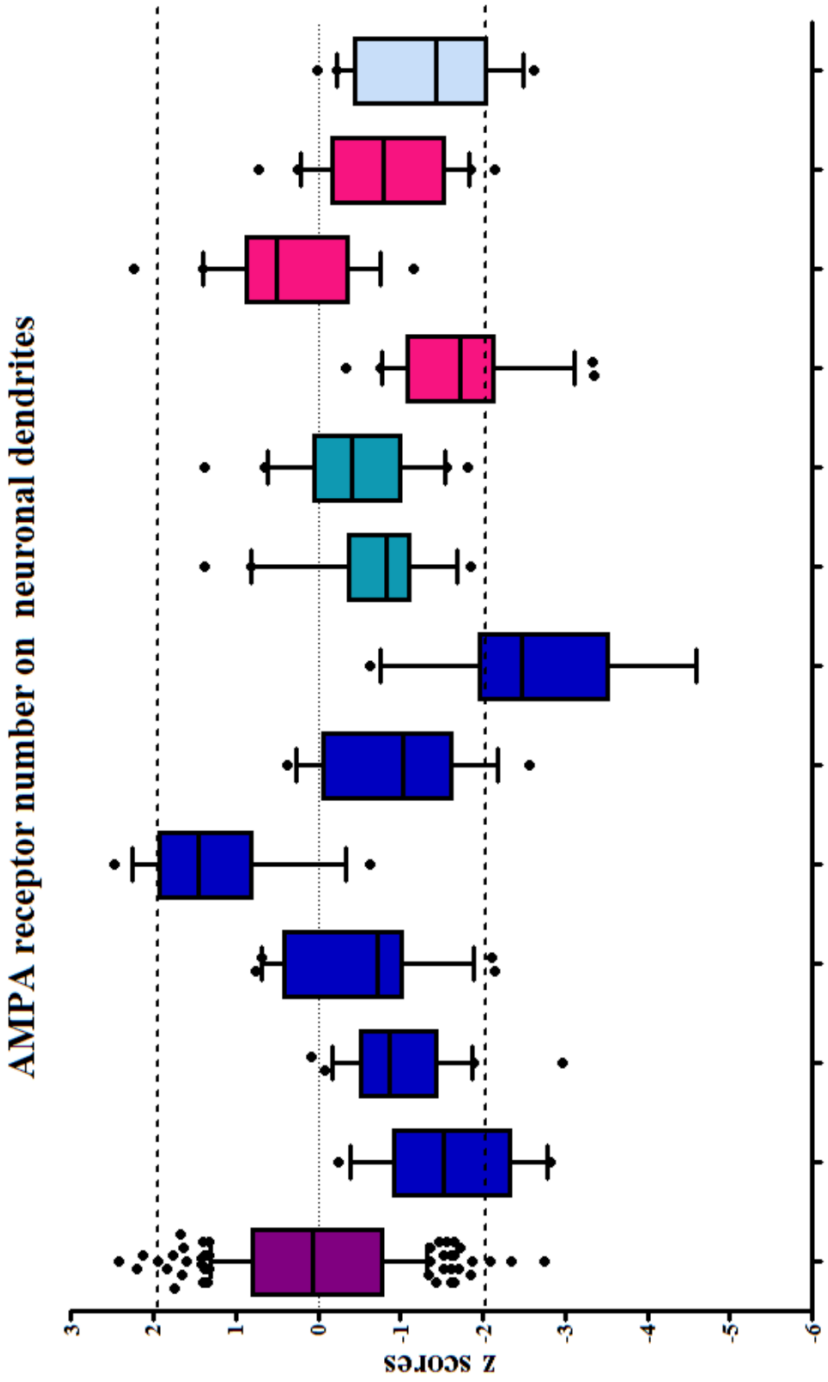

Figure 5- 9: The number of glutamate receptors counted on dentate nucleus neuronal dendrites expressed as z score values.

Most of the patients included in this study (10 out of 12) demonstrated decreased in Glutamate receptor density, whilst only patient 6 (m.3243A>G) was significantly different to controls. Each data point represents the number of puncta detected per µm length of dendrite (n=20 dentate nucleus neurons).

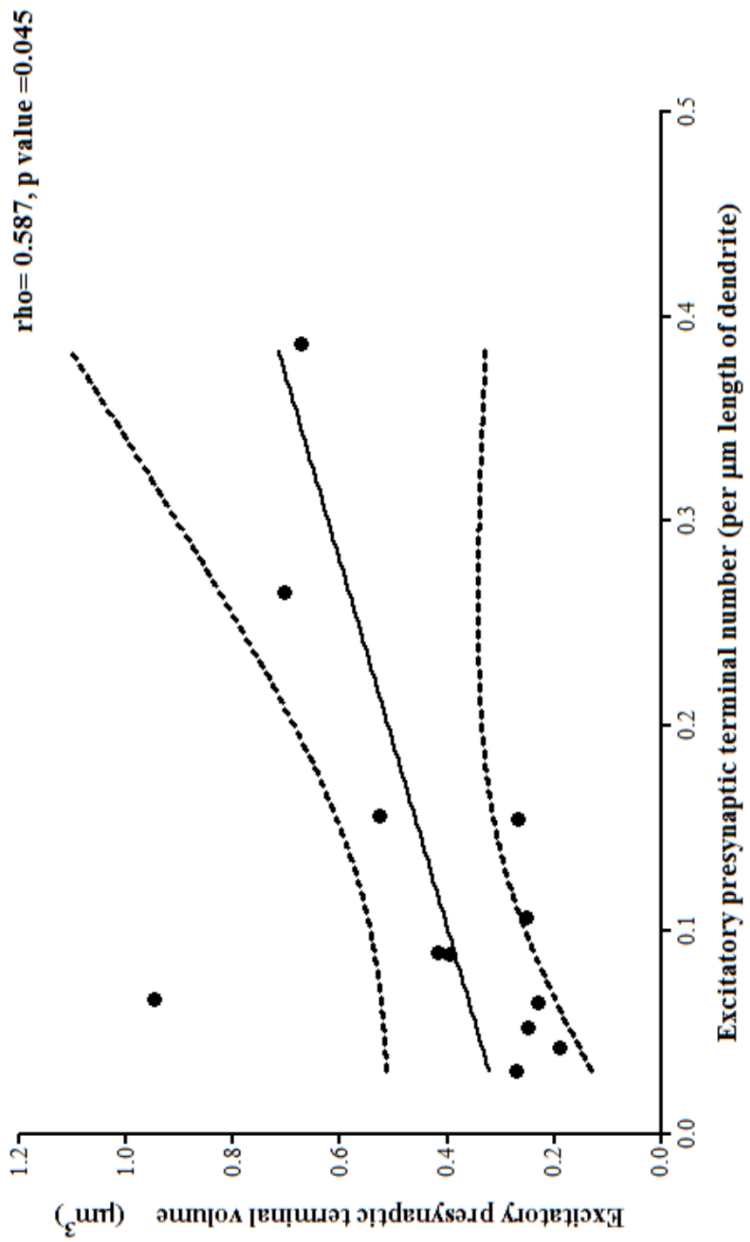

Figure 5- 10: Correlation between the number of excitatory presynaptic terminals and terminal volume.

In those patients whose dendrites possess the less excitatory presynaptic terminals, the terminal punctum volume (measured in μm^3) was also smaller (Spearman's rho= 0.587, p value= 0.045).

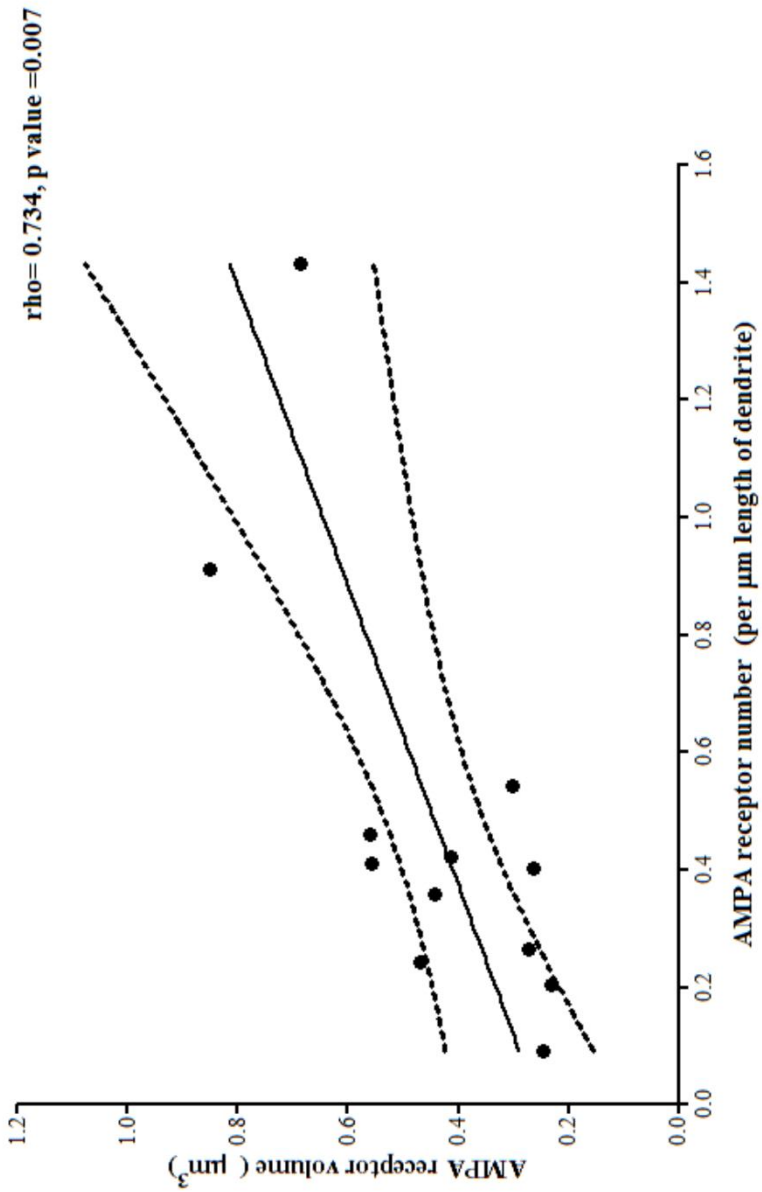

Figure 5- 11: Correlation between the numbers of AMPA receptors detected on dentate nucleus neuronal dendrites and receptor volume.

In those patients whose dendrites possess the less AMPA receptors, receptor volume (measured in μm^3) was also smaller (Spearman's rho= 0.734, p value=0.007).

5.5 Discussion

Cerebellar ataxia, with associated cognitive and motor balance disturbances, frequently affects patients with mitochondrial disease (Hudson *et al.*, 2008; McFarland *et al.*, 2010). The progressive nature of the condition emphasizes the need for elucidating the mechanisms behind neuronal loss that is documented across the olivo-cerebellar pathway of ataxic patients (Lax *et al.*, 2012). Taking into careful consideration the far-reaching evidence for synaptic pathology in common neurodegenerative diseases (Marcello *et al.*, 2012; Picconi *et al.*, 2012) and in fact, the proposed mechanisms for synaptic dysfunction occurring early in neurodegeneration (Li *et al.*, 2003; Janezic *et al.*, 2013), I have decided to study the intracerebellar circuitry in greater detail. Quantitative quadruple immunofluorescence was performed in order to assign the degree of complex I deficiency in dentate nucleus neurons and to further characterise the GABAergic synapse that link these with Purkinje cells. The degree of glutamatergic innervation to the dentate nucleus was also determined to gain further insights into the aetiology of dentate nucleus neuronal death and its impact on circuitry.

Patient dentate nucleus neuronal cell bodies have variably decreased complex I protein expression, relative to controls, whilst the great extent of inter-patient variability implies that the severity of complex I deficiency occurs independent of genetic defect. The degree of dentate nucleus neuronal loss correlates with complex I protein expression in remaining cells, which suggests that respiratory chain deficiency is detrimental to neuronal viability and is in agreement with previous observations (Lax *et al.*, 2012). Interestingly, there is a strong positive relationship for the level of complex I protein expression between Purkinje cell efferents (inhibitory presynaptic terminals) (Chapter 4) and dentate nucleus neuronal cell bodies, which could be indicative for the presence of trans-synaptic effects exerted between the presynaptic terminal and the postsynaptic neuron. Recent evidence for the presence of unique cell-to-cell communication mechanisms, namely tunnelling nanotubes, that facilitate small organelle transport between neighbouring cells (Gerdes *et al.*, 2007; Wang and Gerdes, 2015), implies that mitochondria may well be transported between presynaptic terminals and postsynaptic neuronal cells. Though highly speculative, mitochondrial transport via tunnelling nanotubes could explain for the comparable protein expression levels between the two subneuronal compartments.

As presented in Chapter 4 of this thesis, patient dentate nucleus neurons lose some of their inhibitory input, exemplified by decreased GABAergic synapse contact numbers onto dentate nucleus neurons. Presynaptic terminal loss is accompanied by a loss in the number of gephyrin-

positive puncta located at inhibitory postsynaptic sites demonstrated here. Whilst decreased presynaptic terminal density is likely due to Purkinje cell loss in the cerebellar cortex, loss of gephyrin from the inhibitory postsynaptic compartment may be unfavourable to the excitatory-inhibitory homeostatic balance necessary for neuronal preservation and circuitry function (Turrigiano, 2011). Previous studies suggest neuronal atrophy within the dentate nucleus since shrunken neuron cell bodies are detected (Zhou *et al*., 1997) and axonal loss is reported in the absence of neuronal degeneration (Sparaco *et al.*, 1993). Although no such investigations have been performed in this study, it would be interesting to assess dentate nucleus axonal morphology in association with neuronal density and inhibitory synapse density/volume.

Gephyrin's established role in localizing inhibitory receptors at postsynaptic terminals (Kneussel and Betz, 2000a; Tretter *et al.*, 2012), via cytoskeletal interactions, signify that decreased gephyrin puncta might negatively affect inhibitory receptor localisation and thus GABAergic neurotransmission (Varley *et al.*, 2011). On the contrary, decreased puncta might simply reflect failure of protein transport to the postsynaptic compartments and/or failure of protein aggregation at the site, despite $GABA_A$ receptor presence (Levi *et al.*, 2004; Lorenzo *et al.*, 2014). Remarkably, there is a significant positive relationship between inhibitory presynaptic terminal (GAD-positive puncta) density and gephyrin punctum density which is suggestive of GABAergic synapse destabilisation via potentially trans-synaptic effects. This is in agreement with gephyrin knock-down experiments performed in cultured hippocampal neurons and demonstrate further presynaptic terminal structural abnormalities with consequent inhibitory neurotransmission defects (Yu *et al.*, 2007). Trans-synaptic effects are likely to be exerted via pre- and postsynaptic transmembrane proteins that are responsible for holding the two terminals in close proximity, namely Neurexins and Neuroligins (Krueger *et al.*, 2012). Regardless of the mechanism that accounts for inhibitory synapse destabilisation, the observed changes suggest dentate nucleus neuronal disinhibition in patients with mitochondrial disease.

Further to dentate nucleus neuronal disinhibition, glutamatergic signalling to the region is in part also altered. Excitatory MF presynaptic terminal density is decreased, so is the density of glutamate receptors detected on dentate nucleus neuronal dendrites. These changes may be secondary to extracerebellar neuronal loss within the brainstem and spinal cord, or may reflect an adaptive response to decreased dentate nucleus neuronal inhibition. Maintenance of the excitatory-inhibitory balance is likely to be neuroprotective since it prevents excitotoxic cell death, contrary to what is the speculated mechanisms of neuronal loss in other neurodegenerative disorders (Doble, 1999; Dong *et al.*, 2009). Moreover, decreased

glutamatergic innervation of the dentate nucleus may be beneficial to already impaired mitochondria since excess glutamatergic signalling would result in neuronal Ca^{2+} overload (Prentice *et al.*, 2015). These hypotheses are in agreement with what is discussed in Chapter 4 of this thesis and suggests that neurodegeneration in patients with mitochondrial disease is not due to excitotoxicity. Nevertheless, residual excitatory synapses are smaller which is in contrast to what was previously found for inhibitory presynaptic terminals to the dentate nucleus, suggesting that excitatory and inhibitory synapses are differentially affected in mitochondrial disease. This may well disturb cerebellar synaptic plasticity and thus cerebellar learning with downstream effects on cognitive and motor tasks (D'Angelo and Casali, 2012; D'Angelo, 2014; Mapelli *et al.*, 2015).

Notwithstanding the observed changes in neuronal respiratory chain protein expression, synaptic density and structure, this study has important limitations that need to be taken into careful consideration. Dentate nucleus neurons were identified on the basis of morphology and localisation, whereas mainly large glutamatergic cells were sampled. Since cerebellar output signals are defined by synergistic DCN function, no definitive conclusions regarding extracerebellar signalling can be drawn after only studying large glutamatergic dentate nucleus neurons. Furthermore, glutamatergic input to the region was assessed using an anti-VGLUT1 antibody which is specific to MF excitatory presynaptic terminals and hence only provides partial information on dentate nucleus excitation. Finally, the above studies are performed on post-mortem human brain and represent end-stage disease, thus results should be interpreted with caution whereas conclusions drawn are hypotheses-driven.

5.5.1 Future work

Given cerebellar vulnerability to mitochondrial disease, its significance in integrating upstream sensory input and fine-tuning downstream motor output and the observed changes that point towards altered intra- and extracerebellar circuitry in mitochondrial disease, one appreciates the necessity for closely investigating cerebellar circuitry.

Recent advances in technologies used to control neuronal excitation and inhibition, known as optogenetics, can be used in conjunction with custom made microfluidic champers in order to understand neuronal connectivity and synaptic function in mitochondrial disease. It would be particularly interesting if induced pluripotent stem cells (iPSCs), reprogrammed from patient skin fibroblasts, could be differentiated into neurons and even into functional Purkinje cells (Wang *et al.*, 2015). These could then be allowed to grow in one site of a microfluidic culture platform (Taylor *et al.*, 2005). The perfusion of media across the chamber combined with

axonal polarity would drive unidirectional synapse formation (Taylor *et al.*, 2010), the structural and physiological properties of which can be assessed. Moreover, manipulation of the excitatory-inhibitory balance by optogenetic approaches (Liske *et al.*, 2013) may shed light into possible mechanisms that account for neuronal loss in patients with mitochondrial disease.

Additional to investigating synaptic connectivity, microfluidic chambers can be employed in an attempt to test for the presence of trans-synaptic effects. Can wild-type cells, grown on one site of the chamber, "correct" the deficiency of the cybrids via anterograde effects or do the cybrids retrogradely negatively affect wild-type neurons?

The above experiments may be performed using different neuronal populations depending on the experimental layout. Further to iPSCs, *trans*-mitochondrial embryonic cybrids differentiated into neurons (Kirby *et al.*, 2009; Trevelyan *et al.*, 2010) or primary cultures from mouse models for mitochondrial disease may be employed in order to model synaptic pathology in mitochondrial disease.

5.6 Conclusions

In this study I have shown that dentate nucleus neurons have variably decreased complex I protein expression which is independent to the genetic defect. Neuronal complex I deficiency strongly correlated with presynaptic terminal deficiency and proposes the presence of trans-synaptic effects. The loss of inhibitory pre- and postsynaptic compartments suggests for GABAergic synapse destabilisation and thus, dentate nucleus neuronal disinhibition. Similarly, glutamatergic innervation of dentate nucleus neurons is partially decreased, likely to protect remaining cells from excitotoxicity. Nonetheless, altered intra- and extracerebellar circuitry detected might be responsible for the cognitive and motor disturbances observed in patients with mitochondrial disease.

Chapter 6

Chapter 6 The microvasculature and its effect on neurodegeneration

Understanding the mechanisms contributing to stroke-like cortical lesions in patients with mitochondrial disease

6.1 Introduction

6.1.1 Stroke-like episodes in patients with mitochondrial disease

The complexity of mitochondrial disease is further exemplified by the plethora of neurological symptoms exhibited by patients, amongst which are stroke-like episodes (SLEs) (McFarland *et al.*, 2002). Though a crucial feature of patients with the syndromic diagnosis of mitochondrial encephalomyopathy with lactic acidosis and stroke-like episode (MELAS), due to the m.3243A>G point mutation, SLEs have also been reported in patients with the m.8344A>G point mutation and with secondary mtDNA changes due to mutations in the polymerase gamma (*POLG*) gene (Pavlakis *et al.*, 1984; Tanji *et al.*, 2003; Deschauer *et al.*, 2007; Tzoulis *et al.*, 2014). The term stroke-like is used to describe recurrent neurological deficits that resemble but do not mimic ischemic stroke. Instead, SLEs are associated with lesions that do not follow the major vascular territories of the brain (Ohama *et al.*, 1987; Suzuki *et al.*, 1990; Sue *et al.*, 1998; Tzoulis *et al.*, 2010), they slowly progress to neighbouring brain regions (Iizuka *et al.*, 2003) and are more likely to be reversible (Iizuka *et al.*, 2002). Approximately 20% of patients with the m.3243A>G point mutation present with the classical MELAS phenotype (SLE manifestation) (DiMauro S, 2001) and SLEs can present at any age (Gorman, Shiau Ng *et al* unpublished observation), contrary to what was previously believed (Sproule and Kaufmann, 2008). They are clinically associated with gradual headache, vomiting, seizures and visual abnormalities and are considered to be the underlying cause of focal stroke-like cortical lesions.

Stroke-like cortical lesions are present in posterior cortical regions, involving the occipital, temporal and parietal lobes, as demonstrated upon neuroradiological imaging (Suzuki *et al.*, 1990; Sue *et al.*, 1998; Tanji *et al.*, 2003; Tzoulis *et al.*, 2010). Lesions primarily affect grey matter areas with relative sparing of the white matter and predominate in different cortical regions depending on the genetic defect (occipito-parietal involvement in MELAS and occipital lobe involvement for m.8344A>G and *POLG* mutations) (Tanji *et al.*, 2003; Haas and Dietrich, 2004; Tzoulis *et al.*, 2010; Gropman, 2013). Histopathological examination in affected areas reveals extensive neuronal loss, gliosis plus astrocytic and capillary proliferation (Mizukami *et al.*, 1992; Sue *et al.*, 1998; Betts *et al.*, 2006; Tzoulis *et al.*, 2014).

6.1.2 Theories of the aetiology of stroke-like episodes

The hypothesised mechanisms to account for stroke-like episodes have long been proposed and an extensive amount of evidence exists to support each of the three hypotheses. These are known as the primary vascular, the primary metabolic and the non-ischemic neurovascular hypotheses (Ohama *et al.*, 1987; Gilchrist *et al.*, 1996; Iizuka and Sakai, 2005).

According to the primary vascular hypothesis, mitochondrial dysfunction within the vascular smooth muscle and endothelial cells triggers stroke-like lesion formation. Electron microscopy observations suggest formation of enlarged mitochondria within the smooth muscle and endothelial cells of pial arterioles and small arteries in brain and skeletal muscle (Ohama *et al.*, 1987; Sakuta and Nonaka, 1989; Hasegawa *et al.*, 1991; Mizukami *et al.*, 1992), as well as the presence of morphologically abnormal mitochondria in capillary pericytes of muscle specimens (Sakuta and Nonaka, 1989) serve as the main supporting evidence to this hypothesis. Furthermore, high heteroplasmy levels for the m.3243A>G point mutation in COX-deficient blood (Betts *et al.*, 2006) and pronounced vascular COX-deficiency (relative to neuronal) in the cerebellum of patients with mitochondrial disease favour this theory (Lax *et al.*, 2012). Additionally, smooth muscle and endothelial cell loss along with evidence of blood-brain barrier breakdown strengthens the notion for mitochondrial angiopathic phenomena (Lax *et al.*, 2012). Lastly, changes in regional blood flow as a consequence of decreased cerebrovascular reactivity in patients with the MELAS syndrome (Rodan *et al.*, 2015) and improvement of stroke-like episode severity following L-arginine supplementation (Koga *et al.*, 2005; Koga *et al.*, 2012) hint towards endothelial-driven vasodilatory defects.

The primary metabolic hypothesis suggests that stroke-like episodes are a consequence of a generalised metabolic crisis, likely an additive effect of neuronal, glial and vascular dysfunction (Gropen *et al.*, 1994; Gilchrist *et al.*, 1996). Work performed by Gilchrist and colleagues was supportive of this hypothesis since neuronal and vascular (both in endothelial and smooth muscle cell layers) mitochondria had abnormal cristae organisation upon electron microscopic investigation. Moreover, high levels for the m.3243A>G point mutation in brain were unlikely to solely be due to high heteroplasmic levels in blood vessels (Gilchrist *et al.*, 1996). Similarly, molecular genetic analysis performed by Betts and co-workers revealed high heteroplasmic levels (for the m.3243A>G point mutation) in neurons, though these did not correlate with lesion severity (Betts *et al.*, 2006).

Lastly, the concept that mitochondrial dysfunction in capillaries, neurons or astrocytes results in neuronal hyperexcitability is the basis to the non-ischemic neurovascular hypothesis (Iizuka

and Sakai, 2005). Acute focal hyperperfusion and local neuronal hyperexcitability may initiate a cascade of depolarising events in neighbouring cortical regions shifting the balance between energetic demand and supply (Iizuka *et al.*, 2002; Iizuka *et al.*, 2003). This leads to capillary permeability, local neuronal loss and progressive lesion spreading (Iizuka *et al.*, 2002; Iizuka and Sakai, 2005).

Despite the fact that SLEs has been at the centre stage for many years none of the proposed hypotheses for the aetiology of these episodes is universally accepted, thus the mechanisms underpinning SLE manifestation remain unresolved. The pathological changes associated with SLEs have previously been characterised (Mizukami *et al.*, 1992; Betts *et al.*, 2006; Lax *et al.*, 2012; Tzoulis *et al.*, 2014). However there needs to be a more detailed investigation of the vascular abnormalities in the CNS of patients who present with SLEs if we are to unravel the mechanisms activated and the molecular pathways involved in SLE manifestation. Extended pathological studies combined with direct clinical observations are likely to help identify good candidates for drug targeting and reverse (at least in part) the symptoms of patients who present with SLEs.

6.1.3 The neurovascular unit

The high energetic demand of the brain necessitates a highly sophisticated and dynamic blood supply system to couple blood flow to neural activity. Blood vessels are hierarchically divided into the pial arteries, parenchymal arterioles and capillaries, each of which provides different structural and functional characteristics (Jones, 1970; Cipolla, 2009). Whilst pial arteries contain a single inner endothelial cell layer and an outer layer composed of smooth muscle cells (Cipolla *et al.*, 2004), parenchymal arterioles are composed of a single smooth muscle and endothelial cell layer and an outermost layer made up of astrocytic end-feet (Iadecola, 2004). The former receive extrinsic input from the peripheral nervous systems, whereas the latter communicate with intrinsic neuronal populations. Capillaries on the other hand, establish coupling between neurons and vessels, giving rise to the so-called neurovascular unit. This is composed of an innermost endothelial cell layer engulfed by capillary pericytes and encased by the end feet of astrocytes (Zlokovic, 2008) and is responsible for the exchange of oxygen and nutrients between the capillary bed and neurons.

The synergistic relationship between pial arteries, arterioles and capillaries along with the constant integration of signals arriving from neurons and astrocytes, assures for homeostatic blood supply to the brain. The anatomy of the neurovascular unit is summarised in Figure 6- 1.

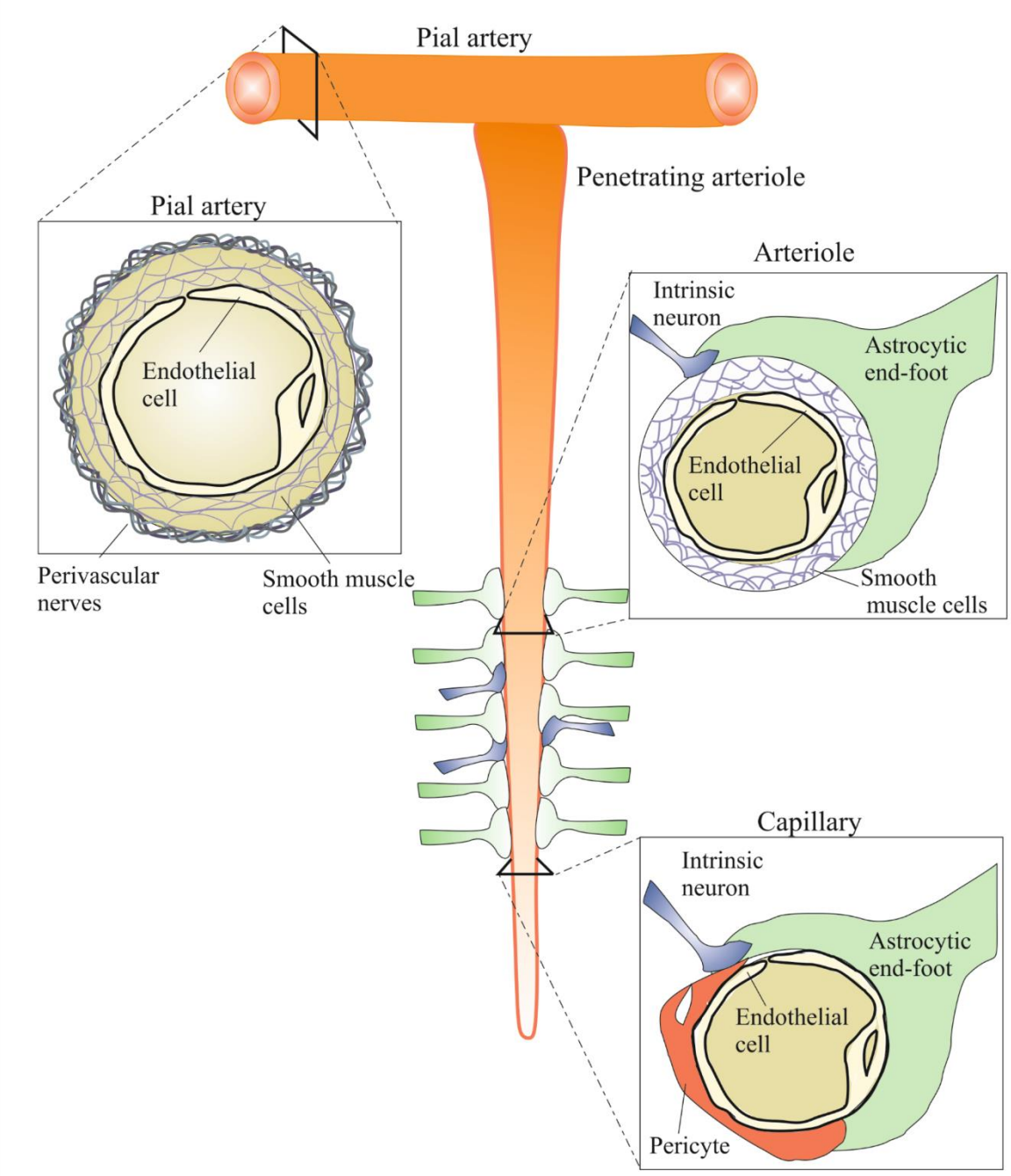

Figure 6- 1: The neurovascular unit.

Pial arteries run along the surface of the brain and branch into arterioles and capillaries that penetrate deeper into the brain. Pial arteries consist of an endothelial cell layer, multiple smooth muscle cell layers (2-3) and an outermost layer of perivascular nerves. Penetrating arterioles are composed of a single endothelial and smooth muscle cell layer and receive intrinsic input through contact with astrocytic end-feet and local neurons. Intrinsic input is also conferred to capillaries which are composed of an innermost endothelial cell layer ensheathed by pericytes.

6.1.4 Mitochondrial function and the vasculature

Although mitochondria are widely known for their capacity for energy production, their function goes beyond ATP synthesis and includes cellular signalling and apoptosis (Quintero *et al.*, 2006; Dromparis and Michelakis, 2013; Tang *et al.*, 2014). The relatively low energetic requirements of the vasculature are met by glycolytic ATP production (Lynch and Paul, 1983; Culic *et al.*, 1997), and vascular mitochondrial density is moderate compared to other tissues (Oldendorf *et al.*, 1977).

The major signalling mechanism utilised by vascular mitochondria involves the production of reactive oxygen species (ROS). Under physiological conditions, ROS production affects vascular tone and cerebral blood flow via regulation of vasoconstrictive and vasodilatory events. Decreased ROS levels promote vascular remodelling, whereas excess ROS drives apoptotic cell death (Dromparis and Michelakis, 2013). Indeed, mitochondrial dysfunction due to excessive ROS production has been demonstrated to contribute to vascular disease (Algahim *et al.*, 2012; Hill *et al.*, 2012).

Likewise, the mitochondrial calcium buffering capacity might have important implications for endothelial function and its response to pathological stimuli (Kluge *et al.*, 2013; Tang *et al.*, 2014), particularly since calcium plays an important role in arteriole dilation (Bubolz *et al.*, 2012) and microvascular response to inflammation (Rowlands *et al.*, 2011). Lastly, mitochondria are crucial to endothelial senescence and apoptosis. Cell senescence is mediated via altered mitochondrial dynamics and elevated mitochondrial ROS in response to normal ageing and/or exposure to cellular stressors (Jendrach *et al.*, 2005; Minamino and Komuro, 2007; Mai *et al.*, 2010; Tang *et al.*, 2014). The apoptotic cell death pathway and consequent endothelial cell loss is triggered by damaging signals and/or disturbed oxygen and nutrient supply to the mitochondria which depolarize the organelles or release pro-apoptotic factors respectively (Wang and Youle, 2009).

6.2 Aims of the investigation

This study primarily aims to explore the consequences of mtDNA defects on the brain vasculature in order to improve our understanding of the aetiology of stroke-like episodes and the underlying pan-necrotic lesions seen in patients with mitochondrial disease. I will achieve this by:

1. Investigating respiratory chain protein abundance in endothelial capillaries and arterioles of posterior cortical regions.
2. Associating neuropathological observations with clinical data available for these patients.

Additionally, since a number of controls were not age-matched, I explored the effect of physiological ageing respiratory chain protein expression and complex IV activity in the vasculature of cognitively normal controls.

6.3 Methodology

6.3.1 Brain tissue samples

For the purposes of this study FFPE cerebellar, occipital and temporal lobe tissue sections from eleven patients who received a genetic and clinical diagnosis confirming mitochondrial disease were neuropathologically investigated (Table 6- 1). Ten cognitively-normal controls acquired from the NBTR were employed to assess the extent of respiratory chain protein deficiency in patients, whereas ten neurologically-normal controls obtained from the MRC Sudden Death Brain and Tissue bank in Edinburgh were used to test for age-related changes in respiratory chain protein expression in the vasculature. Control and patient tissue neuropathological details are summarised in Table 6- 2.

	Pt1	*Pt2*	*Pt3*	*Pt4*	*Pt5*	*Pt7*	*Pt8*	*Pt9*	*Pt10*	*Pt11*	*Pt12*
Age	36	60	30	45	20	42	58	59	79	55	24
Gender	Female	Female	Male	Male	Female	Female	Male	Male	Male	Male	Female
Genotype	m.3243A>G	m.3243A>G	m.3243A>G	m.3243A>G	m.3243A>G	m.8344A>G	m.8344A>G	*POLG* (p.Gly848Ser and p.Ser1104Cys)	*POLG* (p.Thr251Ile/p.Pro587Leu; p.Ala467Thr)	*POLG* (p.Trp748Ser and p.Arg1096Cys)	*POLG* (p.Ala467Thr and p.Trp748Ser)
Disease duration (y)	15	33	11	ND	10	37	23	37	23	50	4
Vascular abnormalities	Granular calcification in putamen and hyalinised vessels in middle frontal gyrus. COX-deficiency, smooth muscle and endothelial abnormalities in the cerebellum	Atherosclerosis in hippocampus and capillary proliferation in frontal lobe. COX-deficiency, smooth muscle and endothelial abnormalities in the cerebellum	-	-	Hyalinisation of cortical and meningeal vessels. COX-deficiency and mineralisation of cerebellar blood vessels	COX-deficient cerebellar vessels	-	Focal haemorrhage in inferior temporal gyrus and hypertrophic capillaries surrounded by macrophages in caudate nucleus	Collagenosis of vessel walls in parietal lobe and globus pallidus	-	-

Clinical information	Multiple stroke-like episodes; first episode associated with imaging changes in right occipital and temporal lobes	Remote history of limb weakness, unclear sight.	No clinical history of stroke-like episodes	Generalised tonic-clonic seizures during stroke-like episodes	No clinical data available	No history of stroke-like episodes	First presentation involved the right temporal, parietal and occipital lobes. The terminal event involved the left hemisphere	No clinical or imaging data. Parkinsonism-like	No history of seizures or stroke-like episodes. Scan 8 years prior to death showed changes in right occipital, parietal and temporal lobe	-	Neuroimaging abnormalities clustered in left parietal and occipital lobes.
Headache	+	-	-	?	?	?	?	?	?	?	?
Stroke-like episodes	+	+	-	+	+	-	+	-	-	-	+
Epilepsy	+	+	-	+	+	+	+	-	-	+	+
Vascular respiratory chain protein expression defects (NDUFB8&COXI)											
Cerebellum	+	+	+	+	+	-	+	-	-	-	+
Occipital lobe	+	+	+	+	+	-	+	-	-	-	+
Temporal lobe	+	+	+	+	+	-	+	-	-	-	-
Stroke-like cortical lesions											
Cerebellum	+	+	-	ND	+	+	-	+	-	+	+
Occipital lobe	+	NT	-	-	+	-	+	-	-	-	-
Temporal lobe	+	NT	-	+	+	-	+	+	+	+	-

Table 6- 1: Clinical and pathological details of patients included in the study.

? = unclear due to limited data; ND – not determined; NT – no tissue available. For the purposes of this study epilepsy is referred to concurrent seizure activity prior to and/or independent to stroke-like episode manifestation.

Type	Age (years)	Sex	Length of fixation (weeks)	Post-mortem delay (hours)	Cause of death	Source
Control 1	69	Female	6	16	Gastric cancer	NBTR
Control 2	68	Male	8	54	Bowel cancer	NBTR
Control 3	78	Female	5	23	metastatic oesophageal carcinoma	NBTR
Control 4	74	Female	13	67	Lung cancer	NBTR
Control 5	55	Male	14	41	Liver cancer	NBTR
Control 6	74	Female	9	53	Heart failure and lung cancer	NBTR
Control 7	70	Male	11	72	Metastatic prostate cancer	NBTR
Control 8	73	Male	7	25		NBTR
Control 9	78	Female	8	34	Metastatic cancer	NBTR
Control 10	45	Male	13	13		NBTR
Control 11	43	Male	1	96	Coronary artery thrombosis and atherosclerosis	Edinburgh
Control 12	74	Female	1	41	Pulmonary thromboembolism	Edinburgh
Control 13	70	Male	1		Hypertensive and ischaemic heart disease, Type 2 diabetes and Fatty degeneration of the liver	Edinburgh
Control 14	52	Male	1	52	Ischaemic heart disease, Coronary artery atherosclerosis and Type 2 Diabetes Mellitus	Edinburgh
Control 15	71	Female	1	41	Ischaemic and hypertensive heart disease	Edinburgh
Control 16	75	Male	1	78	Ischaemic heart disease and Coronary artery atherosclerosis	Edinburgh
Control 17	51	Male	1	71	Ischaemic heart disease and Coronary artery atherosclerosis	Edinburgh
Control 18	41	Female	1	50	Unascertained	Edinburgh
Control 19	33	Male	1	47	Ischaemic heart disease and Coronary artery atherosclerosis	Edinburgh
Control 20	68	Male	1	96	Complications of familial amyloid polyneuropathy	Edinburgh
Patient 1	36	Female	1	42	Cardiac arrest	NBTR
Patient 2	60	Female	6	10	Multi-organ failure	NBTR
Patient 3	30	Male	10	69	Mitochondrial disease	NBTR
Patient 4	45	Female	8	43	Mitochondrial disease	NBTR
Patient 5	20	Male	6	187	Aspiration, pneumonia and MELAS	NBTR
Patient 7	42	Male	8	59	Respiratory failure	NBTR
Patient 8	58	Male	6	66	Stroke-like episodes	NBTR
Patient 9	59	Female	4	67	Pneumonia	NBTR
Patient 10	79	Female	8	85	Respiratory failure	NBTR
Patient 11	55	Male	7	112	Respiratory failure	NBTR
Patient 12	24	Female	18	83	Suppurative tracheobronchitis	NBTR

Table 6- 2: Neuropathological details of control and patient tissue included in the study

6.3.2 Dual COX/SDH histochemistry

15µm-thick frozen brain tissue sections (cerebellum, occipital and temporal lobe) from cognitively normal controls (nine acquired from the NBTR and four from the MRC Sudden Death Brain and Tissue bank, Edinburgh) were subjected to a dual COX/SDH histochemical assay as previously described (section 2.5).

Microvessels were rated according to a semi-quantitative rating scale to ascertain the level of deficiency as follow:

Rating scale	**Criteria**
+	Mild vascular COX-deficiency (~10% of vessels deficient)
++	Intermediate vascular COX-deficiency (~30% of vessels deficient)
+++	Pronounced vascular COX-deficiency (~60% of vessels deficient)
++++	Severe vascular COX-deficiency (~80% vessels deficient)
+++++	COX-deficient vessels present throughout neuropil

The rating system described above relies on the subjective categorisation of vascular COX deficiency, highlighting the need to study respiratory chain protein expression in the brain vasculature using a more reliable, objective and quantitative method.

6.3.3 Immunofluorescence, confocal microscopy and image processing

A previously developed quantitative quadruple immunofluorescent technique (Chapter 3 of this thesis) was used to ascertain the loss of respiratory chain protein subunits within the vasculature of patients with mitochondrial disease compared to cognitively normal controls (section 2.7.1). Glucose transporter 1 (GLUT-1) and alpha smooth muscle actin (α-SMA) were employed to detect the endothelial and smooth muscle cell layer of capillaries and arterioles respectively. The outer mitochondrial membrane protein porin (VDAC1) was used as a mitochondrial mass marker, whereas NADH dehydrogenase [ubiquinone] I beta subcomplex subunit 8 (NDUFB8) and cytochrome *c* oxidase (COX) subunit 1 (COXI) were used to investigate complex I and IV protein expression respectively. All primary and secondary antibodies employed along with their optimal working conditions are listed in Table 6- 3.

Twenty cortical arterioles and twenty cortical capillaries were randomly selected using a point scanning confocal microscope (Nikon A1R) (section 2.8.1). Laser settings were kept constant throughout imaging and z stacking was performed according to the recommended microscope settings (section 2.8.1).

Complex I and IV subunit expression in microvessels was assessed using Volocity®. Once arterioles and capillaries were identified (using α-SMA and GLUT-1 as a reference channel respectively), mitochondria were detected based on their immunoreactivity with porin. Vascular mitochondria were isolated after compartmentalising the mitochondrial population between the vascular population (either arterioles or capillaries). These were then used to obtain fluorescent intensity measurements for porin, NDUFB8 and COXI.

Quadruple immunofluorescence						
Primary antibodies	**Host and isotype**	**Source**	**Catalogue No.**	**Antigen retrieval**	**Optimal dilution**	**Optimal incubation conditions**
Glucose transporter 1 (GLUT-1)*	Rabbit polyclonal - IgG	Thermo Scientific	PA1-21041	EDTA (1mM); 2100 antigen retriever	1 in 100	O/N at 4°C
Alpha- Smooth muscle actin (SMA)*	Rabbit polyclonal - IgG	Abcam	ab5694	EDTA (1mM); 2100 antigen retriever	1 in 100	O/N at 4°C
Voltage-dependent anion channel 1 (VDAC1)	monoclonal - IgG2b	Abcam	ab14734	EDTA (1mM); 2100 antigen retriever	1 in 200	O/N at 4°C
Complex I subunit NDUFB8	Mouse monoclonal - IgG1	Abcam	ab110242	EDTA (1mM); 2100 antigen retriever	1 in 100	O/N at 4°C
Complex IV subunit I	Mouse monoclonal - IgG2a	Abcam	ab14705	EDTA (1mM); 2100 antigen retriever	1 in 200	O/N at 4°C
Secondary antibodies	**Host and epitope**	**Source**	**Catalogue No.**	**Antigen retrieval**	**Optimal dilution**	**Optimal incubation conditions**
Biotin-SP	Goat Anti-Mouse IgG1 (γ1)	Jackson ImmunoResearch	115-065-205	N/A	1 in 200	2 hours, 4°C
Streptavidin, Alexa Fluor® 647 Conjugate	N/A	Life technologies	S32357	N/A	1 in 100	2 hours, 4°C
Alexa Fluor® 405	Goat Anti-Rabbit IgG (H+L)	Life technologies	A31556	N/A	1 in 100	2 hours, 4°C
Alexa Fluor® 488	Goat Anti-Mouse IgG2a (γ2a)	Life technologies	A21131	N/A	1 in 100	2 hours, 4°C
Alexa Fluor® 546	Goat Anti-Mouse IgG2b (γ2b)	Life technologies	A21143	N/A	1 in 100	2 hours, 4°C

Table 6- 3: Primary and secondary antibodies used in this study and their optimised working conditions.

* Indicates antibodies used in alteration.

6.3.4 Statistical analysis

The mean OD values for porin, NDUFB8 and COXI were employed to derive z score for complex I and IV protein expression. A previously described protocol was used (section 3.4.7) with the following modifications:

For each arteriole or capillary the z score for NDUFB8 and COXI levels deviated from the linear regression based on the level of porin.

Each microvessel was classified based on the standard deviation limits for NDUFB8 and COX1 as normal, low, deficient or very deficient. Any other statistical testing was performed as before (section 4.3.5).

6.4 Results

6.4.1 COX-deficiency in the vasculature of neurologically normal controls

Controls obtained from the NBTR and from the MRC Sudden Death Brain and tissue Bank, Edinburgh, exhibited different vascular porin protein expression levels. This was initially speculated to be due to intrinsic tissue processing differences between the two brain tissue resources, thus the controls used to ascertain respiratory chain protein deficiencies in the vasculature of patients with mitochondrial disease were obtained from the same resource as patient samples (NBTR).

Prior to investigating the level of respiratory chain protein expression in the vasculature of patients with mitochondria disease, the accuracy/validity of the dual COX/SDH histochemical assay in determining vascular respiratory chain protein deficiency was tested. Surprisingly, controls obtained both from the NBTR and the MRC Sudden Death Brain and Tissue Bank, Edinburgh, (where frozen tissue was available – 13 out of 20 controls) harboured COX-deficient vessels in the cerebellum, occipital and temporal lobe as observed following COX/SDH histochemistry (Figure 6- 2). Remarkably, some microvessels had absence of COX and SDH reactivity implying that they might be depleted of mitochondria (control 7 – occipital lobe (Figure 6- 2)). Semi-quantitative scores for the severity of vascular COX-deficiency is suggestive of considerable mitochondrial dysfunction in the cerebellar, occipital lobe and temporal lobe vasculature of neurologically normal controls (Table 6- 4).

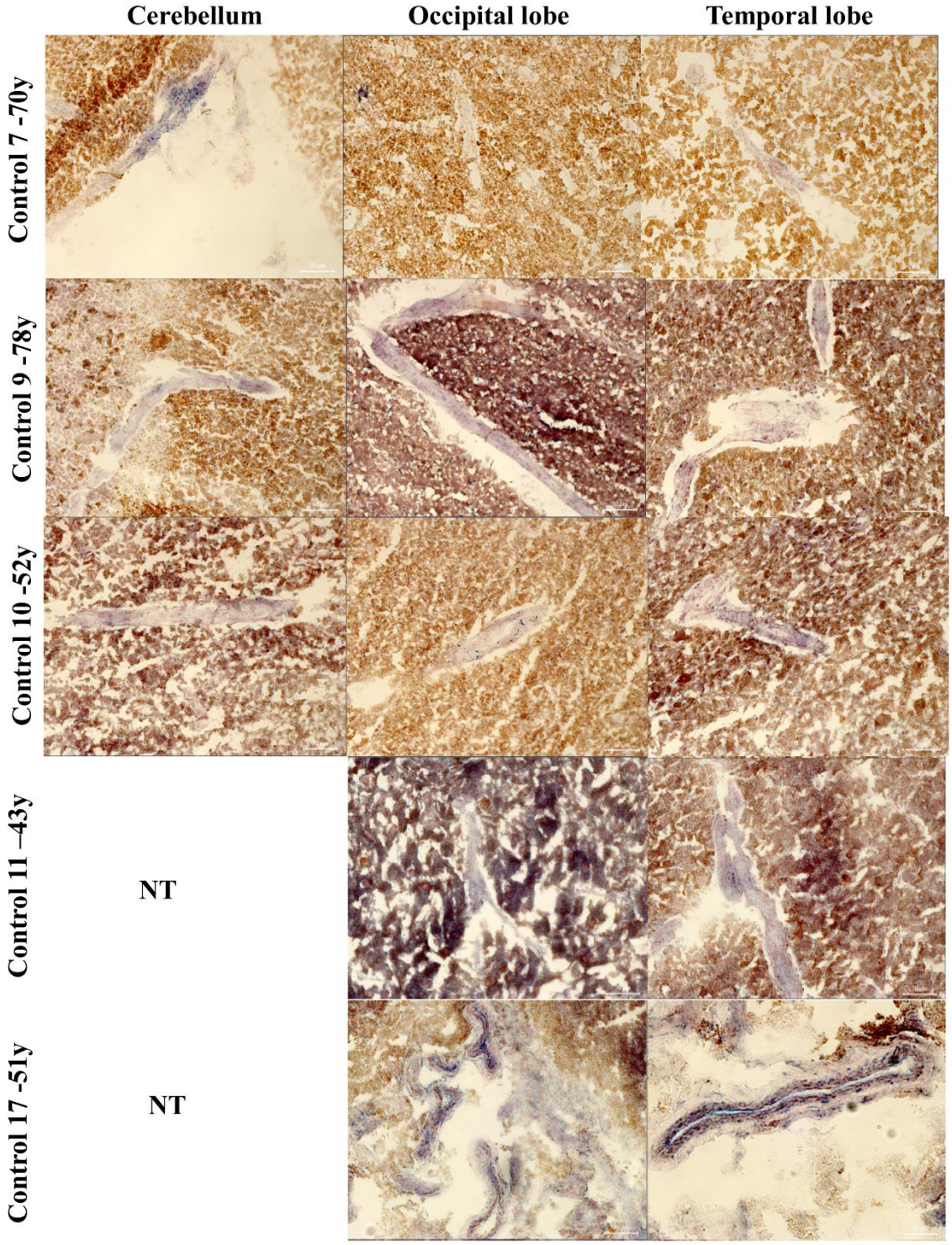

Figure 6- 2: Respiratory chain deficiency in the control vasculature.

Grey matter microvessels stained brown are positive for COX activity, those stained blue (control 11, temporal lobe) are COX deficient, whist microvessels stained purple/grey (control 9, occipital lobe) display intermediate COX deficiency. Scale bar: 50µm. NT- no tissue available

Sample ID	Cerebellum	Occipital	Temporal
Control 1	+++	++++	+++
Control 2	++	++	+++
Control 3	+++	+	NT
Control 4	++++	+	++++
Control 5	++++	++	+++++
Control 6	+++	++	++++
Control 7	+++	+++	++
Control 9	++++	+++++	+++++
Control 10	++++	++++	+++
Control 11	NT	+++++	++++
Control 14	++++	+++	++++
Control 17	NT	++++	++++
Control 18	+++	+++	++++

Table 6- 4: The severity of COX deficiency in control microvessels.

Though neurologically normal, all controls sampled have some degree of vascular COX deficiency in the cerebellum, occipital and temporal lobes. NT – no tissue available.

6.4.2 Respiratory chain protein expression in the cerebellar vasculature

Control cerebellar endothelial capillaries, as judged by the expression of GLUT-1, contained distinct porin-positive puncta indicative of mitochondrial mass (Figure 6- 3). In control capillaries, these mitochondria co-localised with NDUFB8 and COXI implying that mitochondria in control capillaries have intact complex I and IV protein expression respectively (Figure 6- 3). Similarly, a patient harbouring the m.8344A>G point mutation (Patient 7) and a patient with recessive *POLG* mutations (Patient 11) (Table 6- 1) demonstrated matched porin, COXI and NDUFB8 protein expression. On the contrary, capillaries that belonged to Patient 5 (m.3243A>G) lacked NDUFB8 and COXI immunoreactivity, compatible with deficiencies of complexes I and IV (Figure 6- 3). Protein expression quantification and z score analysis helped assign the level of respiratory chain protein deficiency and precisely determine the percentage of microvessels that were normal, low, deficient or very deficient for each of the two proteins (NDUFB8 and COXI). As demonstrated in Figure 6- 4A, patients harbouring the m.3243A>G point mutation have variably decreased levels of NDUFB8 (coloured boxplots) and COXI (clear boxplots), whereas patients harbouring the m.8344A>G point mutation (patient 7 and 8) and those with recessive *POLG* mutations (Patients 9-12) are generally comparable to controls. Patient 8 (m.8344A>G) has isolated COXI defects and patient 12 is the only patient amongst those with recessive *POLG* mutations to show mildly decreased NDUFB8 and COXI protein expression (Table 6- 1) (Figure 6- 4A). Microvessel characterisation exemplifies the presence of combined complex I and IV defects in patients harbouring the m.3243A>G point mutation relative to others (m.8344A>G point mutation and recessive *POLG* mutations) (Table 6- 5).

Z scores derived for complex I and IV protein expression in the cerebellar endothelial cell layer were not affected by PMI (NDUFB8: rho= -0.155, p value= 0.65; COXI: rho= -0.091, p value= 0.79) (Appendix A) or by the length of formalin fixation (NDUFB8: rho= 0.046, p value= 0.892; COXI: rho= 0.593, p value= 0.055) (Spearman's rank correlation).

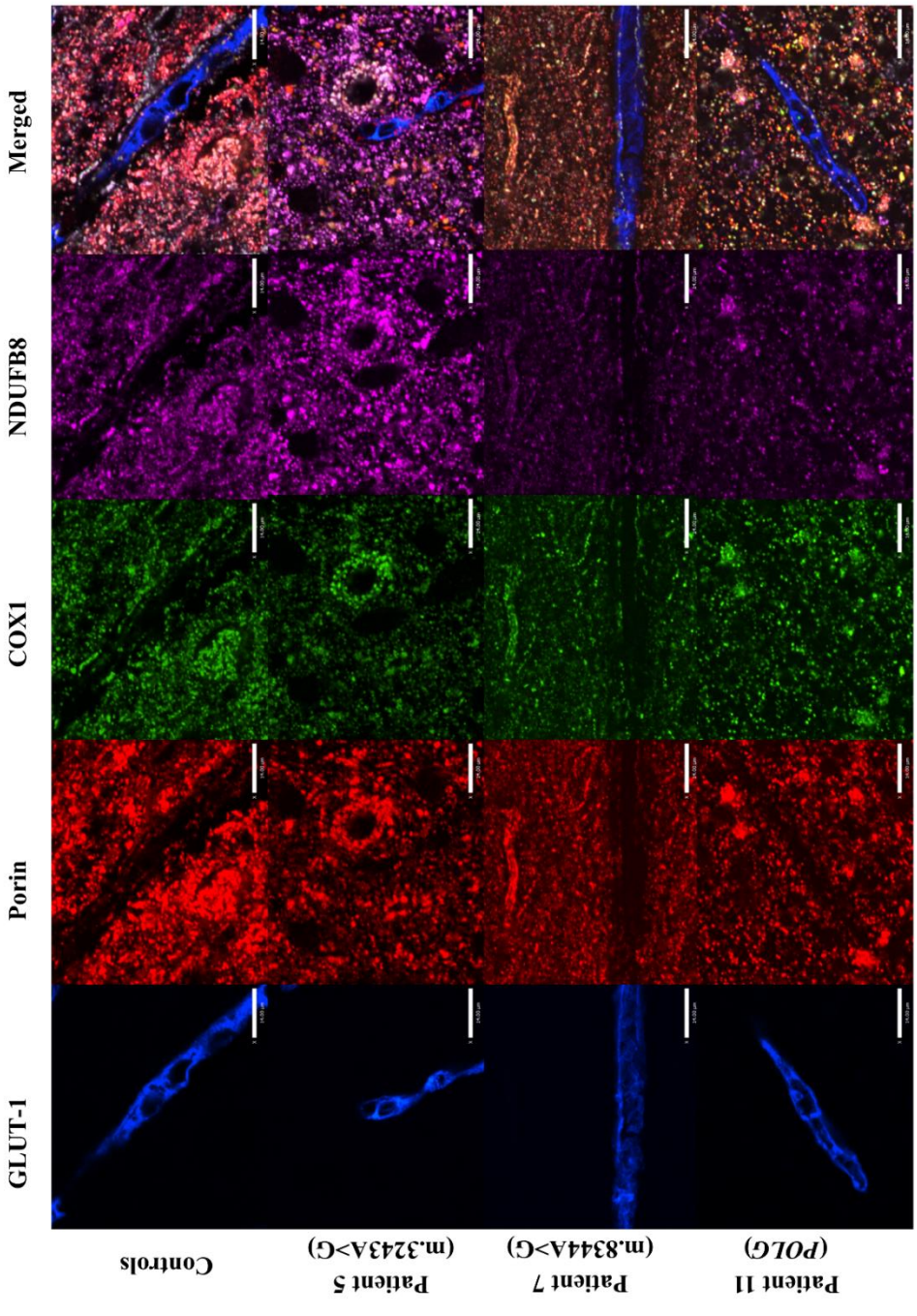

Figure 6- 3: Cerebellar microvessels immunofluorescently stained against glucose transporter 1 (GLUT-1), porin, cytochrome c oxidase subunit 1 (COXI) and NADH Dehydrogenase [ubiquinone] 1 beta subcomplex subunit 8 (NDUFB8).

Porin-positive puncta (representing mitochondria) located within the endothelial cell layer of controls are co-localised with NDUFB8 and COXI, indicative of intact complex I and IV protein expression. Whilst this is also true for patient 7 (m.8344A>G) and 11 (recessive *POLG* mutations), patient 5 (m.3243A>G) possesses microvessels that are immunoreactive only for porin. Thus, there is vascular respiratory chain protein deficiency in this patient. Scale bar: 14µm.

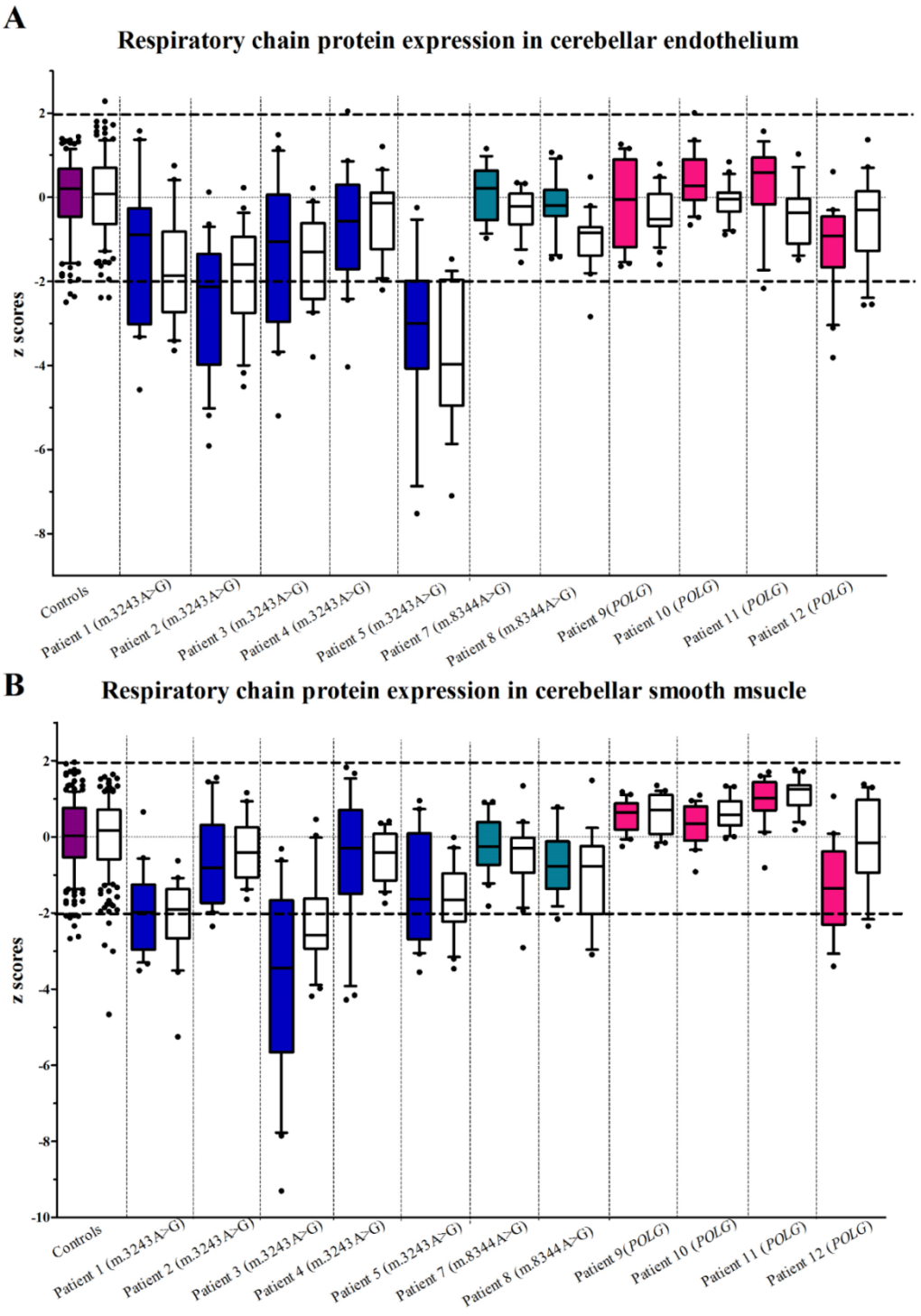

Figure 6- 4: Respiratory chain protein expression quantification in the cerebellar vasculature.

Z score values for the levels of NDUFB8 (coloured boxplots) and COXI (clear boxplots) in the cerebellar endothelial (**A**) and smooth muscle (**B**) cell layers. (**A**) Patients with the m.3243A>G point mutation have combined complex I and IV defects, whereas patient 5 is the one most severely affected. Amongst patients with other genetic defects, mild protein expression changes are evident in patient 8 (m.8344A>G) and 12 (recessive *POLG*). **(B)** Likewise, patients harbouring the m.3243A>G point mutation demonstrate marked changes in NDUFB8 and COXI protein expression in cerebellar arterioles relative to controls. Protein expression changes are also evident in patients 8 (m.8344A>G) and 12 (recessive *POLG*), though to a lesser extent. Each data point reflects a single arteriole or capillary (n=20).

	Controls	Pt1	Pt2	Pt3	Pt4	Pt5	Pt7	Pt8	Pt9	Pt10	Pt11	Pt12
Endothelial cell layer												
Complex I												
Normal (-2< CI_z <2)	97%	60%	43%	65%	85%	22%	100%	100%	100%	100%	94%	81%
Low (CI_z <-2)	3%	15%	24%	10%	10%	28%	0%	0%	0%	0%	6%	10%
Deficient (CI_z <-3)	0%	20%	10%	20%	0%	22%	0%	0%	0%	0%	0%	10%
Very deficient (CI_z <-4)	0%	5%	24%	5%	5%	28%	0%	0%	0%	0%	0%	0%
Complex IV												
Normal (-2< CI_z <2)	98%	60%	57%	65%	95%	28%	100%	95%	100%	100%	100%	90%
Low (CI_z <-2)	2%	25%	24%	30%	5%	6%	0%	5%	0%	0%	0%	10%
Deficient (CI_z <-3)	0%	15%	10%	5%	0%	17%	0%	0%	0%	0%	0%	0%
Very deficient (CI_z <-4)	0%	0%	10%	0%	0%	50%	0%	0%	0%	0%	0%	0%
Smooth muscle cell layer												
Complex I												
Normal (-2< CI_z <2)	96%	50%	95%	30%	80%	55%	100%	94%	100%	100%	100%	63%
Low (CI_z <-2)	4%	25%	5%	5%	10%	35%	0%	6%	0%	0%	0%	26%
Deficient (CI_z <-3)	0%	25%	0%	20%	0%	10%	0%	0%	0%	0%	0%	11%
Very deficient (CI_z <-4)	0%	0%	0%	45%	10%	0%	0%	0%	0%	0%	0%	0%
Complex IV												
Normal (-2< CI_z <2)	98%	55%	100%	30%	100%	60%	95%	78%	100%	100%	100%	89%
Low (CI_z <-2)	1%	25%	0%	50%	0%	30%	5%	17%	0%	0%	0%	11%
Deficient (CI_z <-3)	1%	15%	0%	15%	0%	10%	0%	6%	0%	0%	0%	0%
Very deficient (CI_z <-4)	1%	5%	0%	5%	0%	0%	0%	0%	0%	0%	0%	0%

Table 6- 5: The percentage of cerebellar capillaries and arterioles that are normal, low, deficient or very deficient for complexes I and IV.

Although the majority of control microvessels are normal for NDUFB8 and COXI (complex I and IV respectively), patients 1 -5 (m.3243A>G), 8 (m.8344A>G) and 12 (recessive POLG) possess a mixture of normal, low, deficient or very deficient microvessels.

Similar to endothelial capillaries, cerebellar arterioles, identified by the expression of α-SMA, contained puncta that were positive for porin, indicative of arteriolar mitochondria (Figure 6- 5). Control arterioles had intact complex I and IV protein expression since porin puncta colocalised with NDUFB8 and COXI respectively (Figure 6- 5). Interestingly, mitochondria in patient arterioles were seemingly aggregated closer to the nuclei (vacuole-like pockets), whereas evidence for nuclear proliferation arise from increased density of vacuole-like nuclear pockets (Patient 3, m.3243A>G; Patient 12, recessive *POLG*) (Figure 6- 5). Additional to morphological abnormalities, arteriolar mitochondria had an absence of NDUFB8 and COXI reactivity in a patient harbouring the m.3243A>G point mutation (patient 3), whereas those that belonged to patients 7 (m.8344A>G) and 12 (recessive *POLG*) demonstrated severely decreased protein expression levels (Figure 6- 5). Standard deviation limits for the amount of respiratory chain protein expression in the smooth muscle cell layer shows variable NDUFB8 and COXI expression, with low protein expression levels in patients with the m.3243A>G point mutation, a patient with the m.8344A>G point mutation (patient 8) and one with recessive *POLG* mutations (patient 12) (Figure 6- 4B). The observed changes are confirmed by the percentage of arterioles that are normal, low, deficient or very deficient for either of the two proteins (Table 6- 5). Indeed, only 30% of patient 3's (m.3243A>G) arterioles have normal NDUFB8 and COXI protein expression, whereas approximately half (~55%) the arterioles sampled from patient 1 and 5 (m.3243A>G) are normal for either of the two proteins (Table 6- 5). Patient 2 and 4 (m.3243A>G) possess arterioles that have normal COXI protein expression levels, though some blood vessels are low (patient 2 and 4) and/or very deficient (patient 4) for NDUFB8 (Table 6- 5). Likewise, the majority (>60%) of arterioles sampled from patient 8 (m.8344A>G) and 12 (recessive POLG) have normal respiratory chain protein expression levels (NDUFB8 and COXI), whereas a small proportion of these are low, deficient or very deficient for NDUFB8 and COXI (Table 6- 5).

Neither PMI (NDUFB: rho= 0.173, p value= 0.612; COXI: rho= 0.291, p value= 0.385) (Appendix A) nor fixation length (NDUFB8: rho= -0.056, p value= 0.871; COXI: rho= 0.093, p value= 0.787) exerted any effect on the z score values for respiratory chain protein expression in cerebellar arterioles (Spearman's rank correlation).

When only taking into consideration respiratory chain protein expression in the vasculature of patients with the m.3243A>G point mutation it is evident that the smooth muscle cell layer is more severely affected. Both complex I and IV deficiencies are more pronounced at the arteriole (median NDUFB8z = -1.640, median COXIz = -1.653) compared to the capillary level (median

NDUFB8z = -1.056, median COXIz = -1.591), though respiratory chain protein expression is not statistically different between the two cellular populations (endothelial vs. smooth muscle cell layer) (Wilcoxon Signed-Rank test).

Figure 6- 5: Cerebellar arterioles immunofluorescently stained against alpha smooth muscle actin (α-SMA), porin, COXI and NDUFB8.

Control smooth muscle cells contain distinct mitochondrial puncta with matched COXI and NDUFB8 protein expression. On contrast, patient arterioles contain clusters of porin-positive puncta (indicative of mitochondrial mass) with severely decreased respiratory chain protein expression. Patient 3 (m.3243A>G) possesses arterioles that are deficient for complex I and IV, whereas patients 7 (m.8344A>G) and 12 (recessive *POLG* mutations) contain vascular mitochondria with pronounced decrease in NDUFB8 and COXI protein expression. Scale bar: 14µm.

6.4.3 Respiratory chain protein expression in the occipital lobe vasculature

Similar to the cerebellum, control capillaries in the occipital lobe contained mitochondria with intact complex I and IV expression (Figure 6- 6). The same was true for patients 7 (m.8344A>G) and 9 (recessive POLG) who contained capillaries with matched porin, NDUFB8 and COXI protein expression (Figure 6- 6). Patient 5 (m.3243A>G) on the other hand, possessed capillaries with severely decreased complex I and IV protein expression since porin puncta (mitochondria) did not co-localise with either NDUFB8 or with COXI (Figure 6- 6). Indeed, respiratory chain protein expression quantification indicated severe complex I deficiencies in 4 out of 5 patients carrying the m.3243A>G point mutation (patients 1, 2, 3 and 5) accompanied with milder COXI protein expression changes (Figure 6- 7A). Of the remaining patients (patients 7-12), only patient 8 (m.8344A>G) and 12 (recessive POLG mutations) demonstrated protein expression levels with z scores at the lower range of normal ±2 SD limits (Figure 6- 7A). Categorizing occipital lobe capillaries according to z score values for NDUFB8 and COXI protein expression highlights extensive complex I and milder complex IV deficiencies in patients harbouring the m.3243A>G point mutation, whereas remaining patients have very low (if any) percentage of microvessels that are abnormal for either of the two proteins (Table 6- 6).

Z scores for the level of NDUFB8 and COXI protein expression in occipital lobe capillaries were not affected by either PMI (NDUFB8: rho= -0.018, p value= 0.958; COXI: rho= -0.045, p value= 0.894) (Appendix A) or fixation length (NDUFB8: rho= 0.185, p value= 0.586; COXI: rho= 0.176, p value= 0.605) (Spearman's rank correlation).

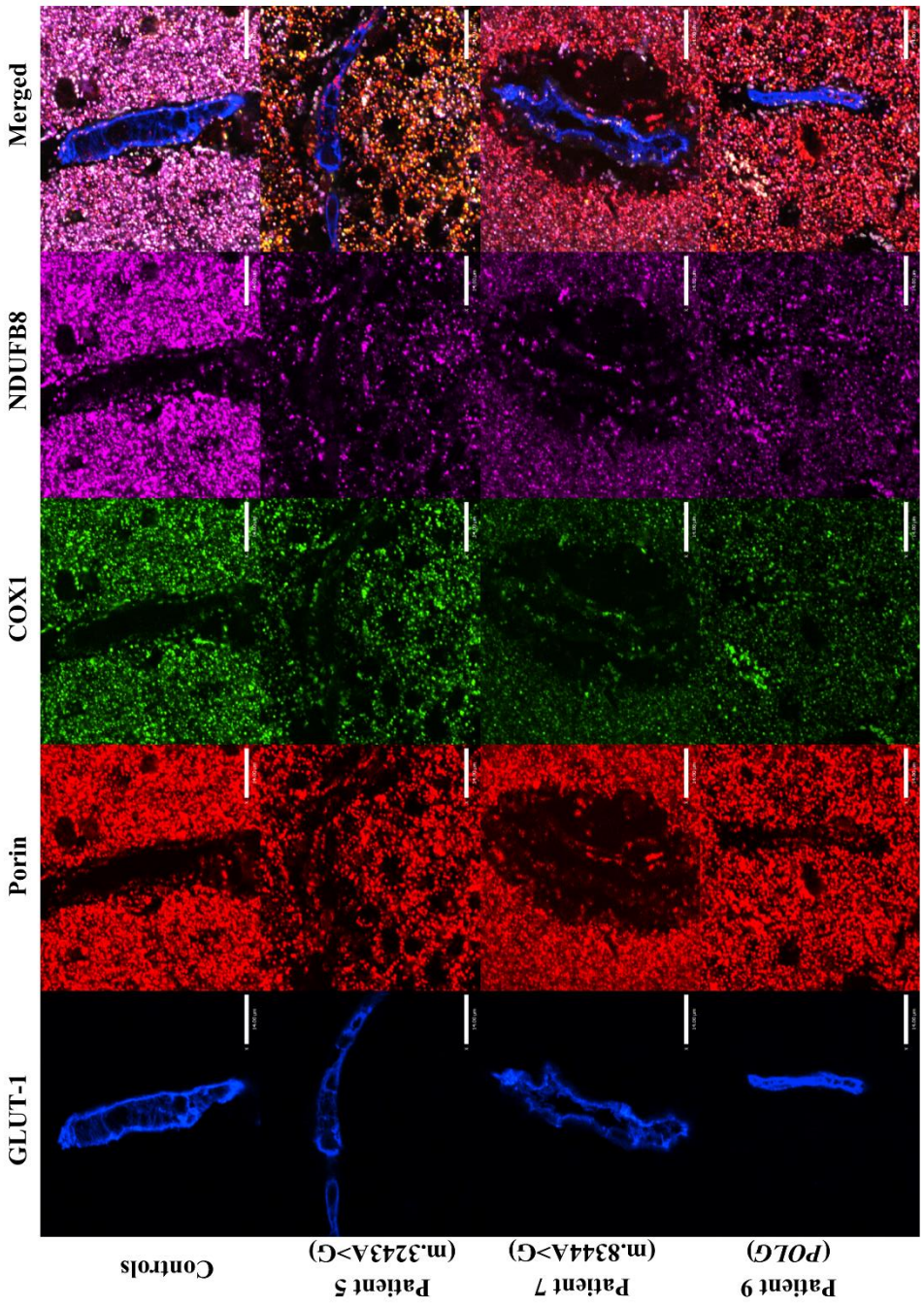

Figure 6- 6: Respiratory chain protein expression in occipital lobe microvessels.

Whilst control capillaries contain mitochondria with preserved complex I and IV protein expression, patient 5 (m.3243A>G) possesses capillarries that are deficient for both complexes since capillary mitochondria lack NDUFB8 and COXI immunoreactivity. On the other hand, patients 7 (m.8344A>G) and 9 (recessive *POLG*) contain cortical capillaries with intact respiratory chain protein expressio. Scale bar: 14µm.

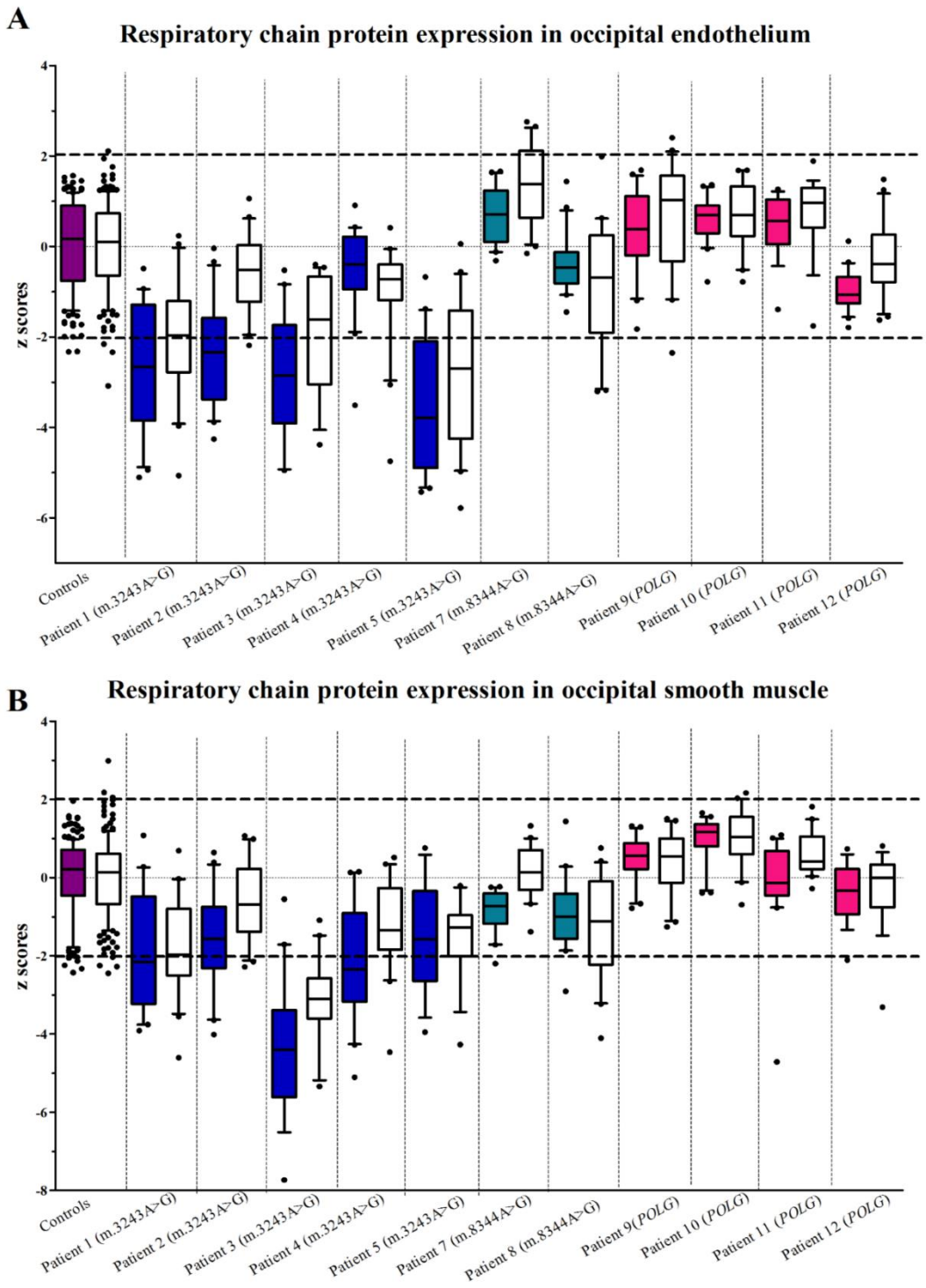

Figure 6- 7: Z score values for the levels of NDUFB8 and COXI expression in occipital lobe vasculature.

(A) Patients harbouring the m.3243A>G point mutation have pronounced NDUFB8 (coloured boxplots) and COXI (clear boxplots) protein expression defects in occipital lobe capillaries. Amongst patients with other genetic defects, mild respiratory chain protein expression decrease is observed in patients 8 (m.8344A>G) and 12 (recessive *POLG*). **(B)** Occipital lobe arterioles that belong to patients 1-5 (m.3243A>G) have combined complex I and IV protein expression changes. Of patients with other genetic defects, decreased protein expression is only evident in patients 7 and 8 (m.8344A>G). Each data point reflects a single arteriole or capillary (n=20).

	Controls	Pt1	Pt2	Pt3	Pt4	Pt5	Pt7	Pt8	Pt9	Pt10	Pt11	Pt12
Endothelial cell layer												
Complex I												
Normal (-2< CI_z <2)	99%	40%	40%	42%	95%	20%	100%	100%	100%	100%	100%	100%
Low (CI_z <-2)	1%	15%	25%	16%	0%	15%	0%	0%	0%	0%	0%	0%
Deficient (CI_z <-3)	0%	20%	30%	21%	5%	15%	0%	0%	0%	0%	0%	0%
Very deficient (CI_z <-4)	0%	25%	5%	21%	0%	50%	0%	0%	0%	0%	0%	0%
Complex IV												
Normal (-2< CI_z <2)	98%	50%	95%	63%	85%	30%	100%	80%	95%	100%	100%	100%
Low (CI_z <-2)	1%	30%	5%	11%	5%	30%	0%	10%	5%	0%	0%	0%
Deficient (CI_z <-3)	1%	15%	0%	16%	5%	10%	0%	10%	0%	0%	0%	0%
Very deficient (CI_z <-4)	0%	5%	0%	11%	5%	30%	0%	0%	0%	0%	0%	0%
Smooth muscle cell layer												
Complex I												
Normal (-2< CI_z <2)	95%	45%	70%	11%	40%	69%	95%	95%	100%	100%	95%	94%
Low (CI_z <-2)	5%	30%	10%	5%	30%	13%	5%	5%	0%	0%	0%	6%
Deficient (CI_z <-3)	0%	25%	15%	21%	10%	19%	0%	0%	0%	0%	0%	0%
Very deficient (CI_z <-4)	0%	0%	5%	63%	20%	0%	0%	0%	0%	0%	5%	0%
Complex IV												
Normal (-2< CI_z <2)	98%	50%	90%	16%	80%	75%	100%	70%	100%	100%	100%	94%
Low (CI_z <-2)	2%	40%	10%	26%	15%	13%	0%	20%	0%	0%	0%	0%
Deficient (CI_z <-3)	0%	5%	0%	37%	0%	6%	0%	5%	0%	0%	0%	6%
Very deficient (CI_z <-4)	0%	5%	0%	21%	5%	6%	0%	5%	0%	0%	0%	0%

Table 6- 6: The percentage of occipital lobe microvessels that are normal, low, deficient or very deficient for complex I and IV.

Despite intact complex I and IV protein expression in the majority of control capillaries and arterioles, patients 1-5 (m.3243A>G) possess microvessels that vary from normal to very deficient for complexes I and IV. Patients 7-12 contain largely normal microvessels.

Arterioles located at the occipital lobe of controls contained distinct mitochondrial puncta with equally high immunoreactivity for NDUFB8 and COXI (Figure 6- 8). In contrast, "mitochondrial aggregates" located in close proximity to the nuclei were evident in the arterioles of patients harbouring the m.3243A>G and m.8344A>G point mutations (Figure 6- 8). These mitochondria were complex I (for both patient 3 and 8) and IV (mainly in patient 8) deficient since they lacked antibody immunoreactivity overall (Figure 6- 8). Instead, patient 9 (recessive POLG mutations) possessed arterioles with morphologically normal mitochondria with intact complex I and IV protein expression (Figure 6- 8). Z score analysis indicated decreased NDUFB8 and COXI expression levels in patients with the m.3243A>G point mutation, compatible with high percentage of vessels that are low, deficient and very deficient for the two proteins (Figure 6- 7B and Table 6- 6). Of the other patients, mild protein expression changes were present in patients 7, 8 (m.8344A>G) 11 and 12 (recessive POLG) (Figure 6- 7B and Table 6- 6).

Protein expression was not affected by PMI (NDUFB8: rho= 0.391, p value= 0.235; COXI: rho= 0.327, p value= 0.326) (Appendix A) or by the length of formalin fixation (NDUFB8: rho= -0.009, p value= 0.987; COXI: rho= 0.028, p value= 0.935) (Spearman's rank correlation).

Remarkably, respiratory chain protein deficiencies in patients with the m.3243A>G are more severe in the endothelial cell layer relative to the smooth muscle layer as exemplified by the lower z score values for NDUFB8 and COXI protein expression (Endothelial cell layer: NDUFB8z= -2.67. COXIz= -1.621; Smooth muscle cell layer: NDUFB8z= -2.161, COXIz= -1.349). Complex I protein expression in arterioles (smooth muscle layer) is not significantly different from that in capillaries (endothelial cell layer), neither is complex IV protein expression (Wilcoxon Singned-Rank test).

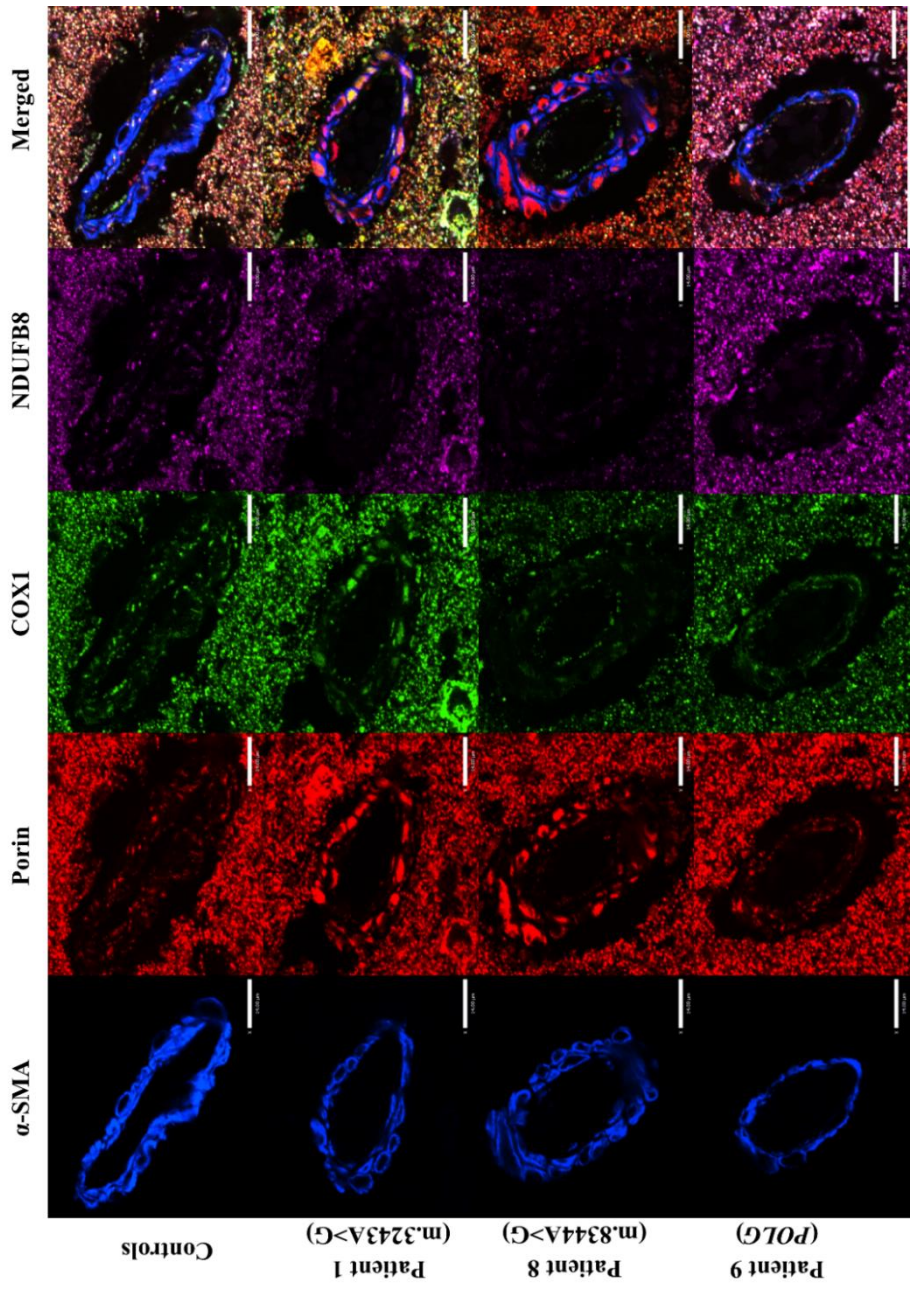

Figure 6- 8: Arterioles located in the occipital lobe immunofluorescently stained against α-SMA, porin, COXI and NDUFB8.

Controls possess arterioles whose mitochondria are located within the smooth muscle cell layer and have matched NUDFB8 and COXI protein expression. This is not the case for patients 1 (m.3243A>G) and 8 (m.8344A>G) whose mitochondrial clusters are located closer to nuclei and have severely decreased NDUFB8 and COXI protein expression. A patient with recessive POLG mutations (patient 9) on the other hand, possesses arterioles with morphologically normal mitochondria with maintained respiratory chain protein expression. Sacle bar: 14µm.

6.4.4 Respiratory chain protein expression in temporal lobe vasculature

Whilst control temporal lobe capillaries contain mitochondria immuno-positive for NDUFB8 and COXI indicating intact complex I and IV protein expression, patient 5 (m.3243A>G) possesses arterioles with marked complex I and IV deficiencies (Figure 6- 9). Capillary complex I deficiency is also evident in patient 12 (recessive POLG mutations), whereas patient 7 (m.8344A>G) contains capillaries with retained respiratory chain protein expression (Figure 6- 9). In agreement with observations made in the cerebellum and occipital lobe, patients harbouring the m.3243A>G point mutation have marked reduction of complex I and IV protein expression relative to controls as revealed by z score analysis (Figure 6- 10A). Patients with other genetic defects (m.8344A>G and recessive POLG mutations) possess microvessels with mainly preserved respiratory chain protein expression as demonstrated by the high percentage (90-100%) of vessels that are normal for both NDUFB8 and COXI (Figure 6- 10A and Table 6- 7).

Z scores for respiratory chain protein expression in temporal lobe capillaries were not affected by PMI (NDUFB8: rho= -0.036, p value= 0.915; COXI: rho= -0.136, p value= 0.689) (Appendix A) or fixation length (NDUFB8: rho= -0.056, p value= 0.445, p value= 0.171) (Spearman's rank correlation).

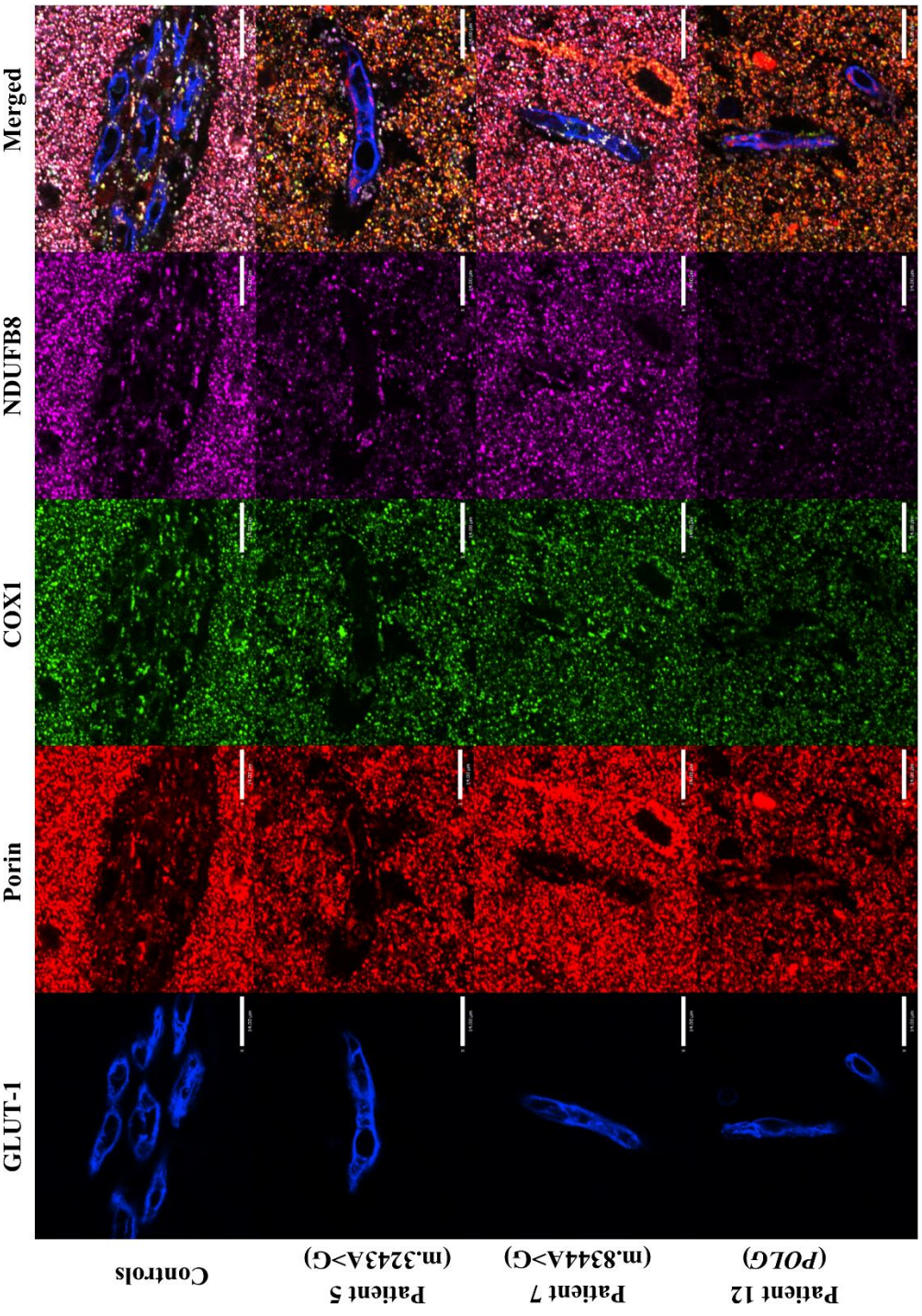

Figure 6- 9: Respiratory chain protein expression in temporal lobe capillaries.

Control capillary mitochondria have matched porin, NDUFB8 and COXI protein expression, indicative of intact respiratory chain protein expression in control microvessels. Patients 5 (m.3243A>G) and 12 (recessive *POLG*) contain capillaries whose mitochondria are deficient for NDUFB8 (both patients) and COXI (patient 5 only). Similar to controls, patient 7 (m.8344A>G) possesses capillaries with preserved respiratory chain protein expression. Scale bar: 14μm.

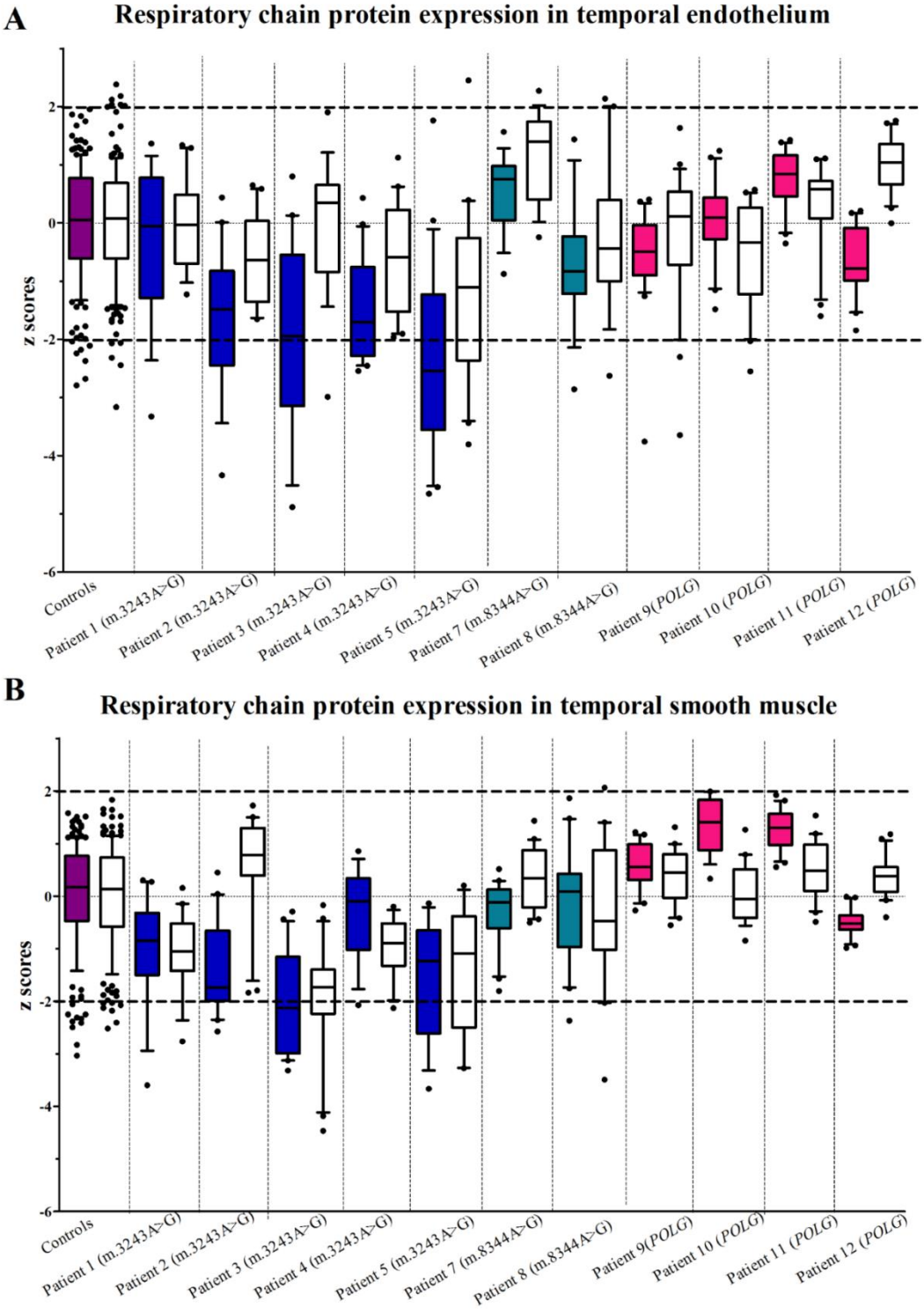

Figure 6- 10: Z score analysis and standard deviation limits for respiratory chain protein expression in temporal lobe vasculature.

(A) Patients 2-5 (m.3243A>G) have decreased NDUFB8 (coloured boxplots) and – to a lesser extent- COXI (clear boxplots) protein expression in temporal lobe capillaries, whereas protein expression defects are also evident for patients 8 (m.8344A>G), 9 and 10 (recessive *POLG*). **(B)** Arteriolar respiratory chain protein expression is decreased in patients 1-5 (m.3243A>G), while moderate changes also occur in patient 8 (m.8344A>G). Each data point reflects a single arteriole or capillary (n=20).

	Controls	Pt1	Pt2	Pt3	Pt4	Pt5	Pt7	Pt8	Pt9	Pt10	Pt11	Pt12
Endothelial cell layer												
Complex I												
Normal (-2< CI_z <2)	96%	84%	53%	58%	70%	43%	100%	89%	95%	100%	100%	100%
Low (CI_z <-2)	4%	11%	37%	16%	30%	19%	0%	11%	0%	0%	0%	0%
Deficient (CI_z <-3)	0%	5%	5%	11%	0%	24%	0%	0%	5%	0%	0%	0%
Very deficient (CI_z <-4)	0%	0%	5%	16%	0%	14%	0%	0%	0%	0%	0%	0%
Complex IV												
Normal (-2< CI_z <2)	97%	100%	100%	95%	100%	67%	100%	95%	91%	90%	100%	100%
Low (CI_z <-2)	2%	0%	0%	5%	0%	19%	0%	5%	5%	10%	0%	0%
Deficient (CI_z <-3)	1%	0%	0%	0%	0%	14%	0%	0%	5%	0%	0%	0%
Very deficient (CI_z <-4)	0%	0%	0%	0%	0%	0%	0%	0%	0%	0%	0%	0%
Smooth muscle cell layer												
Complex I												
Normal (-2< CI_z <2)	94%	84%	75%	45%	93%	69%	100%	95%	100%	100%	100%	100%
Low (CI_z <-2)	6%	11%	25%	30%	7%	19%	0%	5%	0%	0%	0%	0%
Deficient (CI_z <-3)	1%	5%	0%	25%	0%	13%	0%	0%	0%	0%	0%	0%
Very deficient (CI_z <-4)	0%	0%	0%	0%	0%	0%	0%	0%	0%	0%	0%	0%
Complex IV												
Normal (-2< CI_z <2)	96%	89%	100%	60%	93%	75%	100%	85%	100%	100%	100%	100%
Low (CI_z <-2)	4%	11%	0%	25%	7%	6%	0%	10%	0%	0%	0%	0%
Deficient (CI_z <-3)	0%	0%	0%	5%	0%	19%	0%	5%	0%	0%	0%	0%
Very deficient (CI_z <-4)	0%	0%	0%	10%	0%	0%	0%	0%	0%	0%	0%	0%

Table 6- 7: Percent normal, low, deficient and very deficient microvessels in temporal lobe.

Patients harbouring the m.3243A>G point mutation (patient 1-5) have a mixture of normal, low, deficient and very deficient capillaries and arterioles for complex I and IV. On the other hand, patients with other genetic defects have mainly vasculature in which the respiratory chain is intact.

In spite of complex I- and IV- intact mitochondria present in control temporal lobe arterioles, the arterioles of patients harbouring the m.3243A>G point mutation contained groupings of mitochondria that are deficient for both complex I and IV (Figure 6- 11). On the contrary, the smooth muscle cell layer in the arterioles of patient 7 (m.8344A>G) contained mitochondria with mildly decreased NDUFB8, whereas patient 10 (recessive *POLG* mutations) possessed arterioles with complex I- and IV-intact mitochondria (Figure 6- 11). Quantification of immunofluorescence demonstrates altered NDUFB8 and COXI protein expression only in the arterioles of patients with the m.3243A>G point mutation (Figure 6- 10B), reflected by the variable percentage of arterioles that are normal, low, deficient or very deficient in these patients (Table 6- 7). Amongst patients with other genetic defects, only patient 8 (m.8344A>G) contained vessels with abnormal respiratory chain protein expression (Figure 6- 10B and Table 6- 7).

Neither PMI (NDUFB8: rho= 0.391, p value= 0.235; COXI: rho= -0.118, p value= 0.729) (Appendix A) nor fixation length (NDUFB8: rho= -0.046, p value= 0.892; COXI: rho= -0.083, p value= 0.808) affected respiratory chain protein expression in temporal lobe arterioles.

Interestingly, in patients with the m.3243A>G point mutation there is more complex I expression defects in the endothelial cell layer (Median NDUFB8z: endothelium= -1.703, smooth muscle= -1.233), whilst complex IV protein expression abnormalities are more pronounced in the smooth muscle cell layer (Median COXIz: endothelium= -0.587, smooth muscle cell layer= -1.052). Nevertheless, the level of NDUFB8 and COX1 expression between the two vascular cell populations is not significantly different (Wilcoxon Signed-Rank test).

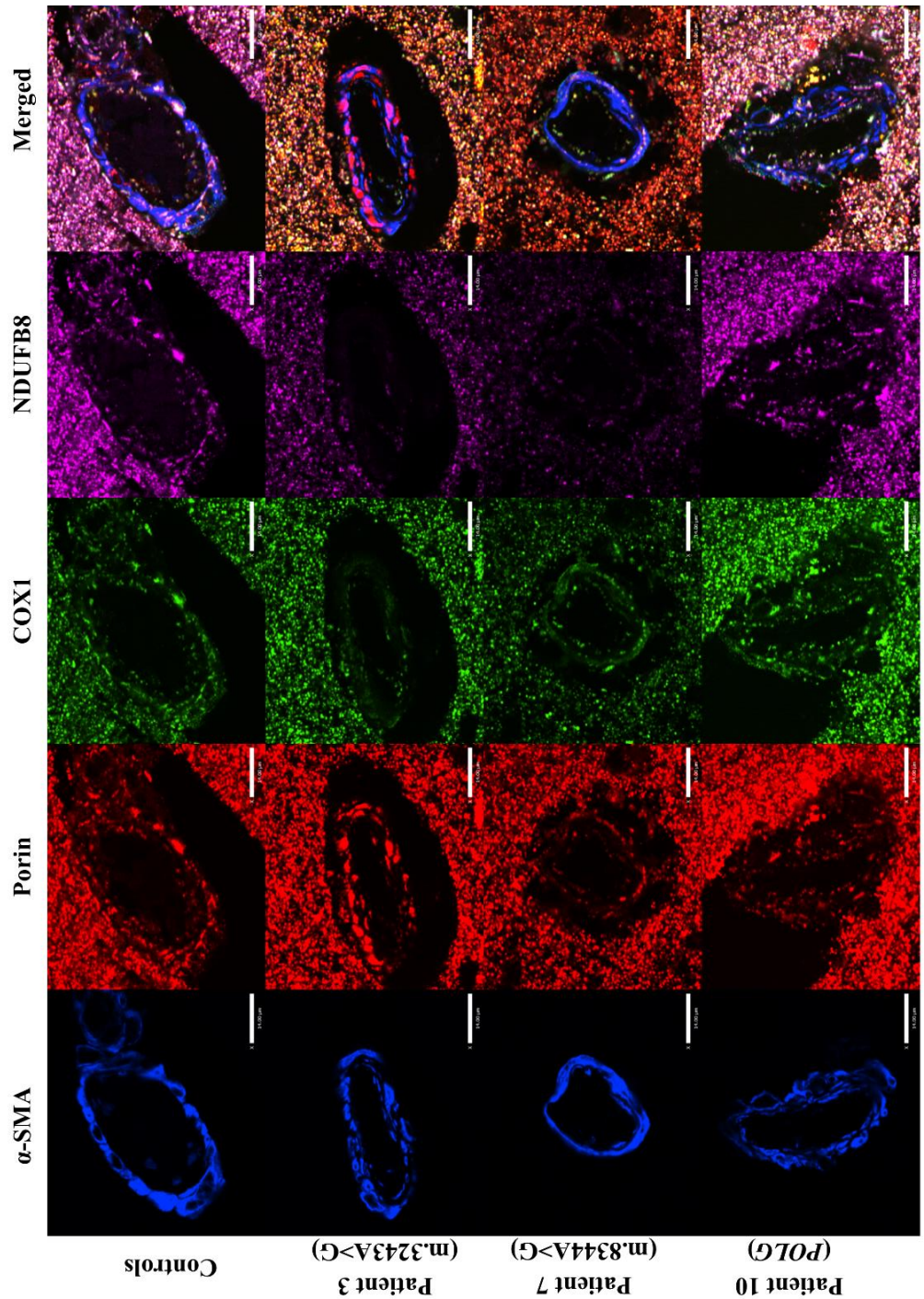

Figure 6- 11: Temporal lobe arterioles and their respiratory chain protein expression.

Controls contain arterioles with respiratory chain intact mitochondria, whereas patient 3 (m.3243A>G) contains microvessels with "grouped" mitochondria that are negative for NDUFB8 and COXI immunoreactivity. Patients' 7 (m.8344A>G) and 10 (recessive POLG) arteriolar mitochondria have largely preserved NDUFB8 and COXI protein expression (slightly decreased NDUFB8 expression for patient 7; m.8344A>G). Scale bar: 14µm.

For both the endothelial and smooth muscle cell layer there is considerable variation in the degree of complex I and IV deficiency observed between patients. Patients with the m.3243A>G point mutation have significantly more severe vascular respiratory chain protein expression defects across all brain regions investigated (cerebellum, occipital and temporal lobe) compared to patients with other genetic defects (m.8344A>G and recessive *POLG* mutations). Complex IV deficiency is more pronounced in the cerebellar vasculature, whereas the occipital and temporal lobe microvessels have more complex I protein expression defects. Moreover, the smooth muscle cell layer of cerebellar arterioles harbours the more severe defects (relative to the endothelial cell layer) contrary to severe respiratory chain deficiency observed in the endothelial cell layer of occipital and temporal lobe capillaries. Generally, and when only taking into account patients with the m.3243A>G point mutation, the occipital lobe vasculature was most severely affected followed by defects in the cerebellum and the temporal lobe.

6.4.5 Investigating respiratory chain protein expression in ageing brain vasculature

Since the controls employed to assess respiratory chain protein expression in the vasculature were not age-matched to patients with mitochondrial disease, we examined whether age exerts any effect on vascular mitochondrial mass and/or respiratory chain protein expression. For this purpose, occipital lobe tissue from ten cognitively normal controls (obtained from the MRC Sudden Death Brain and Tissue Bank in Edinburgh) was subjected to quadruple immunofluorescence (see section 6.3.3). The control age-range varied between 33-75 years of age whilst all controls had a standard 1 week of formalin fixation (Controls 11-20) (Table 6- 2). As demonstrated in Figure 6- 12, all controls contained distinct porin–positive puncta, representing mitochondria, with matched NDUFB8 and COXI protein expression. No changes in protein expression within the smooth muscle cell layer were evident between controls of different ages (Figure 6- 12). Indeed, z scores for the level of porin (Figure 6- 13A), NDUFB8 (Figure 6- 13B) and COXI (Figure 6- 13C) expression are indicative of equally high protein expression regardless of age (Figure 6- 13). Likewise, the vast majority of control arterioles have normal mitochondrial mass and intact respiratory chain protein expression (Table 6- 8). This is further exemplified by the lack of correlation between age and median z scores for the level of porin, NDUFB8 and COXI expression (Age vs. porin: rho= -0.018, p value= 0.973; age vs. NDUFB8: rho= -0.006 p value= 1; age vs. COXI: rho= -0.042, p value= 0.919) (Spearman's rank correlation).

The derived z score values were not affected by PMI (porin: rho= -0.109, p value= 0.780; NDUFB8: rho= -0.728, p value= 0.056; COXI: rho= -0.597, p value= 0.089).

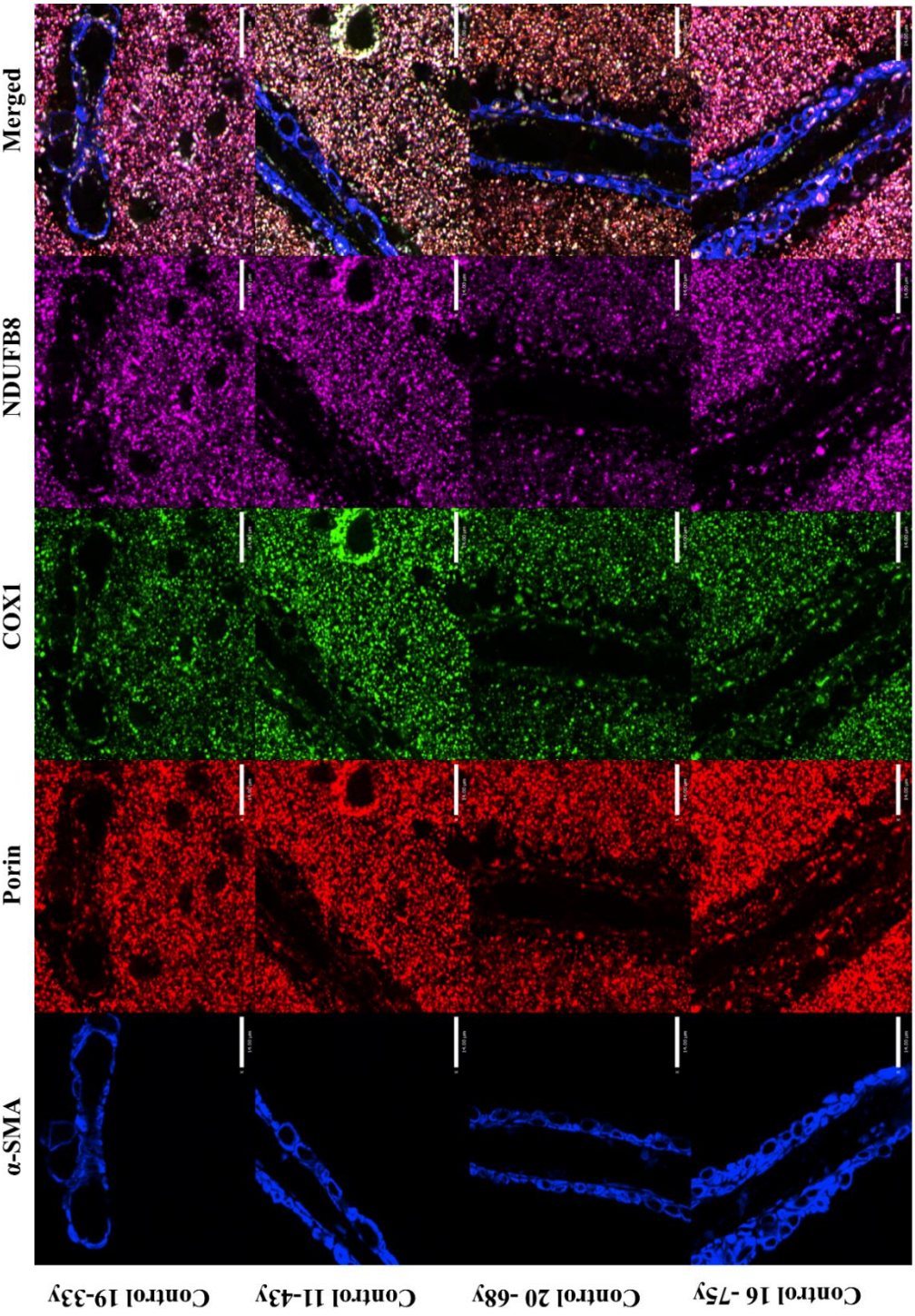

Figure 6- 12: Control occipital lobe arterioles immunofluorescently stained against α-SMA, porin, COXI and NDUFB8.

Regardless of age, the smooth muscle cell layer contained porin-positive puncta with comparable NDUFB8 and COXI protein expression. Hence, all control arterioles are occupied by mitochondria with intact complex I and IV protein expression. Scale bar: 14μm.

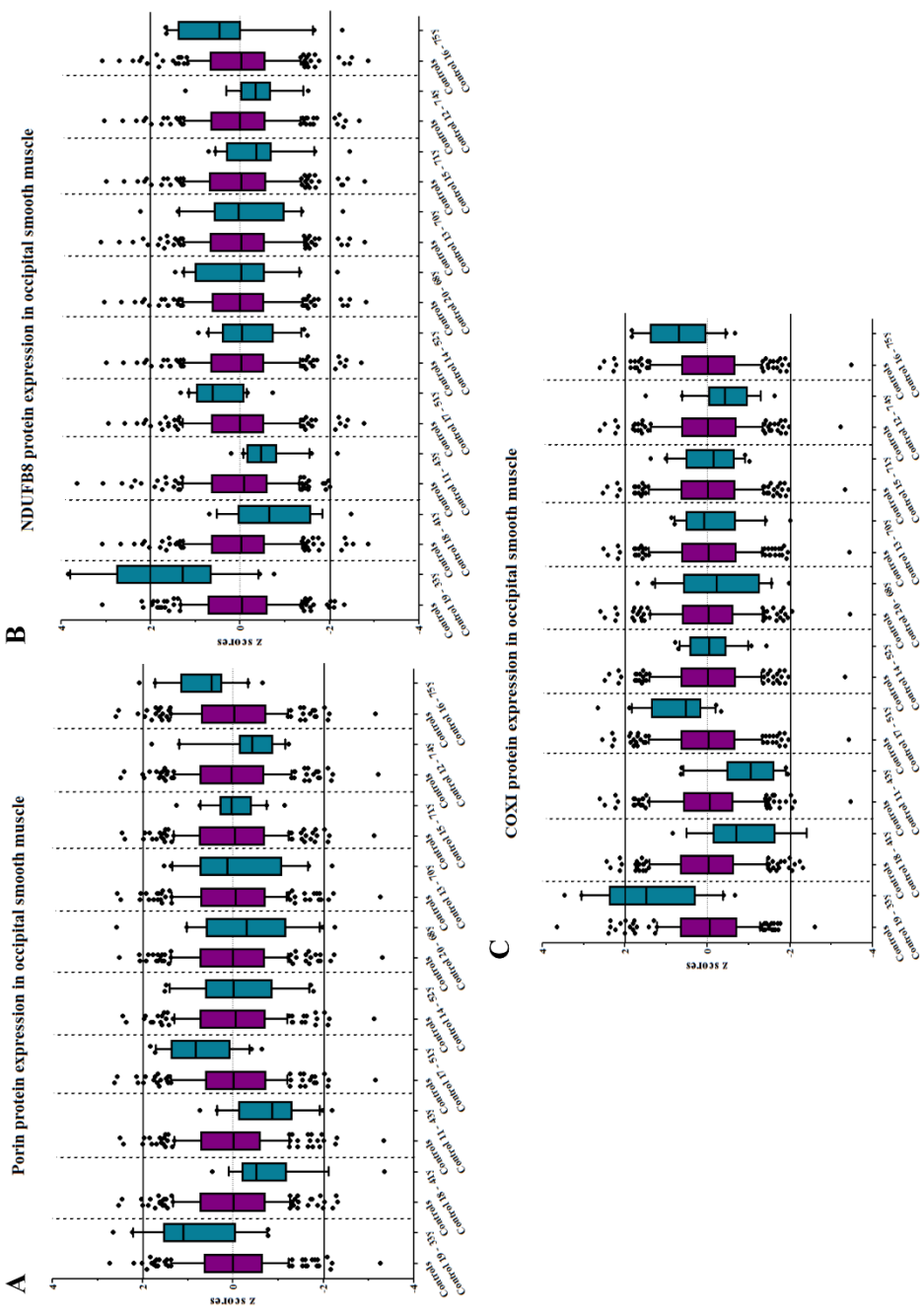

Figure 6- 13: Mitochondrial protein expression in control occipital lobe arterioles.

The level of porin **(A)**, NDUFB8 **(B)** and COXI **(C)** protein expression in the arterioles of controls. **(A)** Z score values for the level of porin protein expression indicate that all control arterioles, regardless of age, have similar mitochondrial mass. **(B)** NDUFB8 protein expression appears to be unaffected by age, since there is very little variation in protein expression amongst controls. **(C)** Likewise, COXI protein expression is identical amongst controls of various ages. Each data point reflects a single arteriole (n=20).

	Controls	Control 11	Control 12	Control 13	Control 14	Control 15	Control 16	Control 17	Control 18	Control 19	Control 20
Porin											
Normal (-2< CI_z <2)	98%	95%	100%	95%	100%	100%	100%	100%	94%	100%	95%
Low (CI_z <-2)	1%	5%	0%	5%	0%	0%	0%	0%	0%	0%	5%
Deficient (CI_z <-3)	1%	0%	0%	0%	0%	0%	0%	0%	6%	0%	0%
Very deficient (CI_z <-4)	0%	0%	0%	0%	0%	0%	0%	0%	0%	0%	0%
Complex I											
Normal (-2< CI_z <2)	99%	95%	100%	100%	100%	95%	100%	100%	100%	100%	100%
Low (CI_z <-2)	1%	5%	0%	0%	0%	5%	0%	0%	0%	0%	0%
Deficient (CI_z <-3)	0%	0%	0%	0%	0%	0%	0%	0%	0%	0%	0%
Very deficient (CI_z <-4)	0%	0%	0%	0%	0%	0%	0%	0%	0%	0%	0%
Complex IV											
Normal (-2< CI_z <2)	98%	100%	100%	100%	95%	100%	100%	90%	94%	100%	100%
Low (CI_z <-2)	2%	0%	0%	0%	5%	0%	0%	10%	6%	0%	0%
Deficient (CI_z <-3)	0%	0%	0%	0%	0%	0%	0%	0%	0%	0%	0%
Very deficient (CI_z <-4)	0%	0%	0%	0%	0%	0%	0%	0%	0%	0%	0%

Table 6- 8: The percentage of control arterioles that are normal, low, deficient or very deficient for porin, complex I and complex IV.

The vast majority of control microvessels have normal mitochondrial mass and intact respiratory chain protein expression, whereas (when present) a small percentage (~5%) of these have low mitochondrial protein expression.

6.5 Discussion

Stroke-like episodes are prominent, but not restricted, to patients with a clinical diagnosis of MELAS and are believed to contribute to the development of ischaemic-like cortical lesions seen neuropathologically in these patients (Sue *et al.*, 1998; Tanji *et al.*, 2003; Deschauer *et al.*, 2007). Posterior cortices are typically affected, within which morphological and functional neuronal and vascular abnormalities have been extensively documented (Betts *et al.*, 2006; Tzoulis *et al.*, 2006; Tzoulis *et al.*, 2010; Lax *et al.*, 2012). Theories on the aetiology of the episodes and mechanisms that account to the progression of the condition have been proposed, yet no single mechanism is universally accepted which negatively impacts the way in which patients with the condition are treated. The above highlight the necessity for an in depth investigation of the extent of vascular respiratory chain defects in patients with mitochondrial disease in an attempt to unravel the mechanisms underpinning SLEs. Dual COX/SDH histochemistry was employed to assess respiratory chain activity in the vasculature of neurologically normal controls and explore the validity of the method in documenting vascular deficiencies. To understand the potential contribution of mitochondrial impairments in the vasculature, a previously developed quantitative quadruple immunofluorescent technique (Chapter 3 of this thesis) was modified to investigate respiratory chain protein expression in cortical blood vessels within the cerebellar, occipital and temporal lobe of eleven patients with mitochondrial disease. Finally, the effect of ageing on mitochondrial mass, complex I and IV protein expression was evaluated using cognitively normal controls.

COX/SDH has initially been developed in order to examine respiratory chain activity (COX activity relative to SDH) in single muscle fibres (Old and Johnson, 1989) and primarily employed to assess the level of COX-deficiency in patients with mitochondrial myopathy (Sciacco *et al.*, 1994). Since then COX/SDH has served as an invaluable tool for detecting cells that are deficient for COX (Ross, 2011) and has been employed in the past to document enzymatic deficiencies in the vessels of patients with mitochondrial disease (Betts *et al.*, 2006; Lax *et al.*, 2012). Surprisingly, COX/SDH histochemistry employed for the purposes of this study revealed that cognitively normal controls possess a significant proportion of microvessels that are deficient for COX. This is true for all posterior brain regions studied (cerebellum, occipital lobe and temporal lobe), for controls obtained from both the NBTR and the MCR, Sudden Death Brain and Tissue Bank (Edinburgh) and for a control cohort with a wide age range (41-78 years of age). Thus, COX/SDH histochemistry is not a trustworthy method for assigning vascular respiratory chain deficiency in patients with mitochondrial disease and any results obtained from the use of this technique alone should be interpreted with caution.

Regardless, there are a number of factors that can explain for vascular COX-deficiency detected in controls included in this study. As mentioned previously, COX/SDH histochemistry was developed to assess respiratory chain activity in muscle fibres and was later optimised for its use in the brain. However, the technique has not been specifically optimised for brain microvessels, thus the results might be reflective of a lack of method optimisation for its use in the vasculature. Moreover, the use of post-mortem tissue is itself an important shortcoming. Post-mortem tissue processing and/or interval might negatively affect respiratory chain activity in the brain vasculature, which might overall be more susceptible to acquiring deficiencies relative to neurons. Lastly, the controls' cause of death (Table 6- 2) might also explain for the results obtained in this study. Vascular disease in some and possible exposure to chemotherapeutics in others, which negatively impacts mitochondrial function, may account for the profound enzymatic deficiencies detected here (Tang *et al.*, 2014; Yoshida *et al.*, 2015).

Quantitative quadruple immunofluorescence has been the preferred method for assessing respiratory chain protein expression in the vasculature of patients with mitochondrial disease and neurologically normal controls. This technique demonstrated the existence of vascular respiratory chain deficiency in patients harbouring the m.3243A>G point mutation. More specifically, capillaries and arterioles located in the cerebellum, occipital and temporal lobe of patients with the m.3243A>G point mutation, have combined complex I and IV protein expression defects, in agreement with severe complex I and milder complex IV deficiencies detected in inhibitory interneurons located in the occipital, temporal and frontal lobe cortices of these patients (Lax *et al.*, 2015). Decreased respiratory chain protein expression is also documented for a patient harbouring the m.8344A>G point mutation (patient 8) and one with recessive *POLG* mutations (patient 12), though to a lesser extent. Vascular respiratory chain protein expression defects detected in this study are in line with vascular COX-deficiency previously reported in patients with the m.3243A>G and m.8344A>G point mutation (Betts *et al.*, 2006; Lax *et al.*, 2012)

When only considering those patients who harbour the m.3243A>G point mutation (patients 1-5), it appears that the occipital lobe vasculature is the one most severely affected since both the endothelial and smooth muscle cell layers have marked complex I and IV deficiencies relative to the same cellular populations of the cerebellum and temporal lobe. This is in agreement with neuroradiological observations in patients with the MELAS syndrome that signify the presence of focal occipital lobe lesions (Sue *et al.*, 1998). Fascinatingly, the cerebellar vasculature (both cell layers) has decreased complex IV protein expression (relative to complex I), whereas

complex I deficiencies are more prominent in the microvessels of the occipital and temporal lobe cortices. Furthermore, respiratory chain protein expression deficiencies are more pronounced in the endothelial cell layer of occipital and temporal lobe microvessels (relative to the smooth muscle layer), whereas the reverse is true for the cerebellum. These could be denotive of differing vulnerability to respiratory chain protein expression deficiencies amongst different brain regions and in fact amongst the two vascular cell layers.

Altered respiratory chain protein expression in the vasculature of patients with mitochondrial disease generally coincides with the incidence of stroke-like episodes and epilepsy across the patient cohort but not necessarily with stroke-like cortical lesions recorded macroscopically (Table 6- 1) (Lax *et al.*, 2012) (unpublished data). Interestingly, respiratory chain protein expression defects have been detected in the microvasculature of patient 3 (m.3243A>G), although there is no clinical history of stroke-like episodes or epilepsy for this patient. In contrast, patient 7 (m.8344A>G) and 11 (recessive *POLG*) have a clinical history of epilepsy, though no vascular respiratory chain protein expression defects are detected and no stroke-like episodes are being reported. These suggest that vascular respiratory chain defects alone cannot explain the presence of stroke-like episodes in patients with mitochondrial disease. This is strengthened by the detection of COX-deficient microvessels in cognitively normal controls and proposes that multiple hits (likely an additive effect between neuronal/interneuronal and vascular deficiency) are required for stroke-like episode manifestation.

Further to vascular respiratory chain protein deficiencies, mitochondrial density and/or dynamics was also altered. Though not quantified, observations suggest mitochondrial accumulation/proliferation mainly in patients harbouring the m.3243A>G point mutation, similar to ragged-red fibres documented in patients with mitochondrial disease (Berkovic *et al.*, 1989; Tokunaga *et al.*, 1993). These mitochondria were mostly deficient for both NDUFB8 and COXI protein expression, implying that nuclear proliferation might occur in affected arterioles in order to support increased mitochondrial biogenesis (Duguez *et al.*, 2002; Trinei *et al.*, 2006), which might occur as means to compensate for mitochondrial deficiency. However, newly synthesised mitochondria are still dysfunctional. Similarly, electron microscopic studies on cerebral and cerebellar blood vessels have reported the presence of enlarged, aggregated and morphologically abnormal mitochondria within the smooth muscle and endothelium of small arteries and within capillary pericytes (Ohama *et al.*, 1987; Sakuta and Nonaka, 1989; Mizukami *et al.*, 1992) .

Mitochondria have previously been shown to act as signalling organelles within the vasculature, acting to maintain calcium homeostasis, produce reactive oxygen species and regulate apoptotic cell death (Quintero *et al.*, 2006; Zhang and Gutterman, 2007; Dromparis and Michelakis, 2013; Tang *et al.*, 2014). Respiratory chain deficiencies detected in the blood vessels of patients with mitochondrial disease combined with inhibitory interneuronal deficiency (Lax *et al.*, 2015) is likely to negatively impact upon vascular tone regulation and cerebral blood flow. Local inhibitory interneurons are known to be important in coupling neuronal activity to blood flow (Vaucher *et al.*, 2000; Cauli *et al.*, 2004; Rancillac *et al.*, 2006), hence failure of interneurons to regulate microvascular tone in combination with aberrant signalling within the microvessels could collectively contribute to stroke-like episode manifestation and stroke-like lesion formation in patients with mitochondrial disease.

Additional to examining respiratory chain protein expression in the vasculature of patients with mitochondrial disease, the effect of age on arteriolar mitochondrial mass and respiratory chain protein expression was assessed. Surprisingly, no changes are observed with regards to mitochondrial mass or respiratory chain protein expression in occipital lobe arterioles of aged controls. This is in contrast to studies performed on aged animals that report age-related decline in vascular mitochondrial mass and function (Burns *et al.*, 1979; Ungvari *et al.*, 2008) or with studies that document age-related structural changes in vascular cell layers and altered regional blood flow in older adults (Martin *et al.*, 1991; Dohi *et al.*, 1995; Chen *et al.*, 2011). However, the control group employed here is small and further research is required before we can extrapolate on these results.

Notwithstanding respiratory chain protein expression deficiencies detected in cerebellar, occipital and temporal lobe microvessels of patients with mitochondrial disease, this study holds significant drawbacks that need to be taken into account. Firstly, pathological examination is performed on post-mortem brain tissue and represents end-stage disease, thus any changes detected are due to chronic abnormalities and should be interpreted with caution. Secondly, studies were performed on FFPE tissue that originates from the right cerebral hemisphere, whereas the majority of patients employed in this study present with left hemisphere changes. Hence, the epicentre of pathology is missed. Thirdly, a clear discrimination of the arteriolar level investigated at the time is needed if we are to comment on the vascular bed more severely affected and develop drug-targeting strategies. Lastly, vascular COX-deficiency was detected in cognitively normal controls upon histochemical examination,

therefore the extent of respiratory chain protein expression defects in patient microvessels may be underestimated highlighting the need to use a more appropriate control group.

6.5.1 Future work

Currently, many theories exist on the triggers, the chronological order and the sequence of events that lead to stroke-like episodes and stroke-like cortical lesion formation in patients with mitochondrial disease. The exact mechanisms that account for the aetiology of stroke-like episodes need to be elucidated if we are to prevent stroke-like episode manifestation and/or improve patient care following an episode.

Impairment of mtDNA transcription in the smooth muscle cell layer of a transgenic mouse model could be greatly beneficial if it was to successfully replicate the human MELAS syndrome (Jawien *et al.*, 2008). Behavioural and physiological mouse testing in parallel with quantitative immunofluorescent techniques would enable the investigation of vascular and neuronal changes, prior, during and after stroke-like episode presentation. Furthermore, the success of therapeutic compounds currently speculated to improve the condition and minimise its severity would be tested, providing the possibility to unravel the compound's mode of action and even the condition mechanisms (Kubota *et al.*, 2004; Koga *et al.*, 2005).

Although transgenic mouse models have significant advances over post-mortem end-stage disease patient samples, the importance of using patient tissue should not be neglected. Investigating respiratory chain protein expression in capillary pericytes might provide with evidence regarding the arteriolar level that accounts for the vascular changes in patients with mitochondrial disease, whereas assessing mitochondrial biogenesis and/or mitochondrial mass in arterioles may help gain further insights into the mechanisms behind stroke-like episodes. Additionally, respiratory chain protein expression investigation in the gut vasculature can be beneficial, since patients with stroke-like episodes usually also present with gastrointestinal dysmotilities (Shimotake *et al.*, 1998).

6.6 Conclusions

In this study I have presented evidence for the occurrence of respiratory chain protein expression defects in the posterior brain region vasculature of patients harbouring the m.3243A>G point mutation accompanied by changes in vascular mitochondrial density and/or localisation. Complex I deficiency is generally more severe compared to complex IV protein expression defects, whereas the endothelial cell layer appears to be more vulnerable to mitochondrial dysfunction. The occipital lobe is most severely affected, followed by vascular defects in the cerebellum and temporal lobe. Vascular respiratory chain defects detected in this

study combined with mitochondrial dysfunction in inhibitory interneurons are likely to additively lead to vascular tone dysregulation and aberrant cerebral blood flow in patients with mitochondrial disease. COX-deficiency in the blood vessels of cognitively normal controls suggests that respiratory chain protein expression deficiency in patients with mitochondrial disease is likely to be underestimated, while it further strengthens the notion that stroke-like episodes result as a consequence of combined neuronal/interneuronal and vascular deficiencies.

Chapter 7

Chapter 7 Final Discussion

The complex and multisystemic nature of mitochondrial disease is exemplified by the presence of neurological and non-neurological symptoms, which progress throughout the patients' life and often lead to disability and death. Neurological deficits are the most frequently reported manifestation in patients with mitochondrial disease and neuropathological investigations performed in the past extensively document brain structural and functional abnormalities. These have contributed significantly towards unravelling the molecular mechanisms responsible for neurodegeneration in patients with mitochondrial disease. Nonetheless no universally accepted hypotheses have been proposed.

The principal aim of this thesis was to further our understanding on the impact of synapses and microvessels upon neuronal degeneration. Synaptic disturbances are increasingly being detected in patients with cerebellar ataxia and vascular abnormalities are prominent in those presenting with stroke-like episodes. Both ataxia and stroke-like episodes are common in patients with mitochondrial disease and are microscopically associated with profound neuronal loss. It is fundamental to identify the cellular and/or subcellular compartments affected early in disease pathogenesis if we are to develop drug targeting strategies which will ultimately prevent and/or delay the degenerative process.

7.1 Quadruple immunofluorescence for investigating protein expression

During the course of this thesis a quantitative quadruple immunofluorescent technique was developed which enables the precise and reliable quantification of protein expression in human post-mortem brain tissues (Chapter 3). This method relies upon conjugation of primary antibodies (targeted against proteins of interest) with spectrally unmixed fluorescent tags, the signal of which is detected following laser excitation. The amount of signal transmitted is linearly related to the amount of protein present, thus allowing quantification of protein expression.

The developed method presents significant advantages over histochemical and immunohistochemical assays, previously employed to study respiratory chain activity and protein expression at the single cell level respectively. Conventional histochemical assays only allow the identification of cells that are positive, intermediate or negative for COX (Old and Johnson, 1989; Ross, 2011), which (the cells) are subjectively and semi-quantitatively classified for respiratory chain enzymatic activity. Likewise, subtle changes in protein expression are likely to be overlooked through indirect immunohistochemistry (Taylor and

Levenson, 2006; Nguyen, 2013), which facilitates the investigation of a singular protein expression without accounting for mitochondrial mass.

In contrast, the newly developed immunofluorescent technique holds the capacity to study the simultaneous expression of four proteins, in a reliable, precise and reproducible manner (Grunewald *et al.*, 2014). Specific neuronal and cellular populations and neuronal domains may be investigated, within which respiratory chain protein expression is quantified and adjusted to mitochondrial presence. Moreover, high-resolution microscopic techniques and three-dimensional image analysis software helped reconstruct and examine the morphological characteristics of sub-cellular compartments. The technique's versatility allowed the incorporation of different markers and/or its use in different tissues depending on the research question at the time, constituting it a valuable tool for the studies performed throughout this thesis.

7.2 Cerebellar ataxia and mitochondrial disease

The high frequency of cerebellar ataxia reported to manifest in patients recruited to the UK MRC Mitochondrial Disease Patient cohort (~70%) (Lax *et al.*, 2012a) highlight the necessity for dissecting out the mechanisms responsible for motor and cognitive impairments in patients with mitochondrial disease. This study provides the first comprehensive documentation of synaptic abnormalities in the intracerebellar circuitry of patients with mitochondrial disease, with a focus on the GABAergic and glutamatergic innervation of the dentate nucleus (summarised in Figure 7- 1).

Variably decreased complex I protein expression is detected in Purkinje cell bodies, their dendrites expanding to the molecular cell layer and their inhibitory presynaptic terminals contacting dentate nucleus neurons (Chapter 4). Protein expression defects are more pronounced in patients harbouring the m.3243A>G point mutation though patients with other genetic defects (m.8344A>G, m.14709T>C and recessive *POLG* mutations) have altered complex I protein expression relative to controls. The level of complex I deficiency was comparable amongst the different neuronal sub-compartments, as were the heteroplasmic levels for the m.3243A>G and m.8344A>G point mutation (where this was applicable) suggesting that synaptic sites are not selectively protected from mitochondrial dysfunction. Taking into account the importance of mitochondria (mainly their capacity to generate ATP and buffer Ca^{2+}) in synaptic activity and plasticity (Brodin *et al.*, 1999; Attwell and Laughlin, 2001; Billups and Forsythe, 2002; Levy *et al.*, 2003), it is likely that synaptic mitochondrial dysfunction will be detrimental to synaptic remodelling and neuronal communication and thus

result in altered information processing in the brain. Indeed, synaptic complex I deficiency is related with poor clinical rating of ataxia implying that mitochondrial deficiency at the synapses contributes to the progression of ataxia.

Three-dimensional reconstruction of GABAergic synapses revealed loss of inhibitory contacts to the dentate nucleus and enlarged remaining presynaptic terminals, providing evidence for the existence of compensatory mechanisms acting to maintain synaptic contact area upon synapse loss (Scheff and Price, 2003). Decreased GABAergic input to the dentate nucleus is accompanied by drop off in the number of Gephyrin-positive puncta located around the periphery of dentate nucleus neuronal cell bodies and directly opposed to inhibitory presynaptic terminals (Chapter 5). Protein loss from inhibitory postsynaptic compartments is reminiscent of GABAergic synapse destabilization - via potential trans-synaptic effects - and subsequent defects in inhibitory neurotransmission (Yu *et al.*, 2007; Varley *et al.*, 2011). Further to dentate nucleus neuronal disinhibition, glutamatergic innervation of these neurons is also partially disturbed. The density of mossy fibre presynaptic terminals and AMPA receptors on dentate nucleus neuronal dendrites is decreased, indicating atypical cerebellar connectivity with precerebellar nuclei.

Postsynaptic neuronal deficiencies (dentate nucleus neurons) are detected and were strongly related to inhibitory presynaptic protein expression defects. Similarly, respiratory chain deficiency in synapses is associated with pronounced dentate nucleus neuronal degeneration, supportive of theories on the exertion of anterograde trans-synaptic effects and potential transneuronal degenerative mechanisms (Cowan, 1970; Linden and Perry, 1983).

Data presented in this study propose for altered intra- and extracerebellar connectivity and consequent loss of trophic support to the dentate nucleus (Figure 7- 1), however the extent of dentate nucleus innervation from climbing fibres remains to be elucidated. When considering the importance of deep cerebellar nuclei in forming local feedback and global signal transduction networks (D'Angelo and Casali, 2012), one can appreciate that aberrant neuronal function and synaptic circuitry detected in patients with mitochondrial disease may contribute to the genesis and progression of ataxia.

These observations are similar to those detected in patients with hereditary ataxias, including Friedrich's ataxia (FRDA). Post-mortem examination of patients with FRDA reveals degeneration of the dentate nucleus accompanied by loss of inhibitory and excitatory input to the region (Koeppen *et al.*, 2011; Koeppen *et al.*, 2013; Koeppen *et al.*, 2015). However, contrary to what is true for mitochondrial disease, no degenerative changes are detected in the

inferior olive or Purkinje cells of patients with FRDA implying that degeneration in mitochondrial disease is likely due to mechanisms unique to patients with the condition.

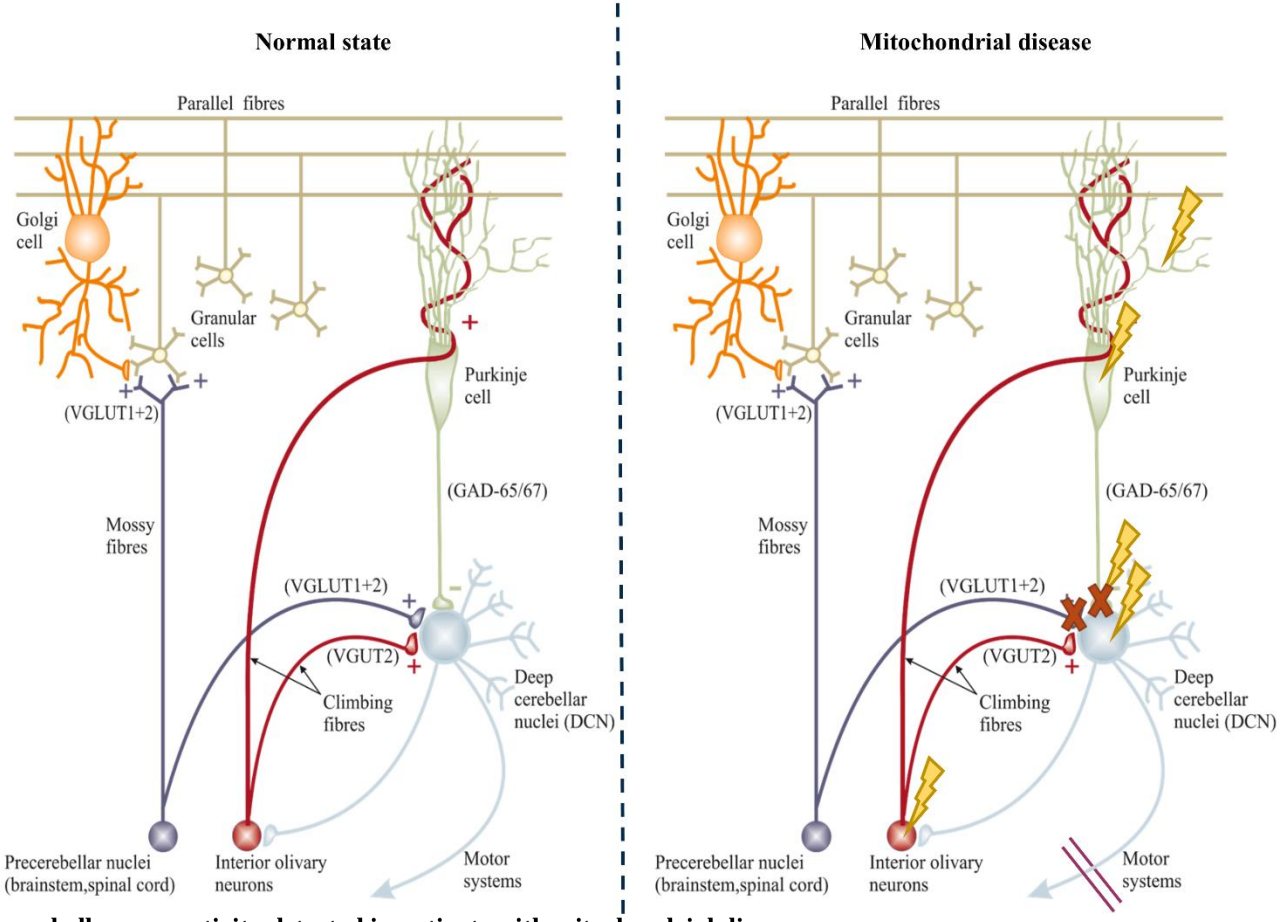

Figure 7- 1: Altered cerebellar connectivity detected in patients with mitochondrial disease.

Under normal conditions, healthy Purkinje cells project their inhibitory synapses to deep cerebellar nuclei neurons (primarily to dentate nucleus neurons) establishing intracerebellar circuitry. Excitatory afferents reach the cerebellum via climbing (from the inferior olive) and mossy fibres (from brainstem and spinal cord), which constitute the main component of extracerebellar connectivity. In patients with mitochondrial disease, decreased neuronal density detected across the olivo-cerebellar pathway is accompanied by respiratory chain deficiencies in remaining neurons (Lax *et al.*, 2012a). In this study, respiratory chain protein expression defects are also detected in Purkinje cell dendrites and inhibitory presynaptic terminals contacting dentate nucleus neurons. Intracerebellar synaptic remodelling is documented and involves decreased inhibitory synapse density and enlarged residual synapses. Partial loss of excitatory input to the dentate nucleus (arising from brainstem and spinal cord) is also detected and may collectively contribute to aberrant cerebellar signalling to premotor and primary motor cortices.

7.3 The vasculature of patients with mitochondrial disease

Additional to neurodegeneration across the olivo-cerebellar pathway, neuropathological investigation of patients with mitochondrial disease reveals the presence of necrotic foci in posterior brain regions. These foci are prominent, but not restricted, to patients with the MELAS syndrome, due to m.3243A>G, and are though to be consequent to stroke-like episodes that manifest in these patients (Pavlakis *et al*., 1984; Ohama *et al*., 1987; Tanji *et al*., 2003; Deschauer *et al*., 2007). Vasogenic oedema and cerebral hyperperfusion are characteristic acute changes which progress into cytotoxic oedema and hypoperfusion during the chronic state (Yonemura *et al*., 2001; Iizuka *et al*., 2007; Kim *et al*., 2011). This study provides important insights regarding respiratory chain protein expression in the cerebellar, occipital and temporal lobe vasculature of patients with a wide range of genetic diagnoses (m.3243A>G, m.8344A>G and recessive *POLG* mutations). Not all patients included in the study have a clinical history of stroke-like episodes and focal stroke-like cortical lesions, documented macroscopically, do not necessarily coincide with the incidence of stroke-like features (Chapter 6).

Combined complex I and IV protein deficiencies are detected in the microvessels of patients harbouring the m.3243A>G point mutation across all brain regions studied. When present, respiratory chain deficiencies in patients with other genetic defects (m.8344A>G and recessive *POLG* mutations) are mild. Interestingly, complex IV protein expression defects predominate in the cerebellar vasculature, whereas complex I deficiency prevails in the occipital and temporal lobe. This might be suggestive of differential vulnerability to respiratory chain deficiency amongst different brain regions. Furthermore, protein expression defects are most noticeable in the smooth muscle cell layer of cerebellar arterioles, whilst the endothelial cells of occipital and temporal lobe capillaries are more severely affected. Vascular respiratory chain deficiency was detected in cognitively-normal controls (upon dual COX/SDH histochemistry) and protein expression defects have also been detected in patients without a clinical history of stroke-like episodes. These data are not in favour of the primary vascular hypothesis and instead suggest that vascular respiratory chain defects alone are not sufficient for the induction of stroke-like episodes.

Generally, microvessels located in the occipital lobe harbour the most severe respiratory chain deficiencies in agreement with stroke-like cortical lesion predilection for this region. Additional to electron transport chain protein expression defects, the arterioles of patients harbouring the m.3243A>G point mutation have altered mitochondrial distribution and/or mass. Mitochondrial clusters deficient for complex I and IV have been detected around smooth muscle cell nuclei,

reminiscent of increased mitochondrial biogenesis and/or aberrant mitochondrial transport. Mitochondrial proliferation may be activated to compensate for vascular mitochondrial dysfunction, though newly synthesised organelles are also malfunctional. Capillary proliferation is not evident, though microvascular density quantification was not the focus of this study and needs to be assessed in greater detail.

Despite the fact that the vascular cell populations are highly glycolytic and do not rely on mitochondria for energy supply, microvascular mitochondria are involved in major signalling pathways affecting cellular survival and function (Quintero *et al.*, 2006; Dromparis and Michelakis, 2013; Tang *et al.*, 2014). Nevertheless, the factors contributing to the development of lesions during a stroke-like episode are likely to be manifold. Respiratory chain deficiency detected in various inhibitory cellular types and sub-cellular domains (Lax *et al.*, 2012a; Chrysostomou *et al.*, 2015; Lax *et al.*, 2015) may result in atypical inhibitory neurotransmission in the brain of patients with mitochondrial disease and consequent lower thresholds for seizure generation. Dysfunctional inhibitory interneurons (Lax *et al.*, 2015) fail to couple blood flow to neuronal hyperexcitability, which combined with mitochondrial dysfunction within and structural abnormalities of microvessels (Lax *et al.*, 2012b) render the seizure foci vulnerable to degeneration. The hypothesised mechanism for stroke-like episode presentation in patients with mitochondrial disease is summarised in Figure 7- 2 and is in agreement with the non-ischemic neurovascular hypothesis proposed by Iizuka and colleagues (Iizuka and Sakai, 2005). According to this, focal neuronal hyperexcitability (as a result of neuronal/interneuronal and/or vascular mitochondrial dysfunction) shifts the balance between energetic demand and supply and results in local neuronal loss (Iizuka and Sakai, 2005).

Figure 7- 2: Potential mechanisms accounting for stroke-like episode manifestation in patients with mitochondrial disease.

According to our hypothesis, multiple hits are required for stroke-like episodes to manifest and cortical lesions to develop in patients with mitochondrial disease. MtDNA defects result in respiratory chain deficiency (mainly involving complex I) in neuronal and interneuronal populations, lowering the threshold for seizure activity and resulting in neuronal hyperexcitability. Respiratory chain defects detected in the vasculature, combined with vascular cell death and blood-brain barrier leakage, confer an extra burden to already dysfunctional neurons. Loss of the neurogenic and vasogenic compartment of vascular autoregulation is likely to account for aberrant blood supply to neurons, rendering the seizure foci vulnerable to degeneration.

7.4 Implications of this study

Studies in this thesis explore the synaptic and vascular abnormalities in a genetically diverse group of patients presenting with cerebellar ataxia and stroke-like episodes. The neuropathological and molecular investigation of neuronal, synaptic and vascular cell populations helped gain further insights into the degenerative changes observed in association with these two different cellular compartments.

Research involving the cerebellar circuitry improved our knowledge with regards to the exact synaptic abnormalities occurring in the cerebellum of ataxic patients. Atypical cerebellar connectivity may be detrimental to local information processing with adverse effects on downstream neuronal signalling, explaining for the cognitive and motor disturbances in a high percentage of patients with mitochondrial disease. However, there is still a lot left to be done before we can confidently report on synaptic anomalies as being the primary event in the degenerative process and the main source of network disruption. Similar experiments in the inferior olive and the thalamus may help unravel whether synaptic changes exist across the olivo- and ponto-cerebellar pathways, whereas investigation of areas with less pronounced neuronal loss will facilitate the assessment of synaptic pathology in the absence of neurodegeneration. Moreover, the use of transgenic mouse models will enable the temporal documentation of synaptic changes with regards to behavioural abnormalities. Regardless, synaptic connections do not appear to be selectively protected from the effects of mitochondrial dysfunction, constituting synapses good candidates for drug targeting. Indeed, the neuroprotective effects of a cold-shock protein (RBM3) have been demonstrated in mouse models of neurodegenerative disease, where maintained structural synaptic plasticity prevented behavioural deficits (Peretti *et al.*, 2015).

The precise quantification of respiratory chain protein expression in the microvascular environment of posterior brain regions has contributed to a better understanding of the aetiology of stroke-like episodes in patients with mitochondrial disease. More severe deficiencies detected primarily in the endothelial cell layer and potentially altered mitochondrial dynamics in the smooth muscle of arterioles may represent pathological changes which might impact upon vascular tone regulation, resulting in abrupt changes in cerebral blood flow. Further characterisation of respiratory chain protein expression defects, including investigation of pericytes, will be crucial for identifying the vascular bed most severely affected holding promises for identifying a valid target for therapeutic intervention.

Mitochondrial dysfunction is directly implicated in the pathophysiology of common neurodegenerative disorders (Duchen, 2004) including Alzheimer's (Du *et al.*, 2010), Parkinson's (Klein and Westenberger, 2012) and Huntington's (Shirendeb *et al.*, 2011) disease. Taking into consideration that neurodegenerative diseases have many parallels and share common themes across neurodegenerative processes, the work performed in this thesis might have wider implications concerning future studies in other neurodegenerative diseases.

7.5 Limitations of this study

Additional to significant advances, this study holds important limitations that need to be considered. These include:

i. Neuropathological investigation is performed on end-stage disease brain tissue, thus does not allow the evaluation of changes during disease progression.
ii. Profound neuronal degeneration is detected prior to the time of neuropathological investigation and implies that interesting cells have already been lost.
iii. Tissue is available for a limited number of patients harbouring the same genetic defect, hence no firm conclusions can be drawn with regards to pathogenic mechanisms specific to a single genetic defect.

7.6 Concluding remarks

In conclusion, the data presented in this thesis expand on current knowledge regarding the extent of synaptic and vascular abnormalities in patients with cerebellar ataxia and stroke-like episodes respectively. The inhibitory synaptic connections linking Purkinje cells to dentate nucleus neurons and the endothelial cell layer of posterior cortical region microvessels could potentially serve as candidates for therapeutic intervention, however further studies are needed in order to fully understand the impact of synaptic and vascular mitochondrial dysfunction in the initiation and progression of neuronal degeneration.

Appendices

Chapter 8 Appendices

8.1 Appendix A: Correlations of post-mortem interval

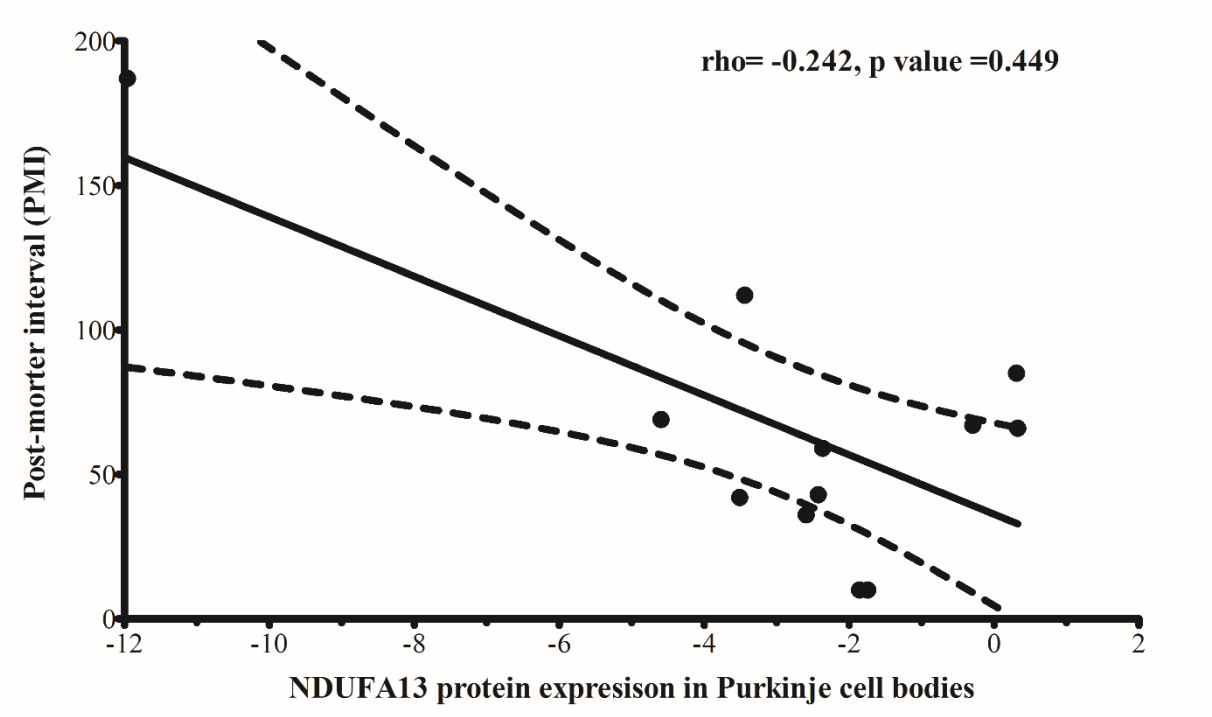

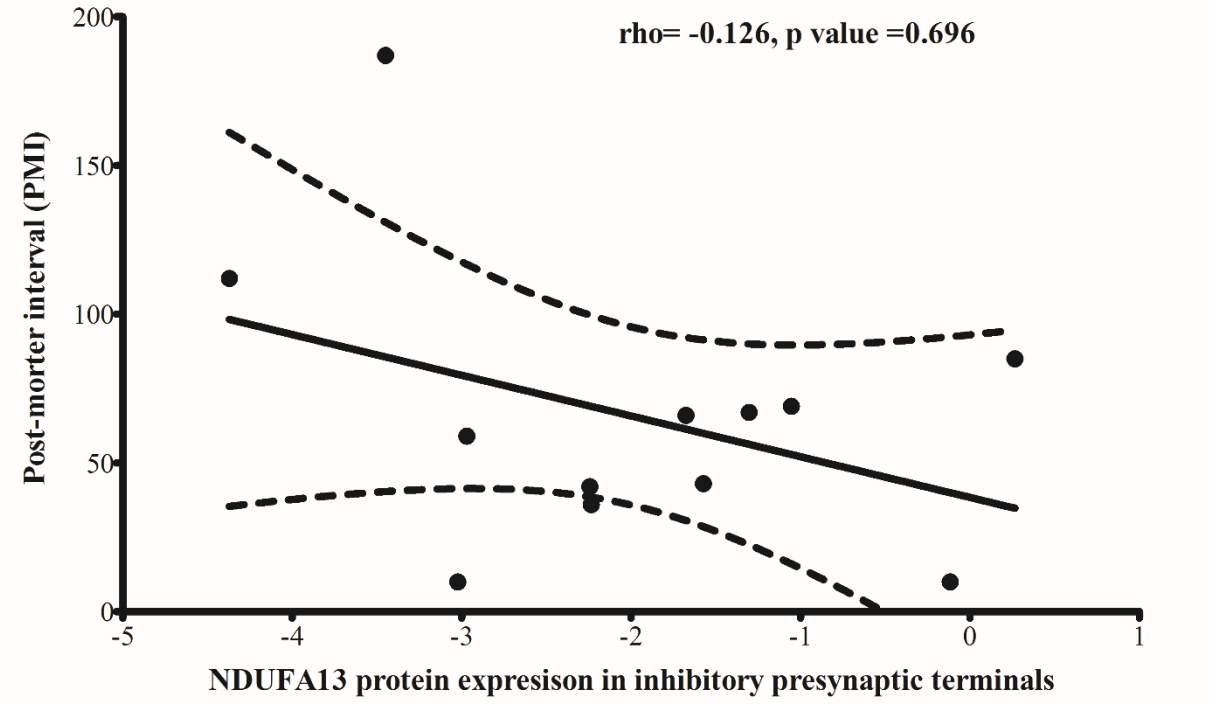

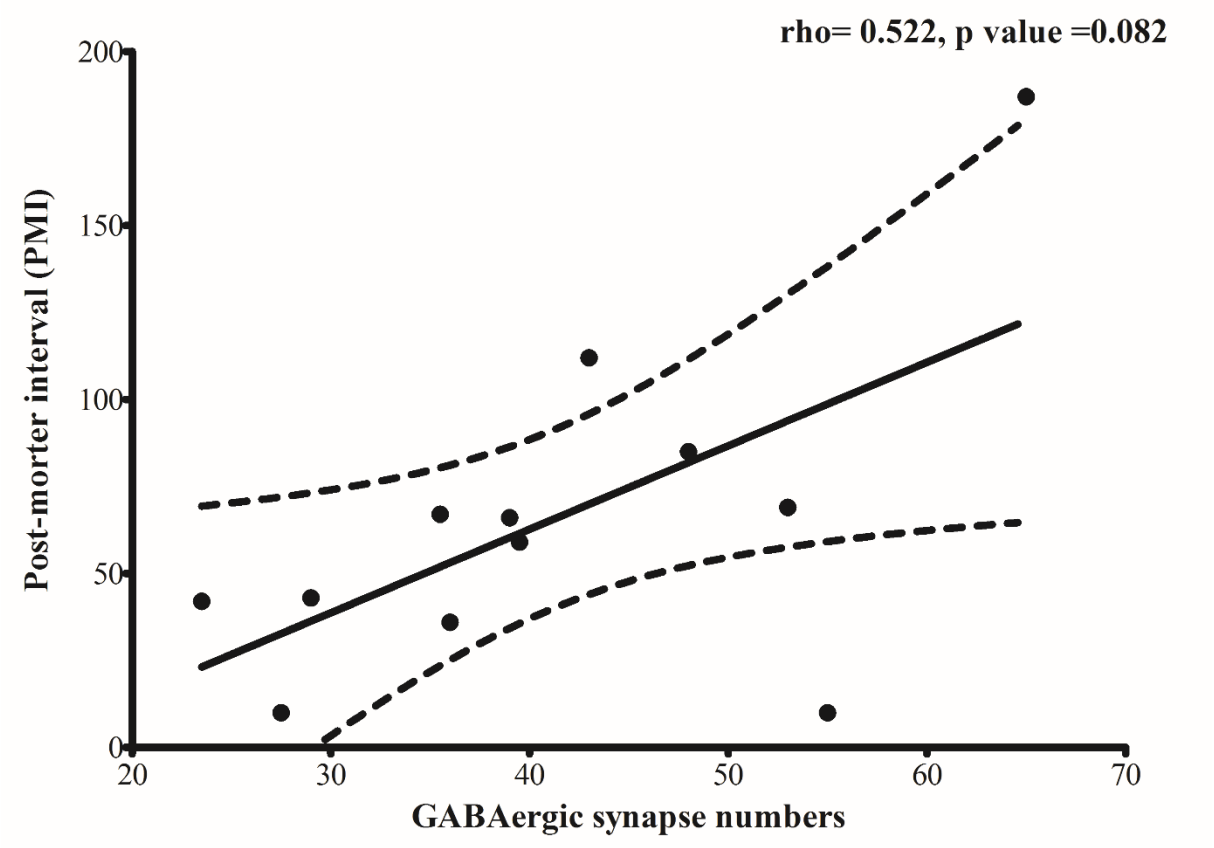
rho= 0.522, p value =0.082
Post-morter interval (PMI)
200
150
100
50
0
20
30
40
50
60
70
GABAergic synapse numbers

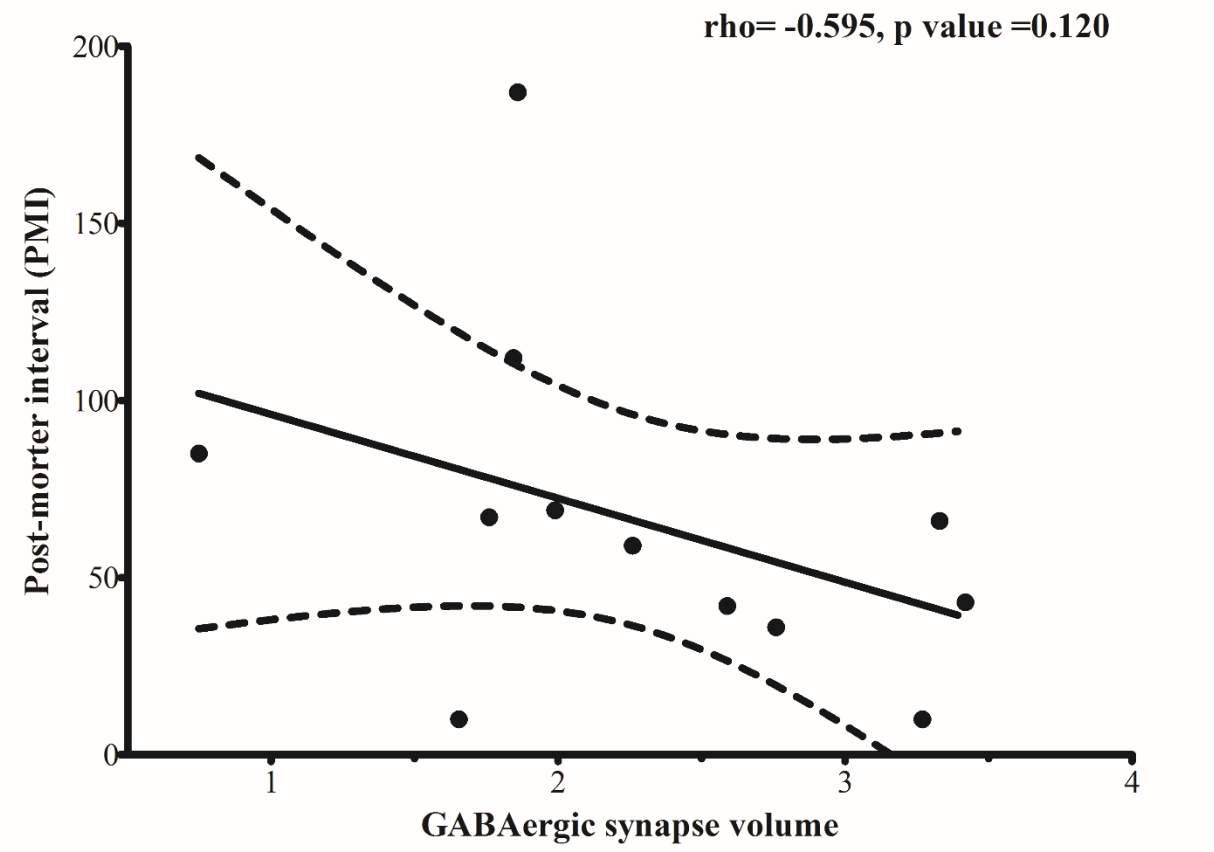
rho= -0.595, p value =0.120
Post-morter interval (PMI)
200
150
100
50
0
1
2
3
4
GABAergic synapse volume

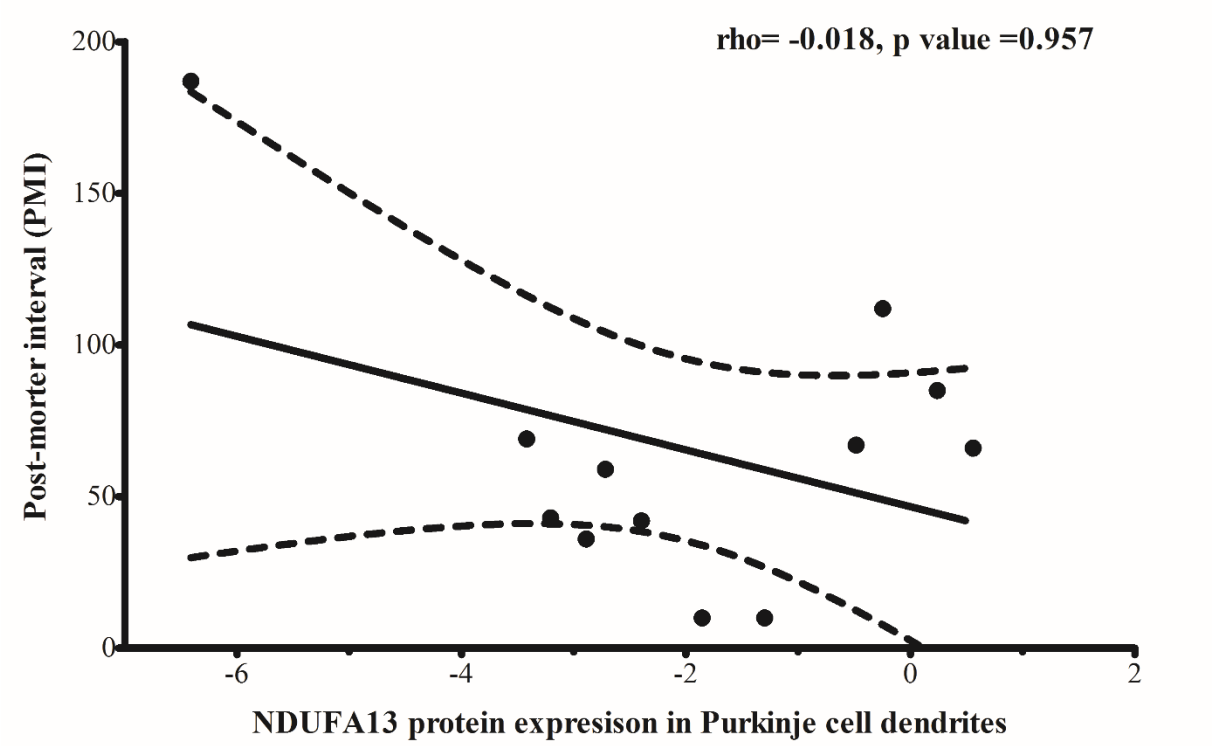
rho= -0.018, p value =0.957
Post-morter interval (PMI)
200
150
100
50
0
-6
-4
-2
0
2
NDUFA13 protein expresison in Purkinje cell dendrites

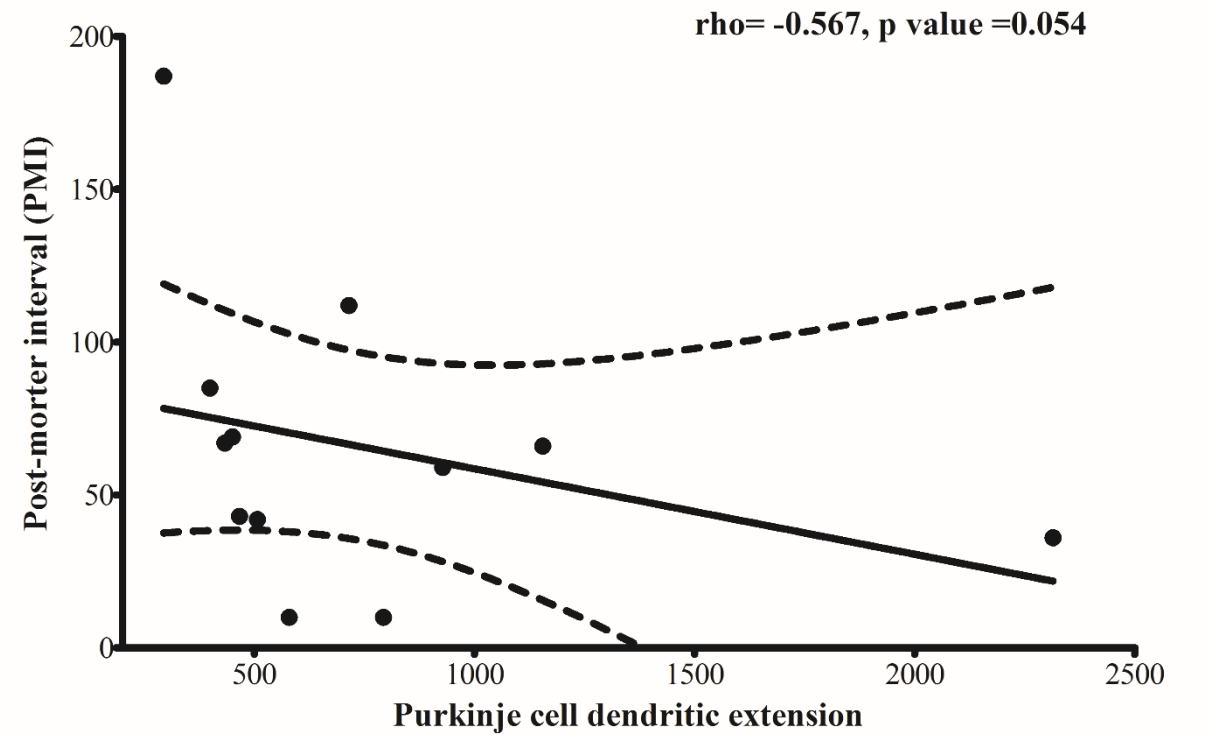
rho= -0.567, p value =0.054
Post-morter interval (PMI)
200
150
100
50
0
500
1000
1500
2000
2500
Purkinje cell dendritic extension

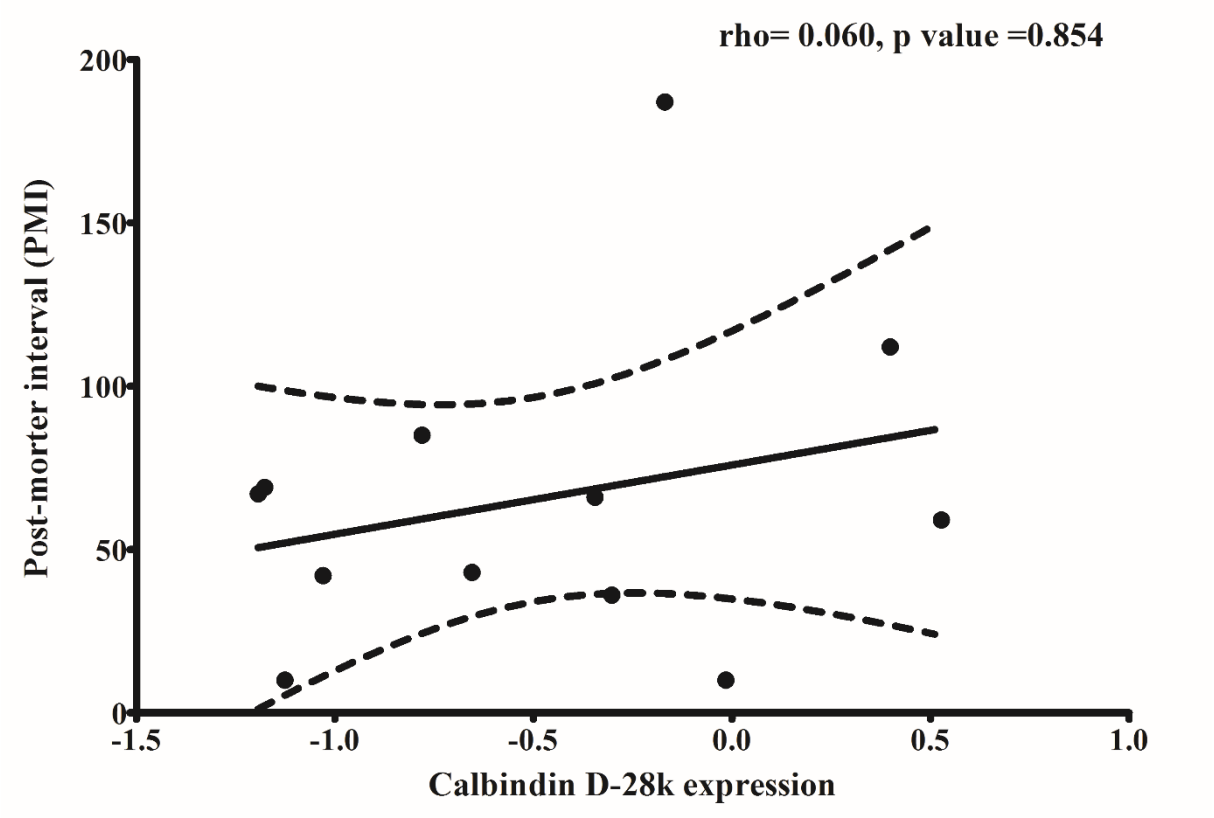
rho= 0.060, p value =0.854
Post-morter interval (PMI)
200
150
100
50
0
-1.5
-1.0
-0.5
0.0
0.5
1.0
Calbindin D-28k expression

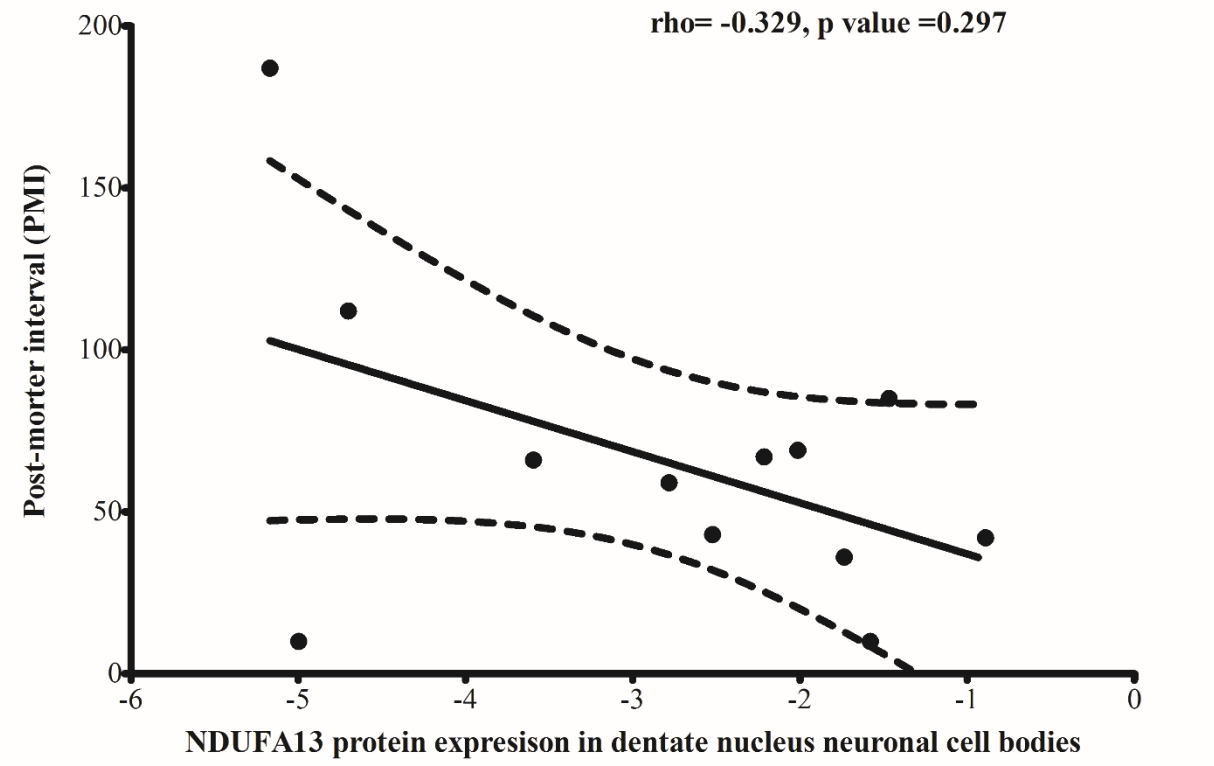
rho= -0.329, p value =0.297
Post-morter interval (PMI)
200
150
100
50
0
-6
-5
-4
-3
-2
-1
0
NDUFA13 protein expresison in dentate nucleus neuronal cell bodies

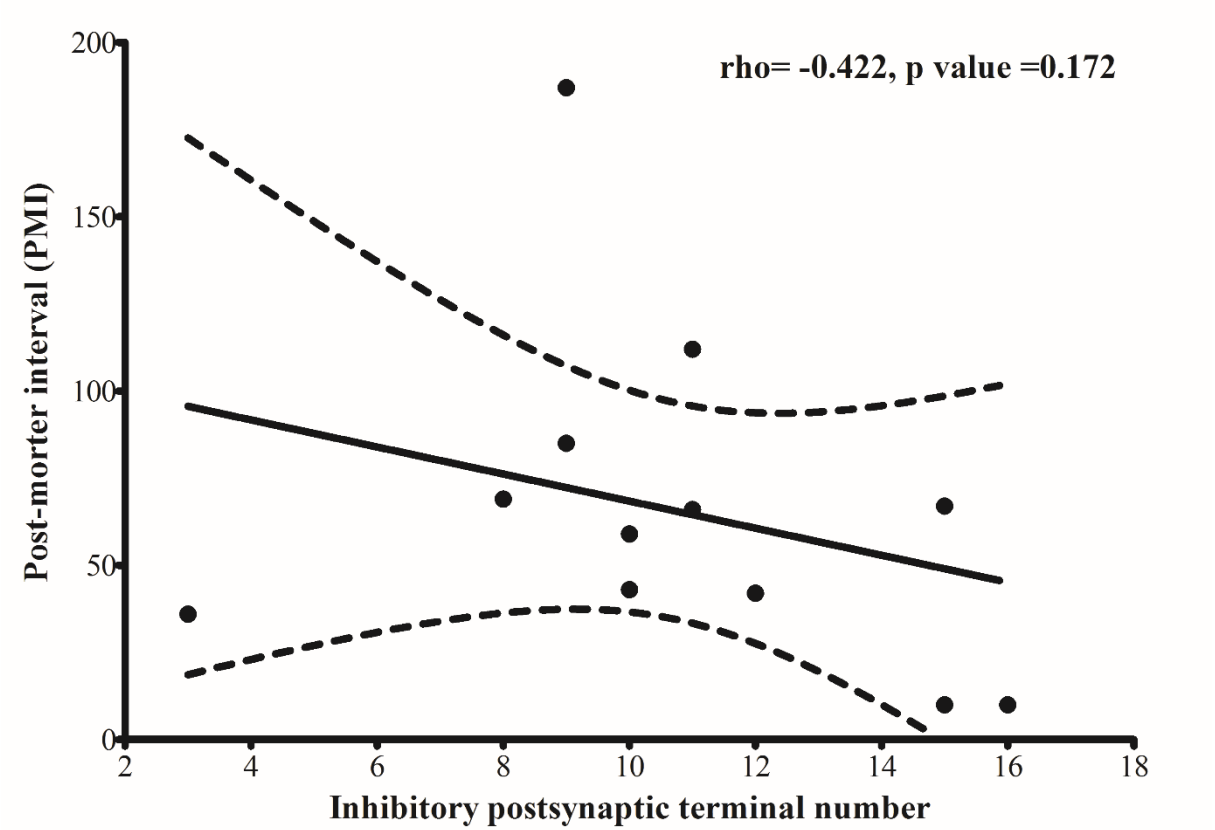
rho= -0.422, p value =0.172
Post-morter interval (PMI)
200
150
100
50
0
2
4
6
8
10
12
14
16
18
Inhibitory postsynaptic terminal number

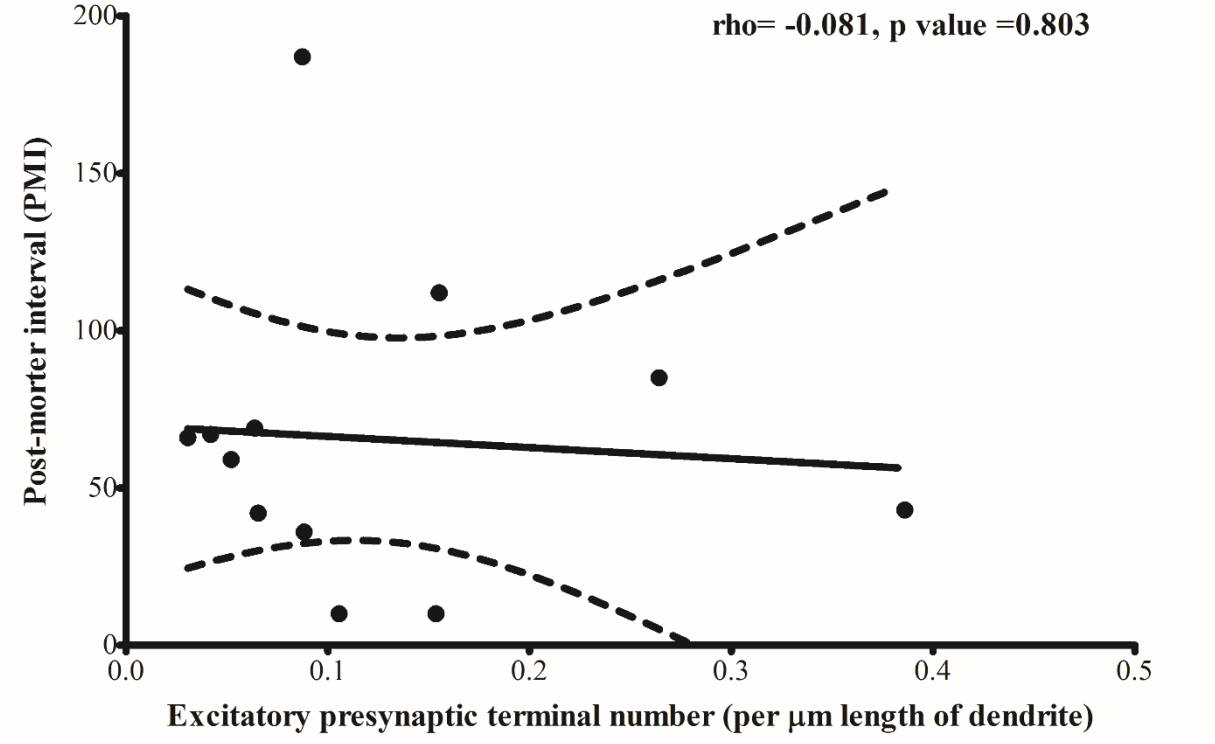
rho= -0.081, p value =0.803
Post-morter interval (PMI)
200
150
100
50
0
0.0
0.1
0.2
0.3
0.4
0.5
Excitatory presynaptic terminal number (per μm length of dendrite)

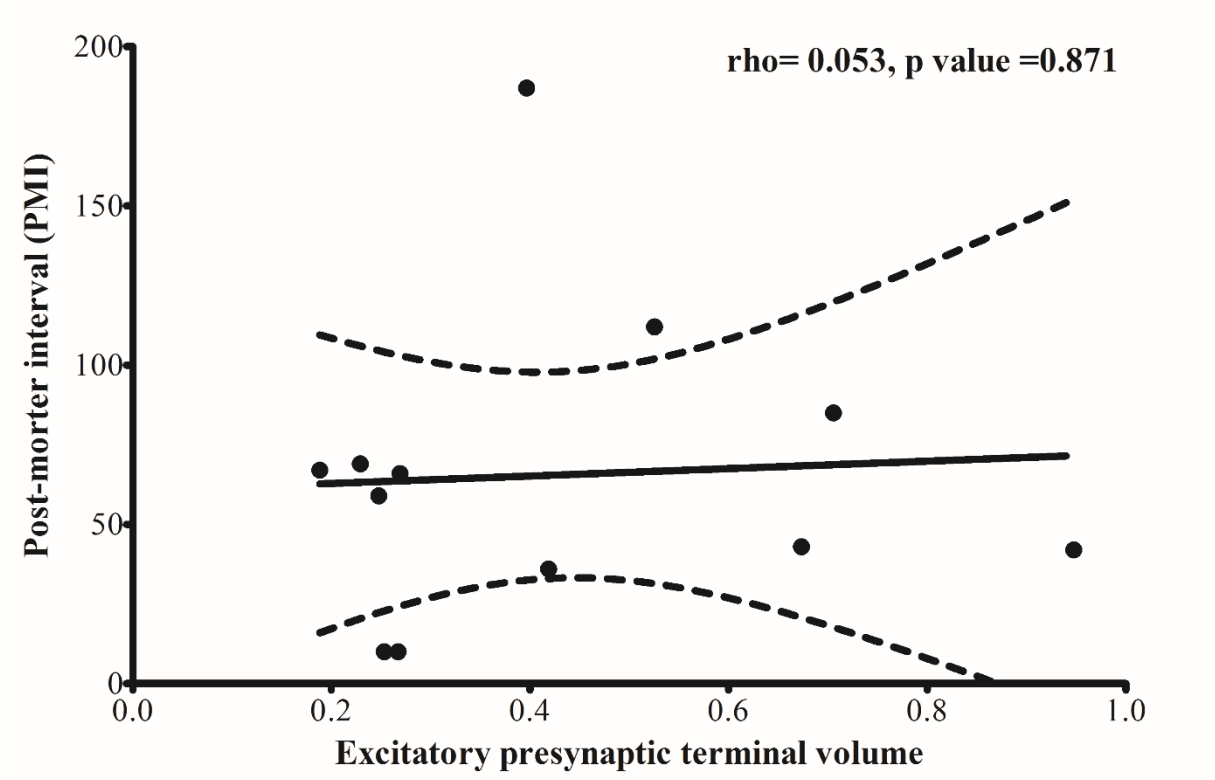
rho= 0.053, p value =0.871
Post-morter interval (PMI)
200
150
100
50
0
0.0
0.2
0.4
0.6
0.8
1.0
Excitatory presynaptic terminal volume

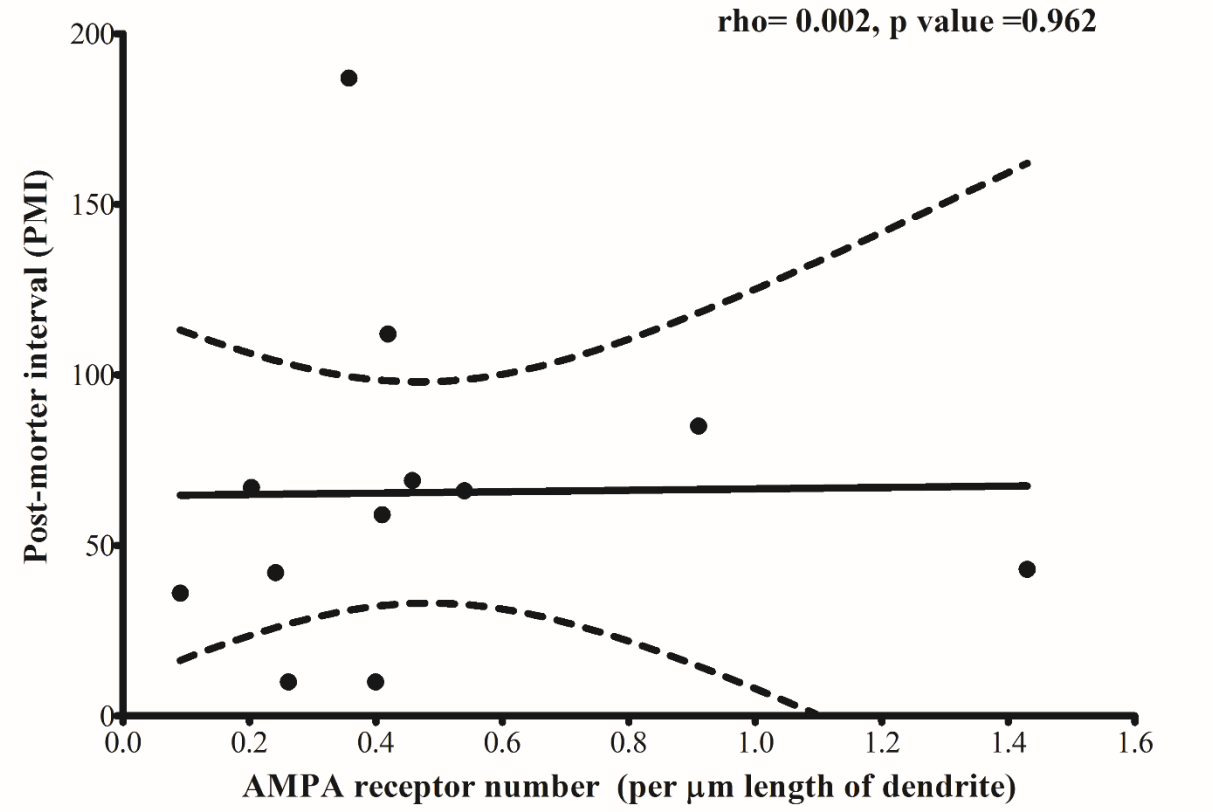
rho= 0.002, p value =0.962
Post-morter interval (PMI)
200
150
100
50
0
0.0
0.2
0.4
0.6
0.8
1.0
1.2
1.4
1.6
AMPA receptor number (per µm length of dendrite)

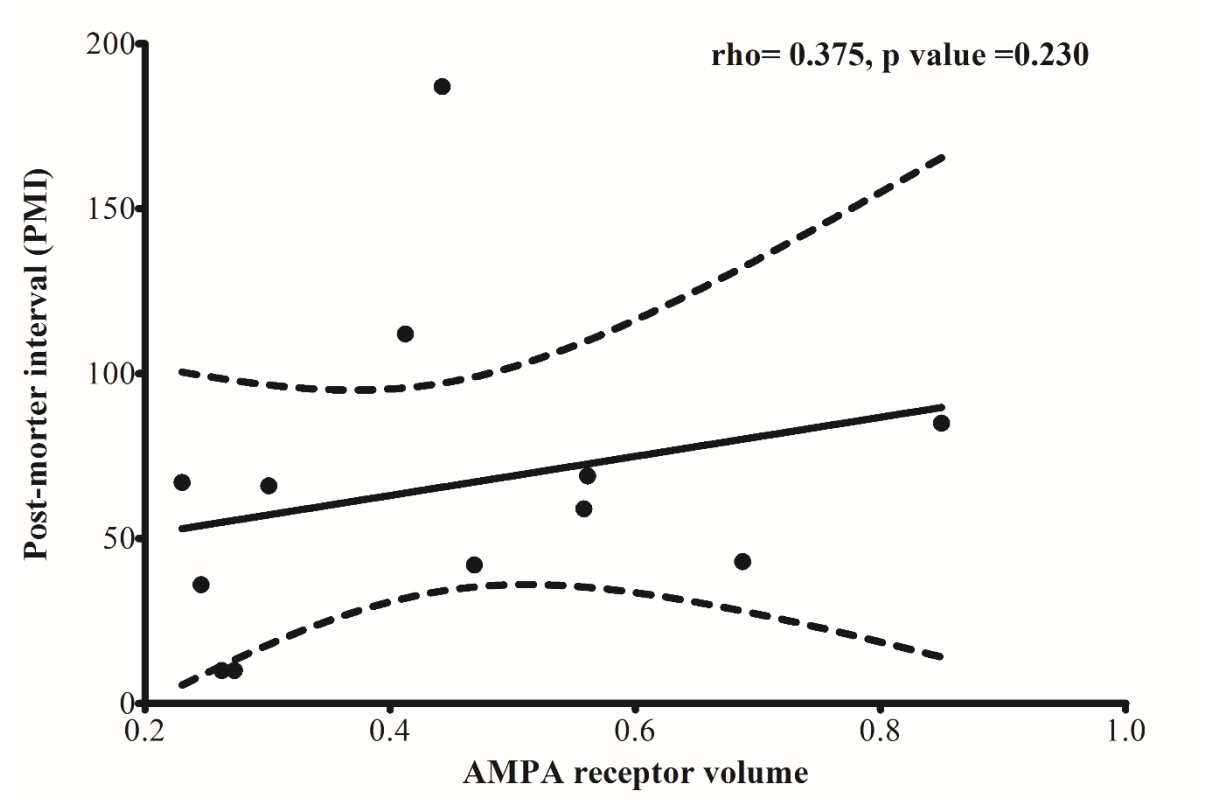
rho= 0.375, p value =0.230
Post-morter interval (PMI)
200
150
100
50
0
0.2
0.4
0.6
0.8
1.0
AMPA receptor volume

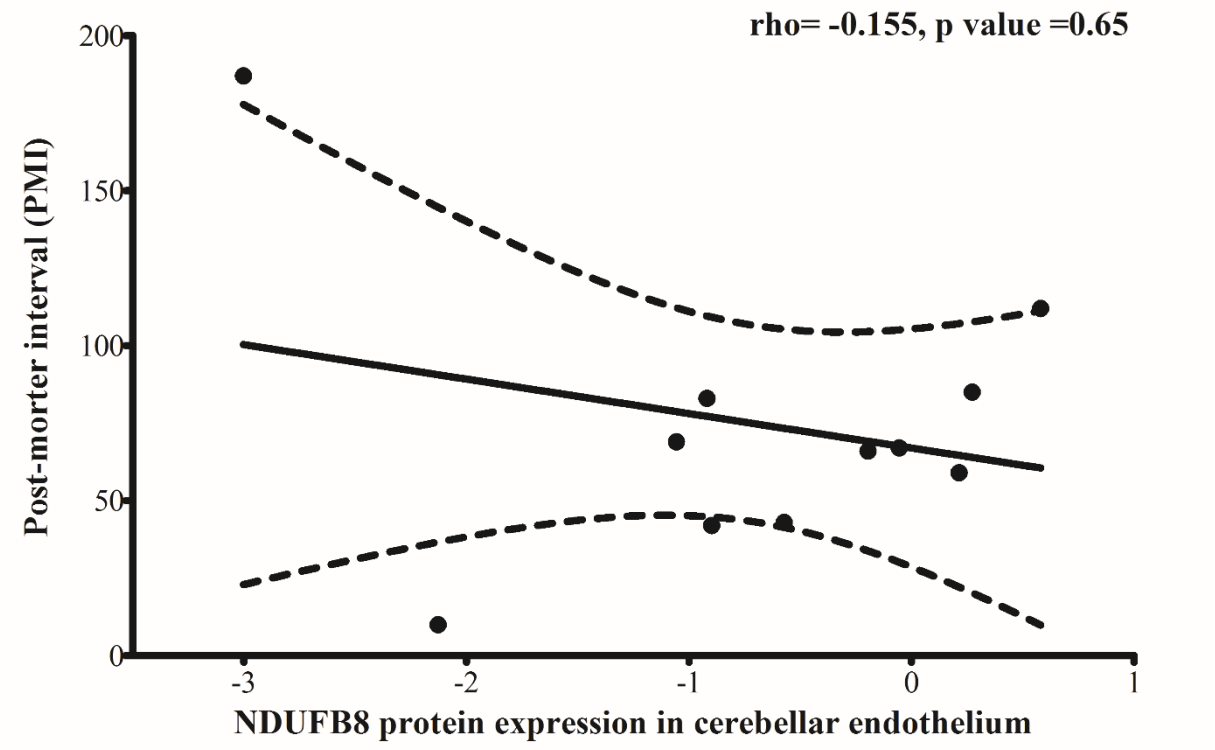
rho= -0.155, p value =0.65
Post-morter interval (PMI)
200
150
100
50
0
-3
-2
-1
0
1
NDUFB8 protein expression in cerebellar endothelium

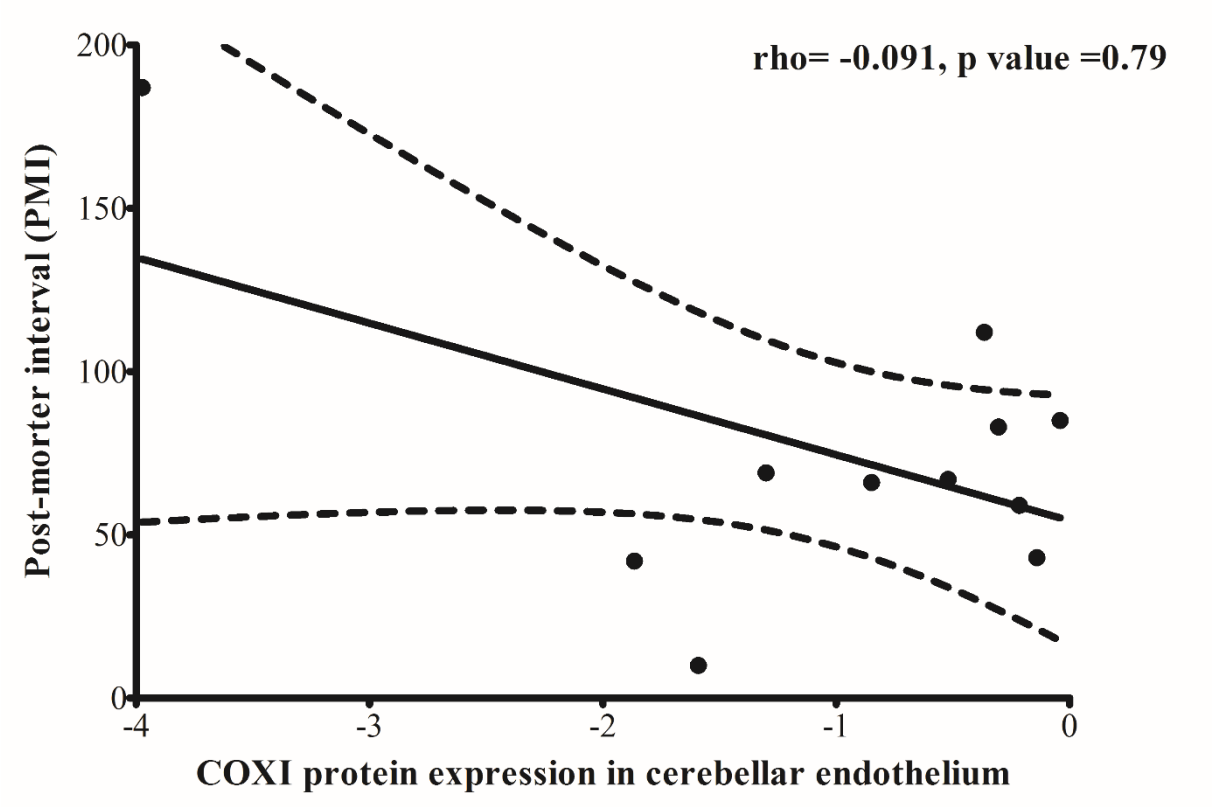
rho= -0.091, p value =0.79
Post-morter interval (PMI)
200
150
100
50
0
-4
-3
-2
-1
0
COXI protein expression in cerebellar endothelium

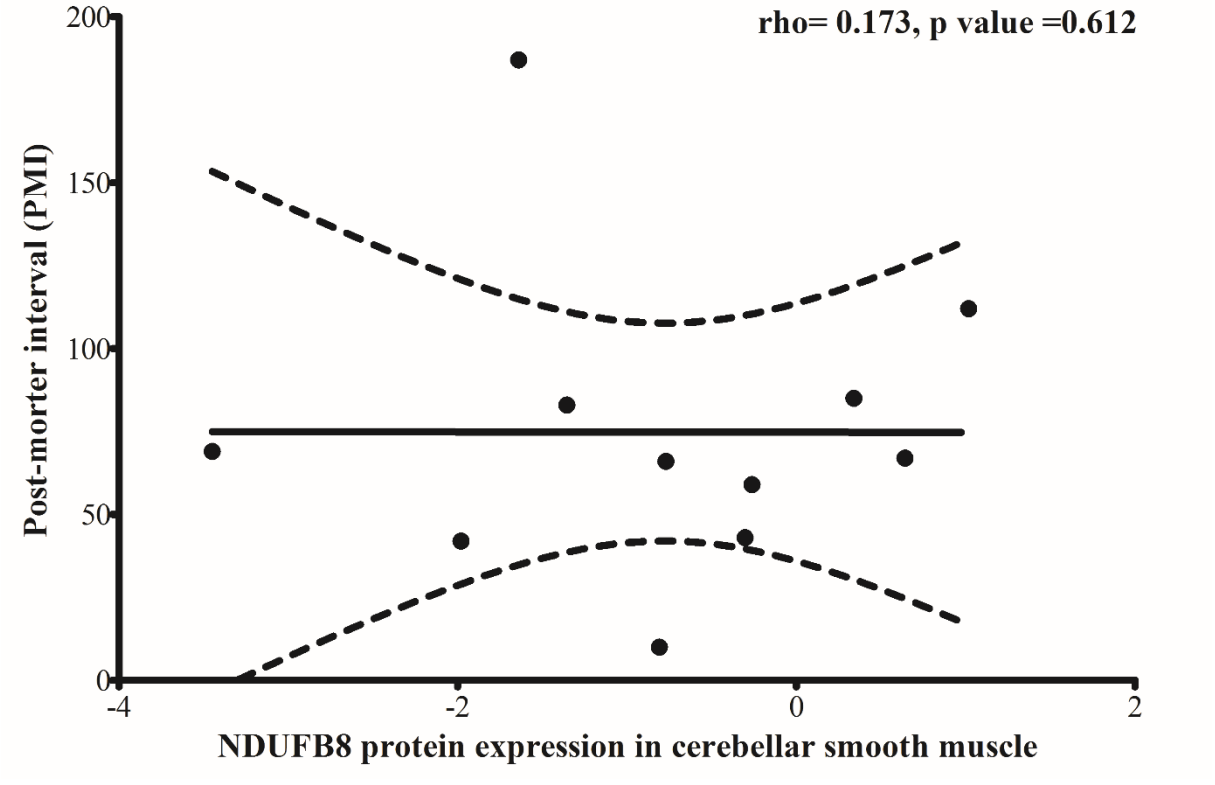
rho= 0.173, p value =0.612
Post-morter interval (PMI)
200
150
100
50
0
-4
-2
0
2
NDUFB8 protein expression in cerebellar smooth muscle

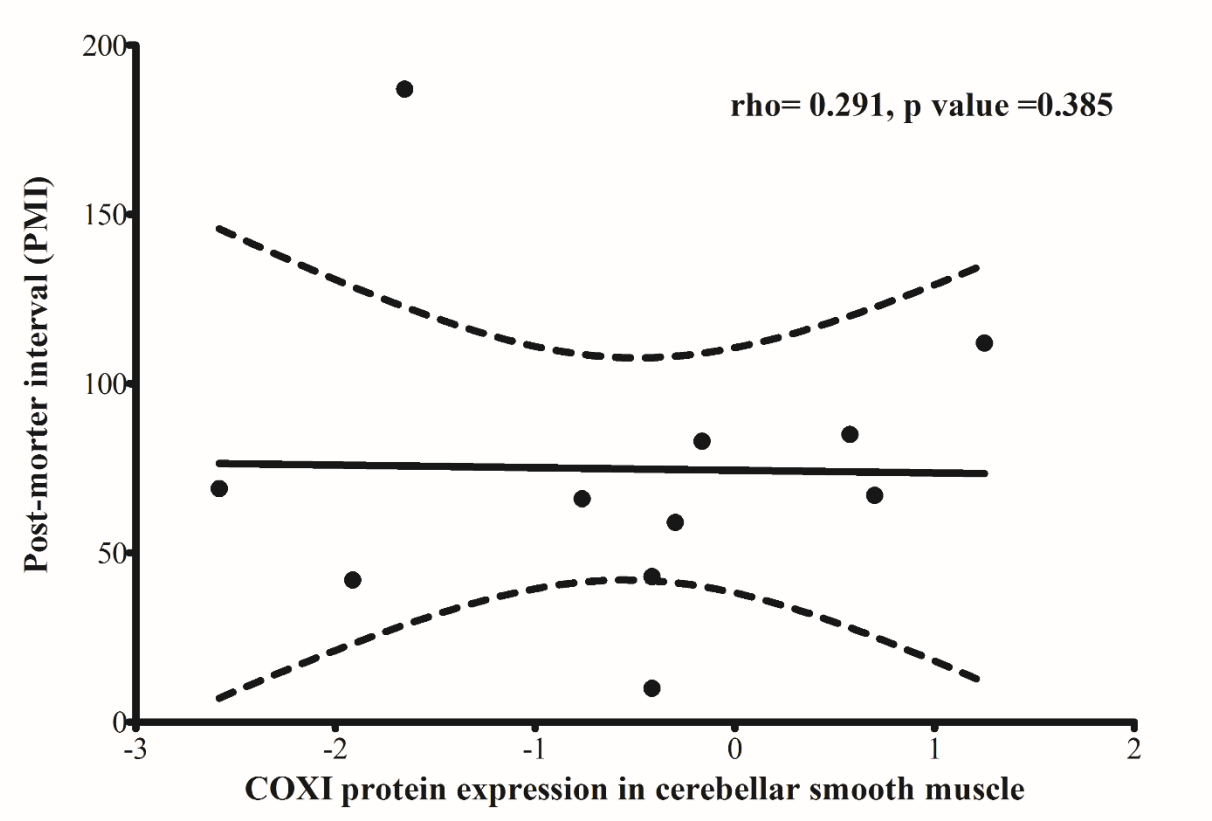
rho= 0.291, p value =0.385
Post-morter interval (PMI)
200
150
100
50
0
-3
-2
-1
0
1
2
COXI protein expression in cerebellar smooth muscle

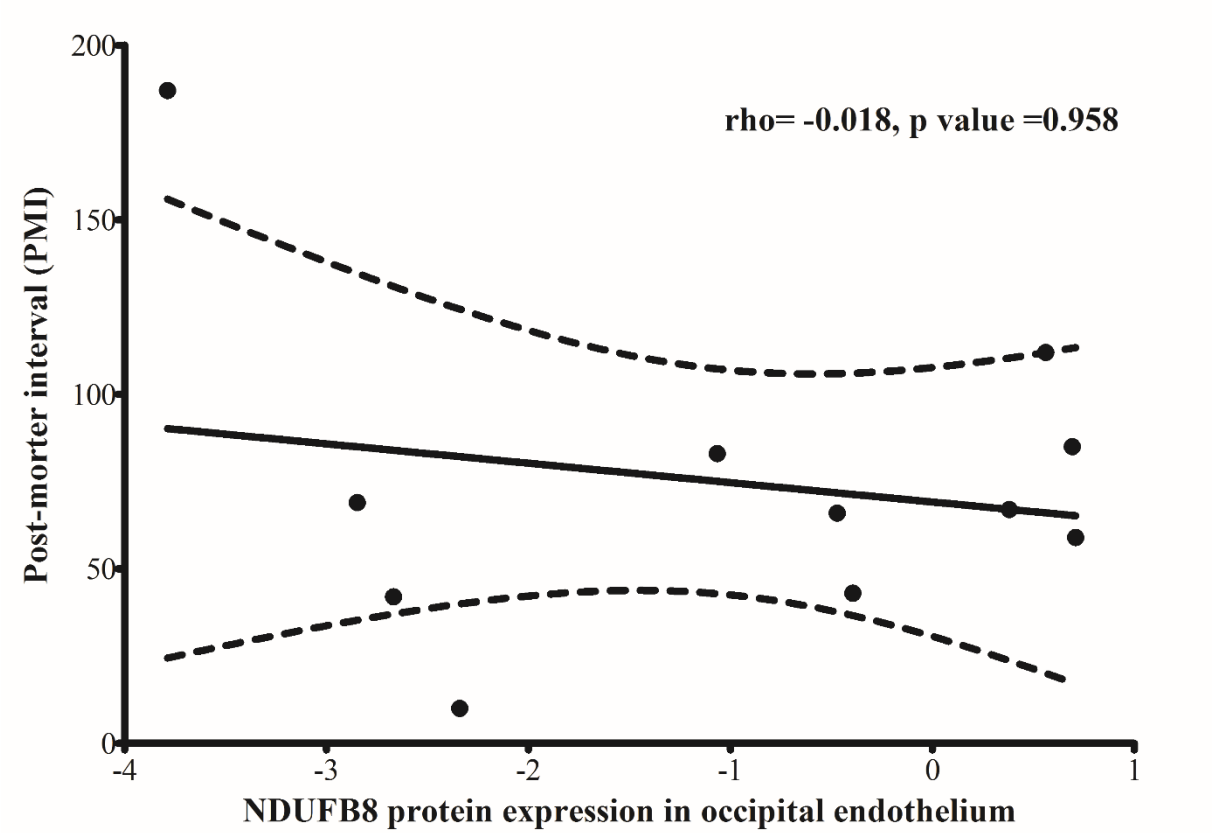
rho= -0.018, p value =0.958
Post-morter interval (PMI)
200
150
100
50
0
-4
-3
-2
-1
0
1
NDUFB8 protein expression in occipital endothelium

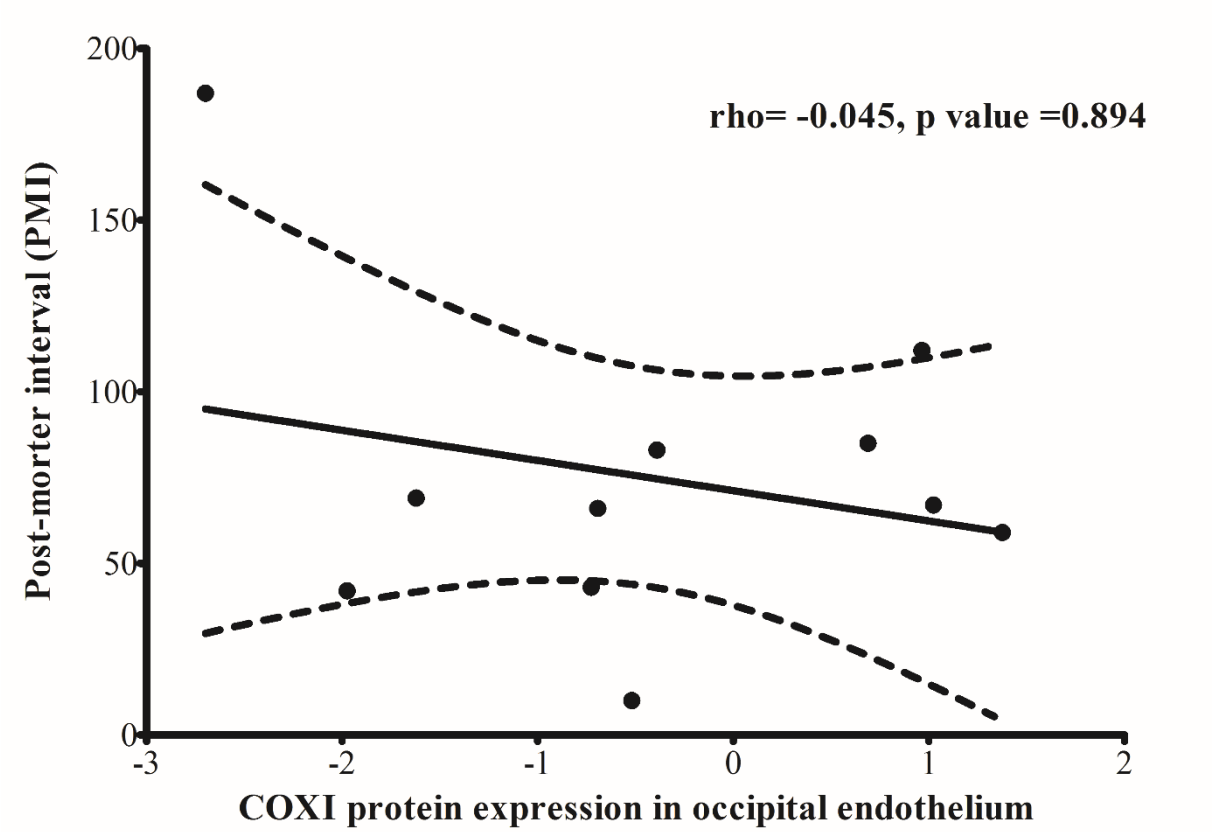
rho= -0.045, p value =0.894
Post-morter interval (PMI)
200
150
100
50
0
-3
-2
-1
0
1
2
COXI protein expression in occipital endothelium

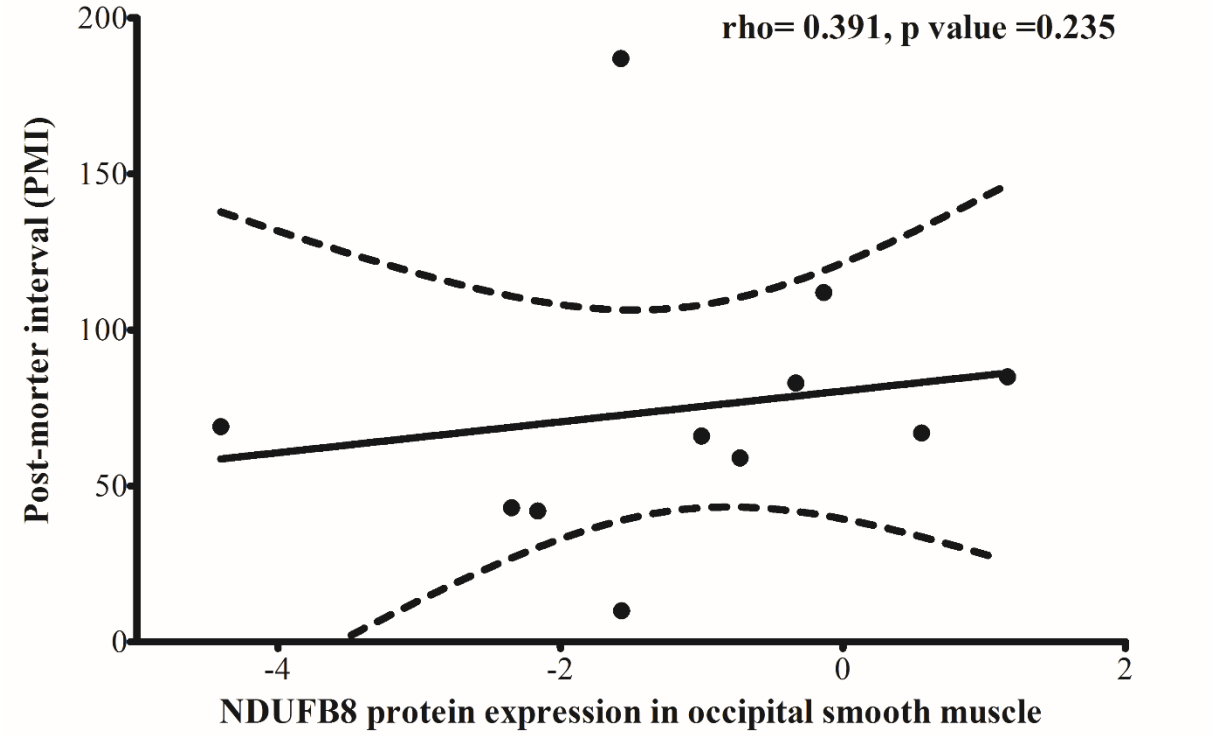
rho= 0.391, p value =0.235
Post-morter interval (PMI)
200
150
100
50
0
-4
-2
0
2
NDUFB8 protein expression in occipital smooth muscle

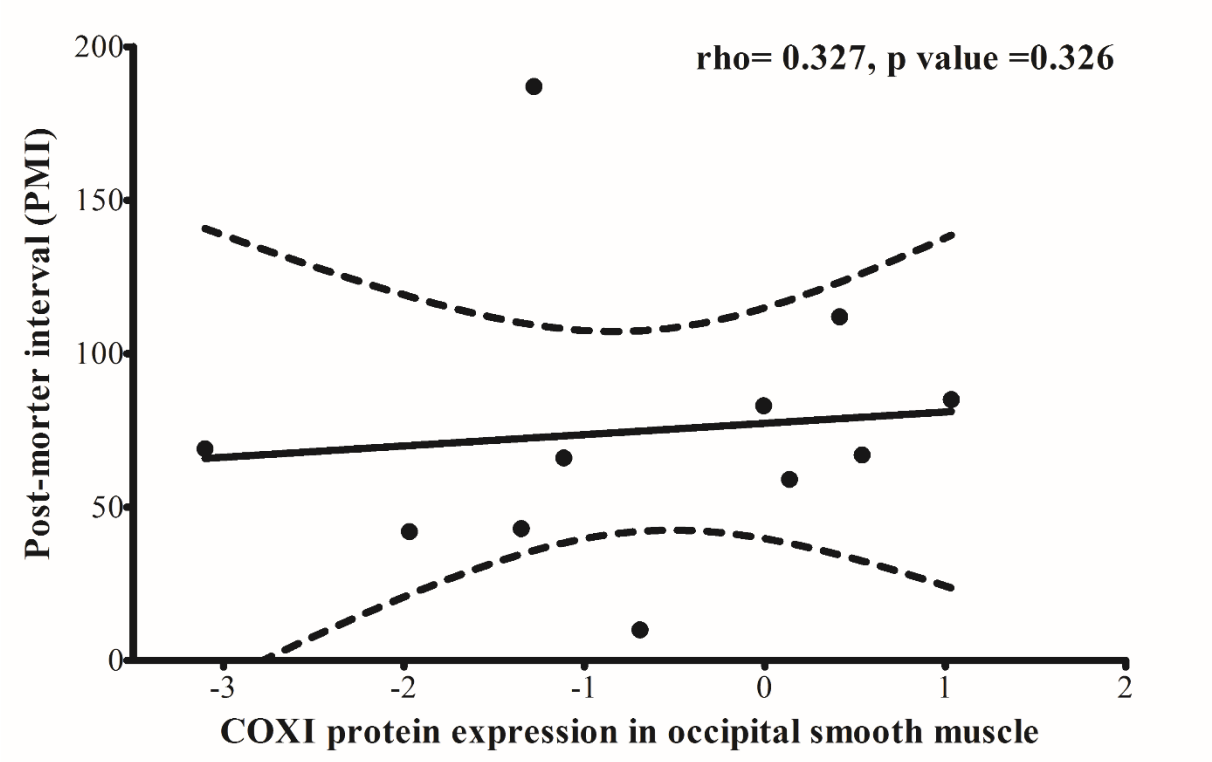
rho= 0.327, p value =0.326
Post-morter interval (PMI)
200
150
100
50
0
-3
-2
-1
0
1
2
COXI protein expression in occipital smooth muscle

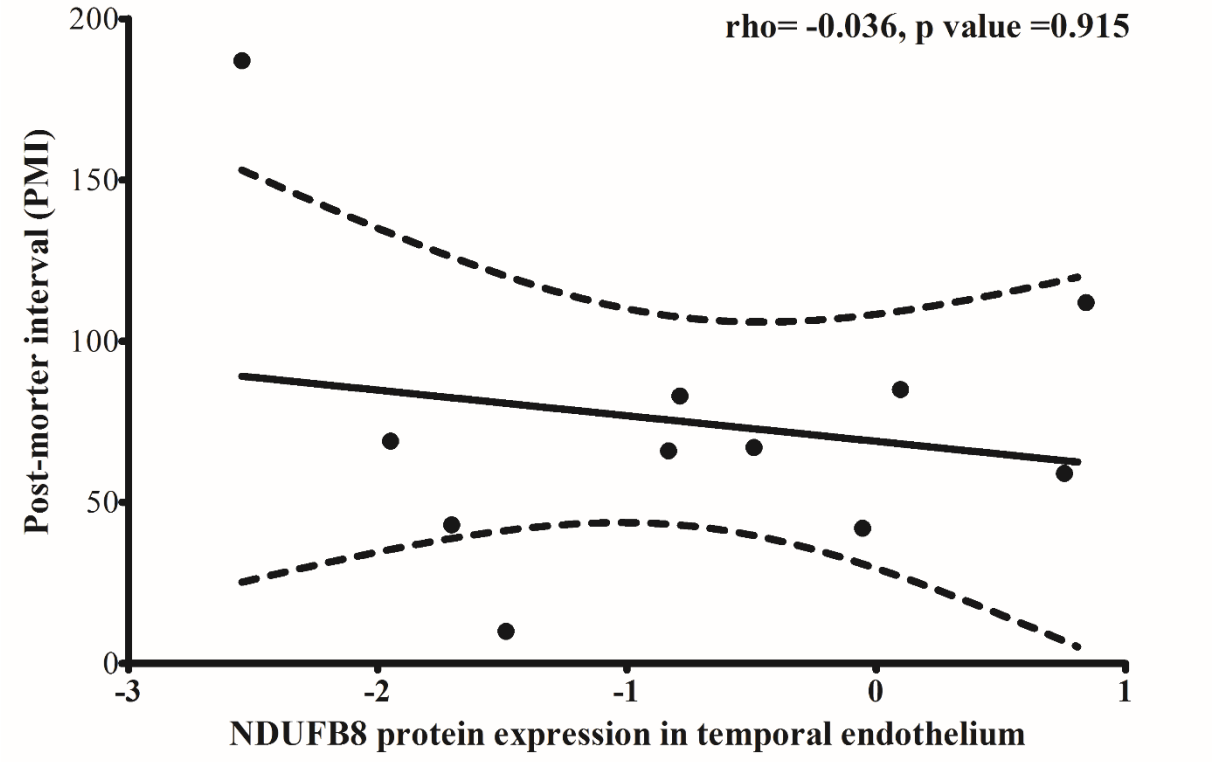
rho= -0.036, p value =0.915
Post-morter interval (PMI)
200
150
100
50
0
-3
-2
-1
0
1
NDUFB8 protein expression in temporal endothelium

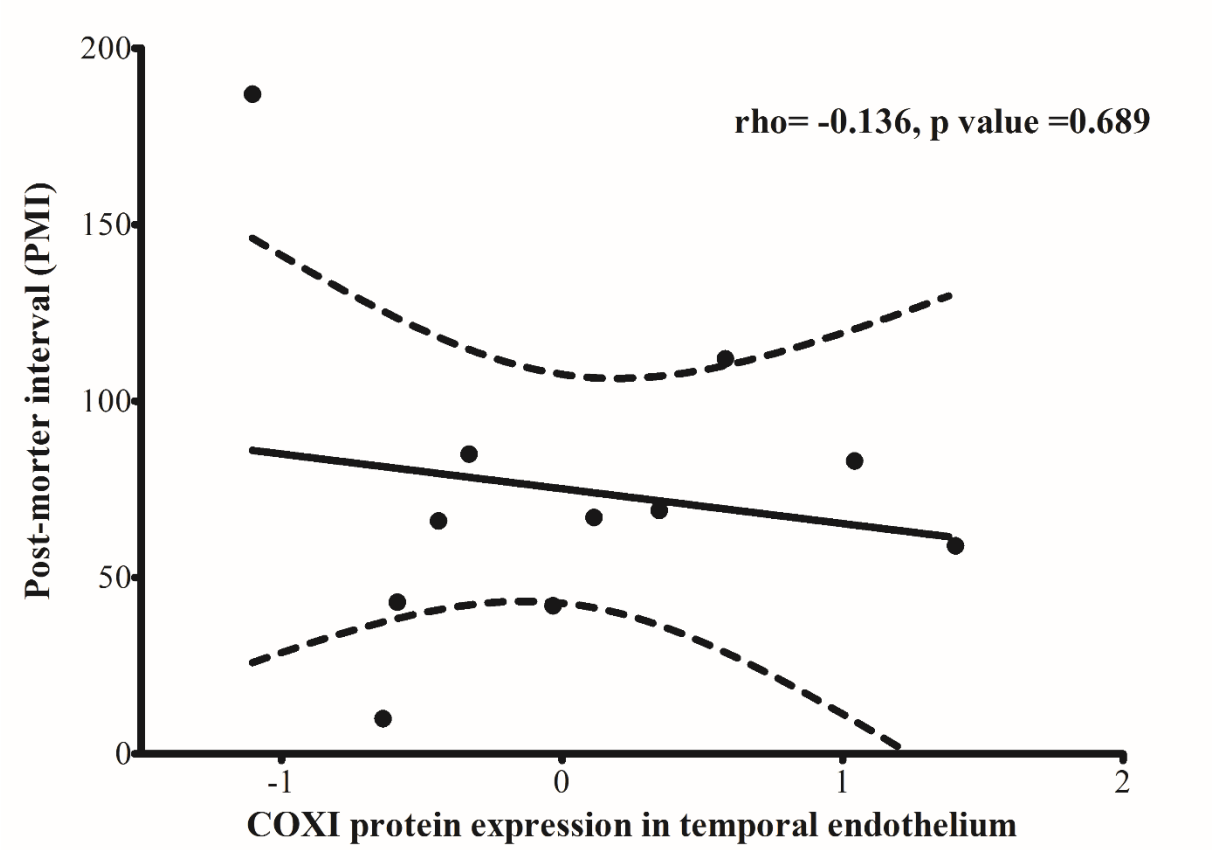
rho= -0.136, p value =0.689
Post-morter interval (PMI)
200
150
100
50
0
-1
0
1
2
COXI protein expression in temporal endothelium

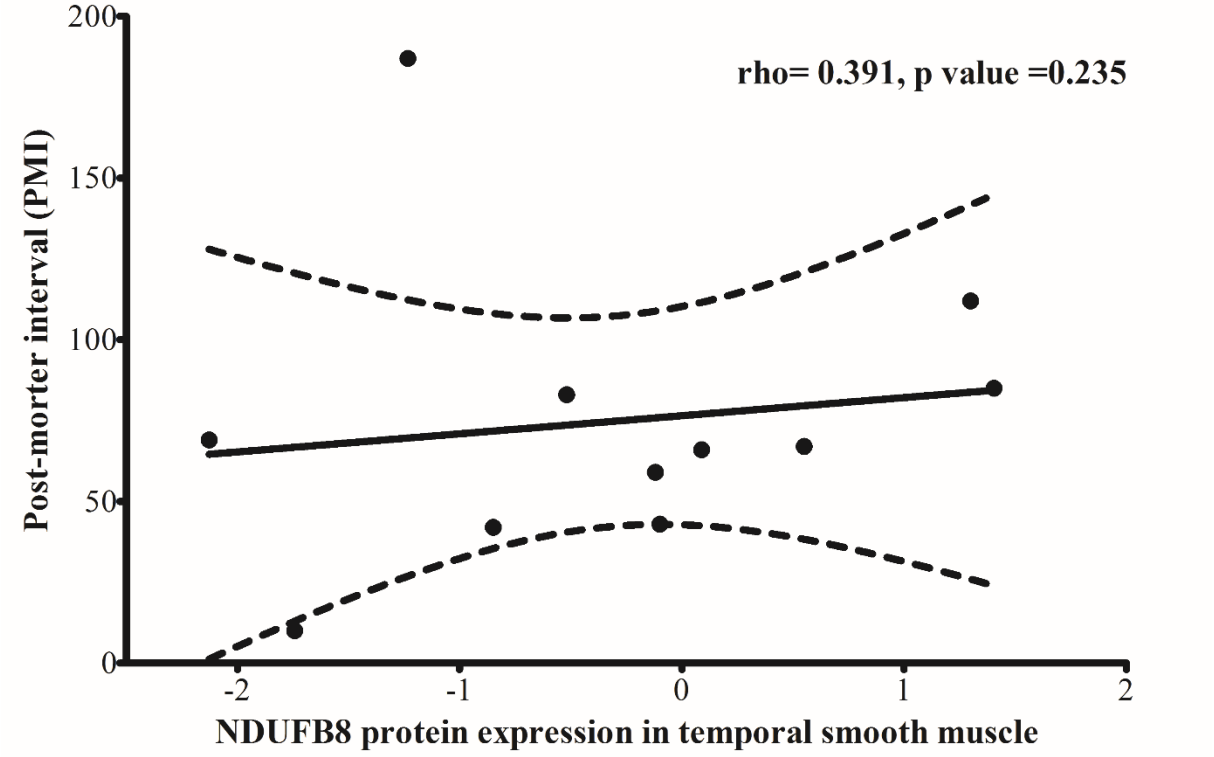
rho= 0.391, p value =0.235
Post-morter interval (PMI)
200
150
100
50
0
-2
-1
0
1
2
NDUFB8 protein expression in temporal smooth muscle

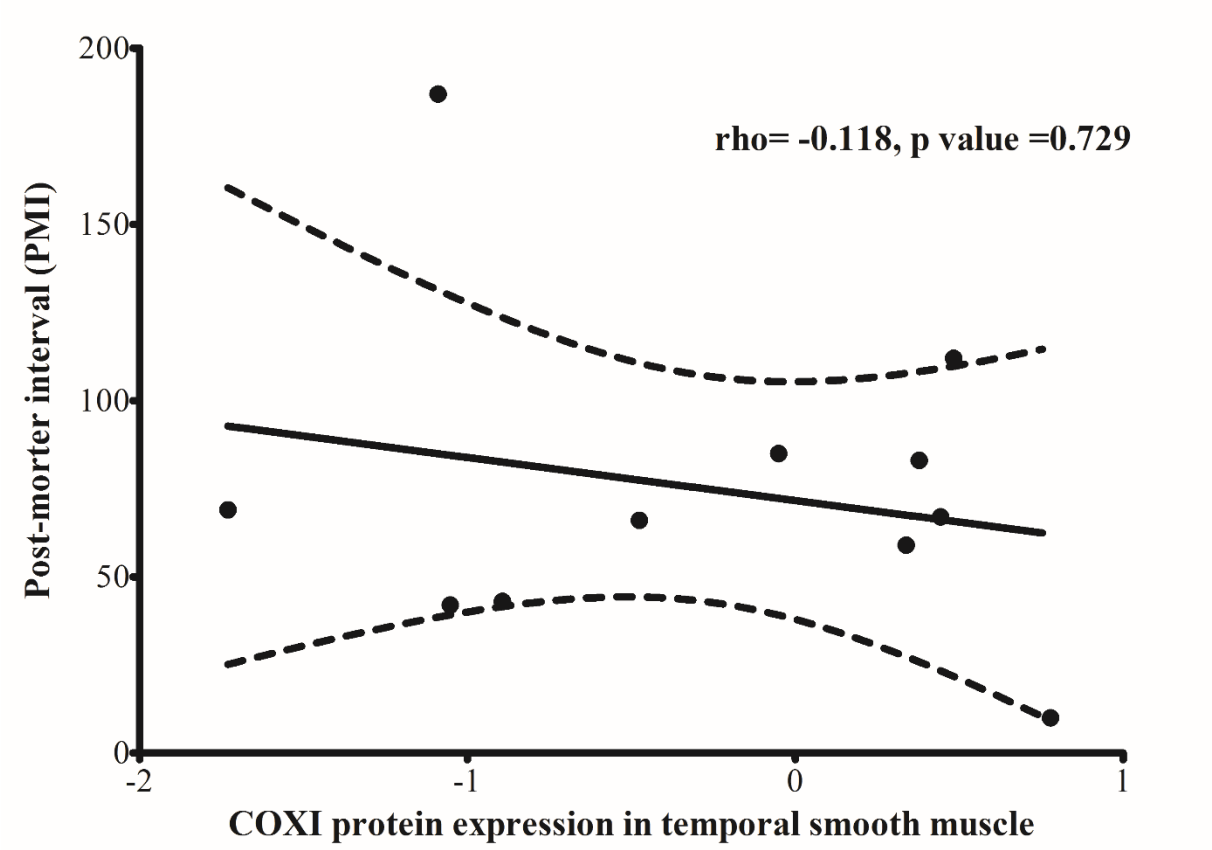
rho= -0.118, p value =0.729
Post-morter interval (PMI)
200
150
100
50
0
-2
-1
0
1
COXI protein expression in temporal smooth muscle

8.2 Appendix B: Inhibitory presynaptic terminal volume

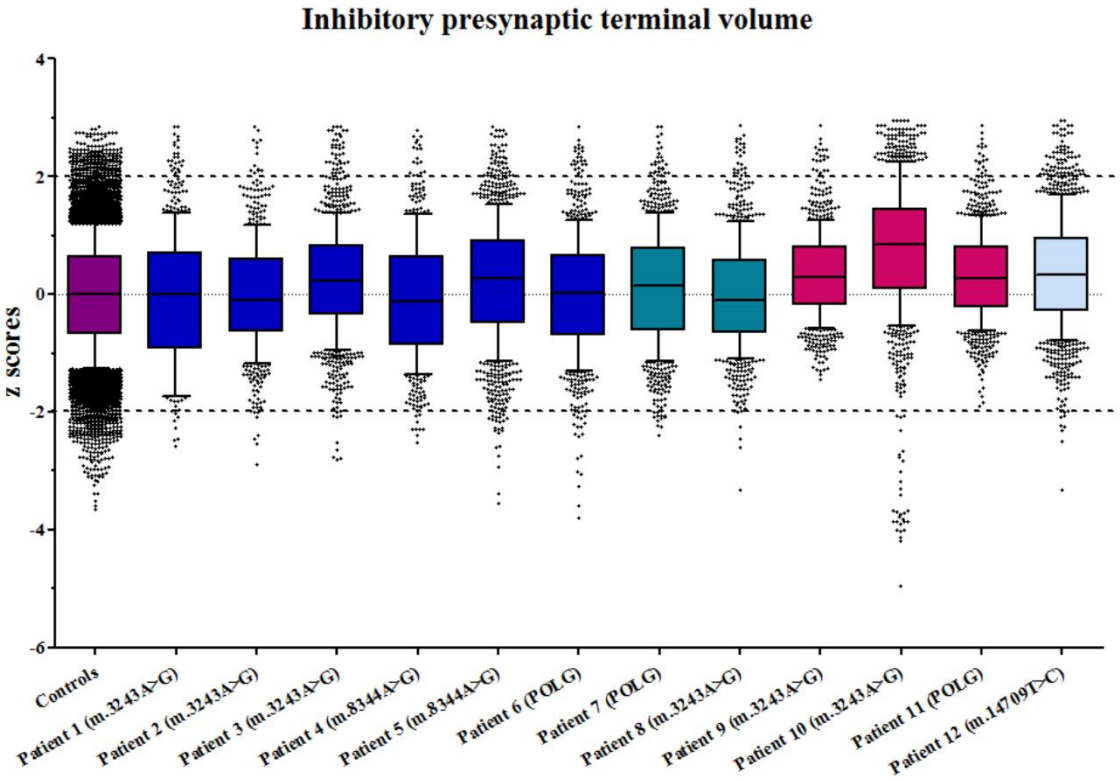

8.3 Appendix C: Inhibitory postsynaptic terminal volume

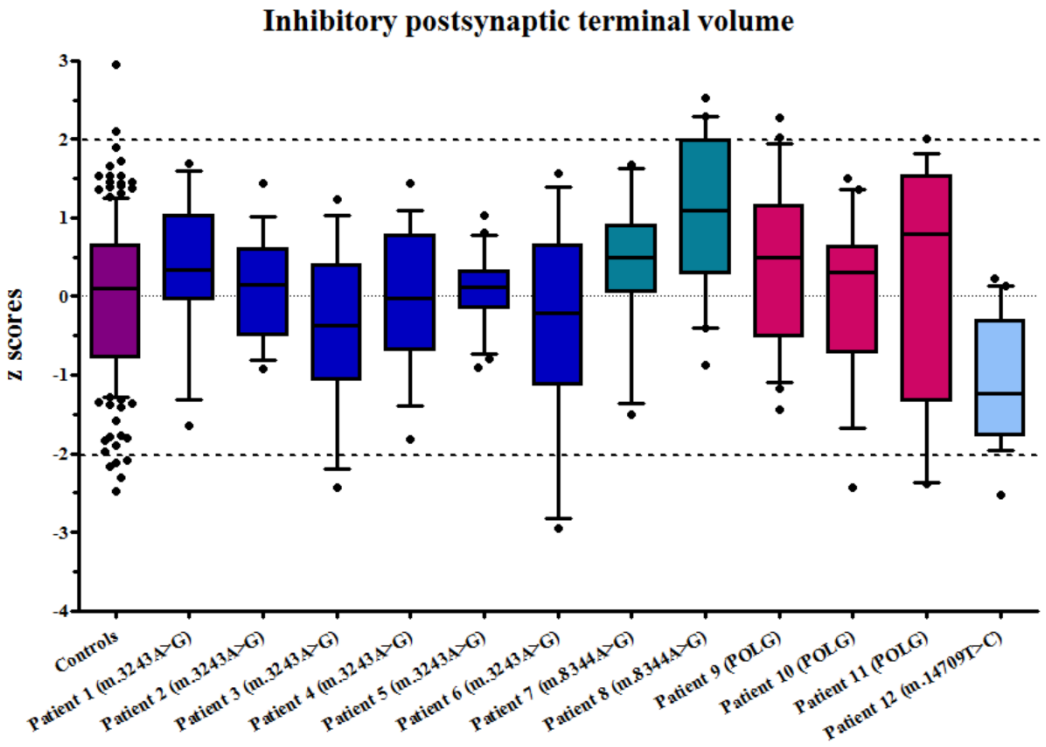

8.4 Appendix D: Excitatory presynaptic terminal volume

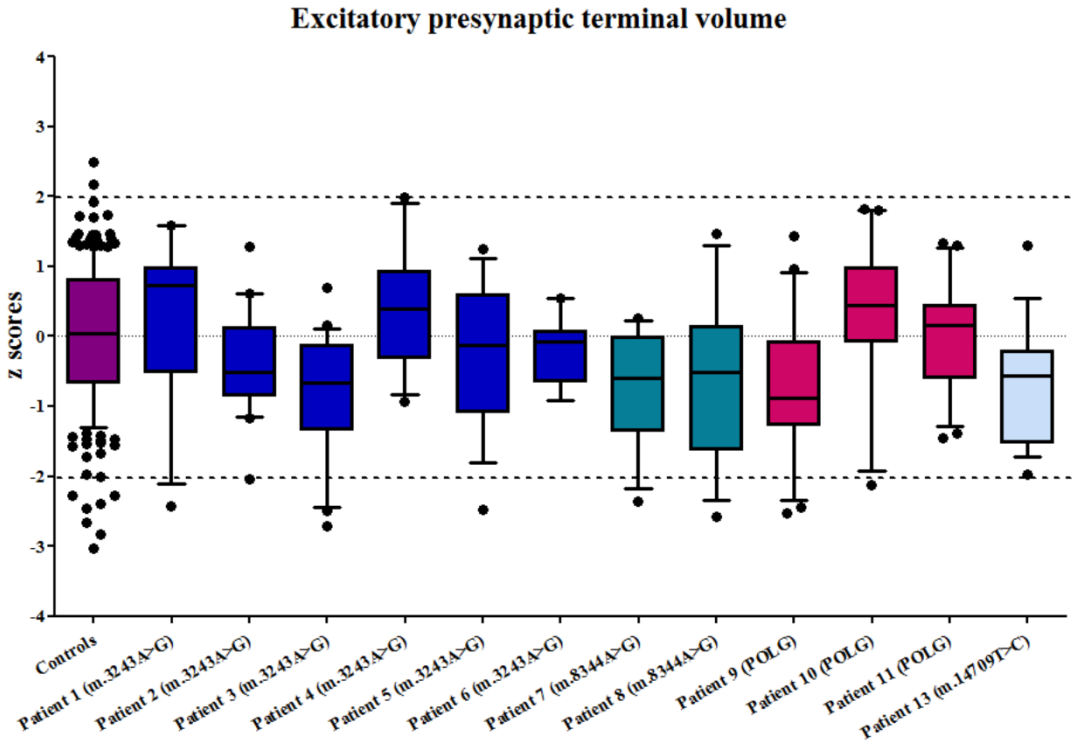

8.5 Appendix E: Excitatory receptor volume

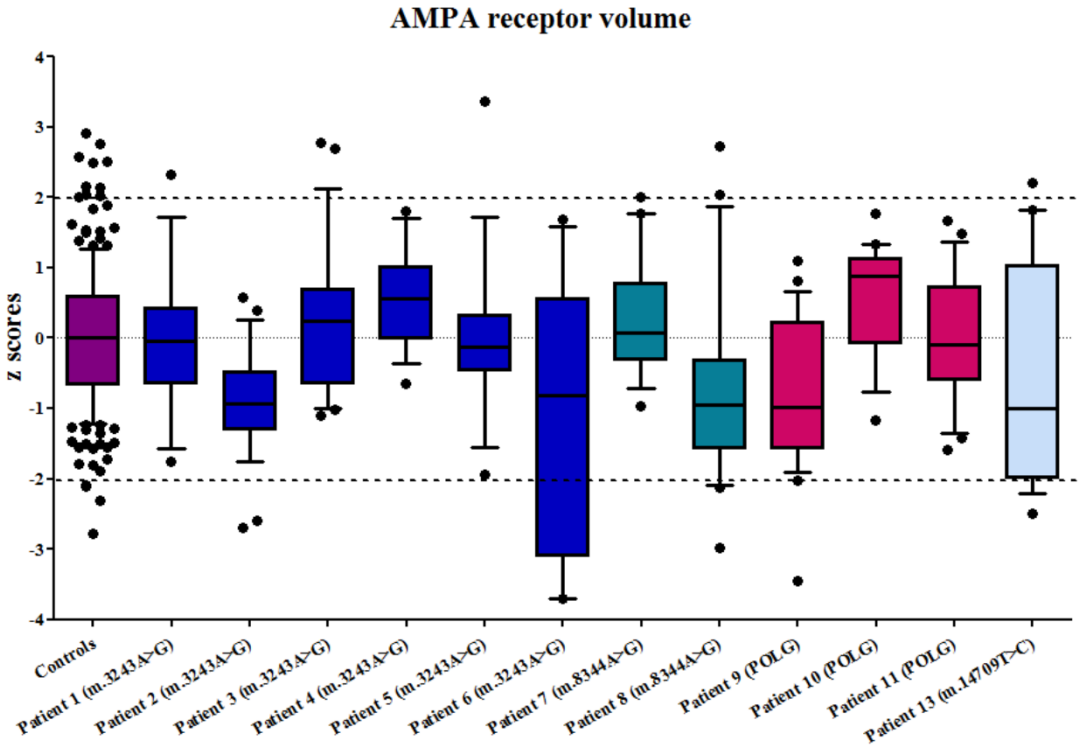

Chapter 9 References

Abramov, A.Y., Smulders-Srinivasan, T.K., Kirby, D.M., Acin-Perez, R., Enriquez, J.A., Lightowlers, R.N., Duchen, M.R. and Turnbull, D.M. (2010) 'Mechanism of neurodegeneration of neurons with mitochondrial DNA mutations', Brain, 133(Pt 3), pp. 797-807.

Acin-Perez, R., Fernandez-Silva, P., Peleato, M.L., Perez-Martos, A. and Enriquez, J.A. (2008) 'Respiratory active mitochondrial supercomplexes', Mol Cell, 32(4), pp. 529-39.

Adachi, M., Torii, J., Volk, B., Briet, P., Wolintz, A. and Schneck, L. (1973) 'Electron microscopic and enzyme histochemical studies of cerebellum, ocular and skeletal muscles in chronic progressive ophthalmoplegia with cerebellar ataxia', Acta Neuropathologica, 23(4), pp. 300-312.

Airaksinen, M.S., Eilers, J., Garaschuk, O., Thoenen, H., Konnerth, A. and Meyer, M. (1997) 'Ataxia and altered dendritic calcium signaling in mice carrying a targeted null mutation of the calbindin D28k gene', Proc Natl Acad Sci U S A, 94(4), pp. 1488-93.

Alberts B, J.A., Lewis J, *et al*. (2002) Molecular Biology of the Cell. 4th edn. New York: Garland Science.

Algahim, M.F., Sen, S. and Taegtmeyer, H. (2012) 'Bariatric surgery to unload the stressed heart: a metabolic hypothesis', Am J Physiol Heart Circ Physiol, 302(8), pp. H1539-45.

Anderson, S., Bankier, A.T., Barrell, B.G., de Bruijn, M.H., Coulson, A.R., Drouin, J., Eperon, I.C., Nierlich, D.P., Roe, B.A., Sanger, F., Schreier, P.H., Smith, A.J., Staden, R. and Young, I.G. (1981) 'Sequence and organization of the human mitochondrial genome', Nature, 290(5806), pp. 457-65.

Angebault, C., Charif, M., Guegen, N., Piro-Megy, C., Mousson de Camaret, B., Procaccio, V., Guichet, P.O., Hebrard, M., Manes, G., Leboucq, N., Rivier, F., Hamel, C.P., Lenaers, G. and Roubertie, A. (2015) 'Mutation in NDUFA13/GRIM19 leads to early onset hypotonia, dyskinesia and sensorial deficiencies, and mitochondrial complex I instability', Hum Mol Genet.

Apps, R. and Garwicz, M. (2005) 'Anatomical and physiological foundations of cerebellar information processing', Nat Rev Neurosci, 6(4), pp. 297-311.

Ardail, D., Privat, J.P., Egret-Charlier, M., Levrat, C., Lerme, F. and Louisot, P. (1990) 'Mitochondrial contact sites. Lipid composition and dynamics', J Biol Chem, 265(31), pp. 18797-802.

Arnberg, A., van Bruggen, E.F. and Borst, P. (1971) 'The presence of DNA molecules with a displacement loop in standard mitochondrial DNA preparations', Biochim Biophys Acta, 246(2), pp. 353-7.

Arpa, J., Cruz-Martinez, A., Campos, Y., Gutierrez-Molina, M., Garcia-Rio, F., Perez-Conde, C., Martin, M.A., Rubio, J.C., Del Hoyo, P., Arpa-Fernandez, A. and Arenas, J. (2003) 'Prevalence and progression of mitochondrial diseases: a study of 50 patients', Muscle Nerve, 28(6), pp. 690-5.

Ashrafi, G., Schlehe, J.S., LaVoie, M.J. and Schwarz, T.L. (2014) 'Mitophagy of damaged mitochondria occurs locally in distal neuronal axons and requires PINK1 and Parkin', J Cell Biol, 206(5), pp. 655-70.

Attwell, D. and Laughlin, S.B. (2001) 'An energy budget for signaling in the grey matter of the brain', J Cereb Blood Flow Metab, 21(10), pp. 1133-45.

Austin, S.A., Vriesendorp, F.J., Thandroyen, F.T., Hecht, J.T., Jones, O.T. and Johns, D.R. (1998) 'Expanding the phenotype of the 8344 transfer RNAlysine mitochondrial DNA mutation', Neurology, 51(5), pp. 1447-50.

Babinski, J. (1899) 'De l' asynergie cérébelleuse', Revue neurologique, 7(22), pp. 806-816.

Bahi, N., Zhang, J., Llovera, M., Ballester, M., Comella, J.X. and Sanchis, D. (2006) 'Switch from caspase-dependent to caspase-independent death during heart development: essential role of endonuclease G in ischemia-induced DNA processing of differentiated cardiomyocytes', J Biol Chem, 281(32), pp. 22943-52.

Barkovich, A.J., Good, W.V., Koch, T.K. and Berg, B.O. (1993) 'Mitochondrial disorders: analysis of their clinical and imaging characteristics', AJNR Am J Neuroradiol, 14(5), pp. 1119-37.

Barrell, B.G., Anderson, S., Bankier, A.T., de Bruijn, M.H., Chen, E., Coulson, A.R., Drouin, J., Eperon, I.C., Nierlich, D.P., Roe, B.A., Sanger, F., Schreier, P.H., Smith, A.J., Staden, R. and Young, I.G. (1980) 'Different pattern of codon recognition by mammalian mitochondrial tRNAs', Proc Natl Acad Sci U S A, 77(6), pp. 3164-6.

Barski, J.J., Hartmann, J., Rose, C.R., Hoebeek, F., Morl, K., Noll-Hussong, M., De Zeeuw, C.I., Konnerth, A. and Meyer, M. (2003) 'Calbindin in cerebellar Purkinje cells is a critical determinant of the precision of motor coordination', J Neurosci, 23(8), pp. 3469-77.

Baschong, W., Suetterlin, R. and Laeng, R.H. (2001) 'Control of Autofluorescence of Archival Formaldehyde-fixed, Paraffin-embedded Tissue in Confocal Laser Scanning Microscopy (CLSM)', Journal of Histochemistry & Cytochemistry, 49(12), pp. 1565-1571.

Bausen, M., Fuhrmann, J.C., Betz, H. and O'Sullivan G, A. (2006) 'The state of the actin cytoskeleton determines its association with gephyrin: role of ena/VASP family members', Mol Cell Neurosci, 31(2), pp. 376-86.

Bellocchio, E.E., Hu, H., Pohorille, A., Chan, J., Pickel, V.M. and Edwards, R.H. (1998) 'The localization of the brain-specific inorganic phosphate transporter suggests a specific presynaptic role in glutamatergic transmission', J Neurosci, 18(21), pp. 8648-59.

Bereiter-Hahn, J. and Voth, M. (1994) 'Dynamics of mitochondria in living cells: shape changes, dislocations, fusion, and fission of mitochondria', Microsc Res Tech, 27(3), pp. 198-219.

Berg JM, T.J., Stryer L. (2002a) 'The Citric Acid Cycle', in Biochemistry. New York: W. H. Freeman.

Berg JM, T.J., Stryer L. (2002b) 'Glycolysis and Gluconeogenesis', in Biochemistry. New York: W. H. Freeman.

Berg JM, T.J., Stryer L. (2002c) 'Oxidative Phosphorylation', in Biochemistry. New York: W. H. Freeman.

Berkovic, S.F., Carpenter, S., Evans, A., Karpati, G., Shoubridge, E.A., Andermann, F., Meyer, E., Tyler, J.L., Diksic, M., Arnold, D., Wolfe, L.S., Andermann, E. and Hakim, A.M. (1989) 'MYOCLONUS EPILEPSY AND RAGGED-RED FIBRES (MERRF)', 1. A CLINICAL, PATHOLOGICAL, BIOCHEMICAL, MAGNETIC RESONANCE SPECTROGRAPHIC AND POSITRON EMISSION TOMOGRAPHIC STUDY, 112(5), pp. 1231-1260.

Betts, J., Jaros, E., Perry, R.H., Schaefer, A.M., Taylor, R.W., Abdel-All, Z., Lightowlers, R.N. and Turnbull, D.M. (2006) 'Molecular neuropathology of MELAS: level of heteroplasmy in individual neurones and evidence of extensive vascular involvement', Neuropathol Appl Neurobiol, 32(4), pp. 359-73.

Betts-Henderson, J., Jaros, E., Krishnan, K.J., Perry, R.H., Reeve, A.K., Schaefer, A.M., Taylor, R.W. and Turnbull, D.M. (2009) 'Alpha-synuclein pathology and Parkinsonism associated with POLG1 mutations and multiple mitochondrial DNA deletions', Neuropathology and Applied Neurobiology, 35(1), pp. 120-124.

Billups, B. and Forsythe, I.D. (2002) 'Presynaptic mitochondrial calcium sequestration influences transmission at mammalian central synapses', J Neurosci, 22(14), pp. 5840-7.

Birky, C.W. (1994) 'Relaxed and Stringent Genomes: Why Cytoplasmic Genes Don't Obey Mendel's Laws', Journal of Heredity, 85(5), pp. 355-365.

Boesch, P., Weber-Lotfi, F., Ibrahim, N., Tarasenko, V., Cosset, A., Paulus, F., Lightowlers, R.N. and Dietrich, A. (2011) 'DNA repair in organelles: Pathways, organization, regulation, relevance in disease and aging', Biochimica et Biophysica Acta (BBA) - Molecular Cell Research, 1813(1), pp. 186-200.

Bogdan, A.R., Miyazawa, M., Hashimoto, K. and Tsuji, Y. (2015) 'Regulators of Iron Homeostasis: New Players in Metabolism, Cell Death, and Disease', Trends in Biochemical Sciences.

Bogenhagen, D. and Clayton, D.A. (1977) 'Mouse L cell mitochondrial DNA molecules are selected randomly for replication throughout the cell cycle', Cell, 11(4), pp. 719-27.

Bosbach, S., Kornblum, C., Schroder, R. and Wagner, M. (2003) 'Executive and visuospatial deficits in patients with chronic progressive external ophthalmoplegia and Kearns-Sayre syndrome', Brain, 126(Pt 5), pp. 1231-40.

Bowmaker, M., Yang, M.Y., Yasukawa, T., Reyes, A., Jacobs, H.T., Huberman, J.A. and Holt, I.J. (2003) 'Mammalian Mitochondrial DNA Replicates Bidirectionally from an Initiation Zone', Journal of Biological Chemistry, 278(51), pp. 50961-50969.

Brand, M.D. (2010) 'The sites and topology of mitochondrial superoxide production', Experimental Gerontology, 45(7–8), pp. 466-472.

Breuer, M.E., Willems, P.H., Smeitink, J.A., Koopman, W.J. and Nooteboom, M. (2013) 'Cellular and animal models for mitochondrial complex I deficiency: a focus on the NDUFS4 subunit', IUBMB Life, 65(3), pp. 202-8.

Brodin, L., Bakeeva, L. and Shupliakov, O. (1999) 'Presynaptic mitochondria and the temporal pattern of neurotransmitter release', Philos Trans R Soc Lond B Biol Sci, 354(1381), pp. 365-72.

Brown, D.T., Samuels, D.C., Michael, E.M., Turnbull, D.M. and Chinnery, P.F. (2001) 'Random Genetic Drift Determines the Level of Mutant mtDNA in Human Primary Oocytes', American Journal of Human Genetics, 68(2), pp. 533-536.

Brown, T.A., Tkachuk, A.N., Shtengel, G., Kopek, B.G., Bogenhagen, D.F., Hess, H.F. and Clayton, D.A. (2011) 'Superresolution fluorescence imaging of mitochondrial nucleoids reveals their spatial range, limits, and membrane interaction', Mol Cell Biol, 31(24), pp. 4994-5010.

Brown, W.M., George, M. and Wilson, A.C. (1979) 'Rapid evolution of animal mitochondrial DNA', Proceedings of the National Academy of Sciences, 76(4), pp. 1967-1971.

Bu, X.D. and Rotter, J.I. (1991) 'X chromosome-linked and mitochondrial gene control of Leber hereditary optic neuropathy: evidence from segregation analysis for dependence on X chromosome inactivation', Proc Natl Acad Sci U S A, 88(18), pp. 8198-202.

Bubolz, A.H., Mendoza, S.A., Zheng, X., Zinkevich, N.S., Li, R., Gutterman, D.D. and Zhang, D.X. (2012) 'Activation of endothelial TRPV4 channels mediates flow-induced dilation in human coronary arterioles: role of Ca2+ entry and mitochondrial ROS signaling', Am J Physiol Heart Circ Physiol, 302(3), pp. H634-42.

Burns, E.M., Kruckeberg, T.W., Comerford, L.E. and Buschmann, M.T. (1979) 'Thinning of capillary walls and declining numbers of endothelial mitochondria in the cerebral cortex of the aging primate, Macaca nemestrina', J Gerontol, 34(5), pp. 642-50.

Cai, Q., Zakaria, H.M., Simone, A. and Sheng, Z.H. (2012) 'Spatial parkin translocation and degradation of damaged mitochondria via mitophagy in live cortical neurons', Curr Biol, 22(6), pp. 545-52.

Calkins, M.J. and Reddy, P.H. (2011) 'Assessment of Newly Synthesized Mitochondrial DNA Using BrdU Labeling in Primary Neurons from Alzheimer's Disease Mice: Implications for Impaired Mitochondrial Biogenesis and Synaptic Damage', Biochimica et biophysica acta, 1812(9), pp. 1182-1189.

Carelli, V., Ross-Cisneros, F.N. and Sadun, A.A. (2004) 'Mitochondrial dysfunction as a cause of optic neuropathies', Progress in Retinal and Eye Research, 23(1), pp. 53-89.

Carrozzo, R., Hirano, M., Fromenty, B., Casali, C., Santorelli, F.M., Bonilla, E., DiMauro, S., Schon, E.A. and Miranda, A.F. (1998) 'Multiple mtDNA deletions features in autosomal dominant and recessive diseases suggest distinct pathogeneses', Neurology, 50(1), pp. 99-106.

Cauli, B., Tong, X.K., Rancillac, A., Serluca, N., Lambolez, B., Rossier, J. and Hamel, E. (2004) 'Cortical GABA interneurons in neurovascular coupling: relays for subcortical vasoactive pathways', J Neurosci, 24(41), pp. 8940-9.

Chambers, W.W. and Sprague, J.M. (1955) 'Functional localization in the cerebellum. II. Somatotopic organization in cortex and nuclei', AMA Arch Neurol Psychiatry, 74(6), pp. 653-80.

Chang, D.D. and Clayton, D.A. (1984) 'Precise identification of individual promoters for transcription of each strand of human mitochondrial DNA', Cell, 36(3), pp. 635-43.

Chen, H. and Chan, D.C. (2004) 'Mitochondrial dynamics in mammals', Curr Top Dev Biol, 59, pp. 119-44.

Chen, H. and Chan, D.C. (2009) 'Mitochondrial dynamics–fusion, fission, movement, and mitophagy–in neurodegenerative diseases', Human Molecular Genetics, 18(R2), pp. R169-R176.

Chen, J.J., Rosas, H.D. and Salat, D.H. (2011) 'Age-associated reductions in cerebral blood flow are independent from regional atrophy', Neuroimage, 55(2), pp. 468-78.

Chen, Q., Vazquez, E.J., Moghaddas, S., Hoppel, C.L. and Lesnefsky, E.J. (2003) 'Production of reactive oxygen species by mitochondria: central role of complex III', J Biol Chem, 278(38), pp. 36027-31.

Chen, W., Zhou, Z., Li, L., Zhong, C.Q., Zheng, X., Wu, X., Zhang, Y., Ma, H., Huang, D., Li, W., Xia, Z. and Han, J. (2013) 'Diverse sequence determinants control human and mouse receptor interacting protein 3 (RIP3) and mixed lineage kinase domain-like (MLKL) interaction in necroptotic signaling', J Biol Chem, 288(23), pp. 16247-61.

Chen, X.J. and Butow, R.A. (2005) 'The organization and inheritance of the mitochondrial genome', Nat Rev Genet, 6(11), pp. 815-825.

Chevalier-Larsen, E. and Holzbaur, E.L.F. (2006) 'Axonal transport and neurodegenerative disease', Biochimica et Biophysica Acta (BBA) - Molecular Basis of Disease, 1762(11–12), pp. 1094-1108.

Chinnery, P.F. (2000) *Mitochondrial Disorders Overview*. Available at: http://www.ncbi.nlm.nih.gov/books/NBK1224/ (Accessed: 1 September).

Chinnery, P.F., Howell, N., Lightowlers, R.N. and Turnbull, D.M. (1997) 'Molecular pathology of MELAS and MERRF. The relationship between mutation load and clinical phenotypes', Brain, 120 (Pt 10), pp. 1713-21.

Chinnery, P.F., Betts, J., Jaros, E., Turnbull, D.M., DiMauro, S. and Perry, R.H. (2008) 'Mitochondrial diseases', in Love, S., Louis, D.N. and Ellison, D.W. (eds.) Greenfield's neuropathology. 8 edn. Hodder Arnold, pp. 601-635.

Chinnery, P.F., Lax, N.Z., Jaros, E., Taylor, R.W., Turnbull, D.M. and DiMauro, S. (2015) 'Mitochondrial Diseases', in Love, S., Perry, A., Ironside, J.W. and Budka, H. (eds.) Greenfiled's neuropathology. London, New York: Boca Raton: CRC Press

Chinnery, P.F., Thorburn, D.R., Samuels, D.C., White, S.L., Dahl, H.-H.M., Turnbull, D.M., Lightowlers, R.N. and Howell, N. (2000) 'The inheritance of mitochondrial DNA heteroplasmy: random drift, selection or both?', Trends in Genetics, 16(11), pp. 500-505.

Chrysostomou, A., Grady, J.P., Laude, A., Taylor, R.W., Turnbull, D.M. and Lax, N.Z. (2015) 'Investigating complex I deficiency in Purkinje cells and synapses in patients with mitochondrial disease', Neuropathol Appl Neurobiol.

Chu, B.C., Terae, S., Takahashi, C., Kikuchi, Y., Miyasaka, K., Abe, S., Minowa, K. and Sawamura, T. (1999) 'MRI of the brain in the Kearns-Sayre syndrome: report of four cases and a review', Neuroradiology, 41(10), pp. 759-64.

Chung, K. and Deisseroth, K. (2013) 'CLARITY for mapping the nervous system', Nat Meth, 10(6), pp. 508-513.

Cipolla, M.J. (2009) 'The Cerebral Circulation', in Anatomy and Ultrastructure. San Rafael (CA): Morgan & Claypool Life Sciences.

Cipolla, M.J., Li, R. and Vitullo, L. (2004) 'Perivascular innervation of penetrating brain parenchymal arterioles', J Cardiovasc Pharmacol, 44(1), pp. 1-8.

Clark, I.E., Dodson, M.W., Jiang, C., Cao, J.H., Huh, J.R., Seol, J.H., Yoo, S.J., Hay, B.A. and Guo, M. (2006) 'Drosophila pink1 is required for mitochondrial function and interacts genetically with parkin', Nature, 441(7097), pp. 1162-6.

Clayton, D.A. (1982) 'Replication of animal mitochondrial DNA', Cell, 28(4), pp. 693-705.

Cohen BH, C.P., Copeland WC (2010) POLG-Related Disorders. Available at: http://www.ncbi.nlm.nih.gov/books/NBK26471/.

Cohen, B.H. and Naviaux, R.K. (2010) 'The clinical diagnosis of POLG disease and other mitochondrial DNA depletion disorders', Methods, 51(4), pp. 364-373.

Cohen, D. (2014) 'Deep Cerebellar Nuclei', in Jaeger, D. and Jung, R. (eds.) Encyclopedia of Computational Neuroscience. Springer New York, pp. 1-4.

Coku, J., Shanske, S., Mehrazin, M., Tanji, K., Naini, A., Emmanuele, V., Patterson, M., Hirano, M. and DiMauro, S. (2010) 'Slowly progressive encephalopathy with hearing loss due to a mutation in the mtDNA tRNA(Leu(CUN)) gene', J Neurol Sci, 290(1-2), pp. 166-8.

Collingridge, G.L. and Lester, R.A. (1989) 'Excitatory amino acid receptors in the vertebrate central nervous system', Pharmacol Rev, 41(2), pp. 143-210.

Cooper, D.W. (1958) 'The Physiology and Pathology of the Cerebellum', The Yale Journal of Biology and Medicine, 31(2), pp. 108-108.

Corona, P., Antozzi, C., Carrara, F., D'Incerti, L., Lamantea, E., Tiranti, V. and Zeviani, M. (2001) 'A novel mtDNA mutation in the ND5 subunit of complex I in two MELAS patients', Ann Neurol, 49(1), pp. 106-10.

Cottrell, D.A., Ince, P.G., Blakely, E.L., Johnson, M.A., Chinnery, P.F., Hanna, M. and Turnbull, D.M. (2000) 'Neuropathological and histochemical changes in a multiple mitochondrial DNA deletion disorder', J Neuropathol Exp Neurol, 59(7), pp. 621-7.

Cowan, W.M. (1970) 'Anterograde and Retrograde Transneuronal Degeneration in the Central and Peripheral Nervous System', in Nauta, W.H. and Ebbesson, S.E. (eds.) Contemporary Research Methods in Neuroanatomy. Springer Berlin Heidelberg, pp. 217-251.

Craven, L., Elson, J.L., Irving, L., Tuppen, H.A., Lister, L.M., Greggains, G.D., Byerley, S., Murdoch, A.P., Herbert, M. and Turnbull, D. (2011) 'Mitochondrial DNA disease: new options for prevention', Human Molecular Genetics, 20(R2), pp. R168-R174.

Craven, L., Tuppen, H.A., Greggains, G.D., Harbottle, S.J., Murphy, J.L., Cree, L.M., Murdoch, A.P., Chinnery, P.F., Taylor, R.W., Lightowlers, R.N., Herbert, M. and Turnbull, D.M. (2010) 'Pronuclear transfer in human embryos to prevent transmission of mitochondrial DNA disease', Nature, 465(7294), pp. 82-85.

Cree, L.M., Samuels, D.C., de Sousa Lopes, S.C., Rajasimha, H.K., Wonnapinij, P., Mann, J.R., Dahl, H.-H.M. and Chinnery, P.F. (2008) 'A reduction of mitochondrial DNA molecules during embryogenesis explains the rapid segregation of genotypes', Nat Genet, 40(2), pp. 249-254.

Culic, O., Gruwel, M.L. and Schrader, J. (1997) 'Energy turnover of vascular endothelial cells', Am J Physiol, 273(1 Pt 1), pp. C205-13.

Dairaghi, D.J., Shadel, G.S. and Clayton, D.A. (1995) 'Human mitochondrial transcription factor A and promoter spacing integrity are required for transcription initiation', Biochim Biophys Acta, 1271(1), pp. 127-34.

Damas, J., Carneiro, J., Goncalves, J., Stewart, J.B., Samuels, D.C., Amorim, A. and Pereira, F. (2012) 'Mitochondrial DNA deletions are associated with non-B DNA conformations', Nucleic Acids Res, 40(16), pp. 7606-21.

D'Angelo, E. (2014) 'The organization of plasticity in the cerebellar cortex: from synapses to control', Prog Brain Res, 210, pp. 31-58.

D'Angelo, E. and Casali, S. (2012) 'Seeking a unified framework for cerebellar function and dysfunction: from circuit operations to cognition', Front Neural Circuits, 6, p. 116.

Das, B.B., Dexheimer, T.S., Maddali, K. and Pommier, Y. (2010) 'Role of tyrosyl-DNA phosphodiesterase (TDP1) in mitochondria', Proceedings of the National Academy of Sciences of the United States of America, 107(46), pp. 19790-19795.

Davey, G.P., Peuchen, S. and Clark, J.B. (1998) 'Energy thresholds in brain mitochondria. Potential involvement in neurodegeneration', J Biol Chem, 273(21), pp. 12753-7.

Davidzon, G., Mancuso, M., Ferraris, S., Quinzii, C., Hirano, M., Peters, H.L., Kirby, D., Thorburn, D.R. and DiMauro, S. (2005) 'POLG mutations and Alpers syndrome', Ann Neurol, 57(6), pp. 921-3.

Day, N.C., Williams, T.L., Ince, P.G., Kamboj, R.K., Lodged, D. and Shaw, P.J. (1995) 'Distribution of AMPA-selective glutamate receptor subunits in the human hippocampus and cerebellum', Molecular Brain Research, 31(1–2), pp. 17-32.

De Coo, I.F., Renier, W.O., Ruitenbeek, W., Ter Laak, H.J., Bakker, M., Schagger, H., Van Oost, B.A. and Smeets, H.J. (1999) 'A 4-base pair deletion in the mitochondrial cytochrome b gene associated with parkinsonism/MELAS overlap syndrome', Ann Neurol, 45(1), pp. 130-3.

de Gottrau, P., Buchi, E.R. and Daicker, B. (1992) 'Distended optic nerve sheaths in Leber's hereditary optic neuropathy', J Clin Neuroophthalmol, 12(2), pp. 89-93.

Del Castillo, P., Llorente, A.R. and Stockert, J.C. (1989) 'Influence of fixation, exciting light and section thickness on the primary fluorescence of samples for microfluorometric analysis', Basic Appl Histochem, 33(3), pp. 251-7.

DeLuca, S.Z. and O'Farrell, P.H. (2012) 'Barriers to male transmission of mitochondrial DNA in sperm development', Dev Cell, 22(3), pp. 660-8.

Deschauer, M., Tennant, S., Rokicka, A., He, L., Kraya, T., Turnbull, D.M., Zierz, S. and Taylor, R.W. (2007) 'MELAS associated with mutations in the POLG1 gene', Neurology, 68(20), pp. 1741-2.

Diedrichsen, J., Maderwald, S., Kuper, M., Thurling, M., Rabe, K., Gizewski, E.R., Ladd, M.E. and Timmann, D. (2011) 'Imaging the deep cerebellar nuclei: a probabilistic atlas and normalization procedure', Neuroimage, 54(3), pp. 1786-94.

DiMauro S, H.M. (2001) MELAS. Available at: http://www.ncbi.nlm.nih.gov/books/NBK1233/ (Accessed: September).

DiMauro S, H.M. (2003) MERRF. Available at: http://www.ncbi.nlm.nih.gov/books/NBK1520/ (Accessed: September 1).

DiMauro, S., Michio, H. and Eric, A.S. (2006) 'The mitochondrial respiratory chain and its disorders', in DiMauro, S., Michio, H. and Eric, A.S. (eds.) *Mitochondrial medicine*. Abingdon: Informa Healthcare, pp. 7-26.

DiMauro, S. and Schon, E.A. (2003) 'Mitochondrial respiratory-chain diseases', N Engl J Med, 348(26), pp. 2656-68.

Dixon, Scott J., Lemberg, Kathryn M., Lamprecht, Michael R., Skouta, R., Zaitsev, Eleina M., Gleason, Caroline E., Patel, Darpan N., Bauer, Andras J., Cantley, Alexandra M., Yang, Wan S., Morrison, B., III and Stockwell, Brent R. (2012) 'Ferroptosis: An Iron-Dependent Form of Nonapoptotic Cell Death', Cell, 149(5), pp. 1060-1072.

Doble, A. (1999) 'The role of excitotoxicity in neurodegenerative disease: implications for therapy', Pharmacol Ther, 81(3), pp. 163-221.

Dohi, Y., Kojima, M., Sato, K. and Luscher, T.F. (1995) 'Age-related changes in vascular smooth muscle and endothelium', Drugs Aging, 7(4), pp. 278-91.

Dong, X.-x., Wang, Y. and Qin, Z.-h. (2009) 'Molecular mechanisms of excitotoxicity and their relevance to pathogenesis of neurodegenerative diseases', Acta Pharmacologica Sinica, 30(4), pp. 379-387.

Dromparis, P. and Michelakis, E.D. (2013) 'Mitochondria in vascular health and disease', Annu Rev Physiol, 75, pp. 95-126.

Du, H., Guo, L., Yan, S., Sosunov, A.A., McKhann, G.M. and ShiDu Yan, S. (2010) 'Early deficits in synaptic mitochondria in an Alzheimer's disease mouse model', Proceedings of the National Academy of Sciences, 107(43), pp. 18670-18675.

Duchen, M.R. (2000) 'Mitochondria and calcium: from cell signalling to cell death', The Journal of Physiology, 529(1), pp. 57-68.

Duchen, M.R. (2004) 'Mitochondria in health and disease: perspectives on a new mitochondrial biology', Molecular Aspects of Medicine, 25(4), pp. 365-451.

Dudkina, N.V., Eubel, H., Keegstra, W., Boekema, E.J. and Braun, H.P. (2005) 'Structure of a mitochondrial supercomplex formed by respiratory-chain complexes I and III', Proc Natl Acad Sci U S A, 102(9), pp. 3225-9.

Dudkina, N.V., Kouřil, R., Peters, K., Braun, H.-P. and Boekema, E.J. (2010) 'Structure and function of mitochondrial supercomplexes', Biochimica et Biophysica Acta (BBA) - Bioenergetics, 1797(6–7), pp. 664-670.

Duguez, S., Féasson, L., Denis, C. and Freyssenet, D. (2002) 'Mitochondrial biogenesis during skeletal muscle regeneration', American Journal of Physiology - Endocrinology and Metabolism, 282(4), pp. E802-E809.

Dum, R.P. and Strick, P.L. (2003) 'An unfolded map of the cerebellar dentate nucleus and its projections to the cerebral cortex', J Neurophysiol, 89(1), pp. 634-9.

El-Hattab, A.W. and Scaglia, F. (2013) 'Mitochondrial DNA Depletion Syndromes: Review and Updates of Genetic Basis, Manifestations, and Therapeutic Options', Neurotherapeutics, 10(2), pp. 186-198.

el-Khamisy, S.F. and Caldecott, K.W. (2007) 'DNA single-strand break repair and spinocerebellar ataxia with axonal neuropathy-1', Neuroscience, 145(4), pp. 1260-6.

Elson, J.L., Samuels, D.C., Turnbull, D.M. and Chinnery, P.F. (2001) 'Random Intracellular Drift Explains the Clonal Expansion of Mitochondrial DNA Mutations with Age', American Journal of Human Genetics, 68(3), pp. 802-806.

Emmanuele, V., Silvers, D.S., Sotiriou, E., Tanji, K., DiMauro, S. and Hirano, M. (2011) 'MERRF and Kearns-Sayre overlap syndrome due to the mitochondrial DNA m.3291T>C mutation', Muscle Nerve, 44(3), pp. 448-51.

Emmanuele, V., Sotiriou, E., Rios, P.G., Ganesh, J., Ichord, R., Foley, A.R., Akman, H.O. and Dimauro, S. (2013) 'A novel mutation in the mitochondrial DNA cytochrome b gene (MTCYB) in a patient with mitochondrial encephalomyopathy, lactic acidosis, and strokelike episodes syndrome', J Child Neurol, 28(2), pp. 236-42.

Erlander, M. and Tobin, A. (1991) 'The structural and functional heterogeneity of glutamic acid decarboxylase: A review', Neurochemical Research, 16(3), pp. 215-226.

Erlander, M.G., Tillakaratne, N.J., Feldblum, S., Patel, N. and Tobin, A.J. (1991) 'Two genes encode distinct glutamate decarboxylases', Neuron, 7(1), pp. 91-100.

Fan, W., Waymire, K.G., Narula, N., Li, P., Rocher, C., Coskun, P.E., Vannan, M.A., Narula, J., MacGregor, G.R. and Wallace, D.C. (2008) 'A Mouse Model of Mitochondrial Disease Reveals Germline Selection Against Severe mtDNA Mutations', Science (New York, N.Y.), 319(5865), pp. 958-962.

Fassati, A., Bordoni, A., Amboni, P., Fortunato, F., Fagiolari, G., Bresolin, N., Prelle, A., Comi, G. and Scarlato, G. (1994) 'Chronic progressive external ophthalmoplegia: a correlative study of quantitative molecular data and histochemical and biochemical profile', J Neurol Sci, 123(1-2), pp. 140-6.

Ferguson, S.J. (2010) 'ATP synthase: From sequence to ring size to the P/O ratio', Proceedings of the National Academy of Sciences, 107(39), pp. 16755-16756.

Ferraro, E., Pulicati, A., Cencioni, M.T., Cozzolino, M., Navoni, F., di Martino, S., Nardacci, R., Carrì, M.T. and Cecconi, F. (2008) 'Apoptosome-deficient Cells Lose Cytochrome c through Proteasomal Degradation but Survive by Autophagy-dependent Glycolysis', Molecular Biology of the Cell, 19(8), pp. 3576-3588.

Ferri, A., Sanes, J.R., Coleman, M.P., Cunningham, J.M. and Kato, A.C. (2003) 'Inhibiting axon degeneration and synapse loss attenuates apoptosis and disease progression in a mouse model of motoneuron disease', Curr Biol, 13(8), pp. 669-73.

Filosto, M., Mancuso, M., Nishigaki, Y., Pancrudo, J., Harati, Y., Gooch, C., Mankodi, A., Bayne, L., Bonilla, E., Shanske, S., Hirano, M. and DiMauro, S. (2003) 'Clinical and genetic heterogeneity in progressive external ophthalmoplegia due to mutations in polymerase gamma', Arch Neurol, 60(9), pp. 1279-84.

Fisher, R.P., Topper, J.N. and Clayton, D.A. (1987) 'Promoter selection in human mitochondria involves binding of a transcription factor to orientation-independent upstream regulatory elements', Cell, 50(2), pp. 247-58.

Fonzo, A.D., Bordoni, A., Crimi, M., Sara, G., Bo, R.D., Bresolin, N. and Comi, G.P. (2003) 'POLG mutations in sporadic mitochondrial disorders with multiple mtDNA deletions', Human Mutation, 22(6), pp. 498-499.

Fremeau Jr, R.T., Troyer, M.D., Pahner, I., Nygaard, G.O., Tran, C.H., Reimer, R.J., Bellocchio, E.E., Fortin, D., Storm-Mathisen, J. and Edwards, R.H. (2001) 'The Expression of Vesicular Glutamate Transporters Defines Two Classes of Excitatory Synapse', Neuron, 31(2), pp. 247-260.

Frey, T.G. and Mannella, C.A. (2000) 'The internal structure of mitochondria', Trends Biochem Sci, 25(7), pp. 319-24.

Fukuhara, N. (1991) 'MERRF: a clinicopathological study. Relationships between myoclonus epilepsies and mitochondrial myopathies', Rev Neurol (Paris), 147(6-7), pp. 476-9.

Fuste, J.M., Wanrooij, S., Jemt, E., Granycome, C.E., Cluett, T.J., Shi, Y., Atanassova, N., Holt, I.J., Gustafsson, C.M. and Falkenberg, M. (2010) 'Mitochondrial RNA polymerase is needed for activation of the origin of light-strand DNA replication', Mol Cell, 37(1), pp. 67-78.

Galluzzi, L., Vanden Berghe, T., Vanlangenakker, N., Buettner, S., Eisenberg, T., Vandenabeele, P., Madeo, F. and Kroemer, G. (2011) 'Programmed necrosis from molecules to health and disease', Int Rev Cell Mol Biol, 289, pp. 1-35.

Gebre, S., Reeber, S. and Sillitoe, R. (2012) 'Parasagittal compartmentation of cerebellar mossy fibers as revealed by the patterned expression of vesicular glutamate transporters VGLUT1 and VGLUT2', Brain Structure and Function, 217(2), pp. 165-180.

Gerdes, H.H., Bukoreshtliev, N.V. and Barroso, J.F. (2007) 'Tunneling nanotubes: a new route for the exchange of components between animal cells', FEBS Lett, 581(11), pp. 2194-201.

Ghavami, S., Shojaei, S., Yeganeh, B., Ande, S.R., Jangamreddy, J.R., Mehrpour, M., Christoffersson, J., Chaabane, W., Moghadam, A.R., Kashani, H.H., Hashemi, M., Owji, A.A. and Łos, M.J. (2014) 'Autophagy and apoptosis dysfunction in neurodegenerative disorders', Progress in Neurobiology, 112, pp. 24-49.

Giesemann, T., Schwarz, G., Nawrotzki, R., Berhorster, K., Rothkegel, M., Schluter, K., Schrader, N., Schindelin, H., Mendel, R.R., Kirsch, J. and Jockusch, B.M. (2003) 'Complex formation between the postsynaptic scaffolding protein gephyrin, profilin, and Mena: a possible link to the microfilament system', J Neurosci, 23(23), pp. 8330-9.

Gilchrist, J.M., Sikirica, M., Stopa, E. and Shanske, S. (1996) 'Adult-onset MELAS. Evidence for involvement of neurons as well as cerebral vasculature in strokelike episodes', Stroke, 27(8), pp. 1420-3.

Giles, R.E., Blanc, H., Cann, H.M. and Wallace, D.C. (1980) 'Maternal inheritance of human mitochondrial DNA', Proceedings of the National Academy of Sciences, 77(11), pp. 6715-6719.

Girard, M., Lariviere, R., Parfitt, D.A., Deane, E.C., Gaudet, R., Nossova, N., Blondeau, F., Prenosil, G., Vermeulen, E.G., Duchen, M.R., Richter, A., Shoubridge, E.A., Gehring, K., McKinney, R.A., Brais, B., Chapple, J.P. and McPherson, P.S. (2012) 'Mitochondrial dysfunction and Purkinje cell loss in autosomal recessive spastic ataxia of Charlevoix-Saguenay (ARSACS)', Proc Natl Acad Sci U S A, 109(5), pp. 1661-6.

Goemans, C.G., Boya, P., Skirrow, C.J. and Tolkovsky, A.M. (2008) 'Intra-mitochondrial degradation of Tim23 curtails the survival of cells rescued from apoptosis by caspase inhibitors', Cell Death Differ, 15(3), pp. 545-54.

Gonzalez-Cabo, P. and Palau, F. (2013) 'Mitochondrial pathophysiology in Friedreich's ataxia', J Neurochem, 126 Suppl 1, pp. 53-64.

Gorman, G.S., Grady, J.P. and Turnbull, D.M. (2015a) 'Mitochondrial Donation — How Many Women Could Benefit?', The New England journal of medicine, 372(9), pp. 885-887.

Gorman, G.S., Schaefer, A.M., Ng, Y., Gomez, N., Blakely, E.L., Alston, C.L., Feeney, C., Horvath, R., Yu-Wai-Man, P., Chinnery, P.F., Taylor, R.W., Turnbull, D.M. and McFarland, R. (2015b) 'Prevalence of nuclear and mitochondrial DNA mutations related to adult mitochondrial disease', Ann Neurol, 77(5), pp. 753-9.

Goto, Y., Nonaka, I. and Horai, S. (1990) 'A mutation in the tRNA(Leu)(UUR) gene associated with the MELAS subgroup of mitochondrial encephalomyopathies', Nature, 348(6302), pp. 651-3.

Goto, Y., Nonaka, I. and Horai, S. (1991) 'A new mtDNA mutation associated with mitochondrial myopathy, encephalopathy, lactic acidosis and stroke-like episodes (MELAS)', Biochim Biophys Acta, 1097(3), pp. 238-40.

Grady, J.P. (2013) Statistical Modelling of Mitochondrial Disease. Newcastle University.

Grady, J.P., Campbell, G., Ratnaike, T., Blakely, E.L., Falkous, G., Nesbitt, V., Schaefer, A.M., McNally, R.J., Gorman, G.S., Taylor, R.W., Turnbull, D.M. and McFarland, R. (2014) 'Disease progression in patients with single, large-scale mitochondrial DNA deletions', Brain, 137(2), pp. 323-334.

Gray, M.W. (2012) 'Mitochondrial Evolution', Cold Spring Harbor Perspectives in Biology, 4(9).

Gropen, T.I., Prohovnik, I., Tatemichi, T.K. and Hirano, M. (1994) 'Cerebral hyperemia in MELAS', Stroke, 25(9), pp. 1873-6.

Gropman, A.L. (2013) 'Neuroimaging in Mitochondrial Disorders', Neurotherapeutics, 10(2), pp. 273-285.

Gross, N.J. and Rabinowitz, M. (1969) 'Synthesis of New Strands of Mitochondrial and Nuclear Deoxyribonucleic Acid by Semiconservative Replication', Journal of Biological Chemistry, 244(6), pp. 1563-1566.

Grunewald, A., Lax, N.Z., Rocha, M.C., Reeve, A.K., Hepplewhite, P.D., Rygiel, K.A., Taylor, R.W. and Turnbull, D.M. (2014) 'Quantitative quadruple-label immunofluorescence of mitochondrial and cytoplasmic proteins in single neurons from human midbrain tissue', J Neurosci Methods, 232, pp. 143-9.

Gustashaw, K.M., Najmabadi, P. and Potts, S.J. (2010) 'Measuring Protein Expression in Tissue: The Complementary Roles of Brightfield and Fluorescence in Whole Slide Scanning', Lab Medicine, 41(3), pp. 135-142.

Haas, R. and Dietrich, R. (2004) 'Neuroimaging of mitochondrial disorders', Mitochondrion, 4(5–6), pp. 471-490.

Hagerhall, C. (1997) 'Succinate: quinone oxidoreductases. Variations on a conserved theme', Biochim Biophys Acta, 1320(2), pp. 107-41.

Hakonen, A.H., Goffart, S., Marjavaara, S., Paetau, A., Cooper, H., Mattila, K., Lampinen, M., Sajantila, A., Lonnqvist, T., Spelbrink, J.N. and Suomalainen, A. (2008) 'Infantile-onset spinocerebellar ataxia and mitochondrial recessive ataxia syndrome are associated with neuronal complex I defect and mtDNA depletion', Hum Mol Genet, 17(23), pp. 3822-35.

Hakonen, A.H., Isohanni, P., Paetau, A., Herva, R., Suomalainen, A. and Lonnqvist, T. (2007) 'Recessive Twinkle mutations in early onset encephalopathy with mtDNA depletion', Brain, 130(Pt 11), pp. 3032-40.

Hamalainen, R.H., Manninen, T., Koivumaki, H., Kislin, M., Otonkoski, T. and Suomalainen, A. (2013) 'Tissue- and cell-type-specific manifestations of heteroplasmic mtDNA 3243A>G mutation in human induced pluripotent stem cell-derived disease model', Proc Natl Acad Sci U S A, 110(38), pp. E3622-30.

Hammarsund, M., Wilson, W., Corcoran, M., Merup, M., Einhorn, S., Grander, D. and Sangfelt, O. (2001) 'Identification and characterization of two novel human mitochondrial elongation factor genes, hEFG2 and hEFG1, phylogenetically conserved through evolution', Hum Genet, 109(5), pp. 542-50.

Hance, N., Ekstrand, M.I. and Trifunovic, A. (2005) 'Mitochondrial DNA polymerase gamma is essential for mammalian embryogenesis', Human Molecular Genetics, 14(13), pp. 1775-1783.

Harris, J.J., Jolivet, R. and Attwell, D. (2012) 'Synaptic energy use and supply', Neuron, 75(5), pp. 762-77.

Hasegawa, H., Matsuoka, T., Goto, Y. and Nonaka, I. (1991) 'Strongly succinate dehydrogenase-reactive blood vessels in muscles from patients with mitochondrial myopathy, encephalopathy, lactic acidosis, and stroke-like episodes', Ann Neurol, 29(6), pp. 601-5.

Hatefi, Y. (1985) 'The mitochondrial electron transport and oxidative phosphorylation system', Annu Rev Biochem, 54, pp. 1015-69.

Hegde, M.L., Izumi, T. and Mitra, S. (2012) 'Oxidized base damage and single-strand break repair in mammalian genomes: role of disordered regions and posttranslational modifications in early enzymes', Prog Mol Biol Transl Sci, 110, pp. 123-53.

Heizmann, C.W. and Braun, K. (1992) 'Changes in Ca(2+)-binding proteins in human neurodegenerative disorders', Trends Neurosci, 15(7), pp. 259-64.

Hill, B.G., Benavides, G.A., Lancaster, J.R., Jr., Ballinger, S., Dell'Italia, L., Jianhua, Z. and Darley-Usmar, V.M. (2012) 'Integration of cellular bioenergetics with mitochondrial quality control and autophagy', Biol Chem, 393(12), pp. 1485-1512.

Hillefors, M., Gioio, A.E., Mameza, M.G. and Kaplan, B.B. (2007) 'Axon viability and mitochondrial function are dependent on local protein synthesis in sympathetic neurons', Cell Mol Neurobiol, 27(6), pp. 701-16.

Hioki, H., Fujiyama, F., Taki, K., Tomioka, R., Furuta, T., Tamamaki, N. and Kaneko, T. (2003) 'Differential distribution of vesicular glutamate transporters in the rat cerebellar cortex', Neuroscience, 117(1), pp. 1-6.

Hirano, M. and DiMauro, S. (1996) 'Clinical features of mitochondrial myopathies and encephalomyopathies', in *Handbook of muscle disease*. New York: Marcel Dekker Inc, pp. 479-504.

Hirano, M., Kaufmann, P., De Vivo, D. and Tanji, K. (2006) 'Mitochondrial neurology I: encephalopathies', in DiMauro, S., Hirano, M. and Schon, E.A. (eds.) *Mitochondrial medicine*. Abingdon: Informa Healthcare, pp. 27-44.

Hirano, M., Ricci, E., Koenigsberger, M.R., Defendini, R., Pavlakis, S.G., DeVivo, D.C., DiMauro, S. and Rowland, L.P. (1992) 'Melas: an original case and clinical criteria for diagnosis', Neuromuscul Disord, 2(2), pp. 125-35.

Hirano, M., Silvestri, G., Blake, D.M., Lombes, A., Minetti, C., Bonilla, E., Hays, A.P., Lovelace, R.E., Butler, I., Bertorini, T.E. and *et al*. (1994) 'Mitochondrial neurogastrointestinal encephalomyopathy (MNGIE): clinical, biochemical, and genetic features of an autosomal recessive mitochondrial disorder', Neurology, 44(4), pp. 721-7.

Hirokawa, N. and Noda, Y. (2008) 'Intracellular Transport and Kinesin Superfamily Proteins, KIFs: Structure, Function, and Dynamics', Physiological Reviews, 88(3), pp. 1089-1118.

Hofer, A.M., Curci, S., Doble, M.A., Brown, E.M. and Soybel, D.I. (2000) 'Intercellular communication mediated by the extracellular calcium-sensing receptor', Nat Cell Biol, 2(7), pp. 392-8.

Hollenbeck, P.J. and Saxton, W.M. (2005) 'The axonal transport of mitochondria', Journal of cell science, 118(Pt 23), pp. 5411-5419.

Holmes, G. (1939) 'THE CEREBELLUM OF MAN', Brain, 62(1), pp. 1-30.

Holt, I.J. and Reyes, A. (2012) 'Human mitochondrial DNA replication', Cold Spring Harb Perspect Biol, 4(12).

Holt, I.J., Harding, A.E. and Morgan-Hughes, J.A. (1988) 'Deletions of muscle mitochondrial DNA in patients with mitochondrial myopathies', Nature, 331(6158), pp. 717-9.

Holt, I.J., Lorimer, H.E. and Jacobs, H.T. (2000) 'Coupled Leading- and Lagging-Strand Synthesis of Mammalian Mitochondrial DNA', Cell, 100(5), pp. 515-524.

Horvath, R., Hudson, G., Ferrari, G., Fütterer, N., Ahola, S., Lamantea, E., Prokisch, H., Lochmüller, H., McFarland, R., Ramesh, V., Klopstock, T., Freisinger, P., Salvi, F., Mayr, J.A., Santer, R., Tesarova, M., Zeman, J., Udd, B., Taylor, R.W., Turnbull, D., Hanna, M., Fialho, D., Suomalainen, A., Zeviani, M. and Chinnery, P.F. (2006) 'Phenotypic spectrum associated with mutations of the mitochondrial polymerase γ gene', Brain, 129(7), pp. 1674-1684.

Howarth, C., Peppiatt-Wildman, C.M. and Attwell, D. (2010) 'The energy use associated with neural computation in the cerebellum', J Cereb Blood Flow Metab, 30(2), pp. 403-14.

Hudson, G., Amati-Bonneau, P., Blakely, E.L., Stewart, J.D., He, L., Schaefer, A.M., Griffiths, P.G., Ahlqvist, K., Suomalainen, A., Reynier, P., McFarland, R., Turnbull, D.M., Chinnery, P.F. and Taylor, R.W. (2008) 'Mutation of OPA1 causes dominant optic atrophy with external ophthalmoplegia, ataxia, deafness and multiple mitochondrial DNA deletions: a novel disorder of mtDNA maintenance', Brain, 131(Pt 2), pp. 329-37.

Huttemann, M., Pecina, P., Rainbolt, M., Sanderson, T.H., Kagan, V.E., Samavati, L., Doan, J.W. and Lee, I. (2011) 'The multiple functions of cytochrome c and their regulation in life and death decisions of the mammalian cell: From respiration to apoptosis', Mitochondrion, 11(3), pp. 369-81.

Iacopino, A., Christakos, S., German, D., Sonsalla, P.K. and Altar, C.A. (1992) 'Calbindin-D28K-containing neurons in animal models of neurodegeneration: possible protection from excitotoxicity', Brain Res Mol Brain Res, 13(3), pp. 251-61.

Iacopino, A.M. and Christakos, S. (1990) 'Specific reduction of calcium-binding protein (28-kilodalton calbindin-D) gene expression in aging and neurodegenerative diseases', Proc Natl Acad Sci U S A, 87(11), pp. 4078-82.

Iadecola, C. (2004) 'Neurovascular regulation in the normal brain and in Alzheimer's disease', Nat Rev Neurosci, 5(5), pp. 347-60.

Iizuka, T. and Sakai, F. (2005) 'Pathogenesis of stroke-like episodes in MELAS: analysis of neurovascular cellular mechanisms', Curr Neurovasc Res, 2(1), pp. 29-45.

Iizuka, T., Sakai, F., Ide, T., Miyakawa, S., Sato, M. and Yoshii, S. (2007) 'Regional cerebral blood flow and cerebrovascular reactivity during chronic stage of stroke-like episodes in MELAS -- implication of neurovascular cellular mechanism', J Neurol Sci, 257(1-2), pp. 126-38.

Iizuka, T., Sakai, F., Kan, S. and Suzuki, N. (2003) 'Slowly progressive spread of the stroke-like lesions in MELAS', Neurology, 61(9), pp. 1238-44.

Iizuka, T., Sakai, F., Suzuki, N., Hata, T., Tsukahara, S., Fukuda, M. and Takiyama, Y. (2002) 'Neuronal hyperexcitability in stroke-like episodes of MELAS syndrome', Neurology, 59(6), pp. 816-24.

Inoue, K., Nakada, K., Ogura, A., Isobe, K., Goto, Y., Nonaka, I. and Hayashi, J.I. (2000) 'Generation of mice with mitochondrial dysfunction by introducing mouse mtDNA carrying a deletion into zygotes', Nat Genet, 26(2), pp. 176-81.

Isohanni, P., Hakonen, A.H., Euro, L., Paetau, I., Linnankivi, T., Liukkonen, E., Wallden, T., Luostarinen, L., Valanne, L., Paetau, A., Uusimaa, J., Lonnqvist, T., Suomalainen, A. and Pihko, H. (2011) 'POLG1 manifestations in childhood', Neurology, 76(9), pp. 811-5.

Ito, S., Shirai, W., Asahina, M. and Hattori, T. (2008) 'Clinical and brain MR imaging features focusing on the brain stem and cerebellum in patients with myoclonic epilepsy with ragged-red fibers due to mitochondrial A8344G mutation', AJNR Am J Neuroradiol, 29(2), pp. 392-5.

Jahn, R., Schiebler, W., Ouimet, C. and Greengard, P. (1985) 'A 38,000-dalton membrane protein (p38) present in synaptic vesicles', Proc Natl Acad Sci U S A, 82(12), pp. 4137-41.

Janezic, S., Threlfell, S., Dodson, P.D., Dowie, M.J., Taylor, T.N., Potgieter, D., Parkkinen, L., Senior, S.L., Anwar, S., Ryan, B., Deltheil, T., Kosillo, P., Cioroch, M., Wagner, K., Ansorge, O., Bannerman, D.M., Bolam, J.P., Magill, P.J., Cragg, S.J. and Wade-Martins, R. (2013)

'Deficits in dopaminergic transmission precede neuron loss and dysfunction in a new Parkinson model', Proc Natl Acad Sci U S A, 110(42), pp. E4016-25.

Jawien, J., Bian, Z., Sheikine, Y., Olofsson, P.S., Pang, Y., Edholm, T., Dou, Y., Metzger, D., Hellstrom, P.M., Feil, R. and Hansson, G.K. (2008) 'Abrogation of mitochondrial transcription in smooth muscle cells impairs smooth muscle contractility and vascular tone', J Physiol Pharmacol, 59(2), pp. 239-52.

Jean-Francois, M.J., Collins, S., Kotsimbos, N., Dennett, X. and Byrne, E. (1997) 'Are mitochondrial DNA deletions causative in chronic progressive external ophthalmoplegia patients?', J Clin Neurosci, 4(2), pp. 163-8.

Jendrach, M., Pohl, S., Voth, M., Kowald, A., Hammerstein, P. and Bereiter-Hahn, J. (2005) 'Morpho-dynamic changes of mitochondria during ageing of human endothelial cells', Mech Ageing Dev, 126(6-7), pp. 813-21.

Jones, E.G. (1970) 'On the mode of entry of blood vessels into the cerebral cortex', J Anat, 106(Pt 3), pp. 507-20.

Jones, J.M., Datta, P., Srinivasula, S.M., Ji, W., Gupta, S., Zhang, Z., Davies, E., Hajnoczky, G., Saunders, T.L., Van Keuren, M.L., Fernandes-Alnemri, T., Meisler, M.H. and Alnemri, E.S. (2003) 'Loss of Omi mitochondrial protease activity causes the neuromuscular disorder of mnd2 mutant mice', Nature, 425(6959), pp. 721-727.

Jornayvaz, F.R. and Shulman, G.I. (2010) 'Regulation of mitochondrial biogenesis', Essays in biochemistry, 47, p. 10.1042/bse0470069.

Kamiya, H. (2003) 'Mutagenic potentials of damaged nucleic acids produced by reactive oxygen/nitrogen species: approaches using synthetic oligonucleotides and nucleotides: SURVEY AND SUMMARY', Nucleic Acids Research, 31(2), pp. 517-531.

Kanaan, N.M., Pigino, G.F., Brady, S.T., Lazarov, O., Binder, L.I. and Morfini, G.A. (2013) 'Axonal degeneration in Alzheimer's disease: When signaling abnormalities meet the axonal transport system', Experimental Neurology, 246(0), pp. 44-53.

Kaneda, H., Hayashi, J., Takahama, S., Taya, C., Lindahl, K.F. and Yonekawa, H. (1995) 'Elimination of paternal mitochondrial DNA in intraspecific crosses during early mouse embryogenesis', Proceedings of the National Academy of Sciences of the United States of America, 92(10), pp. 4542-4546.

Kaneko, T., Fujiyama, F. and Hioki, H. (2002) 'Immunohistochemical localization of candidates for vesicular glutamate transporters in the rat brain', The Journal of Comparative Neurology, 444(1), pp. 39-62.

Kang, J.S., Tian, J.H., Pan, P.Y., Zald, P., Li, C., Deng, C. and Sheng, Z.H. (2008) 'Docking of axonal mitochondria by syntaphilin controls their mobility and affects short-term facilitation', Cell, 132(1), pp. 137-48.

Kasamatsu, H. and Vinograd, J. (1973) 'Unidirectionality of replication in mouse mitochondrial DNA', Nat New Biol, 241(108), pp. 103-5.

Kasamatsu, H., Robberson, D.L. and Vinograd, J. (1971) 'A Novel Closed-Circular Mitochondrial DNA with Properties of a Replicating Intermediate', Proceedings of the National Academy of Sciences, 68(9), pp. 2252-2257.

Kasparek, T.R. and Humphrey, T.C. (2011) 'DNA double-strand break repair pathways, chromosomal rearrangements and cancer', Semin Cell Dev Biol, 22(8), pp. 886-97.

Kaufman, D.L., Houser, C.R. and Tobin, A.J. (1991) 'Two forms of the gamma-aminobutyric acid synthetic enzyme glutamate decarboxylase have distinct intraneuronal distributions and cofactor interactions', J Neurochem, 56(2), pp. 720-3.

Kearns, T.P. and Sayre, G.P. (1958) 'Retinitis pigmentosa, external ophthalmoplegia, and complete heart block: Unusual syndrome with histologic study in one of two cases', A.M.A. Archives of Ophthalmology, 60(2), pp. 280-289.

Kermode, A.G., Moseley, I.F., Kendall, B.E., Miller, D.H., MacManus, D.G. and McDonald, W.I. (1989) 'Magnetic resonance imaging in Leber's optic neuropathy', Journal of Neurology, Neurosurgery, and Psychiatry, 52(5), pp. 671-674.

Kerrison, J.B., Howell, N., Miller, N.R., Hirst, L. and Green, W.R. (1995) 'Leber hereditary optic neuropathy. Electron microscopy and molecular genetic analysis of a case', Ophthalmology, 102(10), pp. 1509-16.

Kim, I., Rodriguez-Enriquez, S. and Lemasters, J.J. (2007) 'Selective degradation of mitochondria by mitophagy', Arch Biochem Biophys, 462(2), pp. 245-53.

Kim, J.H., Lim, M.K., Jeon, T.Y., Rha, J.H., Eo, H., Yoo, S.-Y. and Shu, C.H. (2011) 'Diffusion and Perfusion Characteristics of MELAS (Mitochondrial Myopathy, Encephalopathy, Lactic

Acidosis, and Stroke-Like Episode) in Thirteen Patients', Korean Journal of Radiology, 12(1), pp. 15-24.

Kirby, D.M., McFarland, R., Ohtake, A., Dunning, C., Ryan, M.T., Wilson, C., Ketteridge, D., Turnbull, D.M., Thorburn, D.R. and Taylor, R.W. (2004) 'Mutations of the mitochondrial ND1 gene as a cause of MELAS', J Med Genet, 41(10), pp. 784-9.

Kirby, D.M., Rennie, K.J., Smulders-Srinivasan, T.K., Acin-Perez, R., Whittington, M., Enriquez, J.A., Trevelyan, A.J., Turnbull, D.M. and Lightowlers, R.N. (2009) 'Transmitochondrial embryonic stem cells containing pathogenic mtDNA mutations are compromised in neuronal differentiation', Cell Prolif, 42(4), pp. 413-24.

Kirby, D.M., Thorburn, D.R., Turnbull, D.M. and Taylor, R.W. (2007) 'Biochemical assays of respiratory chain complex activity', Methods Cell Biol, 80, pp. 93-119.

Kirichok, Y., Krapivinsky, G. and Clapham, D.E. (2004) 'The mitochondrial calcium uniporter is a highly selective ion channel', Nature, 427(6972), pp. 360-364.

Klein, C. and Westenberger, A. (2012) 'Genetics of Parkinson's Disease', Cold Spring Harbor Perspectives in Medicine, 2(1), p. a008888.

Klockgether, T. (2000) 'Clinical approach to ataxic patients', in Klockgether, T. (ed.) Handbook of ataxia disorders. New York, Basel: Marcel Dekker, Inc, pp. 101-114.

Kluge, M.A., Fetterman, J.L. and Vita, J.A. (2013) 'Mitochondria and endothelial function', Circ Res, 112(8), pp. 1171-88.

Kneussel, M. and Betz, H. (2000a) 'Clustering of inhibitory neurotransmitter receptors at developing postsynaptic sites: the membrane activation model', Trends Neurosci, 23(9), pp. 429-35.

Kneussel, M. and Betz, H. (2000b) 'Receptors, gephyrin and gephyrin-associated proteins: novel insights into the assembly of inhibitory postsynaptic membrane specializations', J Physiol, 525 Pt 1, pp. 1-9.

Knierim, J. (1997) Cerebellum. Available at: http://neuroscience.uth.tmc.edu/s3/chapter05.html

Koc, E.C. and Spremulli, L.L. (2002) 'Identification of Mammalian Mitochondrial Translational Initiation Factor 3 and Examination of Its Role in Initiation Complex Formation with Natural mRNAs', Journal of Biological Chemistry, 277(38), pp. 35541-35549.

Kodaira, M., Hatakeyama, H., Yuasa, S., Seki, T., Egashira, T., Tohyama, S., Kuroda, Y., Tanaka, A., Okata, S., Hashimoto, H., Kusumoto, D., Kunitomi, A., Takei, M., Kashimura, S., Suzuki, T., Yozu, G., Shimojima, M., Motoda, C., Hayashiji, N., Saito, Y., Goto, Y.-i. and Fukuda, K. (2015) 'Impaired respiratory function in MELAS-induced pluripotent stem cells with high heteroplasmy levels', FEBS Open Bio, 5, pp. 219-225.

Koeppen, A.H., Davis, A.N. and Morral, J.A. (2011) 'The cerebellar component of Friedreich's ataxia', Acta Neuropathol, 122(3), pp. 323-30.

Koeppen, A.H., Ramirez, R.L., Becker, A.B., Feustel, P.J. and Mazurkiewicz, J.E. (2015) 'Friedreich ataxia: failure of GABA-ergic and glycinergic synaptic transmission in the dentate nucleus', J Neuropathol Exp Neurol, 74(2), pp. 166-76.

Koeppen, A.H., Ramirez, R.L., Bjork, S.T., Bauer, P. and Feustel, P.J. (2013) 'The reciprocal cerebellar circuitry in human hereditary ataxia', Cerebellum, 12(4), pp. 493-503.

Koga, Y., Akita, Y., Nishioka, J., Yatsuga, S., Povalko, N., Tanabe, Y., Fujimoto, S. and Matsuishi, T. (2005) 'L-arginine improves the symptoms of strokelike episodes in MELAS', Neurology, 64(4), pp. 710-2.

Koga, Y., Akita, Y., Takane, N., Sato, Y. and Kato, H. (2000) 'Heterogeneous presentation in A3243G mutation in the mitochondrial tRNA(Leu(UUR)) gene', Arch Dis Child, 82(5), pp. 407-11.

Koga, Y., Povalko, N., Nishioka, J., Katayama, K., Yatsuga, S. and Matsuishi, T. (2012) 'Molecular pathology of MELAS and L-arginine effects', Biochim Biophys Acta, 1820(5), pp. 608-14.

Kroemer, G., Dallaporta, B. and Resche-Rigon, M. (1998) 'The mitochondrial death/life regulator in apoptosis and necrosis', Annu Rev Physiol, 60, pp. 619-42.

Krueger, D.D., Tuffy, L.P., Papadopoulos, T. and Brose, N. (2012) 'The role of neurexins and neuroligins in the formation, maturation, and function of vertebrate synapses', Curr Opin Neurobiol, 22(3), pp. 412-22.

Kubota, M., Sakakihara, Y., Mori, M., Yamagata, T. and Momoi-Yoshida, M. (2004) 'Beneficial effect of L-arginine for stroke-like episode in MELAS', Brain Dev, 26(7), pp. 481-3; discussion 480.

Kukat, C., Wurm, C.A., Spåhr, H., Falkenberg, M., Larsson, N.-G. and Jakobs, S. (2011) 'Super-resolution microscopy reveals that mammalian mitochondrial nucleoids have a uniform size and frequently contain a single copy of mtDNA', Proceedings of the National Academy of Sciences of the United States of America, 108(33), pp. 13534-13539.

Kwittken, J. and Barest, H.D. (1958) 'The neuropathology of hereditary optic atrophy (Leber's disease); the first complete anatomic study', Am J Pathol, 34(1), pp. 185-207.

Kwon, S.E. and Chapman, E.R. (2011) 'Synaptophysin regulates the kinetics of synaptic vesicle endocytosis in central neurons', Neuron, 70(5), pp. 847-854.

Labauge, P., Durant, R., Castelnovo, G. and Dubois, A. (2002) 'MNGIE: diarrhea and leukoencephalopathy', Neurology, 58(12), p. 1862.

Larsen, N.B., Rasmussen, M. and Rasmussen, L.J. (2005) 'Nuclear and mitochondrial DNA repair: similar pathways?', Mitochondrion, 5(2), pp. 89-108.

Larsson, N.G. and Clayton, D.A. (1995) 'Molecular genetic aspects of human mitochondrial disorders', Annu Rev Genet, 29, pp. 151-78.

Lartigue, L., Kushnareva, Y., Seong, Y., Lin, H., Faustin, B. and Newmeyer, D.D. (2009) 'Caspase-independent mitochondrial cell death results from loss of respiration, not cytotoxic protein release', Mol Biol Cell, 20(23), pp. 4871-84.

Lax, N. and Jaros, E. (2012) 'Neurodegeneration in Primary Mitochondrial Disorders', in Reeve, A.K., Krishnan, K.J., Duchen, M.R. and Turnbull, D.M. (eds.) Mitochondrial Dysfunction in Neurodegenerative Disorders. Springer London, pp. 21-41.

Lax, N.Z., Campbell, G.R., Reeve, A.K., Ohno, N., Zambonin, J., Blakely, E.L., Taylor, R.W., Bonilla, E., Tanji, K., DiMauro, S., Jaros, E., Lassmann, H., Turnbull, D.M. and Mahad, D.J. (2012a) 'Loss of Myelin-Associated Glycoprotein in Kearns-Sayre Syndrome', Archives of neurology, 69(4), pp. 490-499.

Lax, N.Z., Grady, J., Laude, A., Chan, F., Hepplewhite, P.D., Gorman, G., Whittaker, R.G., Ng, Y., Cunningham, M.O. and Turnbull, D.M. (2015) 'Extensive respiratory chain defects in inhibitory interneurones in patients with mitochondrial disease', Neuropathology and Applied Neurobiology, pp. n/a-n/a.

Lax, N.Z., Hepplewhite, P.D., Reeve, A.K., Nesbitt, V., McFarland, R., Jaros, E., Taylor, R.W. and Turnbull, D.M. (2012b) 'Cerebellar ataxia in patients with mitochondrial DNA disease: a molecular clinicopathological study', J Neuropathol Exp Neurol, 71(2), pp. 148-61.

Lax, N.Z., Pienaar, I.S., Reeve, A.K., Hepplewhite, P.D., Jaros, E., Taylor, R.W., Kalaria, R.N. and Turnbull, D.M. (2012c) 'Microangiopathy in the cerebellum of patients with mitochondrial DNA disease', Brain, 135(Pt 6), pp. 1736-50.

Lax, N.Z., Whittaker, R.G., Hepplewhite, P.D., Reeve, A.K., Blakely, E.L., Jaros, E., Ince, P.G., Taylor, R.W., Fawcett, P.R.W. and Turnbull, D.M. (2012d) 'Sensory neuronopathy in patients harbouring recessive polymerase γ mutations', Brain, 135(1), pp. 62-71.

Lee, H.-C. and Wei, Y.-H. (2005) 'Mitochondrial biogenesis and mitochondrial DNA maintenance of mammalian cells under oxidative stress', The International Journal of Biochemistry & Cell Biology, 37(4), pp. 822-834.

Lennie, P. (2003) 'The cost of cortical computation', Curr Biol, 13(6), pp. 493-7.

Lerman-Sagie, T., Leshinsky-Silver, E., Watemberg, N., Luckman, Y. and Lev, D. (2005) 'White matter involvement in mitochondrial diseases', Mol Genet Metab, 84(2), pp. 127-36.

Levi, S., Logan, S.M., Tovar, K.R. and Craig, A.M. (2004) 'Gephyrin is critical for glycine receptor clustering but not for the formation of functional GABAergic synapses in hippocampal neurons', J Neurosci, 24(1), pp. 207-17.

Levy, M., Faas, G.C., Saggau, P., Craigen, W.J. and Sweatt, J.D. (2003) 'Mitochondrial regulation of synaptic plasticity in the hippocampus', J Biol Chem, 278(20), pp. 17727-34.

Li, J.Y., Plomann, M. and Brundin, P. (2003) 'Huntington's disease: a synaptopathy?', Trends Mol Med, 9(10), pp. 414-20.

Li, Z., Okamoto, K., Hayashi, Y. and Sheng, M. (2004) 'The importance of dendritic mitochondria in the morphogenesis and plasticity of spines and synapses', Cell, 119(6), pp. 873-87.

Liesa, M., Palacin, M. and Zorzano, A. (2009) 'Mitochondrial dynamics in mammalian health and disease', Physiol Rev, 89(3), pp. 799-845.

Lightowlers, R.N., Chinnery, P.F., Turnbull, D.M. and Howell, N. (1997) 'Mammalian mitochondrial genetics: heredity, heteroplasmy and disease', Trends Genet, 13(11), pp. 450-5.

Lightowlers, R.N., Taylor, R.W. and Turnbull, D.M. (2015) 'Mutations causing mitochondrial disease: What is new and what challenges remain?', Science, 349(6255), pp. 1494-1499.

Liguz-Lecznar, M. and Skangiel-Kramska, J. (2007) 'Vesicular glutamate transporters (VGLUTs): the three musketeers of glutamatergic system', Acta Neurobiol Exp (Wars), 67(3), pp. 207-18.

Linden, R. and Perry, V.H. (1983) 'Retrograde and anterograde-transneuronal degeneration in the parabigeminal nucleus following tectal lesions in developing rats', J Comp Neurol, 218(3), pp. 270-81.

Ling, M., Merante, F., Chen, H.S., Duff, C., Duncan, A.M. and Robinson, B.H. (1997) 'The human mitochondrial elongation factor tu (EF-Tu) gene: cDNA sequence, genomic localization, genomic structure, and identification of a pseudogene', Gene, 197(1-2), pp. 325-36.

Liolitsa, D., Rahman, S., Benton, S., Carr, L.J. and Hanna, M.G. (2003) 'Is the mitochondrial complex I ND5 gene a hot-spot for MELAS causing mutations?', Ann Neurol, 53(1), pp. 128-32.

Liske, H., Qian, X., Anikeeva, P., Deisseroth, K. and Delp, S. (2013) 'Optical control of neuronal excitation and inhibition using a single opsin protein, ChR2', Sci. Rep., 3.

Lorenzo, L.E., Godin, A.G., Wang, F., St-Louis, M. and Carbonetto, S. (2014) 'Gephyrin clusters are absent from small diameter primary afferent terminals despite the presence of GABA(A) receptors', 34(24), pp. 8300-17.

Lynch, R.M. and Paul, R.J. (1983) 'Compartmentation of glycolytic and glycogenolytic metabolism in vascular smooth muscle', Science, 222(4630), pp. 1344-6.

Ma, L. and Spremulli, L.L. (1995) 'Cloning and sequence analysis of the human mitochondrial translational initiation factor 2 cDNA', J Biol Chem, 270(4), pp. 1859-65.

MacAskill, A.F. and Kittler, J.T. (2010) 'Control of mitochondrial transport and localization in neurons', Trends Cell Biol, 20(2), pp. 102-12.

Maceluch, J.A. and Niedziela, M. (2006) 'The clinical diagnosis and molecular genetics of kearns-sayre syndrome: a complex mitochondrial encephalomyopathy', Pediatr Endocrinol Rev, 4(2), pp. 117-37.

Mackey, D.A., Oostra, R.J., Rosenberg, T., Nikoskelainen, E., Bronte-Stewart, J., Poulton, J., Harding, A.E., Govan, G., Bolhuis, P.A. and Norby, S. (1996) 'Primary pathogenic mtDNA mutations in multigeneration pedigrees with Leber hereditary optic neuropathy', American Journal of Human Genetics, 59(2), pp. 481-485.

Mai, S., Klinkenberg, M., Auburger, G., Bereiter-Hahn, J. and Jendrach, M. (2010) 'Decreased expression of Drp1 and Fis1 mediates mitochondrial elongation in senescent cells and enhances resistance to oxidative stress through PINK1', J Cell Sci, 123(Pt 6), pp. 917-26.

Maier, D., Farr, C.L., Poeck, B., Alahari, A., Vogel, M., Fischer, S., Kaguni, L.S. and Schneuwly, S. (2001) 'Mitochondrial Single-stranded DNA-binding Protein Is Required for Mitochondrial DNA Replication and Development in Drosophila melanogaster', Molecular Biology of the Cell, 12(4), pp. 821-830.

Majamaa-Voltti, K.A., Winqvist, S., Remes, A.M., Tolonen, U., Pyhtinen, J., Uimonen, S., Karppa, M., Sorri, M., Peuhkurinen, K. and Majamaa, K. (2006) 'A 3-year clinical follow-up of adult patients with 3243A>G in mitochondrial DNA', Neurology, 66(10), pp. 1470-5.

Malfatti, E., Bugiani, M., Invernizzi, F., de Souza, C.F., Farina, L., Carrara, F., Lamantea, E., Antozzi, C., Confalonieri, P., Sanseverino, M.T., Giugliani, R., Uziel, G. and Zeviani, M. (2007) 'Novel mutations of ND genes in complex I deficiency associated with mitochondrial encephalopathy', Brain, 130(Pt 7), pp. 1894-904.

Mancuso, M., Filosto, M., Bellan, M., Liguori, R., Montagna, P., Baruzzi, A., DiMauro, S. and Carelli, V. (2004) 'POLG mutations causing ophthalmoplegia, sensorimotor polyneuropathy, ataxia, and deafness', Neurology, 62(2), pp. 316-8.

Manfredi, G., Schon, E.A., Bonilla, E., Moraes, C.T., Shanske, S. and DiMauro, S. (1996) 'Identification of a mutation in the mitochondrial tRNA(Cys) gene associated with mitochondrial encephalopathy', Hum Mutat, 7(2), pp. 158-63.

Manfredi, G., Schon, E.A., Moraes, C.T., Bonilla, E., Berry, G.T., Sladky, J.T. and DiMauro, S. (1995) 'A new mutation associated with MELAS is located in a mitochondrial DNA polypeptide-coding gene', Neuromuscul Disord, 5(5), pp. 391-8.

Mapelli, L., Pagani, M., Garrido, J.A. and D'Angelo, E. (2015) 'Integrated plasticity at inhibitory and excitatory synapses in the cerebellar circuit', Frontiers in Cellular Neuroscience, 9, p. 169.

Marcello, E., Epis, R., Saraceno, C. and Di Luca, M. (2012) 'Synaptic dysfunction in Alzheimer's disease', Adv Exp Med Biol, 970, pp. 573-601.

Margulis, L. (1970) Origin of eukaryotic cells. New Haven, CT: Yell University press.

Marsden, J. and Harris, C. (2011) 'Cerebellar ataxia: pathophysiology and rehabilitation', Clin Rehabil, 25(3), pp. 195-216.

Martin, A.J., Friston, K.J., Colebatch, J.G. and Frackowiak, R.S. (1991) 'Decreases in regional cerebral blood flow with normal aging', J Cereb Blood Flow Metab, 11(4), pp. 684-9.

Martin, J.H. (2002) 'The Cerebellum', in Neuroanatomy: text and atlas. London.

Martin, W. and Muller, M. (1998) 'The hydrogen hypothesis for the first eukaryote', Nature, 392(6671), pp. 37-41.

Mason, P.A., Matheson, E.C., Hall, A.G. and Lightowlers, R.N. (2003) 'Mismatch repair activity in mammalian mitochondria', Nucleic Acids Res, 31(3), pp. 1052-8.

Mattson, M.P. and Partin, J. (1999) 'Evidence for mitochondrial control of neuronal polarity', J Neurosci Res, 56(1), pp. 8-20.

McFarland, R. and Turnbull, D.M. (2009) 'Batteries not included: diagnosis and management of mitochondrial disease', J Intern Med, 265(2), pp. 210-28.

McFarland, R., Taylor, R.W. and Turnbull, D.M. (2002) 'The neurology of mitochondrial DNA disease', Lancet Neurol, 1(6), pp. 343-51.

McFarland, R., Taylor, R.W. and Turnbull, D.M. (2010) 'A neurological perspective on mitochondrial disease', Lancet Neurol, 9(8), pp. 829-40.

McKenzie, M., Liolitsa, D., Akinshina, N., Campanella, M., Sisodiya, S., Hargreaves, I., Nirmalananthan, N., Sweeney, M.G., Abou-Sleiman, P.M., Wood, N.W., Hanna, M.G. and Duchen, M.R. (2007) 'Mitochondrial ND5 gene variation associated with encephalomyopathy and mitochondrial ATP consumption', J Biol Chem, 282(51), pp. 36845-52.

Minamino, T. and Komuro, I. (2007) 'Vascular cell senescence: contribution to atherosclerosis', Circ Res, 100(1), pp. 15-26.

Mink, J.W., Blumenschine, R.J. and Adams, D.B. (1981) 'Ratio of central nervous system to body metabolism in vertebrates: its constancy and functional basis', Am J Physiol, 241(3), pp. R203-12.

Mita, S., Rizzuto, R., Moraes, C.T., Shanske, S., Arnaudo, E., Fabrizi, G.M., Koga, Y., DiMauro, S. and Schon, E.A. (1990) 'Recombination via flanking direct repeats is a major cause of large-scale deletions of human mitochondrial DNA', Nucleic Acids Res, 18(3), pp. 561-7.

Mitchell, P. (1976) 'Possible molecular mechanisms of the protonmotive function of cytochrome systems', Journal of Theoretical Biology, 62(2), pp. 327-367.

Mizukami, K., Sasaki, M., Suzuki, T., Shiraishi, H., Koizumi, J., Ohkoshi, N., Ogata, T., Mori, N., Ban, S. and Kosaka, K. (1992) 'Central nervous system changes in mitochondrial encephalomyopathy: light and electron microscopic study', Acta Neuropathol, 83(4), pp. 449-52.

Mizukami, K., Sasaki, M., Suzuki, T., Shiraishi, H., Koizumi, J., Ohkoshi, N., Ogata, T., Mori, N., Ban, S. and Kosaka, K. (1992) 'Central nervous system changes in mitochondrial encephalomyopathy: light and electron microscopic study', Acta Neuropathol, 83(4), pp. 449-52.

Moggio, M., Colombo, I., Peverelli, L., Villa, L., Xhani, R., Testolin, S., Di Mauro, S. and Sciacco, M. (2014) 'Mitochondrial disease heterogeneity: a prognostic challenge', Acta Myologica, 33(2), pp. 86-93.

Monaghan, D.T., Bridges, R.J. and Cotman, C.W. (1989) 'The excitatory amino acid receptors: their classes, pharmacology, and distinct properties in the function of the central nervous system', Annu Rev Pharmacol Toxicol, 29, pp. 365-402.

Montoya, J., Christianson, T., Levens, D., Rabinowitz, M. and Attardi, G. (1982) 'Identification of initiation sites for heavy-strand and light-strand transcription in human mitochondrial DNA', Proc Natl Acad Sci U S A, 79(23), pp. 7195-9.

Moraes, C.T., DiMauro, S., Zeviani, M., Lombes, A., Shanske, S., Miranda, A.F., Nakase, H., Bonilla, E., Werneck, L.C., Servidei, S. and *et al*. (1989) 'Mitochondrial DNA deletions in progressive external ophthalmoplegia and Kearns-Sayre syndrome', N Engl J Med, 320(20), pp. 1293-9.

Moraes, C.T., Ricci, E., Bonilla, E., DiMauro, S. and Schon, E.A. (1992) 'The mitochondrial tRNA(Leu(UUR)) mutation in mitochondrial encephalomyopathy, lactic acidosis, and strokelike episodes (MELAS): genetic, biochemical, and morphological correlations in skeletal muscle', Am J Hum Genet, 50(5), pp. 934-49.

Moreno-Lastres, D., Fontanesi, F., Garcia-Consuegra, I., Martin, M.A., Arenas, J., Barrientos, A. and Ugalde, C. (2012) 'Mitochondrial complex I plays an essential role in human respirasome assembly', *Cell Metab*, 15(3), pp. 324-35.

Morfini, G.A., Burns, M., Binder, L.I., Kanaan, N.M., LaPointe, N., Bosco, D.A., Brown, R.H., Jr., Brown, H., Tiwari, A., Hayward, L., Edgar, J., Nave, K.A., Garberrn, J., Atagi, Y., Song, Y., Pigino, G. and Brady, S.T. (2009) 'Axonal transport defects in neurodegenerative diseases', J Neurosci, 29(41), pp. 12776-86.

Mori, O., Yamazaki, M., Ohaki, Y., Arai, Y., Oguro, T., Shimizu, H. and Asano, G. (2000) 'Mitochondrial encephalomyopathy with lactic acidosis and stroke like episodes (MELAS) with prominent degeneration of the intestinal wall and cactus-like cerebellar pathology', Acta Neuropathol, 100(6), pp. 712-7.

Moslemi, A.R., Melberg, A., Holme, E. and Oldfors, A. (1999) 'Autosomal dominant progressive external ophthalmoplegia: distribution of multiple mitochondrial DNA deletions', Neurology, 53(1), pp. 79-84.

Motor Learning and Synaptic Plasticity in the Cerebellum. Cambridge University Press.

Nakamura, M., Fujiwara, Y. and Yamamoto, M. (1993) 'The two locus control of Leber hereditary optic neuropathy and a high penetrance in Japanese pedigrees', Hum Genet, 91(4), pp. 339-41.

Nass, S. and Nass, M.M. (1963) 'Intramitochondrial fibers with DNA characteristics. II. Enzymatic and other hydrolytic treatments', J Cell Biol, 19, pp. 613-29.

Natera-Naranjo, O., Aschrafi, A., Gioio, A.E. and Kaplan, B.B. (2010) 'Identification and quantitative analyses of microRNAs located in the distal axons of sympathetic neurons', Rna, 16(8), pp. 1516-29.

Naviaux, R.K. and Nguyen, K.V. (2004) 'POLG mutations associated with Alpers' syndrome and mitochondrial DNA depletion', Ann Neurol, 55(5), pp. 706-12.

Nesbitt, V., Pitceathly, R.D., Turnbull, D.M., Taylor, R.W., Sweeney, M.G., Mudanohwo, E.E., Rahman, S., Hanna, M.G. and McFarland, R. (2013) 'The UK MRC Mitochondrial Disease Patient Cohort Study: clinical phenotypes associated with the m.3243A>G mutation--implications for diagnosis and management', J Neurol Neurosurg Psychiatry, 84(8), pp. 936-8.

Newman, N.J. (2002) 'From genotype to phenotype in Leber hereditary optic neuropathy: still more questions than answers', J Neuroophthalmol, 22(4), pp. 257-61.

Nguyen, D. (2013) 'Quantifying chromogen intensity in immunohistochemistry via reciprocal intensity'.

Nikali, K., Suomalainen, A., Saharinen, J., Kuokkanen, M., Spelbrink, J.N., Lonnqvist, T. and Peltonen, L. (2005) 'Infantile onset spinocerebellar ataxia is caused by recessive mutations in mitochondrial proteins Twinkle and Twinky', Hum Mol Genet, 14(20), pp. 2981-90.

Nishigaki, Y., Tadesse, S., Bonilla, E., Shungu, D., Hersh, S., Keats, B.J., Berlin, C.I., Goldberg, M.F., Vockley, J., DiMauro, S. and Hirano, M. (2003) 'A novel mitochondrial tRNA(Leu(UUR)) mutation in a patient with features of MERRF and Kearns-Sayre syndrome', Neuromuscul Disord, 13(4), pp. 334-40.

Nishimura, Y., Yoshinari, T., Naruse, K., Yamada, T., Sumi, K., Mitani, H., Higashiyama, T. and Kuroiwa, T. (2006) 'Active digestion of sperm mitochondrial DNA in single living sperm revealed by optical tweezers', Proceedings of the National Academy of Sciences, 103(5), pp. 1382-1387.

Nishino, I., Spinazzola, A. and Hirano, M. (1999) 'Thymidine phosphorylase gene mutations in MNGIE, a human mitochondrial disorder', Science, 283(5402), pp. 689-92.

Noonberg, S.B., Weiss, T.L., Garovoy, M.R. and Hunt, C.A. (1992) 'Characterization and minimization of cellular autofluorescence in the study of oligonucleotide uptake using confocal microscopy', Antisense Res Dev, 2(4), pp. 303-13.

O'Brien, T.W. (2003) 'Properties of human mitochondrial ribosomes', IUBMB Life, 55(9), pp. 505-13.

Ohama, E. and Ikuta, F. (1987) 'Involvement of choroid plexus in mitochondrial encephalomyopathy (MELAS)', Acta Neuropathol, 75(1), pp. 1-7.

Ohama, E., Ohara, S., Ikuta, F., Tanaka, K., Nishizawa, M. and Miyatake, T. (1987) 'Mitochondrial angiopathy in cerebral blood vessels of mitochondrial encephalomyopathy', Acta Neuropathol, 74(3), pp. 226-33.

Old, S.L. and Johnson, M.A. (1989) 'Methods of microphotometric assay of succinate dehydrogenase and cytochrome c oxidase activities for use on human skeletal muscle', Histochem J, 21(9-10), pp. 545-55.

Oldendorf, W.H., Cornford, M.E. and Brown, W.J. (1977) 'The large apparent work capability of the blood-brain barrier: a study of the mitochondrial content of capillary endothelial cells in brain and other tissues of the rat', Ann Neurol, 1(5), pp. 409-17.

Oldfors, A., Fyhr, I.M., Holme, E., Larsson, N.G. and Tulinius, M. (1990) 'Neuropathology in Kearns-Sayre syndrome', Acta Neuropathol, 80(5), pp. 541-6.

Olsson, K.S. and Norrby, A. (2008) 'Comment to: Hepcidin: from discovery to differential diagnosis. Haematologica 2008; 93:90-7', Haematologica, 93(6), p. e51; discussion e52.

Orrenius, S., Zhivotovsky, B. and Nicotera, P. (2003) 'Regulation of cell death: the calcium-apoptosis link', Nat Rev Mol Cell Biol, 4(7), pp. 552-65.

Osawa, S., Jukes, T.H., Watanabe, K. and Muto, A. (1992) 'Recent evidence for evolution of the genetic code', Microbiol Rev, 56(1), pp. 229-64.

Palade, G.E. (1952) 'The fine structure of mitochondria', The Anatomical Record, 114(3), pp. 427-451.

Palade, G.E. (1953) 'An electron microcope study of the mitochondrial structure', Journal of Histochemistry & Cytochemistry, 1(4), pp. 188-211.

Parisi, M.A. and Clayton, D.A. (1991) 'Similarity of human mitochondrial transcription factor 1 to high mobility group proteins', Science, 252(5008), pp. 965-9.

Park, J., Lee, S.B., Lee, S., Kim, Y., Song, S., Kim, S., Bae, E., Kim, J., Shong, M., Kim, J.M. and Chung, J. (2006) 'Mitochondrial dysfunction in Drosophila PINK1 mutants is complemented by parkin', Nature, 441(7097), pp. 1157-61.

Parsons, L.M. and Fox, P.T. (1997) 'Sensory and Cognitive Functions', in Ronald J. Bradley, R.A.H.P.J. and Jeremy, D.S. (eds.) International Review of Neurobiology. Academic Press, pp. 255-271.

Pavlakis, S.G., Phillips, P.C., DiMauro, S., De Vivo, D.C. and Rowland, L.P. (1984) 'Mitochondrial myopathy, encephalopathy, lactic acidosis, and strokelike episodes: a distinctive clinical syndrome', Ann Neurol, 16(4), pp. 481-8.

Peretti, D., Bastide, A., Radford, H., Verity, N., Molloy, C., Martin, M.G., Moreno, J.A., Steinert, J.R., Smith, T., Dinsdale, D., Willis, A.E. and Mallucci, G.R. (2015) 'RBM3 mediates structural plasticity and protective effects of cooling in neurodegeneration', Nature, 518(7538), pp. 236-239.

Perkins, G., Renken, C., Martone, M.E., Young, S.J., Ellisman, M. and Frey, T. (1997) 'Electron tomography of neuronal mitochondria: three-dimensional structure and organization of cristae and membrane contacts', J Struct Biol, 119(3), pp. 260-72.

Perkins, G.A., Tjong, J., Brown, J.M., Poquiz, P.H., Scott, R.T., Kolson, D.R., Ellisman, M.H. and Spirou, G.A. (2010) 'The micro-architecture of mitochondria at active zones: electron tomography reveals novel anchoring scaffolds and cristae structured for high-rate metabolism', J Neurosci, 30(3), pp. 1015-26.

Petruzzella, V., Moraes, C.T., Sano, M.C., Bonilla, E., DiMauro, S. and Schon, E.A. (1994) 'Extremely high levels of mutant mtDNAs co-localize with cytochrome c oxidase-negative ragged-red fibers in patients harboring a point mutation at nt 3243', Hum Mol Genet, 3(3), pp. 449-54.

Picconi, B., Piccoli, G. and Calabresi, P. (2012) 'Synaptic dysfunction in Parkinson's disease', Adv Exp Med Biol, 970, pp. 553-72.

Poulopoulos, A., Aramuni, G., Meyer, G., Soykan, T., Hoon, M., Papadopoulos, T., Zhang, M., Paarmann, I., Fuchs, C., Harvey, K., Jedlicka, P., Schwarzacher, S.W., Betz, H., Harvey, R.J., Brose, N., Zhang, W. and Varoqueaux, F. (2009) 'Neuroligin 2 drives postsynaptic assembly at perisomatic inhibitory synapses through gephyrin and collybistin', Neuron, 63(5), pp. 628-42.

Prentice, H., Modi, J.P. and Wu, J.Y. (2015) 'Mechanisms of Neuronal Protection against Excitotoxicity, Endoplasmic Reticulum Stress, and Mitochondrial Dysfunction in Stroke and Neurodegenerative Diseases', *Oxid Med Cell Longev*, 2015, p. 964518.

Purves. D, Augustine. GJ and D., F. (2001) 'Glutamate Receptors', in Neuroscience. 2nd edn. Sunderland (MA): Sinauer Associates

Quintana, A., Kruse, S.E., Kapur, R.P., Sanz, E. and Palmiter, R.D. (2010) 'Complex I deficiency due to loss of Ndufs4 in the brain results in progressive encephalopathy resembling Leigh syndrome', Proc Natl Acad Sci U S A, 107(24), pp. 10996-1001.

Quintero, M., Colombo, S.L., Godfrey, A. and Moncada, S. (2006) 'Mitochondria as signaling organelles in the vascular endothelium', Proceedings of the National Academy of Sciences of the United States of America, 103(14), pp. 5379-5384.

Rajakumar, j.A.K.R. (2013) 'Cerebellum', in The human nervous system: an anatomical viewpoint. Philadelphia, pp. 157-172.

Rancillac, A., Rossier, J., Guille, M., Tong, X.K., Geoffroy, H., Amatore, C., Arbault, S., Hamel, E. and Cauli, B. (2006) 'Glutamatergic Control of Microvascular Tone by Distinct GABA Neurons in the Cerebellum', J Neurosci, 26(26), pp. 6997-7006.

Rangaraju, V., Calloway, N. and Ryan, Timothy A. (2014) 'Activity-Driven Local ATP Synthesis Is Required for Synaptic Function', Cell, 156(4), pp. 825-835.

Rebelo, A.P., Dillon, L.M. and Moraes, C.T. (2011) 'Mitochondrial DNA transcription regulation and nucleoid organization', J Inherit Metab Dis, 34(4), pp. 941-51.

Reeve, A., Meagher, M., Lax, N., Simcox, E., Hepplewhite, P., Jaros, E. and Turnbull, D. (2013) 'The Impact of Pathogenic Mitochondrial DNA Mutations on Substantia Nigra Neurons', The Journal of Neuroscience, 33(26), pp. 10790-10801.

Renard, D. and Labauge, P. (2012) 'Posterior leukoencephalopathy in NARP syndrome', Acta Neurologica Belgica, 112(4), pp. 417-418.

Richter, C., Park, J.W. and Ames, B.N. (1988) 'Normal oxidative damage to mitochondrial and nuclear DNA is extensive', Proc Natl Acad Sci U S A, 85(17), pp. 6465-7.

Roberti, M., Polosa, P.L., Bruni, F., Manzari, C., Deceglie, S., Gadaleta, M.N. and Cantatore, P. (2009) 'The MTERF family proteins: Mitochondrial transcription regulators and beyond', Biochimica et Biophysica Acta (BBA) - Bioenergetics, 1787(5), pp. 303-311.

Rodan, L.H., Poublanc, J., Fisher, J.A., Sobczyk, O., Wong, T., Hlasny, E., Mikulis, D. and Tein, I. (2015) 'Cerebral hyperperfusion and decreased cerebrovascular reactivity correlate with neurologic disease severity in MELAS', Mitochondrion, 22, pp. 66-74.

Ross, J.M. (2011) 'Visualization of mitochondrial respiratory function using cytochrome c oxidase/succinate dehydrogenase (COX/SDH) double-labeling histochemistry', J Vis Exp, (57), p. e3266.

Rossignol, R., Malgat, M., Mazat, J.-P. and Letellier, T. (1999) 'Threshold Effect and Tissue Specificity: IMPLICATION FOR MITOCHONDRIAL CYTOPATHIES', Journal of Biological Chemistry, 274(47), pp. 33426-33432.

Rouault, T.A. and Tong, W.-H. (2005) 'Iron-sulphur cluster biogenesis and mitochondrial iron homeostasis', Nat Rev Mol Cell Biol, 6(4), pp. 345-351.

Rowland, K.C., Irby, N.K. and Spirou, G.A. (2000) 'Specialized synapse-associated structures within the calyx of Held', J Neurosci, 20(24), pp. 9135-44.

Rowlands, D.J., Islam, M.N., Das, S.R., Huertas, A., Quadri, S.K., Horiuchi, K., Inamdar, N., Emin, M.T., Lindert, J., Ten, V.S., Bhattacharya, S. and Bhattacharya, J. (2011) 'Activation of TNFR1 ectodomain shedding by mitochondrial Ca2+ determines the severity of inflammation in mouse lung microvessels', J Clin Invest, 121(5), pp. 1986-99.

Ruiter, E.M., Siers, M.H., van den Elzen, C., van Engelen, B.G., Smeitink, J.A.M., Rodenburg, R.J. and Hol, F.A. (2006) 'The mitochondrial 13513G>A mutation is most frequent in Leigh syndrome combined with reduced complex I activity, optic atrophy and//or Wolff-Parkinson-White', Eur J Hum Genet, 15(2), pp. 155-161.

Sadun, A.A., Win, P.H., Ross-Cisneros, F.N., Walker, S.O. and Carelli, V. (2000) 'Leber's hereditary optic neuropathy differentially affects smaller axons in the optic nerve', Transactions of the American Ophthalmological Society, 98, pp. 223-235.

Sajadi, A., Schneider, B.L. and Aebischer, P. (2004) 'Wlds-mediated protection of dopaminergic fibers in an animal model of Parkinson disease', Curr Biol, 14(4), pp. 326-30.

Sakuta, R. and Nonaka, I. (1989) 'Vascular involvement in mitochondrial myopathy', Ann Neurol, 25(6), pp. 594-601.

Saneto, R.P., Friedman, S.D. and Shaw, D.W.W. (2008) 'Neuroimaging of Mitochondrial Disease', Mitochondrion, 8(5-6), pp. 396-413.

Santorelli, F.M., Tanji, K., Kulikova, R., Shanske, S., Vilarinho, L., Hays, A.P. and DiMauro, S. (1997) 'Identification of a novel mutation in the mtDNA ND5 gene associated with MELAS', Biochem Biophys Res Commun, 238(2), pp. 326-8.

Santos, R.X., Correia, S.C., Carvalho, C., Cardoso, S., Santos, M.S. and Moreira, P.I. (2011) 'Mitophagy in neurodegeneration: an opportunity for therapy?', Curr Drug Targets, 12(6), pp. 790-9.

Saraste, M. (1999) 'Oxidative Phosphorylation at the fin de siècle', Science, 283(5407), pp. 1488-1493.

Sarder, P. and Nehorai, A. (2006) 'Deconvolution methods for 3-D fluorescence microscopy images', Signal Processing Magazine, IEEE, 23(3), pp. 32-45.

Sarzi, E., Goffart, S., Serre, V., Chretien, D., Slama, A., Munnich, A., Spelbrink, J.N. and Rotig, A. (2007) 'Twinkle helicase (PEO1) gene mutation causes mitochondrial DNA depletion', Ann Neurol, 62(6), pp. 579-87.

Sato, M. and Sato, K. (2011) 'Degradation of Paternal Mitochondria by Fertilization-Triggered Autophagy in C. elegans Embryos', Science, 334(6059), pp. 1141-1144.

Sato, M. and Sato, K. (2013) 'Maternal inheritance of mitochondrial DNA by diverse mechanisms to eliminate paternal mitochondrial DNA', Biochimica et Biophysica Acta (BBA) - Molecular Cell Research, 1833(8), pp. 1979-1984.

Scacco, S., Petruzzella, V., Budde, S., Vergari, R., Tamborra, R., Panelli, D., van den Heuvel, L.P., Smeitink, J.A. and Papa, S. (2003) 'Pathological Mutations of the Human NDUFS4 Gene of the 18-kDa (AQDQ) Subunit of Complex I Affect the Expression of the Protein and the Assembly and Function of the Complex', Journal of Biological Chemistry, 278(45), pp. 44161-44167.

Scaglia, F., Towbin, J.A., Craigen, W.J., Belmont, J.W., Smith, E.O., Neish, S.R., Ware, S.M., Hunter, J.V., Fernbach, S.D., Vladutiu, G.D., Wong, L.J. and Vogel, H. (2004) 'Clinical spectrum, morbidity, and mortality in 113 pediatric patients with mitochondrial disease', Pediatrics, 114(4), pp. 925-31.

Scaglia, F., Wong, L.J., Vladutiu, G.D. and Hunter, J.V. (2005) 'Predominant cerebellar volume loss as a neuroradiologic feature of pediatric respiratory chain defects', AJNR Am J Neuroradiol, 26(7), pp. 1675-80.

Schacher, S. and Wu, F. (2002) 'Synapse formation in the absence of cell bodies requires protein synthesis', J Neurosci, 22(5), pp. 1831-9.

Schaefer, A.M., McFarland, R., Blakely, E.L., He, L., Whittaker, R.G., Taylor, R.W., Chinnery, P.F. and Turnbull, D.M. (2008) 'Prevalence of mitochondrial DNA disease in adults', Annals of Neurology, 63(1), pp. 35-39.

Schaefer, A.M., Phoenix, C., Elson, J.L., McFarland, R., Chinnery, P.F. and Turnbull, D.M. (2006) 'Mitochondrial disease in adults: a scale to monitor progression and treatment', Neurology, 66(12), pp. 1932-4.

Schäfer, E., Seelert, H., Reifschneider, N.H., Krause, F., Dencher, N.A. and Vonck, J. (2006) 'Architecture of Active Mammalian Respiratory Chain Supercomplexes', Journal of Biological Chemistry, 281(22), pp. 15370-15375.

Schagger, H. and Pfeiffer, K. (2000) 'Supercomplexes in the respiratory chains of yeast and mammalian mitochondria', Embo j, 19(8), pp. 1777-83.

Scheff, S.W. and Price, D.A. (2003) 'Synaptic pathology in Alzheimer's disease: a review of ultrastructural studies', Neurobiol Aging, 24(8), pp. 1029-46.

Scherzed, W., Brunt, E.R., Heinsen, H., de Vos, R.A., Seidel, K., Burk, K., Schols, L., Auburger, G., Del Turco, D., Deller, T., Korf, H.W., den Dunnen, W.F. and Rub, U. (2012) 'Pathoanatomy of cerebellar degeneration in spinocerebellar ataxia type 2 (SCA2) and type 3 (SCA3)', Cerebellum, 11(3), pp. 749-60.

Schon, E.A., Rizzuto, R., Moraes, C.T., Nakase, H., Zeviani, M. and DiMauro, S. (1989) 'A direct repeat is a hotspot for large-scale deletion of human mitochondrial DNA', Science, 244(4902), pp. 346-9.

Schultz, B.E. and Chan, S.I. (2001) 'Structures and proton-pumping strategies of mitochondrial respiratory enzymes', Annu Rev Biophys Biomol Struct, 30, pp. 23-65.

Schwartz, M. and Vissing, J. (2002) 'Paternal inheritance of mitochondrial DNA', N Engl J Med, 347(8), pp. 576-80.

Schwarz, T.L. (2013) 'Mitochondrial trafficking in neurons', Cold Spring Harb Perspect Biol, 5(6).

Sciacco, M., Bonilla, E., Schon, E.A., DiMauro, S. and Moraes, C.T. (1994) 'Distribution of wild-type and common deletion forms of mtDNA in normal and respiration-deficient muscle fibers from patients with mitochondrial myopathy', Human Molecular Genetics, 3(1), pp. 13-19.

Sena, Laura A. and Chandel, Navdeep S. (2012) 'Physiological Roles of Mitochondrial Reactive Oxygen Species', Molecular Cell, 48(2), pp. 158-167.

Shadel, G.S. and Clayton, D.A. (1997) 'Mitochondrial DNA maintenance in vertebrates', Annu Rev Biochem, 66, pp. 409-35.

Shaw, G.C., Cope, J.J., Li, L., Corson, K., Hersey, C., Ackermann, G.E., Gwynn, B., Lambert, A.J., Wingert, R.A., Traver, D., Trede, N.S., Barut, B.A., Zhou, Y., Minet, E., Donovan, A., Brownlie, A., Balzan, R., Weiss, M.J., Peters, L.L., Kaplan, J., Zon, L.I. and Paw, B.H. (2006) 'Mitoferrin is essential for erythroid iron assimilation', Nature, 440(7080), pp. 96-100.

Sheng, Z.H. (2014) 'Mitochondrial trafficking and anchoring in neurons: New insight and implications', J Cell Biol, 204(7), pp. 1087-98.

Shimotake, T., Furukawa, T., Inoue, K., Iwai, N. and Takeuchi, Y. (1998) 'Familial occurrence of intestinal obstruction in children with the syndrome of mitochondrial encephalomyopathy, lactic acidosis, and stroke-like episodes (MELAS)', J Pediatr Surg, 33(12), pp. 1837-9.

Shirendeb, U., Reddy, A.P., Manczak, M., Calkins, M.J., Mao, P., Tagle, D.A. and Reddy, P.H. (2011) 'Abnormal mitochondrial dynamics, mitochondrial loss and mutant huntingtin oligomers in Huntington's disease: implications for selective neuronal damage', Hum Mol Genet, 20(7), pp. 1438-55.

Shoffner, J.M., Lott, M.T., Lezza, A.M., Seibel, P., Ballinger, S.W. and Wallace, D.C. (1990) 'Myoclonic epilepsy and ragged-red fiber disease (MERRF) is associated with a mitochondrial DNA tRNA(Lys) mutation', Cell, 61(6), pp. 931-7.

Shtilbans, A., Shanske, S., Goodman, S., Sue, C.M., Bruno, C., Johnson, T.L., Lava, N.S., Waheed, N. and DiMauro, S. (2000) 'G8363A mutation in the mitochondrial DNA transfer ribonucleic acidLys gene: another cause of Leigh syndrome', J Child Neurol, 15(11), pp. 759-61.

Silvestri, G., Servidei, S., Rana, M., Ricci, E., Spinazzola, A., Paris, E. and Tonali, P. (1996) 'A novel mitochondrial DNA point mutation in the tRNA(Ile) gene is associated with progressive external ophtalmoplegia', Biochem Biophys Res Commun, 220(3), pp. 623-7.

Simamura, E., Shimada, H., Hatta, T. and Hirai, K. (2008) 'Mitochondrial voltage-dependent anion channels (VDACs) as novel pharmacological targets for anti-cancer agents', J Bioenerg Biomembr, 40(3), pp. 213-7.

Sligh, J.E., Levy, S.E., Waymire, K.G., Allard, P., Dillehay, D.L., Nusinowitz, S., Heckenlively, J.R., MacGregor, G.R. and Wallace, D.C. (2000) 'Maternal germ-line transmission of mutant mtDNAs from embryonic stem cell-derived chimeric mice', Proceedings of the National Academy of Sciences of the United States of America, 97(26), pp. 14461-14466.

Smith, J.L., Tse, D.T., Byrne, S.F., Johns, D.R. and Stone, E.M. (1990) 'Optic nerve sheath distention in Leber's optic neuropathy and the significance of the "Wallace mutation"', J Clin Neuroophthalmol, 10(4), pp. 231-8.

Smits, P., Smeitink, J. and van den Heuvel, L. (2010) 'Mitochondrial translation and beyond: processes implicated in combined oxidative phosphorylation deficiencies', J Biomed Biotechnol, 2010, p. 737385.

Sparaco, M., Bonilla, E., DiMauro, S. and Powers, J.M. (1993) 'Neuropathology of mitochondrial encephalomyopathies due to mitochondrial DNA defects', J Neuropathol Exp Neurol, 52(1), pp. 1-10.

Sparaco, M., Schon, E.A., DiMauro, S. and Bonilla, E. (1995) 'Myoclonic epilepsy with ragged-red fibers (MERRF): an immunohistochemical study of the brain', Brain Pathol, 5(2), pp. 125-33.

Sparaco, M., Simonati, A., Cavallaro, T., Bartolomei, L., Grauso, M., Piscioli, F., Morelli, L. and Rizzuto, N. (2003) 'MELAS: clinical phenotype and morphological brain abnormalities', Acta Neuropathologica, 106(3), pp. 202-212.

Spelbrink, J.N., Li, F.Y., Tiranti, V., Nikali, K., Yuan, Q.P., Tariq, M., Wanrooij, S., Garrido, N., Comi, G., Morandi, L., Santoro, L., Toscano, A., Fabrizi, G.M., Somer, H., Croxen, R., Beeson, D., Poulton, J., Suomalainen, A., Jacobs, H.T., Zeviani, M. and Larsson, C. (2001) 'Human mitochondrial DNA deletions associated with mutations in the gene encoding Twinkle, a phage T7 gene 4-like protein localized in mitochondria', Nat Genet, 28(3), pp. 223-31.

Spinazzola, A. and Zeviani, M. (2005) 'Disorders of nuclear-mitochondrial intergenomic signaling', Gene, 354, pp. 162-8.

Sproule, D.M. and Kaufmann, P. (2008) 'Mitochondrial encephalopathy, lactic acidosis, and strokelike episodes: basic concepts, clinical phenotype, and therapeutic management of MELAS syndrome', Ann N Y Acad Sci, 1142, pp. 133-58.

Stierum, R.H., Dianov, G.L. and Bohr, V.A. (1999) 'Single-nucleotide patch base excision repair of uracil in DNA by mitochondrial protein extracts#', Nucleic Acids Research, 27(18), pp. 3712-3719.

Su, M., Yoshida, Y., Hirata, Y., Satoh, Y. and Nagata, K. (2000) 'Degeneration of the cerebellar dentate nucleus in corticobasal degeneration: neuropathological and morphometric investigations', Acta Neuropathol, 99(4), pp. 365-70.

Sue, C.M., Crimmins, D.S., Soo, Y.S., Pamphlett, R., Presgrave, C.M., Kotsimbos, N., Jean-Francois, M.J., Byrne, E. and Morris, J.G. (1998) 'Neuroradiological features of six kindreds with MELAS tRNA(Leu) A2343G point mutation: implications for pathogenesis', J Neurol Neurosurg Psychiatry, 65(2), pp. 233-40.

Sutovsky, P., Moreno, R.D., Ramalho-Santos, J., Dominko, T., Simerly, C. and Schatten, G. (1999) 'Ubiquitin tag for sperm mitochondria', Nature, 402(6760), pp. 371-2.

Suzuki, T., Koizumi, J., Shiraishi, H., Ishikawa, N., Ofuku, K., Sasaki, M., Hori, T., Ohkoshi, N. and Anno, I. (1990) 'Mitochondrial encephalomyopathy (MELAS) with mental disorder. CT, MRI and SPECT findings', Neuroradiology, 32(1), pp. 74-6.

Swalwell, H., Kirby, D.M., Blakely, E.L., Mitchell, A., Salemi, R., Sugiana, C., Compton, A.G., Tucker, E.J., Ke, B.X., Lamont, P.J., Turnbull, D.M., McFarland, R., Taylor, R.W. and Thorburn, D.R. (2011) 'Respiratory chain complex I deficiency caused by mitochondrial DNA mutations', Eur J Hum Genet, 19(7), pp. 769-75.

Sykora, P., Croteau, D.L., Bohr, V.A. and Wilson, D.M., 3rd (2011) 'Aprataxin localizes to mitochondria and preserves mitochondrial function', Proc Natl Acad Sci U S A, 108(18), pp. 7437-42.

Tait, S.W. and Green, D.R. (2008) 'Caspase-independent cell death: leaving the set without the final cut', Oncogene, 27(50), pp. 6452-61.

Tait, S.W., Ichim, G. and Green, D.R. (2014) 'Die another way--non-apoptotic mechanisms of cell death', J Cell Sci, 127(Pt 10), pp. 2135-44.

Tait, S.W., Oberst, A., Quarato, G., Milasta, S., Haller, M., Wang, R., Karvela, M., Ichim, G., Yatim, N., Albert, M.L., Kidd, G., Wakefield, R., Frase, S., Krautwald, S., Linkermann, A. and Green, D.R. (2013) 'Widespread mitochondrial depletion via mitophagy does not compromise necroptosis', Cell Rep, 5(4), pp. 878-85.

Takamori, S., Holt, M., Stenius, K., Lemke, E.A., Gronborg, M., Riedel, D., Urlaub, H., Schenck, S., Brugger, B., Ringler, P., Muller, S.A., Rammner, B., Grater, F., Hub, J.S., De Groot, B.L., Mieskes, G., Moriyama, Y., Klingauf, J., Grubmuller, H., Heuser, J., Wieland, F. and Jahn, R. (2006) 'Molecular anatomy of a trafficking organelle', Cell, 127(4), pp. 831-46.

Takamori, S., Rhee, J.S., Rosenmund, C. and Jahn, R. (2000a) 'Identification of a vesicular glutamate transporter that defines a glutamatergic phenotype in neurons', Nature, 407(6801), pp. 189-94.

Takamori, S., Riedel, D. and Jahn, R. (2000b) 'Immunoisolation of GABA-specific synaptic vesicles defines a functionally distinct subset of synaptic vesicles', J Neurosci, 20(13), pp. 4904-11.

Tam, E.W., Feigenbaum, A., Addis, J.B., Blaser, S., Mackay, N., Al-Dosary, M., Taylor, R.W., Ackerley, C., Cameron, J.M. and Robinson, B.H. (2008) 'A novel mitochondrial DNA mutation in COX1 leads to strokes, seizures, and lactic acidosis', Neuropediatrics, 39(6), pp. 328-34.

Tanahashi, C., Nakayama, A., Yoshida, M., Ito, M., Mori, N. and Hashizume, Y. (2000) 'MELAS with the mitochondrial DNA 3243 point mutation: a neuropathological study', Acta Neuropathol, 99(1), pp. 31-8.

Tang, X., Luo, Y.X., Chen, H.Z. and Liu, D.P. (2014) 'Mitochondria, endothelial cell function, and vascular diseases', Front Physiol, 5, p. 175.

Tang, Y.-g. and Zucker, R.S. (1997) 'Mitochondrial Involvement in Post-Tetanic Potentiation of Synaptic Transmission', Neuron, 18(3), pp. 483-491.

Tanji, K., DiMauro, S. and Bonilla, E. (1999) 'Disconnection of cerebellar Purkinje cells in Kearns-Sayre syndrome', J Neurol Sci, 166(1), pp. 64-70.

Tanji, K., Gamez, J., Cervera, C., Mearin, F., Ortega, A., de la Torre, J., Montoya, J., Andreu, A.L., DiMauro, S. and Bonilla, E. (2003) 'The A8344G mutation in mitochondrial DNA associated with stroke-like episodes and gastrointestinal dysfunction', Acta Neuropathol, 105(1), pp. 69-75.

Tanji, K., Gamez, J., Cervera, C., Mearin, F., Ortega, A., de la Torre, J., Montoya, J., Andreu, A.L., DiMauro, S. and Bonilla, E. (2003) 'The A8344G mutation in mitochondrial DNA associated with stroke-like episodes and gastrointestinal dysfunction', Acta Neuropathol, 105(1), pp. 69-75.

Tanji, K., Kunimatsu, T., Vu, T.H. and Bonilla, E. (2001) 'Neuropathological features of mitochondrial disorders', Semin Cell Dev Biol, 12(6), pp. 429-39.

Tarasov, A.I., Griffiths, E.J. and Rutter, G.A. (2012) 'Regulation of ATP production by mitochondrial Ca(2+)', Cell Calcium, 52(1), pp. 28-35.

Taylor, A.M., Blurton-Jones, M., Rhee, S.W., Cribbs, D.H., Cotman, C.W. and Jeon, N.L. (2005) 'A microfluidic culture platform for CNS axonal injury, regeneration and transport', Nat Methods, 2(8), pp. 599-605.

Taylor, A.M., Dieterich, D.C., Ito, H.T., Kim, S.A. and Schuman, E.M. (2010) 'Microfluidic local perfusion chambers for the visualization and manipulation of synapses', Neuron, 66(1), pp. 57-68.

Taylor, C.R. and Levenson, R.M. (2006) 'Quantification of immunohistochemistry—issues concerning methods, utility and semiquantitative assessment II', Histopathology, 49(4), pp. 411-424.

Taylor, R.W. and Turnbull, D.M. (2005) 'Mitochondrial DNA mutations in human disease', Nat Rev Genet, 6(5), pp. 389-402.

Taylor, R.W., Barron, M.J., Borthwick, G.M., Gospel, A., Chinnery, P.F., Samuels, D.C., Taylor, G.A., Plusa, S.M., Needham, S.J., Greaves, L.C., Kirkwood, T.B. and Turnbull, D.M. (2003) 'Mitochondrial DNA mutations in human colonic crypt stem cells', J Clin Invest, 112(9), pp. 1351-60.

Taylor, R.W., Chinnery, P.F., Bates, M.J., Jackson, M.J., Johnson, M.A., Andrews, R.M. and Turnbull, D.M. (1998) 'A novel mitochondrial DNA point mutation in the tRNA(Ile) gene: studies in a patient presenting with chronic progressive external ophthalmoplegia and multiple sclerosis', Biochem Biophys Res Commun, 243(1), pp. 47-51.

Taylor, R.W., Chinnery, P.F., Haldane, F., Morris, A.A., Bindoff, L.A., Wilson, J. and Turnbull, D.M. (1996) 'MELAS associated with a mutation in the valine transfer RNA gene of mitochondrial DNA', Ann Neurol, 40(3), pp. 459-62.

Taylor, R.W., Pyle, A., Griffin, H. and *et al*. (2014) 'USe of whole-exome sequencing to determine the genetic basis of multiple mitochondrial respiratory chain complex deficiencies', JAMA, 312(1), pp. 68-77.

Telford, J.E., Kilbride, S.M. and Davey, G.P. (2009) 'Complex I is rate-limiting for oxygen consumption in the nerve terminal', J Biol Chem, 284(14), pp. 9109-14.

Teune, T.M., van der Burg, J., de Zeeuw, C.I., Voogd, J. and Ruigrok, T.J. (1998) 'Single Purkinje cell can innervate multiple classes of projection neurons in the cerebellar nuclei of the rat: a light microscopic and ultrastructural triple-tracer study in the rat', J Comp Neurol, 392(2), pp. 164-78.

Thach, W.T. and Thach, W.T. (1997) On the specific role of the cerebellum in motor learning and cognition: Clues from PET activation and lesion studies in man

Timmis, J.N., Ayliffe, M.A., Huang, C.Y. and Martin, W. (2004) 'Endosymbiotic gene transfer: organelle genomes forge eukaryotic chromosomes', Nat Rev Genet, 5(2), pp. 123-135.

Tokunaga, M., Mita, S., Sakuta, R., Nonaka, I. and Araki, S. (1993) 'Increased mitochondrial DNA in blood vessels and ragged-red fibers in mitochondrial myopathy, encephalopathy, lactic acidosis, and stroke-like episodes (MELAS)', Ann Neurol, 33(3), pp. 275-80.

Tretter, V., Mukherjee, J., Maric, H.M., Schindelin, H., Sieghart, W. and Moss, S.J. (2012) 'Gephyrin, the enigmatic organizer at GABAergic synapses', Front Cell Neurosci, 6, p. 23.

Trevelyan, A.J., Kirby, D.M., Smulders-Srinivasan, T.K., Nooteboom, M., Acin-Perez, R., Enriquez, J.A., Whittington, M.A., Lightowlers, R.N. and Turnbull, D.M. (2010) 'Mitochondrial DNA mutations affect calcium handling in differentiated neurons', Brain, 133(3), pp. 787-796.

Trifunovic, A., Hansson, A., Wredenberg, A., Rovio, A.T., Dufour, E., Khvorostov, I., Spelbrink, J.N., Wibom, R., Jacobs, H.T. and Larsson, N.G. (2005) 'Somatic mtDNA mutations cause aging phenotypes without affecting reactive oxygen species production', Proc Natl Acad Sci U S A, 102(50), pp. 17993-8.

Trifunovic, A., Wredenberg, A., Falkenberg, M., Spelbrink, J.N., Rovio, A.T., Bruder, C.E., Bohlooly, Y.M., Gidlof, S., Oldfors, A., Wibom, R., Tornell, J., Jacobs, H.T. and Larsson, N.G. (2004) 'Premature ageing in mice expressing defective mitochondrial DNA polymerase', Nature, 429(6990), pp. 417-23.

Trinei, M., Berniakovich, I., Pelicci, P.G. and Giorgio, M. (2006) 'Mitochondrial DNA copy number is regulated by cellular proliferation: A role for Ras and p66Shc', Biochimica et Biophysica Acta (BBA) - Bioenergetics, 1757(5–6), pp. 624-630.

Turrigiano, G. (2011) 'Too many cooks? Intrinsic and synaptic homeostatic mechanisms in cortical circuit refinement', Annu Rev Neurosci, 34, pp. 89-103.

Twig, G., Elorza, A., Molina, A.J., Mohamed, H., Wikstrom, J.D., Walzer, G., Stiles, L., Haigh, S.E., Katz, S., Las, G., Alroy, J., Wu, M., Py, B.F., Yuan, J., Deeney, J.T., Corkey, B.E. and Shirihai, O.S. (2008) 'Fission and selective fusion govern mitochondrial segregation and elimination by autophagy', Embo j, 27(2), pp. 433-46.

Tyagarajan, S.K. and Fritschy, J.-M. (2014) 'Gephyrin: a master regulator of neuronal function?', Nat Rev Neurosci, 15(3), pp. 141-156.

Tyynismaa, H., Mjosund, K.P., Wanrooij, S., Lappalainen, I., Ylikallio, E., Jalanko, A., Spelbrink, J.N., Paetau, A. and Suomalainen, A. (2005) 'Mutant mitochondrial helicase Twinkle causes multiple mtDNA deletions and a late-onset mitochondrial disease in mice', Proc Natl Acad Sci U S A, 102(49), pp. 17687-92.

Tyynismaa, H., Sembongi, H., Bokori-Brown, M., Granycome, C., Ashley, N., Poulton, J., Jalanko, A., Spelbrink, J.N., Holt, I.J. and Suomalainen, A. (2004) 'Twinkle helicase is essential

for mtDNA maintenance and regulates mtDNA copy number', Human Molecular Genetics, 13(24), pp. 3219-3227.

Tzoulis, C., Engelsen, B.A., Telstad, W., Aasly, J., Zeviani, M., Winterthun, S., Ferrari, G., Aarseth, J.H. and Bindoff, L.A. (2006) 'The spectrum of clinical disease caused by the A467T and W748S POLG mutations: a study of 26 cases', Brain, 129(Pt 7), pp. 1685-92.

Tzoulis, C., Neckelmann, G., Mørk, S.J., Engelsen, B.E., Viscomi, C., Moen, G., Ersland, L., Zeviani, M. and Bindoff, L.A. (2010) Localized cerebral energy failure in DNA polymerase gamma-associated encephalopathy syndromes.

Tzoulis, C., Papingji, M., Fiskestrand, T., Roste, L.S. and Bindoff, L.A. (2009) 'Mitochondrial DNA depletion in progressive external ophthalmoplegia caused by POLG1 mutations', Acta Neurol Scand Suppl, (189), pp. 38-41.

Tzoulis, C., Tran, G.T., Coxhead, J., Bertelsen, B., Lilleng, P.K., Balafkan, N., Payne, B., Miletic, H., Chinnery, P.F. and Bindoff, L.A. (2014) 'Molecular Pathogenesis of Polymerase Gamma–Related Neurodegeneration', Annals of Neurology, 76(1), pp. 66-81.

Ugalde, C., Janssen, R.J., van den Heuvel, L.P., Smeitink, J.A. and Nijtmans, L.G. (2004a) 'Differences in assembly or stability of complex I and other mitochondrial OXPHOS complexes in inherited complex I deficiency', Hum Mol Genet, 13(6), pp. 659-67.

Ugalde, C., Vogel, R., Huijbens, R., Van Den Heuvel, B., Smeitink, J. and Nijtmans, L. (2004b) 'Human mitochondrial complex I assembles through the combination of evolutionary conserved modules: a framework to interpret complex I deficiencies', Hum Mol Genet, 13(20), pp. 2461-72.

Ungvari, Z., Labinskyy, N., Gupte, S., Chander, P.N., Edwards, J.G. and Csiszar, A. (2008) 'Dysregulation of mitochondrial biogenesis in vascular endothelial and smooth muscle cells of aged rats', Am J Physiol Heart Circ Physiol, 294(5), pp. H2121-8.

Uusisaari, M. and De Schutter, E. (2011) 'The mysterious microcircuitry of the cerebellar nuclei', J Physiol, 589(Pt 14), pp. 3441-57.

Uusisaari, M. and Knopfel, T. (2011) 'Functional classification of neurons in the mouse lateral cerebellar nuclei', Cerebellum, 10(4), pp. 637-46.

Uusisaari, M. and Knöpfel, T. (2013) 'Neurons of the Deep Cerebellar Nuclei', in Manto, M., Schmahmann, J., Rossi, F., Gruol, D. and Koibuchi, N. (eds.) Handbook of the Cerebellum and Cerebellar Disorders. Springer Netherlands, pp. 1101-1110.

Uusisaari, M., Obata, K. and Knöpfel, T. (2007) Morphological and Electrophysiological Properties of GABAergic and Non-GABAergic Cells in the Deep Cerebellar Nuclei.

Valanne, L., Ketonen, L., Majander, A., Suomalainen, A. and Pihko, H. (1998) 'Neuroradiologic findings in children with mitochondrial disorders', AJNR Am J Neuroradiol, 19(2), pp. 369-77.

Vallee, R.B., Williams, J.C., Varma, D. and Barnhart, L.E. (2004) 'Dynein: An ancient motor protein involved in multiple modes of transport', J Neurobiol, 58(2), pp. 189-200.

Valsecchi, F., Grefte, S., Roestenberg, P., Joosten-Wagenaars, J., Smeitink, J.A., Willems, P.H. and Koopman, W.J. (2013) 'Primary fibroblasts of NDUFS4(-/-) mice display increased ROS levels and aberrant mitochondrial morphology', Mitochondrion, 13(5), pp. 436-43.

Van Goethem, G., Dermaut, B., Lofgren, A., Martin, J.J. and Van Broeckhoven, C. (2001) 'Mutation of POLG is associated with progressive external ophthalmoplegia characterized by mtDNA deletions', Nat Genet, 28(3), pp. 211-2.

Van Goethem, G., Luoma, P., Rantamaki, M., Al Memar, A., Kaakkola, S., Hackman, P., Krahe, R., Lofgren, A., Martin, J.J., De Jonghe, P., Suomalainen, A., Udd, B. and Van Broeckhoven, C. (2004) 'POLG mutations in neurodegenerative disorders with ataxia but no muscle involvement', Neurology, 63(7), pp. 1251-7.

Vandecasteele, G., Szabadkai, G. and Rizzuto, R. (2001) 'Mitochondrial Calcium Homeostasis: Mechanisms and Molecules', IUBMB Life, 52(3-5), pp. 213-219.

Varley, Z.K., Pizzarelli, R., Antonelli, R., Stancheva, S.H., Kneussel, M., Cherubini, E. and Zacchi, P. (2011) 'Gephyrin regulates GABAergic and glutamatergic synaptic transmission in hippocampal cell cultures', J Biol Chem, 286(23), pp. 20942-51.

Varoqueaux, F., Jamain, S. and Brose, N. (2004) 'Neuroligin 2 is exclusively localized to inhibitory synapses', European Journal of Cell Biology, 83(9), pp. 449-456.

Vaucher, E., Tong, X.K., Cholet, N., Lantin, S. and Hamel, E. (2000) 'GABA neurons provide a rich input to microvessels but not nitric oxide neurons in the rat cerebral cortex: a means for direct regulation of local cerebral blood flow', J Comp Neurol, 421(2), pp. 161-71.

Verstreken, P., Ly, C.V., Venken, K.J., Koh, T.W., Zhou, Y. and Bellen, H.J. (2005) 'Synaptic mitochondria are critical for mobilization of reserve pool vesicles at Drosophila neuromuscular junctions', Neuron, 47(3), pp. 365-78.

Viegas, M.S., Martins, T.C., Seco, F. and do Carmo, A. (2007) 'An improved and cost-effective methodology for the reduction of autofluorescence in direct immunofluorescence studies on formalin-fixed paraffin-embedded tissues', Eur J Histochem, 51(1), pp. 59-66.

Vogel, F., Bornhövd, C., Neupert, W. and Reichert, A.S. (2006) 'Dynamic subcompartmentalization of the mitochondrial inner membrane', The Journal of Cell Biology, 175(2), pp. 237-247.

Voogd, J. and Glickstein, M. (1998) 'The anatomy of the cerebellum', Trends Neurosci, 21(9), pp. 370-5.

Waldvogel, H.J., Baer, K., Snell, R.G., During, M.J., Faull, R.L.M. and Rees, M.I. (2003) 'Distribution of gephyrin in the human brain: an immunohistochemical analysis', Neuroscience, 116(1), pp. 145-156.

Wallace, D.C. (2010) 'Mitochondrial DNA mutations in disease and aging', Environmental and Molecular Mutagenesis, 51(5), pp. 440-450.

Wallace, D.C., Singh, G., Lott, M.T., Hodge, J.A., Schurr, T.G., Lezza, A.M., Elsas, L.J., 2nd and Nikoskelainen, E.K. (1988) 'Mitochondrial DNA mutation associated with Leber's hereditary optic neuropathy', Science, 242(4884), pp. 1427-30.

Wang, C. and Youle, R.J. (2009) 'The role of mitochondria in apoptosis*', Annu Rev Genet, 43, pp. 95-118.

Wang, G.J., Nutter, L.M. and Thayer, S.A. (1997) 'Insensitivity of cultured rat cortical neurons to mitochondrial DNA synthesis inhibitors: evidence for a slow turnover of mitochondrial DNA', Biochem Pharmacol, 54(1), pp. 181-7.

Wang, J. and Pantopoulos, K. (2011) 'Regulation of cellular iron metabolism', Biochemical Journal, 434(Pt 3), pp. 365-381.

Wang, M.S., Fang, G., Culver, D.G., Davis, A.A., Rich, M.M. and Glass, J.D. (2001) 'The WldS protein protects against axonal degeneration: a model of gene therapy for peripheral neuropathy', Ann Neurol, 50(6), pp. 773-9.

Wang, S., Wang, B., Pan, N., Fu, L., Wang, C., Song, G., An, J., Liu, Z., Zhu, W., Guan, Y., Xu, Z.-Q.D., Chan, P., Chen, Z. and Zhang, Y.A. (2015) 'Differentiation of human induced pluripotent stem cells to mature functional Purkinje neurons', Sci. Rep., 5.

Wang, X. and Gerdes, H.H. (2015) 'Transfer of mitochondria via tunneling nanotubes rescues apoptotic PC12 cells', Cell Death Differ, 22(7), pp. 1181-1191.

Wang, Z., Jiang, H., Chen, S., Du, F. and Wang, X. (2012) 'The mitochondrial phosphatase PGAM5 functions at the convergence point of multiple necrotic death pathways', Cell, 148(1-2), pp. 228-43.

Watt, I.N., Montgomery, M.G., Runswick, M.J., Leslie, A.G.W. and Walker, J.E. (2010) 'Bioenergetic cost of making an adenosine triphosphate molecule in animal mitochondria', Proceedings of the National Academy of Sciences of the United States of America, 107(39), pp. 16823-16827.

Weber, K., Wilson, J.N., Taylor, L., Brierley, E., Johnson, M.A., Turnbull, D.M. and Bindoff, L.A. (1997) 'A new mtDNA mutation showing accumulation with time and restriction to skeletal muscle', Am J Hum Genet, 60(2), pp. 373-80.

Williams, P.A., Piechota, M., von Ruhland, C., Taylor, E., Morgan, J.E. and Votruba, M. (2012) 'Opa1 is essential for retinal ganglion cell synaptic architecture and connectivity', Brain, 135(Pt 2), pp. 493-505.

Wishart, T.M., Paterson, J.M., Short, D.M., Meredith, S., Robertson, K.A., Sutherland, C., Cousin, M.A., Dutia, M.B. and Gillingwater, T.H. (2007) 'Differential proteomics analysis of synaptic proteins identifies potential cellular targets and protein mediators of synaptic neuroprotection conferred by the slow Wallerian degeneration (Wlds) gene', Mol Cell Proteomics, 6(8), pp. 1318-30.

Wong, L.J., Naviaux, R.K., Brunetti-Pierri, N., Zhang, Q., Schmitt, E.S., Truong, C., Milone, M., Cohen, B.H., Wical, B., Ganesh, J., Basinger, A.A., Burton, B.K., Swoboda, K., Gilbert, D.L., Vanderver, A., Saneto, R.P., Maranda, B., Arnold, G., Abdenur, J.E., Waters, P.J. and Copeland, W.C. (2008) 'Molecular and clinical genetics of mitochondrial diseases due to POLG mutations', Hum Mutat, 29(9), pp. E150-72.

Xin, H., Woriax, V., Burkhart, W. and Spremulli, L.L. (1995) 'Cloning and expression of mitochondrial translational elongation factor Ts from bovine and human liver', J Biol Chem, 270(29), pp. 17243-9.

Yagoda, N., von Rechenberg, M., Zaganjor, E., Bauer, A.J., Yang, W.S., Fridman, D.J., Wolpaw, A.J., Smukste, I., Peltier, J.M., Boniface, J.J., Smith, R., Lessnick, S.L., Sahasrabudhe, S. and Stockwell, B.R. (2007) 'RAS-RAF-MEK-dependent oxidative cell death involving voltage-dependent anion channels', Nature, 447(7146), pp. 865-869.

Yang, M.Y., Bowmaker, M., Reyes, A., Vergani, L., Angeli, P., Gringeri, E., Jacobs, H.T. and Holt, I.J. (2002) 'Biased incorporation of ribonucleotides on the mitochondrial L-strand accounts for apparent strand-asymmetric DNA replication', Cell, 111(4), pp. 495-505.

Yang, W.S. and Stockwell, B.R. (2015) 'Ferroptosis: Death by Lipid Peroxidation', Trends in Cell Biology.

Yarana, C., Sanit, J., Chattipakorn, N. and Chattipakorn, S. (2012) 'Synaptic and nonsynaptic mitochondria demonstrate a different degree of calcium-induced mitochondrial dysfunction', Life Sci, 90(19-20), pp. 808-14.

Yasui, A., Yajima, H., Kobayashi, T., Eker, A.P. and Oikawa, A. (1992) 'Mitochondrial DNA repair by photolyase', Mutat Res, 273(2), pp. 231-6.

Yasukawa, T., Reyes, A., Cluett, T.J., Yang, M.Y., Bowmaker, M., Jacobs, H.T. and Holt, I.J. (2006) 'Replication of vertebrate mitochondrial DNA entails transient ribonucleotide incorporation throughout the lagging strand', Embo Journal, 25(22), pp. 5358-5371.

Yeh, K.Y., Yeh, M., Mims, L. and Glass, J. (2009) 'Iron feeding induces ferroportin 1 and hephaestin migration and interaction in rat duodenal epithelium', Am J Physiol Gastrointest Liver Physiol, 296(1), pp. G55-65.

Yoneda, M., Miyatake, T. and Attardi, G. (1995) 'Heteroplasmic mitochondrial tRNA(Lys) mutation and its complementation in MERRF patient-derived mitochondrial transformants', Muscle Nerve Suppl, 3, pp. S95-101.

Yonemura, K., Hasegawa, Y., Kimura, K., Minematsu, K. and Yamaguchi, T. (2001) 'Diffusion-weighted MR Imaging in a Case of Mitochondrial Myopathy, Encephalopathy, Lactic Acidosis, and Strokelike Episodes', American Journal of Neuroradiology, 22(2), pp. 269-272.

Yoon, K.L., Ernst, S.G., Rasmussen, C., Dooling, E.C. and Aprille, J.R. (1993) 'Mitochondrial disorder associated with newborn cardiopulmonary arrest', Pediatr Res, 33(5), pp. 433-40.

Yoshida, T., Okuyama, H., Nakayama, M., Endo, H., Nonomura, N., Nishimura, K. and Inoue, M. (2015) 'High-dose chemotherapeutics of intravesical chemotherapy rapidly induce mitochondrial dysfunction in bladder cancer-derived spheroids', Cancer Sci, 106(1), pp. 69-77.

Yu, W., Jiang, M., Miralles, C.P., Li, R.-w., Chen, G. and De Blas, A.L. (2007) 'Gephyrin clustering is required for the stability of GABAergic synapses', Molecular and cellular neurosciences, 36(4), pp. 484-500.

Yum, H.R., Chae, H., Shin, S.Y., Kim, Y., Kim, M. and Park, S.H. (2014) 'Pathogenic mitochondrial DNA mutations and associated clinical features in Korean patients with Leber's hereditary optic neuropathy', Invest Ophthalmol Vis Sci, 55(12), pp. 8095-101.

Zeviani, M., Moraes, C.T., DiMauro, S., Nakase, H., Bonilla, E., Schon, E.A. and Rowland, L.P. (1988) 'Deletions of mitochondrial DNA in Kearns-Sayre syndrome', Neurology, 38(9), pp. 1339-46.

Zhang, D.X. and Gutterman, D.D. (2007) 'Mitochondrial reactive oxygen species-mediated signaling in endothelial cells', Am J Physiol Heart Circ Physiol, 292(5), pp. H2023-31.

Zhou, L., Chomyn, A., Attardi, G. and Miller, C.A. (1997) 'Myoclonic epilepsy and ragged red fibers (MERRF) syndrome: selective vulnerability of CNS neurons does not correlate with the level of mitochondrial tRNAlys mutation in individual neuronal isolates', J Neurosci, 17(20), pp. 7746-53.

Zlokovic, B.V. (2008) 'The blood-brain barrier in health and chronic neurodegenerative disorders', Neuron, 57(2), pp. 178-201.